SOME CHARACTERISTICS AND APPLICATIONS OF A GENERAL PURPOSE OPTIMUM MULTICHANNEL STACKING FILTER

A thesis submitted by

Peter Hubral, Diplomgeophysiker

for the degree of

Doctor of Philosophy

of the

University of London

September, 1970

Department of Geophysics
Imperial College
London, S.W. 7

ABSTRACT

An exclusive study of a general class of multichannel stacking filters is made. They are designed in the time domain as optimum multichannel Wiener filters for various models of random stationary processes and include some known stacking filters as special cases. It is shown that filters of this class may be specified as two- and three-dimensional velocity filters, polarisation filters and stacking filters for the rejection or enhancement of signals with differential normal moveout. The two- and three-dimensional Fourier transforms are used as valuable tools for the characterisation of velocity filters. Transforms for special differential moveout filters are also given. The concept of a stacking filter transfer function is defined and it is shown under which conditions it can be obtained from the two- or three-dimensional Fourier transform of a filter. It gives a deep insight into the filter characteristics.

A discussion of the given multichannel normal equations shows how to select special time windows to obtain zero phase transfer functions. Zero phase stacking filter components do not necessarily guarantee zero phase transfer functions, while non-zero phase components may give phasefree transfer functions.

Some rules for the characteristics of the class of filters are presented. They are used in the design of special velocity filters, which have superior properties over known velocity filters. A study of the presented multichannel normal equations leads as well to the discovery of the 'scaling effect'. This effect helps to reduce computer calculations of filters. It also explains observations connected with their characterisation and application. Because the filter design depends on a host of design parameters, computational experiments were done to show in which way important parameters influence filter characteristics. A short re-appraisal of the basic theory of time series analysis is given. The theory of continuous and discrete stacking filters is also reviewed.

CONTENTS

CHAPTER 1

INTRODUCTION

Seismics is one of the most widely accepted and successful methods in exploration and the study of the solid earth. As most geophysical disciplines it is primarily concerned with the extraction of useful subsurface information from surface observations. The measurements are available in the form of seismograms; the problem (often referred to as the inverse seismic problem) is their proper interpretation in geological terms. In particular, one wishes to replace the mass of original data, which is of a complicated nature, by a small number of descriptive characteristics.

A large part of basic seismic research is therefore directed towards a better understanding of the physical processes involved in the seismic method. A seismogram may be regarded as the response of the system consisting of the earth and recording apparatus to an impulsive source, for instance an explosion. This system, although usually very complicated, is susceptible to basically three seismic approaches towards its analysis.

1. Computation of synthetic seismograms and comparison with actual field data.
2. Model seismic experiments and comparison with field data.
3. Application of different techniques based on various principles of communication theory.

The third technical approach was given a large impetus with the arrival of digital computers because most processing is in fact only possible on fast computers with large storage facilities. For all three basic techniques it is necessary to simplify to develop a working model. There can never be a unique all-embracing model in any case. A compromise between simplicity and reality is always necessary. Nevertheless, there is great hope that the combination of all different approaches will lead to

an understanding of the inverse seismic problem which is not obtainable with one technique alone. Therefore experience and knowledge gained in all seismic disciplines are most valuable for the design of digital processing techniques. There may sometimes even be a creative phase necessary for the design of processes beyond the reach of any specified mathematical theory. Within digital processes applicable to seismograms most techniques are filtering procedures. There exist basically three types of digital filters:

1. The single channel filter.
2. The n-dimensional filter based on the mathematical theory of n-dimensional Fourier transforms.
3. The multichannel filter based on the theory of matrix polynomials.

The last two filters are logical extensions of the single channel filter concept and as such include it as a special case. This work is confined to multichannel input - single channel output filters. This is a special case of a multichannel filter. The application of these filters is often referred to as multichannel stacking and their design is based on stochastic models. The design in this thesis is also partly done in analog and partly in discrete form. The analog version of the normal equations which usually specifies two-sided filter responses (Wiener, 1949) is used because of its simplicity for mathematical considerations. The discrete version (Robinson, 1967) is used for actual filter computations. The sampling theorem as given in Chapter 11 is of utmost importance in understanding the relationship between the two formulations. To help distinguish between them, t^* is used throughout the thesis as a discrete and t as a continuous time parameter. For the sake of simplicity the sampling interval is always taken as one time unit. Sampling therefore implies throughout this work, taking samples of a continuous function separated by this unit.

The design of any kind of filter has to be based on mathematical concepts. Random stationary functions are chosen in this work as models for seismic record sections. The theory of random stationary functions is reviewed and should be sufficient to appreciate the mathematical rules, which have been obeyed in the filter design. In particular it is reminded that the usual Fourier integral as presented in chapter 11 is not defined for a stationary function and that auto- and crosscorrelations are conceptual functions, which can be only obtained in a limiting process.

Although one may use a purely functional approach for the filter design, it is not until the theory of random stationary functions is introduced that certain procedures become meaningful in a physical sense. This theory, as conceived by Yule (1921,1927) and established in full generality by Khintchine (1934) makes use of averaging procedures, which were arrived at from the probability point of view. The full importance of the theory towards the solution of various engineering problems is emphasized by Wiener (1949) and Kolmogorov (1942).

The statistical approach has become very popular and sucessful in connection with the processing of seismograms and is justified by various authors as for instance Wadsworth (1953) and Robinson (1967).
A full understanding of the theory of stationary functions is not possible without having conceived various basic theorems as for instance the predictive decomposition theorem (Wold,1938) and the power spectrum factorisation (Kolmogorov, 1939). With the help of both theorems it can be shown that any stationary function with a continuous power spectrum can be thought to be a convolution of a minimum delay wavelet with a random stationary function, which has a white (broad band) spectrum. It is this property of random stationary functions, which brings them so near to the concept of the nature of a seismogram as given by Ricker (1953). A seismogram according to Ricker is an elaborate wavelet complex and the analysis of a

seismogram consists of breaking the record down into its components. The filtering process of predictive deconvolution (Robinson, 1957) is a classical example for the usefulness of the assumption that seismogram sections are stationary.

The particular stochastic model chosen in this treatment is the following one. It is assumed, that a seismic record section can be represented as a multichannel process, where each trace is the sum of three components, a signal (often primaries), correlated noise (often multiples) and uncorrelated noise. Signal and correlated noise are the common components in the record section, which differ only by their moveout from trace to trace. The stacking filter is designed to optimally filter the signal component and reject simultaneously all noise components. The fact that the filters are designed in the time domain allows the incorporation of various information available from the input traces. It is shown that the given design is very general and that the investigated class of filters may find application in various seismic problems. The two- and three- dimensional Fourier transforms are used to characterise some stacking filters.

It must be generally emphasized, that it was not the intention to give strict proofs for all individual steps. It was more the aim to discuss and characterise a useful class of stacking filters and outline applications for various seismic problems. The notation used in this thesis corresponds to the notation used by Robinson (1963, 1967 b).

CHAPTER II

BASIC CONCEPTS OF TIME SERIES ANALYSIS AND COMMUNICATION THEORY

The most important concepts essential for the understanding of this thesis are reviewed. The inclusion of various topics from time series analysis and communication theory in this chapter is intended as a reminder of their importance and an introduction to the special notation used in this thesis. The treatment includes a discussion of the Fourier-transform, the sampling theorem, time series, convolution, Z-transform and random processes. (Wiener, 1949; Lee,1960; Jury,1964; Papoulis,1962)

2.1 Fourier Transform

From a mathematical point of view Fourier transforms exist for various classes of functions and various conditions (Papoulis, 1962; Lanczos, 1966; Lighthill, 1966). It is always assumed that the necessary mathematical conditions are fulfilled to guarantee the existence of the transform. As Fourier transforms, the following pair is used in this thesis:

$$G(f) = \int_{-\infty}^{\infty} g(t) e^{-2\pi i f t} dt \qquad (2.1.1)$$

$$g(t) = \int_{-\infty}^{\infty} G(f) e^{+2\pi i f t} df \qquad (2.1.2)$$

G(f) is the Fourier transform of g(t) and g(t) is the inverse Fourier transform of G(f). t is time (e.g. milliseconds) and f is frequency (e.g. cycles per millisecond). The spectrum G(f) is generally a complex function which extends over all frequencies from minus to plus infinity. In polar form one may write:

$$G(f) = |G(f)| e^{i\Phi(f)} \qquad (2.1.3)$$

G(f) is called the amplitude spectrum and $\Phi(f)$ the phase spectrum. If g(t) is real valued, then $G(f) = G^*(-f)$, where $G^*(f)$ is the complex conjugate of G(f). The knowledge of G(f) for $f>0$ is then sufficient to describe g(t). Extensive use is made of the following Fourier transform pairs:

$$\int_{-\infty}^{\infty} g_1(t_1)\, g_2\,(t-t_1)\, dt_1 \quad \text{——} \quad G_1(f)\, G_2(f)$$

$$g\left(\frac{t-\beta}{\alpha}\right) \quad \text{——} \quad \alpha G(\alpha f)\, e^{-2\pi i f \beta}$$

$$\text{rec}\,(t) \quad \text{——} \quad \text{sinc}\,(f)$$

$$\text{sinc}\,(t) \quad \text{——} \quad \text{rec}\,(f)$$

where $\text{rec}\,(t) = \begin{cases} 1 \text{ for } |t| \leq \frac{1}{2} \\ 0 \text{ for } |t| > \frac{1}{2} \end{cases}$

and $\text{sinc}\,(t) = \dfrac{\sin(\pi t)}{\pi t}$

Also the following abbreviation for convolution is used:

$$\int_{-\infty}^{\infty} g_1(t_1)\, g_2(t-t_1)\, dt_1 = g_1(t) * g_2(t) = g_2(t) * g_1(t)$$

Further it is reminded that if a sampled function is given in form of q equidistant values in the time domain, q values transform into q complex values in the frequency domain (Cooley and Tuckey, 1965).

For the q values of the sampled function

$$(g\,(0),\ g\,(1),\ \ldots\ ,\ g\,(q-1)) \tag{2.1.4}$$

these are the q complex values

$$G(j/q) = \sum_{k=0}^{q-1} g(k) e^{-2\pi i k j/q} \quad (j=0,1,2,\ \ldots\ ,\ q-1) \tag{2.1.5}$$

The inverse transform of (2.1.5) is:

$$g(j) = (1/q) \sum_{k=0}^{q-1} G(k/q)\, e^{2\pi i k j/q} \quad (j=0,1,2,\ \ldots\ ,\ q-1) \tag{2.1.6}$$

One usually defines however, as the Fourier transform for the sampled values (2.1.4) the following continuous expression :

$$G(f) = \sum_{k=0}^{q-1} g(k)\, e^{-2\pi i f k} \tag{2.1.7}$$

The Fourier transform has three inherent attributes in communication theory -

1. It is a tool of analysis for time functions.

2. It is a concept to describe theoretical considerations of time functions often in an easier form in the frequency domain.

3. It is a tool for processing which is due to an existing fast discrete Fourier transform algorithm (Cooley and Tuckey, 1965), which may be applied to do a fast convolution of two sampled functions.

2.2 Sampling Theorem

In this section a short introduction to the sampling theorem is given, which is essential to describe the connection between discrete and analog formulations of time functions (Papoulis, 1962). It can be expressed as follows:

Let $$G(f) = \int_{-\infty}^{+\infty} g(t)\, e^{-2\pi i f t} dt \qquad (2.2.1)$$

be the Fourier transform of the analog function g(t) and

$$\bar{G}(f) = \sum_{n=-\infty}^{+\infty} g(n)\, e^{-2\pi i f n} \qquad (2.2.2)$$

the corresponding function of the sampled values

g_t = (.... g(-2), g(-1), g(0), g(1), g(2), ...),

then both transforms are connected with each other by the expression

$$\bar{G}(f) = \sum_{n=-\infty}^{+\infty} G(f+n) \qquad (2.2.3)$$

From (2.2.3) one may immediately conclude -

1. If G(f) is confined to $|f| \leq \frac{1}{2}$ then $\bar{G}(f) = G(f)$ for $|f| \leq \frac{1}{2}$. In this case no information gets lost due to sampling.

2. If $G(f) \neq 0$ for $|f| > \frac{1}{2}$, then $\bar{G}(f) \neq G(f)$ for $|f| \leq \frac{1}{2}$ and the functions G(f+n) $(-\infty < n < +\infty)$ overlap in expression

(2.2.3). This effect is known as aliasing. To prevent it, G(f) may be multiplied with rec (f) before sampling. This process is referred to as anti-aliasing.

3. An analog function with the same Fourier transform for $|f| \leq \frac{1}{2}$ as the discrete function g_t is

$$\tilde{g}(t) = \sum_{n=-\infty}^{+\infty} g(n) \text{ sinc } (t-n) \qquad (2.2.4)$$

This equation is obtained by taking the inverse Fourier transform of $\bar{G}(f)$ rec (f). It is of great help in later chapters to associate sampled values with the continuous function $\tilde{g}(t)$. Note that $\tilde{g}(t^*)=g(t^*)$.

2.3 Time Series

In this section the concept of discrete time series is presented. A discrete time series is a sequence of equidistant observations which are associated with the discrete time parameter t^*. Without loss of generality one may take the spacing between each successive observation to be one unit of time and thus represent the time series as

$$x_t = x(t^*) = (\ldots., x(-3), x(-2), x(-1), x(0), x(1) \ldots.)$$

An M-channel time series (multichannel time series) is then represented by

$$x_t = \begin{bmatrix} x_1(t^*) \\ x_2(t^*) \\ \\ x_M(t^*) \end{bmatrix} = \begin{bmatrix} \ldots., x_1(-2), x_1(-1), x_1(0), x_1(1), \ldots. \\ \ldots., x_2(-2), x_2(-1), x_2(0), x_2(1), \ldots. \\ \\ \ldots., x_M(-2), x_M(-1), x_M(0), x_M(1), \ldots. \end{bmatrix}$$

The following definitions (Robinson, 1967) are used in connection with discrete time series:

1. If a time series is one-sided in the way that $x(\hat{t}^*)=0$ for $\hat{t}^*<0$, the series is called physically realizable.
2. If for a realizable time series the equation

$\sum_{\hat{t}^*=0}^{\infty} x^2(\hat{t}^*) < \infty$ holds, then the time series is called a wavelet.

3. If $\sum_{\hat{t}^*=-\infty}^{\infty} x^2(\hat{t}^*) < \infty$, the time series is called an energy signal.

4. If $\lim_{T\to\infty} \frac{1}{T} \sum_{\hat{t}^*=-T/2}^{T/2} x^2(\hat{t}^*) < \infty$, the time series is called a power signal.

2.4 Convolution

Convolution is a mathematical concept, which describes the physical process of time domain filtering. When a wavelet y(t) passes through a linear time invariant filter, the output z(t) is known to be the convolution of the input wavelet y(t) with the unit impulse response of the filter a(t). The expression for convolution in continuous form is:

$$z(t) = \int_{-\infty}^{\infty} a(\tau)\, y(t-\tau)\, d\tau = a(t)^* y(t) = y(t)^* a(t) \qquad (2.4.1)$$

For the discrete case, where the sampling interval is chosen to be one, the expression is:

$$z(t^*) = \sum_{\tau^*=-\infty}^{\infty} a(\tau^*)\, y(t^* - \tau^*) \equiv a(t^*)^* y(t^*) = y(t^*)^* a(t^*) \qquad (2.4.2)$$

This is a numerical process done in the time domain. One is therefore able to specify many mathematical filters in the computer which have no equivalent electrical circuits. Examples are the class of Wiener single and multichannel filters, all-pass phase shift filters, phase-free reject and band-pass filters. Other linear operations, such as static corrections and inter-polation are also examples of convolution. Thus convolution is an extremely powerful tool for processing seismic data. The concept is strongly related to stationary linear systems and linear ordinary differential equations with constant coefficients (Doetsch, 1961; Cheng, 1959). The relation with linear systems is expressed in the fact that

the convolution integral can be interpreted as a superposition integral (Lee, 1960 , p. 323). There is also another strong connection between convolution and harmonic functions. This finds its expression in the convolution theorem. This theorem states that the Fourier transform of a convolution is the product of the Fourier transforms of the convolved functions.

2.5 Z-Transform

The Z-transform of a digital signal x_t is defined as

$$X(z) = \sum_{\hat{t}^*=-\infty}^{+\infty} x(\hat{t}^*)\, z^{\hat{t}^*} \qquad (2.5.1)$$

where z is supposed to be a complex variable (Jury, 1967). There are strong connections with the Laplace and Fourier transforms which are treated elsewhere. The importance of the Z-transform lies in the fact that many concepts related to digital functions find an easier formulation and explanation with this transform. So for instance may the Z-transform of the convolution of two time series x_t and y_t be simply expressed as the following product $Z(z) = X(z)\, Y(z)$ where $X(z)$ is the Z-transform of x_t and $Y(z)$ the Z-transform of y_t. The Fourier transform of an energy signal is easily obtained by substituting $z = e^{-2\pi if}$ in the corresponding Z-transform. A further concept most easily defined in the Z-domain is the concept of minimum, mixed and maximum delay. A discrete wavelet is called minimum delay if all its roots are outside the unit circle in the Z-domain. It is called maximum delay if all its roots are inside and it is called mixed delay if there are roots both inside and outside the unit circle.

2.6 Random Processes

In Chapter IV a multichannel filter is designed. The procedure for this is purely mathematical and therefore has to be based on mathematical concepts. On the other hand it is expected that these filters will also operate on real seismic traces. A mathematical concept which

seems to be a good approximation for actual seismic traces is the concept of a random stationary process. Random stationary processes will be used in this thesis as so-called 'stochastic models' for the design of optimum stacking filters. They can be defined for the continuous and discrete case. A short description of random stationary functions for the discrete case is given below.

Random is every function x_t, whose instantaneous value $x(\hat{t}^*)$ cannot be determined precisely. It is however assumed that a range of possible values $\{x(\hat{t}^*)\}$ exists with an associated probability distribution describing the likeliness of each possible value. In the language of probability theory, one says that for each $\hat{t}^*$, $x(\hat{t}^*)$ is a random variable. The complete function $\{x_t\}$ is called a random process. One must bear in mind, that an observed record of a random process is merely one record of a whole infinite collection of possible records, which might have been observed. This collection of possible records is called an 'ensemble' and any particular record is called a 'realization' or 'member' of the process. When dealing with random processes, one describes the 'steady state' type of behaviour by the term - stationary. More precisely, $\{x_t\}$ is called 'completely stationary' if all the statistical properties of $\{x(\hat{t}^*)\}$ do not change with time. If the first and second moments of $\{x(\hat{t}^*)\}$ do not change with time, one says that $\{x_t\}$ is 'stationary up to the second order' or simply 'stationary'.

The classical theory of spectral analysis which is used in this thesis, applies only to stationary random processes. This is still a severe restriction and it is doubtful whether any 'real-life' process possesses this property. In fact, stationarity is a mathematical idealisation and it is well known that every physical behaviour can only be described approximately with mathematical concepts. Therefore in practical applications the most one could hope for is that over a certain time interval on a seismogram the process would not depart 'too far' from stationarity for

the results of the analysis to be invalid. Statistical tests exist to verify the hypothesis of stationarity of seismograms (Bryan, 1967) and extensive tests showed that this assumption is in fact often justified on seismogram sections. Because the given design of digital filters is also based on stationarity, a satisfactory performance of these filters can be regarded as an indirect justification for the assumption.

Often one refers to functions having all the attributes of random stationary functions, though known for all time, also as random functions. This is, strictly speaking, of course wrong. In actual fact, one always operates with these 'known random' functions, unless 'real time' processing is done. A recorded seismogram section is a typical example for such an assumed 'known random' function. The general harmonic analysis however, applies to both types of functions if the basic assumptions are the same.

2.7 Basic functions of spectral analysis

There is a number of important functions related to stationary random processes. Some of them are reviewed in this section. For any random process, one may form averages with respect to the ensemble of realizations $\{x(\hat{t}^*)\}$ for a fixed integer valued time. Such averages are called ensemble averages and are denoted by the expectation symbol E. In particular the mean value $m = E\{x(\hat{t}^*)\}$ and the variance $\sigma = E\{(x(\hat{t}^*)-m)^2\}$ of a stationary random process are independent of time $\hat{t}^*$. Likewise, the autocorrelation coefficients $\varphi_{xx}(\tau^*) = E\{x(\hat{t}^* + \tau^*)\, x(\hat{t}^*)\}$ are independent of $\hat{t}^*$.

There is another type of average known as time average, in which the averaging process is carried out with respect to all values of time for a given realization. A stationary process is called ergodic if the ensemble and time averages are equal with probability one. As a result, the autocorrelation of an ergodic process may be expressed as the time average:

$$\varphi_{xx}(\tau^*) = \lim_{T\to\infty} \frac{1}{2T+1} \sum_{\hat{t}^*=-T}^{T} x(\hat{t}^* + \tau^*)\, x(\hat{t}^*) \qquad (2.7.1)$$

The crosscorrelation of two stationary processes $\{ x_t \}$ and $\{ y_t \}$ is defined as

$\varphi_{xy}(\tau^*) = E\{x(\hat{t}^* + \tau^*)\, y(\hat{t}^*)\}$ whose time average presentation is

$$\varphi_{xy}(\tau^*) = \lim_{T\to\infty} \frac{1}{2T+1} \sum_{\hat{t}^*=-T}^{T} x(\hat{t}^* + \tau^*)\, y(\hat{t}^*) \qquad (2.7.2)$$

The Fourier transform of (2.7.1) is known as the power spectrum and the transform of (2.7.2) is called the crosspower spectrum.

It can be shown that autocorrelation functions are symmetric and that all functions with the same amplitude spectrum have the same autocorrelation. It seems therefore clear that the autocorrelation is of utmost importance in the harmonic analysis of a random process where variety in waveform of the realizations is an inherent attribute. Crosscorrelations of random functions are used in communication theory in various ways. They are of utmost importance for the design of multichannel filters.

CHAPTER III

INTRODUCTION TO MULTICHANNEL FILTER THEORY

A seismogram generally consists of more than one trace. Events which may be followed from trace to trace and record to record, usually have more value to the seismic interpreter and hence are statistically more important than events which appear on only one trace. A function describing this inter-relation from trace to trace is, for instance, the crosscorrelation of two traces. All crosscorrelations between individual traces are incorporated in the autocorrelation matrix of a multichannel system. This matrix is a basic element for the design of a multichannel filter. Because a multichannel filter uses more information of the input traces, one should expect that it generally works better than individually designed filters for each trace. It is however also logical that if there are no essential crosscorrelations among the traces, then there is hardly any use in applying a multichannel filter. The geophysicist is therefore interested in characteristics and performance of these filters for individual cases which are related to practical problems.

The theory of multichannel stacking filters can be presented in analog form (Wiener, 1949) and in digital form (Robinson, 1967 b) Optimum least squares filters can be designed as realizable and non-realizable filters. The analog version of the normal equations presented in the geophysical literature (Meyerhoff, 1966; Foster, et al., 1968; Davies ,et al. 1968; Burg,1964) is the one which will usually specify physically non-realizable analog filters. A short introduction to this special version is given below. In more detail the digital form is treated which is actually used for the computation of filters.

3.1 The theory of optimum multichannel stacking filters in continuous form

Let N random stationary ergodic functions $x_i(t)$,(i=1,..,N) be the input to the multichannel stacking filter as shown in figure 3.1.1.

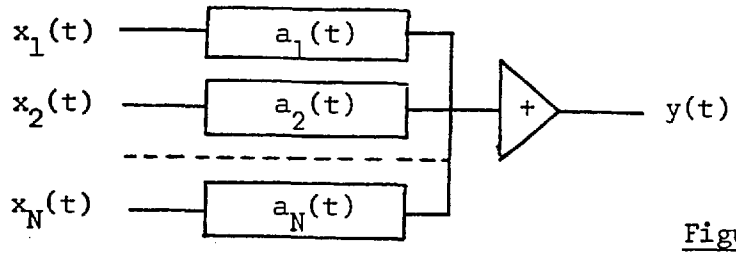

Figure 3.1.1 Stacking filter

z(t) and y(t) are stationary processes representing the desired and actual output of the filter. The N linear filters $a_i(t)$ $(-\infty < t < \infty)$, which operate on the input traces $x_i(t)$ to minimize

$$I = \lim_{T\to\infty} \frac{1}{2T} \int_{-T}^{T} (z(t) - y(t))^2 \, dt$$

where $y(t) = \sum_{i=1}^{N} a_i(t) * x_i(t)$ satisfy the set of simultaneous equations:

$$\sum_{i=1}^{N} a_i(t) * \varphi_{x_i x_j}(t) = \varphi_{z x_j}(t), \quad (j=1,..,N) \tag{3.1.1}$$

$$\varphi_{x_i x_j}(\tau) = \lim_{T\to\infty} \frac{1}{2T} \int_{-T}^{T} x_i(t+\tau) x_j(t) \, dt \tag{3.1.2}$$

$$\varphi_{z x_j}(\tau) = \lim_{T\to\infty} \frac{1}{2T} \int_{-T}^{T} z(t+\tau) x_j(t) \, dt \tag{3.1.3}$$

The proof is usually given by making use of concepts from the theory of functions (Wiener, 1949; Robinson, 1962). If equations (3.1.1) are to be used on multichannel traces right away, the auto- and crosscorrelations have to be necessarily estimated from finite length record sections. To do the best estimation is a problem in its own and is extensively treated by Blackman and Tuckey (1968).

As the treatment in chapter IV will show, equations (3.1.1) are however used differently in this thesis. They can be looked upon as the basic equations for a further theoretical design procedure.

In the frequency domain equations (3.1.1) become

$$\sum_{i=1}^{N} A_i(f)\Phi_{x_i x_j}(f) = \Phi_{zx_j}(f) \qquad (j=1,\ldots,N) \qquad (3.1.5)$$

where the hermitian matrix $\Phi_{x_i x_j}(f)$ is called the coherency matrix of the input traces. The inverse Fourier transform of this matrix is the autocorrelation matrix. A special case for equation (3.1.5) is the single channel case where for only one input trace $x_i(t) = x(t)$ the optimum filter is

$$A(f) = \Phi_{zx}(f)/\Phi_{xx}(f) \qquad (3.1.6)$$

Another very important case which is generally treated in the geophysical literature is the following one where the stochastic model of the seismic traces is assumed to have the presentation

$$x_i(t) = s_i(t) + r_i(t) + n_i(t) \quad , (i=1,\ldots,N) \; ; \; z(t)=s(t), \qquad (3.1.7)$$

and signals $s_i(t)$, correlated noise $r_i(t)$ and uncorrelated noise $n_i(t)$ satisfy the conditions

$$\varphi_{x_i x_j}(\tau) = \varphi_{s_i s_j}(\tau)+\varphi_{r_i r_j}(\tau)+\varphi_{n_i n_j}(\tau)\,\delta_{ij} \quad , (i,j=1,\ldots,N) \qquad (3.1.8)$$

$$\varphi_{zx_j}(\tau) = \varphi_{ss_j}(\tau), \qquad (j=1,\ldots,N) \qquad (3.1.9)$$

This means that signals and noise are uncorrelated with each other. The normal equations under this condition become in the time domain

$$\sum_{i=1}^{N} a_i(\tau)*\left[\varphi_{s_i s_j}(\tau) + \varphi_{r_i r_j}(\tau) + \varphi_{n_i n_j}(\tau)\,\delta_{ij}\right] = \varphi_{ss_j}(\tau), \qquad (j=1,\ldots,N) \qquad (3.1.10)$$

or in the frequency domain

$$\sum_{i=1}^{N} A_i(f)\left[\Phi_{s_i s_j}(f) + \Phi_{r_i r_j}(f)+\Phi_{n_i n_j}(f)\delta_{ij}\right] = \Phi_{ss_j}(f), (j=1,..,N) \qquad (3.1.11)$$

By choosing the minimization criterion

$$I = \lim_{T\to\infty} \frac{1}{2T}\left[\int_{-T}^{T}\Big(s(t)-\sum_{i=1}^{N} a_i(t)*s_i(t)\Big)^2+\rho\int_{-T}^{T}\Big(\sum_{i=1}^{N} a_i(t)*r_i(t)\Big)^2+\nu\int_{-T}^{T}\Big(\sum_{i=1}^{N} a_i(t)*n(t)\Big)^2\right]$$

one would again obtain (3.1.10), however with the weighted correlation functions $\rho\varphi_{r_i r_j}(\tau)$ and $\nu\varphi_{n_i n_j}(\tau)$. (See also section 3.2.5.)

3.2 The theory of multichannel filters in discrete form

The introduction to the theory of digital multichannel filters in this thesis is given in more detail because it is the theory which is most adapted to actual digital computer processing. To make this treatment more general, the theory for the N-input and M-output channel case is presented.

3.2.1 Introduction to the theory of matrix polynomials

For the sake of understanding the basic concepts of the theory of discrete multichannel filters a very short introduction to the most important properties of matrix polynomials is given. They are also called polynomial matrices or λ-matrices (Lambda-matrices). The theory of matrix polynomials is a logical extension of the theory of constant matrices and it is the basis for the theory of discrete multichannel filters. A matrix polynomial is defined as $\bar{\bar{A}}(z) = \sum_{i=0}^{m} a_i z^i$ where z denotes an indeterminate which is assumed to be commutative with itself and the constant M x N matrices $a_i (i=0,..m)$. For a constant value of z a matrix polynomial reduces to a constant matrix. For operations with λ-matrices it is therefore demanded that the usual matrix algebra applies. Regarding a λ-matrix as a polynomial with matrix coefficients leads to the name matrix polynomial. Regarding it as a matrix with polynomial entries leads to the name polynomial matrix.

The product of two polynomial matrices $\bar{\bar{A}}(z)$ and $\bar{\bar{B}}(z)$, is not necessarily commutative. It is a polynomial matrix $\bar{\bar{C}}(z)=\bar{\bar{A}}(z)\,\bar{\bar{B}}(z)$, whose coefficients are obtained by convolving the coefficients of $\bar{\bar{A}}(z)$ and $\bar{\bar{B}}(z)$. Further and detailed treatment of this theory is given in various works as for instance: Frazer, Duncan, Collar, 1963; Gantmacher, 1959.

3.2.2 Basic concepts of a digital multichannel filter

A box with N inputs and M outputs is shown in figure 3.2.2.1.

FIGURE 3.2.2.1 Multichannel filter.

Exciting input channel 1 with a spike (1, 0, ...), a multichannel response on all M outputs is expected whose Z-transforms are $A_{11}(z)$, $A_{21}(z)$, ... , $A_{M1}(z)$.

$A_{11}(z)$ is the Z-transform of the response on output channel 1, $A_{21}(z)$ on output channel 2, etc. Putting a spike on input channel K will result again in M different outputs $A_{1K}(z)$, ... , $A_{MK}(z)$. The behaviour of the box is fully described by the M x N responses $A_{ij}(z)$,(i=1,.M; j=1,.,N). Such a box is called a digital multichannel filter. To keep the theory within reasonable limits, it is demanded that the following mathematical conditions are fulfilled:

1. The multichannel filter has to be time invariant. (The application of the same input spikes at different times results in the same outputs).
2. The responses of the multichannel filter have to be wavelets.
3. The multichannel filter has to be linear. This means:
   (a) Applying more spikes on different input channels or at different times or both results in the superposition of the corresponding output wavelets.
   (b) Scaling of an input spike results in the same scaling of the output wavelets.

Condition 3 leads to the superposition principle. This principle states that, regarding each input trace as a sequence of differently scaled spikes at subsequent times, the overall output is the superposition of all the

scaled corresponding stimulus responses belonging to each individual spike. It describes in single channel filter theory the fact that the filter output can be expressed as a convolution of the input with the stimulus response. For a multichannel filter the principle demands that the multichannel output is connected with the multichannel input by the following matrix multiplication.

$$\begin{bmatrix} A_{11}(z) & A_{12}(z) & \dots & A_{1N}(z) \\ & & & \\ & & & \\ A_{M1}(z) & & & A_{MN}(z) \end{bmatrix} \begin{bmatrix} X_1(z) \\ X_2(z) \\ \\ X_N(z) \end{bmatrix} = \begin{bmatrix} Y_1(z) \\ Y_2(z) \\ \\ Y_M(z) \end{bmatrix} \qquad (3.2.2.1)$$

Or in short, $\underline{\underline{A}}(z)\ X(z) = Y(z)$ where $X(z)$ is the Z-transform of the multichannel input and $Y(z)$ the Z-transform of the multichannel output. The Z-transform of a multichannel filter therefore has the mathematical representation of a polynomial matrix. It may also be written in the form of a matrix polynomial

$$\underline{\underline{A}}(z) = a_o + a_1 z + \dots + a_m z^m \qquad (3.2.2.2)$$

Each coefficient is a constant M x N matrix. Multichannel convolution is expressed in the time domain in concise form as:

$$a_o x_t + a_1 x_{t-1} + \dots + a_m x_{t-m} = y_t \qquad (3.2.2.3)$$

where $y_t = \begin{bmatrix} y_1(t^*) \\ \\ y_M(t^*) \end{bmatrix}$ and $x_t = \begin{bmatrix} x_1(t^*) \\ \\ x_N(t^*) \end{bmatrix}$

A polynomial matrix with only one entry is the special case of a single channel filter. When all the entries of an N x N polynomial matrix are zero except those on the main diagonal, the matrix describes the application of N filters to N traces. It is shown below how even two-dimensional filters can be included as special cases in the theory of multichannel filters.

Having two two-dimensional operators a_{ij} ,(i=1,.n;k=1,.m) and b_{ij},(i=1,..,k;j=1,..,$\tilde{l}$) and defining the two functions

$$A(t,y) = \sum_{i=1}^{n} \sum_{j=1}^{m} a_{ij} t^{i-1} y^{j-1} \qquad (3.2.2.4)$$

$$B(t,y) = \sum_{i=1}^{k} \sum_{j=1}^{\tilde{l}} b_{ij} t^{i-1} y^{j-1} \qquad (3.2.2.5)$$

the coefficients of the function $C(t,y) = A(t,y)\,B(t,y)$ are called the convolution of a_{ij} and b_{ij}: $c_{ij} = \sum_{r=0}^{n} \sum_{s=0}^{m} a_{rs} b_{i-r+1,j-s+1}$

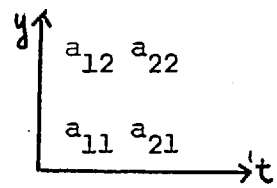

Figure 3.2.2.2

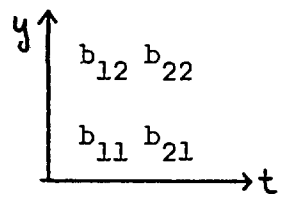

Figure 3.2.2.3

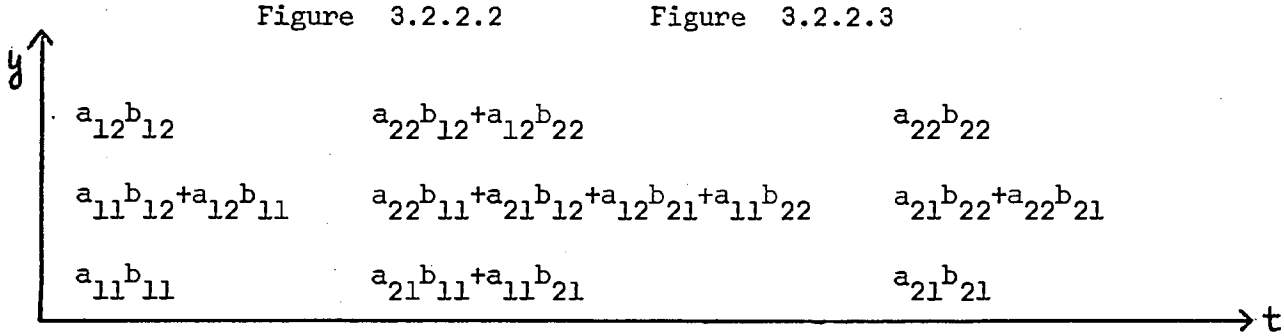

Figure 3.2.2.4

To give an example the 2 x 2 operator of figure 3.2.2.2 was convolved with the 2 x 2 operator of figure 3.2.2.3. The result is shown in figure 3.2.2.4. This operation can be formulated as a multichannel filter process. For this purpose a_{ij}(i,j = 1,2) is regarded as two single channel filters and b_{ij}(i,j = 1,2) as two input time series of length two. C_{ij} are then three output time series of length three. Taking the Z-transforms

$A_1(z)=a_{11}+a_{21}z$ $\qquad$ $B_1(z)=b_{11}+b_{21}z$

$A_2(z)=a_{12}+a_{22}z$ $\qquad$ $B_2(z)=b_{12}+b_{22}z$

and letting the Z-transforms of the three output traces be

$C_1(z)=a_{11}b_{11}+(a_{21}b_{11}+a_{11}b_{21})z+a_{21}b_{21}z^2$

$C_2(z)=(a_{11}b_{12}+a_{12}b_{11})+(a_{22}b_{11}+a_{21}b_{12}+a_{12}b_{21}+a_{11}b_{22})z+(a_{21}b_{22}+a_{22}b_{21})z^2$

$C_3(z)=a_{12}b_{12}+(a_{22}b_{12}+a_{12}b_{22})z+a_{22}b_{22}z^2$

it may be seen that two-dimensional convolution for the above example can be written as

$$\begin{bmatrix} A_1(z) & 0 & 0 \\ A_2(z) & A_1(z) & 0 \\ 0 & A_2(z) & A_1(z) \end{bmatrix} \begin{bmatrix} B_1(z) \\ B_2(z) \\ 0 \end{bmatrix} = \begin{bmatrix} C_1(z) \\ C_2(z) \\ C_3(z) \end{bmatrix}$$

For the general case the Z-transforms are

$$A_j(z) = \sum_{i=1}^{n} a_{ij} z^{i-1} \qquad (j=1,\ldots,m) \qquad (3.2.2.6)$$

$$B_j(z) = \sum_{i=1}^{k} b_{ij} z^{i-1} \qquad (j=1,\ldots,\tilde{l}) \qquad (3.2.2.7)$$

With these terms the following $(\tilde{l} + m) \times (\tilde{l} + m)$ matrix

$$\bar{\bar{A}}(z) = \begin{bmatrix} A_1(z) & 0 & 0 & . & . & . & . \\ A_2(z) & A_1(z) & 0 & . & . & . & . \\ A_3(z) & A_2(z) & A_1(z) & . & . & 0 & 0 \\ . & . & . & . & . & . & . \\ A_m(z) & . & . & . & . & . & . \\ 0 & A_m(z) & . & . & . & 0 & 0 \\ . & . & . & . & . & A_1(z) & 0 \\ 0 & 0 & 0 & A_m(z) & . & A_2(z) & A_1(z) \end{bmatrix} \qquad (3.2.2.8)$$

and the $(m + \tilde{l})$ - length vector

$B^T(z) = (B_1(z), B_2(z), \ldots. B_i(z) \ldots.0)$ is defined. It can be easily verified that the matrix product $\bar{\bar{A}}(z)\, B(z) = C(z)$, which now corresponds to a multichannel process, possesses the coefficients of the two-dimensional convolution. Note that $B^T(z)$ is the transpose of $B(z)$. In particular, when N input traces $B_i(z)$ have to be convolved with an N-trace filter $A_i(z)$ then 2N-1 output traces result. Of special importance in this case is

then, as shown in Chapter VI the centre trace of the output

$$C_N(z) = \sum_{i=1}^{N} A_i(z) B_{N+1-i}(z) \qquad (3.2.2.9)$$

This description of two-dimensional convolution in multichannel filter terms can be easily extended to three and higher dimensional convolution. Two-dimensional convolution can be done by taking the discrete two-dimensional Fourier transforms of the input traces and the filter, multiplying both and taking again the inverse transform of the product (See Chapter VI).

3.2.3 Auto- and crosscorrelation matrix of a multichannel time series

A p channel stochastic process may be presented by the column vector $x_t = \begin{bmatrix} x_1(t^*) \\ x_p(t^*) \end{bmatrix}$

where each element $x_i(t^*)$ denotes a single channel process. The multi-channel autocorrelation coefficient for time shift s is given by the p xp matrix.

$$\varphi_{xx}(s) = \varphi_s = E\{x_{t+s} x_t^T\} = \begin{bmatrix} \varphi_{11}(s) & \varphi_{12}(s) & \cdots & \varphi_{1p}(s) \\ & & & \\ \varphi_{p1}(s) & & & \varphi_{pp}(s) \end{bmatrix}$$

$\varphi_{ij}(s) = \varphi_{x_i x_j}(s) = E\left\{x_i(\hat{t}^* + s)\, x_j(\hat{t}^*)\right\}$ is the single-channel auto-correlation for i=j or the dual channel crosscorrelation for i≠j. If $y_t = \begin{bmatrix} y_1(t^*) \\ y_q(t^*) \end{bmatrix}$ represents another q channel stochastic process, then

$\varphi_{xy}(s) = E\left\{x_{t+s} y_t^T\right\}$ correspondingly is called a crosscorrelation matrix coefficient for time shift s. Under the assumption that correlation functions are of finite length 2n + 1, the Z-transform of a multichannel autocorrelation matrix can be written as

$$\begin{vmatrix} \sum_{i=-n}^{n} \varphi_{11}(i)z^i & \cdots & \sum_{i=-n}^{n} \varphi_{1p}(i)z^i \\ \sum_{i=-n}^{n} \varphi_{p1}(i)\, z^i & \cdots & \sum_{i=-n}^{n} \varphi_{pp}(i)\, z^i \end{vmatrix} \qquad (3.2.3.1)$$

n may be any integer value between one and infinity. This is an extended symmetric λ-matrix (Robinson, 1967) . Due to this fact, it is sufficient to know only the one-sided autocorrelation matrix, where the summation is from i=0 to i=n.

3.2.4 Design of a digital multichannel - Wiener filter

It was shown that multichannel convolution can be expressed as $y_t = \sum_{i=0}^{m} a_i x_{t-i}$, where x_t is the multichannel input, y_t the multichannel output and $a_i (i=0,\ldots m)$ are constant matrices. One would like to know how to determine the numerical values of a_i in order to optimize the specific problem, where a known x_t has to be transformed into a desired output z_t.

Below a short review of the solution to this problem (Robinson, 1967) is given. The solution rests on three main assumptions:

1. The time series representing the input x_t and the output z_t are random stationary functions.
2. The approximation criterion is taken in such a way as to minimize the trace of the mean-square-error matrix between the desired output z_t and the actual output y_t. This trace is given by
$$I = \text{tr } E\left\{(z_t - y_t)(z_t - y_t)^T\right\}$$
where $(z_t - y_t)^T$ is the transpose of $(z_t - y_t)$.
3. The filter is time invariant, physically realizable and stable.

3.2.5 Derivation of the multichannel normal equations

An (m+1) length multichannel filter is chosen where the coefficients are M x N matrices

$$a_s = a(s) = \begin{bmatrix} a_{11}(s) & a_{12}(s) \,..\, a_{1N}(s) \\ \\ a_{M1}(s) & a_{M2}(s) \,..\, a_{MN}(s) \end{bmatrix} \quad (s=0,\ldots,m) \qquad (3.2.5.1)$$

The input time series are given by the N x 1 vector valued time series $x_t = x(t^*) = \begin{bmatrix} x_1(t^*) \\ x_N(t^*) \end{bmatrix}$ and the desired output by the (M x 1) vector - valued time series $z_t = z(t^*) = \begin{bmatrix} z_1(t^*) \\ z_N(t^*) \end{bmatrix}$.

The actual output is given by the matrix equation $y_t = a_0 x_t + a_1 x_{t-1} + \ldots + a_m x_{t-m}$

The error between the desired output and actual output is then

$$e_t = z_t - y_t = z_t - (a_0 x_t + \ldots + a_m x_{t-m}) \qquad (3.2.5.2)$$

Defining the mean-square error-matrix by

$$E\left\{e_t e_t^T\right\} = \begin{bmatrix} E\left\{e_1^2(t)\right\} & E\left\{e_1(t)e_2(t)\right\} & \ldots & E\left\{e_1(t)e_M(t)\right\} \\ \\ E\left\{e_M(t)e_1(t)\right\} & \ldots\ldots\ldots\ldots & & E\left\{e_M^2(t)\right\} \end{bmatrix} \qquad (3.2.5.3)$$

the trace of this matrix is then the sum of the diagonal entries

$$I = \operatorname{tr} E\left\{e_t e_t^T\right\} = E\left\{e_1^2(t)\right\} + E\left\{e_2^2(t)\right\} + \ldots + E\left\{e_M^2(t)\right\} \qquad (3.2.5.4)$$

This means in other words, the sum of the squared errors resulting on all outputs is going to be minimized. Because the error

$e_t = z_t - y_t = z_t - \sum_{s=0}^{m} a_s x_{t-s}$ and $e_t e_t^T = (z_t - \sum_{s=0}^{m} a_s x_{t-s})(z_t - \sum_{s=0}^{m} a_s x_{t-s})^T$ the mean-square-error matrix becomes

$$E\{e_t e_t^T\} = E\{z_t z_t^T\} - \sum_{r=0}^{m} E\{z_t x_{t-r}^T\} a_r^T - \sum_{s=0}^{m} a_s E\{x_{t-s} z_t^T\}$$

$$+ \sum_{r=0}^{m} \sum_{s=0}^{m} a_s E\{x_{t-s} x_{t-r}^T\} a_r^T$$

This can be written by making use of the definition of the auto- and crosscorrelation matrix

$$E\{x_{t-s} x_{t-r}^T\} = \varphi_{xx}(r-s)$$

$$E\{z_{t-s} x_{t-r}^T\} = \varphi_{zx}(r-s)$$

as $$E\{e_t e_t^T\} = E\{z_t z_t^T\} - \sum_{r=0}^{m} \varphi_{zx}(r) a_r^T - \sum_{s=0}^{m} a_s \varphi_{xz}(-s)$$

$$+ \sum_{r=0}^{m} \sum_{s=0}^{m} a_s \varphi_{xx}(r-s) a_r^T$$

Setting the partial derivatives of the trace $I = \mathrm{tr}\, E\{e_t e_t^T\}$ in respect to the (m+1)xMxN filter coefficients equal to zero results in the set of simultaneous equations

$$\begin{aligned} a_o \varphi_{xx}(0) + a_1 \varphi_{xx}(-1) + \ldots + a_m \varphi_{xx}(-m) &= \varphi_{zx}(0) \\ a_o \varphi_{xx}(1) + a_1 \varphi_{xx}(0) + \ldots + a_m \varphi_{xx}(1-m) &= \varphi_{zx}(1) \\ &\vdots \\ a_o \varphi_{xx}(m) + a_1 \varphi_{xx}(m-1) + \ldots + a_m \varphi_{xx}(0) &= \varphi_{zx}(m) \end{aligned} \qquad (3.2.5.5)$$

These are the discrete multichannel normal equations. All $a_s(s=0,m)$ are M x N matrices, all $\varphi_{xx}(s)(s=-m,m)$ are N x N matrices and all $\varphi_{zx}(s)(s=0,m)$ are M x N matrices.

In concise form equations (3.2.55) may be written as

$$\sum_{r=0}^{m} a_r \varphi_{xx}(s-r) = \varphi_{zx}(s), \quad (s=0,\ldots,m)$$

As already mentioned, Wiggins and Robinson (1965) presented a recursive

solution of these equations which is generally available. With the help of the computed filter coefficients the minimum value of the trace of the mean-square-error matrix is

$$I_{min} = tr\varphi_{zz}(0) - tr\sum_{r=0}^{m} \varphi_{zx}(r)a_r^T \qquad (3.2.5.6)$$

For the design of a multichannel Wiener-filter the only elements necessary are therefore the one-sided auto- and crosscorrelation matrices.

In case a more detailed assumption is made about the input and output, a least squares error criterion may be chosen, which leads to slightly different normal equations. Let $x_t = s_t+r_t+n_t$, where s_t is a multichannel process of N signals and r_t, n_t are multichannel processes representing correlated and uncorrelated noise. It is also assumed that the signals s_t are not correlated with the noise and that the desired N-trace output array is chosen as s_t. The error vector (3.2.5.2) may now be decomposed into the three components

$$e_t = s_t - \sum_{s=0}^{m} a_s(s_{t-s}+r_{t-s}+n_{t-s})$$

$$e_t = {}^{s}e_t + {}^{r}e_t + {}^{n}e_t$$

where

$${}^{s}e_t = s_t - \sum_{s=0}^{m} a_s s_{t-s}$$

$${}^{r}e_t = -\sum_{s=0}^{m} a_s r_{t-s}$$

$${}^{n}e_t = -\sum_{s=0}^{m} a_s n_{t-s}$$

Instead of taking (3.2.5.4) for the computation of the normal equations, one may also choose

$$I_{\varrho\nu} = trE\left\{{}^{s}e_t\,{}^{s}e_t^T\right\} + \varrho\, trE\left\{{}^{r}e_t\,{}^{r}e_t^T\right\} + \nu\, trE\left\{{}^{n}e_t\,{}^{n}e_t^T\right\} \qquad (3.2.5.7)$$

thus giving different weights to the errors caused by the signal and noise components. Setting the partial derivatives of $I_{\rho\nu}$ with respect to all filter coefficients equal to zero leads to the normal equations

$$\sum_{r=0}^{m} a_r \left[\varphi_{ss}(s-r) + \rho \varphi_{rr}(s-r) + \nu \varphi_{nn}(s-r) \right] = \varphi_{ss}(s), (s=0,..,m) \quad (3.2.5.8)$$

where φ_{ss} is the N x N autocorrelation matrix of the signal vector s_t and $\varphi_{rr}, \varphi_{nn}$ the N x N autocorrelation matrices of the noise vectors.

It is a known fact that the assignment of a weighting factor to the autocorrelation matrix of the correlated noise (Galbraith and Wiggins, 1968) may lead to considerable improvement in the signal to correlated noise ratio. The above treatment shows that such a weighting factor can be already included in the least squares criterion which for a big value of ρ exaggerates the importance of correlated noise in the design. Computational experiments are done in later chapters which show the effect of ρ and ν on the filtering process.

3.3 Exact and approximate solutions of multichannel normal equations

In the previous two sections normal equations for optimum multichannel stacking filters for the discrete (3.2.5.5) and analog case (3.1.1) were presented. Complete analog solutions are generally not available while discrete solutions of (3.2.5.5) are easily obtained with the fast multichannel - Levinson algorithm.

Throughout the rest of this work normal equations are discussed in analog form. Below it is shown under which conditions the discrete algorithm can be applied to give (at least approximate) solutions for the analog case. The analog normal equations (3.1.5) can be written in concise form as:

$$\sum_{j=1}^{N} \hat{A}_j(f)\,\Phi_{ij}(f) = \Phi_i(f), \quad (i=1,..,N) \tag{3.3.1}$$

They generally specify two-sided continuous responses where $\hat{A}_j(f)(j=1,\ldots,N)$ covers the range $|f|<\infty$. These solutions can never be obtained with the discrete normal equations. Discrete solutions are always physically realizable and have a spectrum which is entirely defined in the range $|f|<\frac{1}{2}$ If (3.3.1) has to be solved with the discrete algorithm, one has to make sure, first of all, that the equations have the form

$$\mathrm{rec}(f) \sum_{j=1}^{N} \tilde{A}_j(f)\,\Phi_{ij}(f) = \Phi_i(f)\,\mathrm{rec}\,(f), \quad (i=1,..,N) \tag{3.3.2}$$

so that their solutions are also confined to the range $|f|<\frac{1}{2}$. The solutions of (3.3.1) and (3.3.2) are connected with each other by the following formula

$$\tilde{A}_j(f) = \hat{A}_j(f)\,\mathrm{rec}\,(f), \quad (j=1,..,N) \tag{3.3.3}$$

This is self explanatory, because solutions of (3.3.1) and (3.3.2.) for a given f do not depend on other frequencies and in particular $\tilde{A}_j(f)$ cannot depend on $|f|>\frac{1}{2}$. Solutions of (3.3.2.) may be physically not realizable. There is the possibility that by multiplying the right side of (3.3.2) with

$e^{-2\pi i f t_d}$ where $t_d > 0$

$$\mathrm{rec}(f)\sum_{j=1}^{N} A_j(f)\,\Phi_{ij}(f) = \Phi_j(f)\,\mathrm{rec}(f)\,e^{-2\pi i f t_d},\ (i=1,..,N) \qquad (3.3.4)$$

one would obtain solutions $A_j(f) = \tilde{A}_j(f)\,e^{-2\pi i f t_d}$ or $a_j(t)=\tilde{a}_j(t-t_d),(j=1,..,N)$ which are shifted into positive times. There is always a value for t_d, such that the remaining negative part of the time responses for (3.3.4) is negligible. If it is therefore assumed, that the time domain solutions $a_j(t)$, $(j=1,..,N)$ of (3.3.4) can be neglected for $t < 0$ (which is justified for large t_d), then they fulfil the same properties as the solutions of the discrete normal equations (3.2.5.5). Solutions for (3.3.4) were therefore computed as follows:

The auto- and crosscorrelations of (3.3.4)

$$\varphi_{ij}(\tau) = \int_{-\infty}^{+\infty} \mathrm{rec}(f)\,\Phi_{ij}(f)\,e^{2\pi i f \tau}\,df \qquad (3.3.5)$$

$$\varphi_j(\tau) = \int_{-\infty}^{\infty} \mathrm{rec}(f)\,\Phi_j(f) e^{-2\pi i f t_d}\,e^{2\pi i f \tau}\,df \qquad (3.3.6)$$

were sampled for $0 \le \tau \le m$ and with

$$\varphi_{xx}(\tau) = \begin{bmatrix} \varphi_{11}(\tau) & \cdots & \varphi_{1N}(\tau) \\ \cdots & \cdots & \cdots \\ \varphi_{N1}(\tau) & \cdots & \varphi_{NN}(\tau) \end{bmatrix} \qquad (\tau=0,\ldots,m)$$

and $$\varphi_{zx}(\tau) = \begin{bmatrix} \varphi_1(\tau) & \cdots & \varphi_N(\tau) \end{bmatrix} \qquad (\tau=0,\ldots,m)$$

the normal equations

$$\sum_{r=0}^{m} a_r\,\varphi_{xx}(\tau-r) = \varphi_{zx}(\tau) \qquad (\tau=0,\ldots,m)$$

were solved with the fast multichannel Levinson algorithm.

The discrete solutions depend very much on the values m and t_d. It is immediately clear that m and t_d must tend towards infinity, if the obtained discrete solutions should represent complete continuous solutions. These practically unobtainable solutions will be refered to as the "exact" solutions.

It is however possible to compute finite length discrete filters with a finite number of $\varphi_{ij}(\tau^*)$ and $\varphi_j(\tau^*)$ and a finite positive t_d. The obtained discrete filters of various possible length m and a given t_d

$$a_j^m(t^*) \quad (0 \leq t^* \leq m) \qquad (j=1,\ldots,N) \qquad (3.3.7)$$

are called the 'approximate' discrete solutions. An approximate analog solution for (3.3.4) is then

$$a_j^m(t) = \sum_{i=0}^{m} a_j^m(i) \operatorname{sinc}(t-i), \quad (j=1,..,N) \qquad (3.3.8)$$

Among the 'approximate' solutions one is only interested in the best approximations to the 'exact' solution for the shortest possible filter length. The least squares error (3.2.5.6) is a good criterion to give an upper limit for the filter length (Galbraith and Wiggins, 1968), from where onwards further convergence becomes very slow. It is also a criterion for the optimal choice of the value t_d. For all solved problems the filters were never longer than thirty samples and the delay t_d was always about half the filter length. If for instance the solutions for the analog normal equations are known to be symmetric to the time origin, then t_d should be chosen as half the filter length. This is generally done in later chapters. In this way discrete symmetric operators of finite length are obtained. The N realizable time responses obtained with (3.2.5.5) for a positive delay t_d can be shifted into negative time by the same amound t_d. Performing subsequently the stacking filter process with this non realizable stacking filter will approximate the zero delay desired output.

CHAPTER IV

MULTICHANNEL STACKING FILTERS

The concept of multichannel stacking filters is already well established and its superiority over single channel filter operations in certain processing techniques is known. The normal equations (3.2.5.5) are used for the computation of stacking filters in basically three different ways

1. Specifying idealized input and output data to obtain the correlation matrices.
2. Presetting the correlation matrices due to specific mathematical considerations.
3. Straightforward application to real seismic data.

The first two approaches are deterministic, and the third one is a practical approach. The first approach is the simplest and is hardly treated in the literature. It has the disadvantage that computed filters are very sensitive to changes in the input traces from the chosen model.

The third approach is known as multichannel deconvolution. It is a straightforward application in the way that the autocorrelation matrix is computed from a section of actual field data. The desired output is chosen as a spike at zero position. Thus the one-sided cross-correlations between the desired output and each input trace also become spikes at zero position. A multichannel deconvolution filter therefore is entirely specified by the autocorrelation matrix of the traces. This special process which can be regarded as the corresponding process for single channel deconvolution, shows generally little improvement (Davies and Mercado, 1968) over single channel processes.

The second approach is the most popular and is also used in this thesis. The main advantage is that with this design procedure, many filters can be computed which would be impossible to obtain with other techniques. For instance, this approach leads to ghost suppression filters (Schneider, et. al., 1964), suboptimum velocity filters (Foster, Sengbush, Watson, 1964), optimum multichannel velocity filters (Sengbush, Foster, 1968) and optimum horizontal stackfilters (Galbraith and Wiggins, 1968). The design procedure is basically the same in all cases. It starts by specifying an analog stochastic model.

$$x_i(t) = s_i(t) + r_i(t) + n_i(t), \quad (i=1,..,N) \tag{4.1}$$

where each trace $x_i(t)$ consists of a signal $s_i(t)$, correlated noise $r_i(t)$ and uncorrelated noise $n_i(t)$. A varied form of this assumption is (Foster, Sengbush, 1968)

$$x_i(t) = s(t-\tau_i) + r(t-\tilde{\tau}_i) + n_i(t) \ , \quad (i=1,..,N) \tag{4.2}$$

where signals and correlated noise are expected to have the same wave form on each trace. In the case of Common Depth Point (CDP) data (Mayne, 1965) the model may even be assumed to be

$$x_i(t) = s(t) + r(t-\tilde{\tau}_i) + n_i(t), \quad (i=1,..,N) \tag{4.3}$$

The specification of models in analog form is necessary, because the relative arrival times τ_i and $\tilde{\tau}_i$ for the signals and correlated noise do not necessarily fall on sample points. τ_i and $\tilde{\tau}_i$ are assumed as random variables for which probability density functions are chosen which seem to fit various filtering problems best. This ensures that the filters will be applicable to a broad class of input traces with similar statistical properties in their arrival times. With the probability density functions, finally expectation values for the correlation functions of the traces are computed. Apart from uncertainties in the arrivals of signals and correlated noise, many other uncertainties may be incorporated into this design procedure.

The necessary compromise between simplicity of a model and the reality should always be oriented on the actual knowledge about traces. Wrong assumptions about input traces may have a strong negative influence on the filtering process. If much is known about given seismic traces, the statistical changes assumed for the model should be confined to small ranges. The performance of a more specifically designed filter will then be better than one of a very general filter where broader assumptions about the statistics of traces were included. The design of a multichannel stacking filter will therefore ultimately, as in the present case,make use of many design parameters. They make it possible to tailor filters for many individual purposes. These design parameters are not equally important. Their importance is revealed by doing computational experiments with the filters. They often influence filter characteristics in a very logical way and there exists a number of general rules about them. Some of the rules are presented in due course.

The following stochastic model is given in this work

$$x_i(t) = s\,(t-\tau_i) + r\,(t-\tilde{\tau}_i) + n_i(t),(i=1,..,N) \qquad (4.4)$$

Initially it is assumed that signals and correlated noise differ only in move-out from trace to trace. τ_i and $\tilde{\tau}_i$ are specially chosen random variables. As desired output $z(t) = s\,(t-t_d)$ is taken, where $s\,(t)$ is the common signal in the input traces . t_d describes various possible delays of the output signal. The value of t_d, where the expected error (3.2.5.6) is minimum, is known as optimum delay.

Generally it is possible to design a N-input M-output channel filter, where all M desired outputs are s (t). Computational experiments (Galbraith and Wiggins, 1968) showed however, that for optimum delay of the specified output, all M actual output traces give nearly the same results. Because the design of a single channel output filter is computationally more efficient, there seems to be enough justification for only concentrating on the multichannel stacking filter case.

4.1 Design of a general purpose multichannel stacking filter

In the following treatment the design of the general class of stacking filters is presented which is investigated in this thesis. Two- and three-dimensional velocity filters, polarisation filters and multichannel stacking filters for differential normal moveouts are included in the given derivation. A certain value of this work may therefore be found in the fact that all these filters can be treated from a general point of view. Characteristics and rules observed with one special type can usually be generalized for the whole class of filters.

Derivation of the autocorrelation matrix

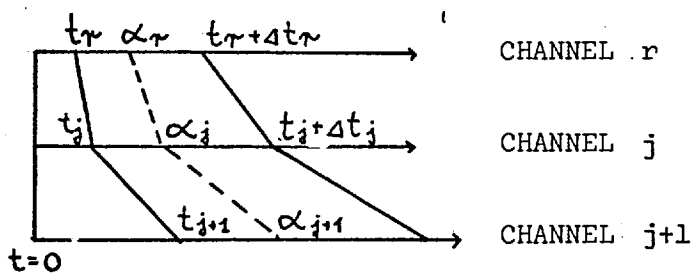

FIGURE 4.1.1 Time window.

N seismic channels are given (figure 4.1.1 shows three of these). It is important to notice that there are no restrictions as to where these channels have been recorded. They need not necessarily have been recorded in sequence along a line with equidistant recording positions. Positions may also be arbitrarily distributed in three-dimensional space. The signal $s_i(t)$ on trace i may arrive at the relative time α_i and the signal $s_j(t)$ on trace j at the relative time α_j. The autocorrelation function of each trace is then $\tilde{\varphi}_{s\,s}(\tau)$ and independent of α_i, while the crosscorrelation between $s_i(t)$ and $s_j(t)$ is given by

$$\varphi_{s_i s_j}(\tau)=\lim_{T\to\infty}\frac{1}{2T}\int_{-T}^{T} s\,(t-\alpha_i)\,s\,(t-\alpha_j-\tau)\,dt \qquad (4.1.1)$$

$$=\tilde{\varphi}_{s\,s}\,(\tau+\alpha_j-\alpha_i) \qquad (4.1.2)$$

and depends on the relative shift $\alpha_j-\alpha_i$.

It is assumed that the relative arrival times α_i and α_j are random variables defined as follows:

$$\alpha_r = t_r + \Delta t_r/2 + \eta + \gamma_r \tag{4.1.3}$$

$$\alpha_j = t_j + \Delta t_j/2 + \eta \Delta t_j/\Delta t_r + \gamma_j \tag{4.1.4}$$

where t_j and Δt_j, (j=1,..,N) describe two limiting curves in figure 4.1.1. η and γ_j are independent random variables, with the following arbitrarily chosen probability density functions

$$p_o(\eta) = \frac{1}{\Delta t_r} \operatorname{rec}(\eta/\Delta t_r) \tag{4.1.5}$$

$$p(\gamma_j) = \frac{1}{t_c} \operatorname{rec}(\gamma_j/t_c), \qquad (j = 1,\ldots,N) \tag{4.1.6}$$

Channel r is an arbitrarily chosen reference trace.

t_c will be referred to as chatter. The meaning of η, γ_j, γ_r becomes clear at once by discussing equations (4.1.3) and (4.1.4) for the special cases where one of the variables η or γ_j equals zero. The random variable η forces the arrival times to fall on non-overlapping curves, which divide Δt_j on each trace in the same ratio, while γ_j permits a certain deviation of these arrivals from the fixed family of curves. Equation (4.1.2) can now be written as

$$\varphi_{s_i s_j}(\tau) = \tilde{\varphi}_{s\,s}(\tau + t_j + \Delta t_j/2 + \eta \Delta t_j/\Delta t_r + \gamma_j - t_i - \Delta t_i/2 - \eta - \gamma_i) \tag{4.1.7}$$

or with the help of the abbreviations

$$\begin{aligned} t_{ij} &= t_j - t_i + (\Delta t_j - \Delta t_i)/2 \\ \tau_{ij} &= \Delta t_j - \Delta t_i \\ \hat{\eta} &= \eta(\Delta t_j/\Delta t_r - 1) \end{aligned} \tag{4.1.8}$$

as

$$\varphi_{s_i s_j}(\tau) = \tilde{\varphi}_{s\,s}\,(\tau + t_{ij} + \hat{\eta} + \gamma_j - \gamma_i) \qquad (4.1.9)$$

This becomes in the frequency domain the crosspower spectrum

$$\Phi_{s_i s_j}(f) = \tilde{\Phi}_{s\,s}(f) e^{2\pi i t_{ij} f} e^{2\pi i \hat{\eta} f} e^{2\pi i \gamma_j f} e^{-2\pi i \gamma_i f}$$

The expectation of this is

$$E\left\{\Phi_{s_i s_j}(f)\right\} = \int_{-\infty}^{+\infty}\int_{-\infty}^{+\infty}\int_{-\infty}^{+\infty} p_1(\hat{\eta}) p(\gamma_1) p(\gamma_2)\, \tilde{\Phi}_{s\,s}(f)\, d\hat{\eta}\, d\gamma_1\, d\gamma_2 \qquad (4.1.10)$$

where the probability density $p_1(\hat{\eta})$ is related to $p_0(\eta)$ by

$$p_1(\hat{\eta}) = \frac{1}{\left|\Delta t_j/\Delta t_r - 1\right|}\; p_0\left(\frac{\hat{\eta}}{\left|\Delta t_j/\Delta t_r - 1\right|}\right)$$

Due to the symmetry of all probability density functions and the statistical independence of the random variables, equation (4.1.10) can be written as a product including three Fourier integrals

$$E\left\{\Phi_{ij}(f)\right\} = E\left\{\Phi_{s_i s_j}(f)\right\} = \tilde{\Phi}_{s\,s}(f) e^{2\pi i f t_{ij}} I_1(f) \cdot I_2(f) \cdot I_3(f) \qquad (4.1.11)$$

where
$$I_1(f) = \int_{-\infty}^{+\infty} p_1(\hat{\eta}) e^{2\pi i \eta f} d\eta = \operatorname{sinc}(\tau_{ij} f)$$

$$I_2(f) = \int_{-\infty}^{+\infty} p(\gamma_1) e^{2\pi i \gamma_1 f} d\gamma_1 = \operatorname{sinc}(t_c f)$$

$$I_3(f) = I_2(f)$$

so that

$$E\left\{\Phi_{ij}(f)\right\} = \operatorname{sinc}^2(t_c f) \operatorname{sinc}(\tau_{ij} f) e^{2\pi i t_{ij} f} \tilde{\Phi}_{s\,s}(f) \qquad (4.1.12)$$

This becomes in the time domain the following convolution integral

$$E\left\{\varphi_{ij}(\tau)\right\} = \frac{1}{|\tau_{ij}|} \operatorname{rec}\left(\frac{\tau + t_{ij}}{|\tau_{ij}|}\right) * \frac{1}{t_c} \operatorname{rec}\left(\frac{\tau}{t_c}\right) * \frac{1}{t_c} \operatorname{rec}\left(\frac{\tau}{t_c}\right) * \tilde{\varphi}_{s\,s}(\tau) \qquad (4.1.13)$$

For the special assumption that $s_i(t)$ and $s_j(t)$ are broad band signals

$$\tilde{\varphi}_{s\,s}(\tau) = \mathrm{sinc}(\tau) \quad \text{or} \quad \Phi_{ss}(f)=\mathrm{rec}(f)$$

the expectation of the crosspower spectrum becomes

$$E\left\{\Phi_{ij}(f)\right\} = \mathrm{rec}(f)\,\mathrm{sinc}^2(t_c f)\mathrm{sinc}(\tau_{ij} f)\, e^{2\pi i f t_{ij}} \qquad (4.1.14)$$

The time domain presentation can be written as

$$E\left\{\varphi_{ij}(\tau)\right\} = \int_{-\frac{1}{2}}^{+\frac{1}{2}} \mathrm{sinc}^2(t_c f)\mathrm{sinc}(\tau_{ij} f)\cos 2\pi f(\tau + t_{ij})\,df \qquad (4.1.15)$$

This integral can be further simplified as shown in appendix 1 and easily computed on a digital computer. The autocorrelation functions under the special broad band condition turn out to be

$$E\left\{\varphi_{ii}(\tau)\right\} = \mathrm{sinc}(\tau) \qquad (4.1.16)$$

Derivation of the crosscorrelation matrix

The crosscorrelation between the desired output signal $s_0(t) = s\,(t-t_d)$ and the input signal on trace j can be written as

$$\varphi_{s_0 s_j}(\tau) = \lim_{T\to\infty} \frac{1}{2T} \int_{-T}^{+T} s\,(t-t_d)\,s\,(t-\alpha_j-\tau)\,dt \qquad (4.1.17)$$

where α_j is given in (4.1.4), so that

$$\varphi_{s_0 s_j}(\tau) = \tilde{\varphi}_{s\,s_j}(\tau + t_j + \Delta t_j/2 + \eta \Delta t_j/\Delta t_r + \gamma_j - t_d) \qquad (4.1.18)$$

Using the following abbreviations

$$\tau_j = t_j + \Delta t_j/2 - t_d$$

$$\hat{\eta} = \frac{\Delta t_j}{\Delta t_r}\eta\,; \qquad p_2(\hat{\eta}) = \left|\frac{\Delta t_r}{\Delta t_j}\right| p_0\left(\frac{\eta}{\frac{\Delta t_j}{\Delta t_r}}\right)$$

one gets for the expectation of this expression

$$E\left\{\varphi_{s_0 s_j}(\tau)\right\} = \frac{1}{t_c}\,\mathrm{rec}\left(\frac{\tau}{t_c}\right) * \frac{1}{|\Delta t_j|}\,\mathrm{rec}\left(\frac{\tau + t_j + \Delta t_j/2 - t_d}{|\Delta t_j|}\right) * \tilde{\varphi}_{s\,s}(\tau) \qquad (4.1.19)$$

This has for the assumption that $s_0(t)$ and $s_j(t)$ is broad band the Fourier transform

$$E\left\{\Phi_{s_0 s_j}(f)\right\} = E\left\{\Phi_j(f)\right\} = \mathrm{rec}(f)\,\mathrm{sinc}\,(t_c f)\,\mathrm{sinc}\,(\Delta t_j f) e^{2\pi i f \tau_j} \qquad (4.1.20)$$

By making use of the inverse Fourier transform the time domain presentation can also be written as

$$E\left\{\varphi_j(\tau)\right\} = \int_{-\frac{1}{2}}^{+\frac{1}{2}} \mathrm{sinc}(t_c f)\,\mathrm{sinc}\,(\Delta t_j f)\cos 2\pi f(\tau + \tau_j)\,df \qquad (4.1.21)$$

This integral can be further simplified and easily programmed on a digital computer as shown in appendix 1.

From a mathematical point of view, correlated noise is expressed in the same way as signals. The expectation of the autocorrelation matrix for the correlated noise is therefore computed exactly in the same way as the autocorrelation matrix for the signals, only for a different moveout window. If more signal- and correlated noise families are known to be present in the input traces which are uncorrelated to each other and fall into different moveout windows, then the total autocorrelation matrix of the traces is the sum of the autocorrelation matrices of the above specified kind.

With the formulae (4.1.15), (4.1.16) and (4.1.21) one now has the possibility of computing discrete filters. If uncorrelated noise is in the input traces, it is clear that the autocorrelation functions of this noise must be added to the diagonal of the autocorrelation matrix. Deterministic multichannel stacking filters can be made less sensitive to gain variations of the input traces. The technique (Baldwin, 1964) may be described as follows. It is assumed that the gain on each channel is a random variable,

independent from the gain on any other channel. The gain value is assumed to be uniformly distributed between $1-\alpha$ and $1+\alpha$. This means the probability density function for the gain is $p_3(g) = \frac{1}{2\alpha} \mathrm{rec}\left(\frac{g-1}{2\alpha}\right)$. If the input traces are given by $\bar{x}_i = g_i x_i$, where g_i is the variable gain, the autocorrelation is $\varphi_{\bar{x}_i \bar{x}_i} = g_i^2 \varphi_{x_i x_i}$. The expectation of this is

$$E\{\varphi_{\bar{x}_i \bar{x}_i}\} = \int_{-\infty}^{+\infty} p_3(g_i) g_i^2 \varphi_{x_i x_i} dg_i = \frac{1}{2\alpha} \varphi_{x_i x_i} \int_{1-\alpha}^{1+\alpha} g_i^2 dg_i = \left(1 + \frac{\alpha^2}{3}\right) \varphi_{x_i x_i}(\tau)$$

The crosscorrelation is $\varphi_{\bar{x}_i \bar{x}_j} = g_i g_j \varphi_{x_i x_j}$ whose expectation is because of the assumed statistical independence for the gains

$$E\{\varphi_{\bar{x}_i \bar{x}_j}\} = \varphi_{x_i x_j}(\tau) \left[\int_{-\infty}^{+\infty} g_i p_3(g_i) dg_i\right]^2 = \varphi_{x_i x_j}(\tau)$$

The technique therefore, is to leave the crosscorrelations unchanged and multiply the autocorrelations by the factor $(1 + \alpha^2/3)$. In the particular case where signals are broad band and $\varphi_{x_i x_i} = \mathrm{sinc}(\tau)$, this corresponds to adding a constant amount of white noise to each trace. This addition of white noise is also important for another reason. The autocorrelation matrix usually tends to be singular, thus leading to unstable filters. This effect is often remedied by adding a spike at zero position to the autocorrelations (Galbraith, Wiggins, 1968).

The broad band assumption for all signals is a restriction which is mainly made for the sake of simplicity. This assumption is known (Schneider, Prince and Giles, 1965) to give already good results, thus showing that the phase relations between signals (or organized noise) are more important in multichannel filter design than their amplitudes. This restriction may be made less severe by making one of the following three assumptions:

1. The autocorrelations $\varphi_{ss}(\tau)$, $\varphi_{rr}(\tau)$ and $\varphi_{n_i n_j}(\tau) = \varphi_{nn}(\tau)\,\delta_{ij}$ are known (or at least an estimate of them is available).
2. The autocorrelation functions of all input components are the same.
3. Signals and noise change in band width from trace to trace.

If in the first case all three autocorrelations are known, they can be incorporated in the design by convolving them with equations (4.1.15), (4.1.16) and (4.1.21). The problem of estimating these functions from traces is discussed in Chapter IX. The second assumption leads to the same results as the broad band assumption, because the input traces could be deconvolved, thus becoming broad band as well. An approach to take care of the third assumption is given in appendix 11.

One may argue that neither signal nor noise on actual seismograms will show much change in band width from trace to trace and that therefore further statistical averaging in this respect is unnecessary. In Chapter VIII enough reason is given to show why the broad band assumption is the most economical one for the design. Nevertheless, the computations in appendix 11 are of general value. They show that, by taking variable band width from trace to trace into account, the above specified power and crosspower spectra have to be further multiplied with certain tapering functions in the frequency domain. Favouring this special feature has therefore to be paid for with some kind of high frequency loss in the correlation functions. This loss is transferred into the high frequency content of the obtained stacking filters. Later it is shown that allowance for chatter as well as high amounts of uncorrelated noise also suppress the high frequency content of filters. Favouring one uncertainty in the design will therefore benefit the other two as well. Because it is not possible to

design a filter which exactly fits the properties of the input traces, it is a consolation to know that the filter shows a certain stability towards changes of design criteria.

4.2 Multichannel normal equations and symmetries of solutions

With the above specified power- and crosspower spectra it is now possible to compute the responses of various kinds of stacking filters. For the rest of this work, it is assumed for the design that the signals are broad band and the correlation functions are given as

$$E\left\{\Phi_{ii}(f)\right\} = \mathrm{rec}(f) \tag{4.2.1}$$

$$E\left\{\Phi_{ij}(f)\right\} = \mathrm{rec}(f)\,\mathrm{sinc}^2(t_c f)\,\mathrm{sinc}(\tau_{ij} f)\,e^{2\pi i t_{ij} f} \quad (i \neq j) \tag{4.2.2}$$

$$E\left\{\Phi_{j}(f)\right\} = \mathrm{rec}(f)\,\mathrm{sinc}(t_c f)\,\mathrm{sinc}(\Delta t_j f)\,e^{2\pi i \tau_j f} \tag{4.2.3}$$

Let t_j^k and Δt_j^k $(j=1,N;\ k=1,L)$ be the parameters for L regions designed for signals, while $\bar{t}_j^k$ and $\Delta \bar{t}_j^k$ $(j=1,N;\ k=1,K)$ are the corresponding parameters for K regions designed for correlated noise. With the parameters ϱ and ν as introduced in 3.2.5 the continuous normal equations in the frequency domain for the most general case of the stacking filter become

$$\sum_{i=1}^{N} A_i(f)\, R_{ij}(f) = G_j(f), \quad (j=1,\ldots,N) \tag{4.2.4}$$

where

$$R_{ij}(f) = \mathrm{rec}(f)\,\mathrm{sinc}^2(t_c f)\left[\sum_{k=1}^{L} \mathrm{sinc}(\tau_{ij}^k f)\,e^{2\pi i f t_{ij}^k} + \varrho \sum_{k=1}^{K} \mathrm{sinc}(\bar{\tau}_{ij}^k f)\,e^{2\pi i f \bar{t}_{ij}^k}\right] + \nu\,\mathrm{rec}(f)\cdot\delta_{ij} \tag{4.2.5}$$

$$G_j(f) = \mathrm{rec}(f)\,\mathrm{sinc}(t_c f)\left[\sum_{k=1}^{L} \mathrm{sinc}(\Delta t_j^k f)\,e^{2\pi i f \tau_j^k}\right] \tag{4.2.6}$$

and

$$t_{ij}^k = t_j^k - t_i^k + \frac{\Delta t_j^k - \Delta t_i^k}{2} \tag{4.2.7}$$

$$\tau_{ij}^k = \Delta t_j^k - \Delta t_i^k\,; \qquad \tau_j^k = t_j^k + \Delta t_j^k/2 \tag{4.2.8}$$

Without solving the system (4.2.4) one may already draw a number of important conclusions concerning the solutions $A_i(f)$ or $a_i(t)$:

1. If $R_{ij}(f) = R_{ij}(-f)$ and $G_j(f) = G_j(-f)$, then all time responses $a_i(t),(i=1,N)$ are symmetric about the origin $t = 0$, thus each component has a zero phase response. This can be immediately verified by replacing $A_i(f)$ with $A_i(-f)$ in (4.2.4) and observing that the expressions for $A_i(f)$ must be the same as for $A_i(-f)$. One may easily verify, that, for instance, a time window satisfying the conditions $t_j = -\Delta t_j/2$ belongs to this case. Special windows of this case are given in figure 4.2.1 and figure 4.2.2. Stacking filters of this type are referred to as trace-symmetric.

2. If $R_{ij}(f),(i,j=1,.....,N)$ is a Toeplitz-matrix (symmetric to the main diagonal and with the same elements along each diagonal) and the following equalities hold $G_i(f) = G_{N+1-i}(f),(i=1,..,N)$

then $A_i(f) = A_{N+1-i}(f),(i=1,..,N)$

or $a_i(t) = a_{N+1-i}(t),(i=1,..,N)$

The proof is easily found by first reflecting the equations with respect to the centre equation (or a fictitious horizontal centre line, if the number of equations is even)and then reflecting the columns of the coherency matrix with respect to the centre column. Time windows fulfilling these conditions are symmetric to the centre trace and the time origin. Two examples of such cases are given in figure 4.2.3 and figure 4.2.4. A more special case is the window of figure 5.1.1.1. Note that condition 1 is automatically fulfilled as well. Filters of this type will be referred to as symmetric filters.

3. If the coherency matrix has the same elements along each diagonal and is in addition hermitian and $G_i(f) = G^*_{N+1-i}(f),(i=1,..,N)$ then the solutions will always fulfil

$$A_i(f)=A^*_{N+1-i}(f); \qquad a_i(t)=a_{N+1-i}(-t),(i=1,..,N)$$

The proof is given for a three channel system, which can generally be

extended to any number of channels.

Let the system be given by

$$\begin{aligned} A_1R_1 + A_2R_2 + A_3R_3 &= G_1 \\ A_1R_2^* + A_2R_1 + A_3R_2 &= G_2 \\ A_1R_3^* + A_2R_2^* + A_3R_1 &= G_1^* \end{aligned} \tag{4.2.9}$$

Substituting A_3^* for A_1, A_2^* for A_2 and A_1^* for A_3 gives

$$\begin{aligned} A_3^*R_1 + A_2^*R_2 + A_1^*R_3 &= G_1 \\ A_3^*R_2^* + A_2^*R_1 + A_1^*R_2 &= G_2 \\ A_3^*R_3^* + A_2^*R_2^* + A_1^*R_1 &= G_1^* \end{aligned} \tag{4.2.10}$$

By interchanging the third row with the first and the third column with first, one obtains

$$\begin{aligned} A_1^*R_1 + A_2^*R_2 + A_3^*R_3^* &= G_1^* \\ A_1^*R_2 + A_2^*R_1 + A_3^*R_2^* &= G_2 \\ A_1^*R_3 + A_2^*R_2 + A_3^*R_1 &= G_1 \end{aligned} \tag{4.2.11}$$

By taking the complex conjugate of each row, again equations (4.2.9) are obtained. Condition 3 is fulfilled by (4.2.4) whenever the time window is centrosymmetric to the centre point. These filters are called centrosymmetric filters. A typical time window for this case is given in figure 4.2.5 or figure 4.2.6.

The various symmetries of the time responses as investigated in this section become of great importance in Chapter Vl, where phase properties of stacking filters are discussed. Two other important relations between time windows and responses of stacking filter components can be expressed as follows:

4. If a given time window has the same t_i and Δt_i on two different traces, then the obtained responses for these traces are the same. In figure 4.2.1 for instance, the responses for trace 3 and trace 5 are the same.

5. If two time windows can be obtained from each other by rearranging the traces, then the responses computed for traces with the same t_i and Δt_i are the same.

The proof for both statements is obtained in a similar way as described above by rearranging the normal equations.

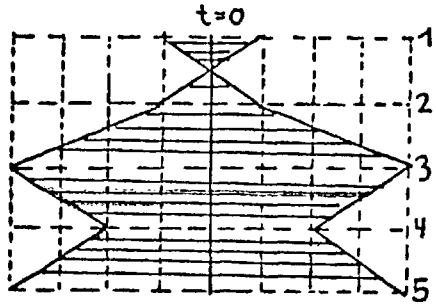

FIGURE 4.2.1 Trace-symmetric time window.

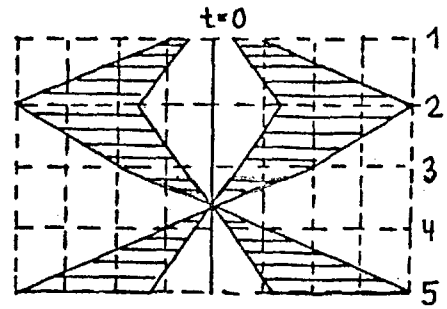

FIGURE 4.2.2 Trace symmetric window.

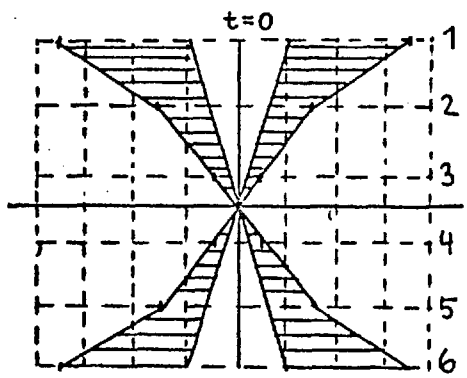

FIGURE 4.2.3 Symmetric time window.

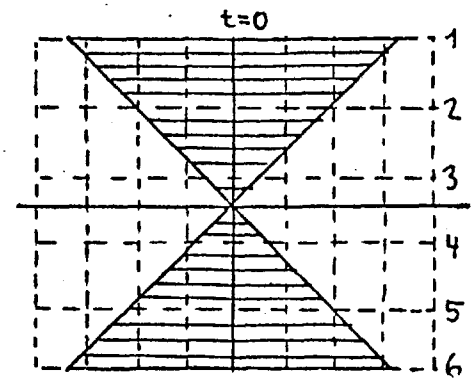

FIGURE 4.2.4 Symmetric time window.

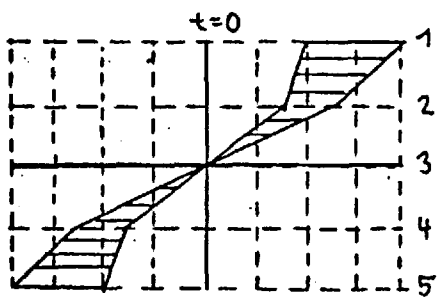

FIGURE 4.2.5 Centro-symmetric window.

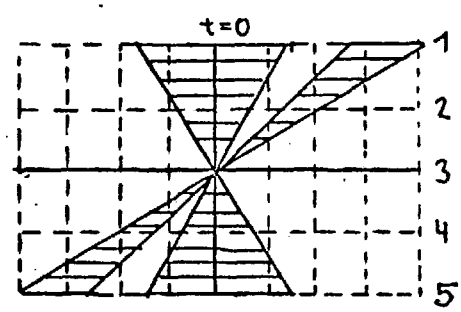

FIGURE 4.2.6 Centrosymmetric window.

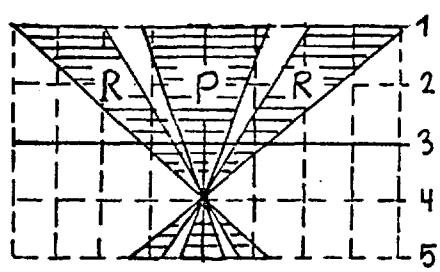

FIGURE 4.2.7

Trace-symmetric window for a optimum multichannel velocity filter.
If R is a reject region then P is a pass region (or vice versa).

CHAPTER V

DISCUSSION OF SPECIAL STACKING FILTERS

The full generality of the normal equations (4.2.4) becomes more clear in this chapter where their application to individual practical cases is treated. It is shown how time window configurations have to be selected for various filtering problems. The choice of a time window for each problem is not unique. Special windows, however, should be selected to obtain filters with simple phase relations. The normal equations (4.2.4) incorporate those presented by Schneider, Prince and Giles (1965).

In section 5.1 it is shown how the normal equations (4.2.4) are used to obtain velocity filters. The equations for optimum multichannel velocity filters (Foster and Sengbush, 1968) are derived. These filters may be regarded as a special case of more generally designed two-dimensional multichannel velocity filters. Equations (4.2.4) are also used in connection with three-dimensional velocity filtering problems. Finally in section 5.2 the application of (4.2.4) for the rejection or enhancement of signals possessing differential normal moveout is discussed.

5.1 Multichannel velocity filters

The concept of filtering seismic signals, based on constant trace to trace moveout, was developed both for nuclear surveillance and for exploration seismology. The filters used for this purpose are known as velocity filters and have already a long history in seismic data processing. A variety of such filters has been discussed, including the 'Fanfilters' of Fail and Grau (1963), the 'Pie-Slice Filters' of Embree et. al. (1963), and 'Doublet' filters of Foster et. al. (1964). A more general and flexible theory of velocity filters based upon a stochastic model of the data generating process and designed in the form of a multichannel Wiener filter was presented by Sengbush and Foster (1968). These filters may be more

adapted to special problems by incorporating more information from the input traces. Comparison of multichannel velocity filters with pie-slice and doublet filters (Sengbush and Foster,1968) has shown the superiority of the former, especially when the velocity pass and reject band is narrow. As long as signals falling into any region of figure 4.2.7 have to be passed or rejected, optimum multichannel velocity filters are flexible enough to solve the problem. There exist, however, a host of problems, where differently designed two-dimensional multichannel velocity filters have better characteristics than optimum multichannel velocity filters. The three-dimensional velocity filters presented in 5.1.3 can be regarded as a logical extension of two-dimensional multichannel velocity filters.

A full insight into properties of computed filters cannot be obtained before Chapter V11 where the two- and three-dimensional Fourier-transforms are applied for the characterisation of filters. Many characteristics of two-dimensional velocity filters are observed in a similar form in the three-dimensional case. Because two-dimensional multichannel velocity filters are superior to other velocity filters, one can expect that, due to the similar design, the same applies to the given three-dimensional multichannel velocity filters.

5.1.1 Optimum multichannel velocity filters

Optimum multichannel velocity filters which are presented and excellently discussed by Sengbush and Foster (1968), can be obtained from (4.2.4). Because their approach for the filter computation was differently chosen, it is shown below how to derive a pass-reject optimum multichannel velocity filter from the given normal equations. For reasons of better comparison, the same parameters are used as by Sengbush and Foster.

t_i and $t_i+\Delta t_i$ in (4.2.4) are forced to fall along straight lines of the time window given in figure 5.1.1.1. The chatter t_c is chosen as zero. Region 1 and 3 are specified as reject regions and region 2 as a pass

region. In this way, the normal equations (4.2.4) give a pass-reject optimum multichannel velocity filter designed without chatter. If alternatively 1 and 3 are pass regions and 2 a reject region, one obtains the normal equations for a reject-pass optimum multichannel velocity filter. Whenever it is referred to optimum multichannel velocity filters in this work, one of these two versions of symmetric filters designed for three regions is meant.

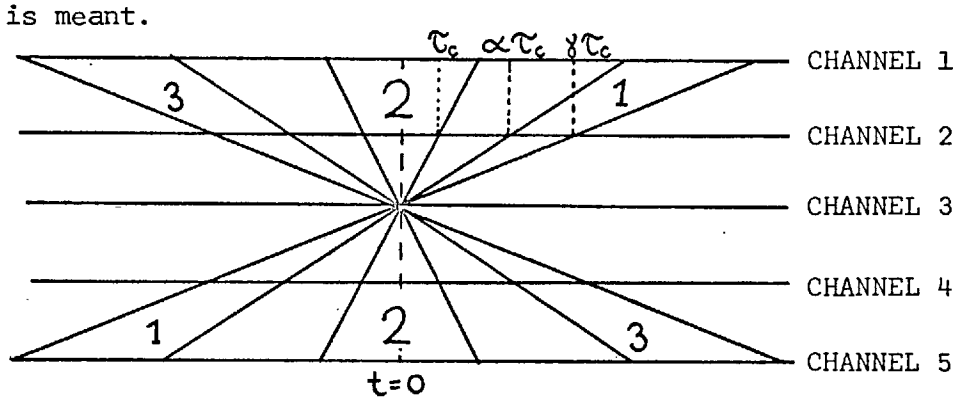

FIGURE 5.1.1.1 Symmetric time window for the centre trace estimate of a optimum multichannel velocity filter.

To have this treatment as general as possible, any number N of input channels is allowed. (Figure 5.1.1.1 presents only a five channel case). $z=(N+1)/2$ is the centre trace number. In case N is even a fictitious reference trace is introduced as centre trace.

Consider reject region 1 of figure 5.1.1.1. The coherency matrix for the broad band case, with no chatter ($t_c = 0$) for this region is fully described by

$$R^1_{ii}(f) = \mathrm{rec}(f) \tag{5.1.1.1}$$

$$R^1_{ij}(f) = \mathrm{rec}(f)\,\mathrm{sinc}(\tau_{ij}f)\,e^{2\pi i f t_{ij}} \quad (i \neq j) \tag{5.1.1.2}$$

The values $t_i, \Delta t_i, \tau_{ij}$ and t_{ij} become, with the help of figure 5.1.1.1

$$t_i = (z-i)\alpha\tau_c \tag{5.1.1.3}$$

$$\Delta t_i = (z-i)\tau_c(\gamma-\alpha) \tag{5.1.1.4}$$

$$\tau_{ij} = (i-j)\tau_c(\gamma-\alpha) \tag{5.1.1.5}$$

$$t_{ij} = \frac{1}{2}(i-j)\tau_c(\gamma+\alpha) \tag{5.1.1.6}$$

Put into equation (5.1.1.2) gives

$$R_{ij}^{1}(f) = \text{rec}(f)\,\text{sinc}(\tau_c f(\gamma-\alpha)(i-j))e^{i\pi f(i-j)\tau_c(\alpha+\gamma)} \tag{5.1.1.7}$$

For reject region 3, one obtains by replacing τ_c with $-\tau_c$ in (5.1.1.7)

$$R_{ij}^{3}(f) = \text{rec}(f)\,\text{sinc}(\tau_c f(\gamma-\alpha)(i-j))e^{-i\pi f(i-j)\tau_c(\alpha+\gamma)} \tag{5.1.1.8}$$

By assuming that the correlated noise, which falls into region 1 and 3 are uncorrelated with each other, the coherency matrix of the total correlated noise becomes $R_{ij}^{r}(f) = R_{ij}^{1}(f) + R_{ij}^{3}(f)$, which is

$$R_{ij}^{r}(f) = -\text{rec}(f)\frac{1}{\gamma-\alpha}\,\frac{\sin 2\pi f\alpha\tau_c(i-j) - \sin 2\pi f\tau_c\gamma(i-j)}{\tau_c(i-j)f} \tag{5.1.1.9}$$

The coherency matrix for the pass region 2 is obtained from (5.1.1.9) by putting $\alpha = 0$ and $\gamma = 1$

$$R_{ij}^{s}(f) = \text{rec}(f)\frac{\sin 2\pi f\tau_c(i-j)}{\tau_c(i-j)f} \tag{5.1.1.10}$$

Correspondingly one gets with formula (4.1.20) and $t_c = 0$ and $t_d = 0$

$$G_j(f) = \frac{\sin 2\pi f\tau_c(j-z)}{\pi(z-j)\tau_c f}\ \text{rec}(f) \tag{5.1.1.11}$$

The normal equations for this special problem may therefore be written as

$$\sum_{i=1}^{N} A_i(f)\left[R_{ij}^{s}(f) + \rho R_{ij}^{r}(f) + \nu\delta_{ij}\text{rec}(f)\right] = G_j(f),\quad (j=1,..,N) \tag{5.1.1.12}$$

where $A_i(f)$, $(i=1,..N)$ are the Fourier transforms of the desired filters. Equations (5.1.1.12) correspond to equations (A-15)(p. 34, Sengbush,

and Foster, 1968) for the case, where signal and noise are broad band.

Taking the limit $\gamma \to \infty$ in (5.1.1.9) for a finite α shows that $R_{ij}^{r}(f)$ becomes zero. In this case (5.1.1.12) reduces to

$$\sum_{i=1}^{N} A_i(f)\left[R_{ij}^{s}(f)+\nu\delta_{ij}\,rec(f)\right] = G_j(f)\ ,\ (j=1,..,N) \qquad (5.1.1.13)$$

Designing a pass filter is therefore the same as specifying a pass-reject filter, where the reject region is given as the total region outside the pass region. In a similar way to the above derivation, one obtains for a reject-pass optimum multichannel velocity filter

$$\sum_{i=1}^{N} A_i(f)\left[R_{ij}^{s}(f)+\rho R_{ij}^{r}(f)+\nu\delta_{ij}\,rec(f)\right] = G_j^{s}(f),\ (j=1,..N)$$

with (5.1.1.14)

$$G_j^{s}(f) = rec(f)\frac{1}{\gamma-\alpha}\ \frac{\sin 2\pi f\gamma\tau_c(j-z)-\sin 2\pi f\alpha\tau_c(j-z)}{\tau_c(j-z)f}$$

The high symmetry of the time window leads to highly symmetric filters which fulfil all conditions 1 to 3 of section 4.2.

With the more general equations (4.2.4) in mind, one can however, immediately draw the following two conclusions concerning optimum multichannel velocity filters.

1. The version which will allow additional chatter in the arrival times of the signals, is easily obtained by multiplying the left side of equations (5.1.1.12), (5.1.1.13) or (5.1.1.14) with term $\mathrm{sinc}(t_c f)$. The necessity of this term seems logical since expecting the signals to have constant moveout seems to be a restriction, which most certainly does more harm than good on actual traces.

2. In the derivation of the normal equations for optimum multichannel velocity filters, it was shown that they actually include three design regions. However, for many seismic problems only two regions are necessary. In section 7.2 it will be shown that characteristics of velocity filters are generally superior for the case when two regions are sufficient for the design.

5.1.2 General two-dimensional multichannel velocity filters

In the design of a stacking filter which passes signals having constant moveout $-\tau_c < \tau < \tau_c$ and rejects signals falling into the region $\alpha\tau_c < \tau < \gamma\tau_c$ one could make use of an optimum multichannel velocity filter which also includes the reject region $-\gamma\tau_c < \tau < -\alpha\tau_c$. In this case however, it is logical to compute a filter for two regions only. The choice of a time window for a multichannel velocity filter is not unique as shown below. Figure 5.1.2.1 shows four cases for a given problem out of an infinite number of possibilities. All windows are chosen in such a way that they appear to operate in the same manner for the given moveout range. The centre point of the time window does not necessarily have to fall upon a trace. It may be on any point along the vertical line VL. For each of these windows different stacking filters are obtained although they all will perform in a very similar way. Sufficient justification is given in Chapter VI for why the centre trace estimate should be selected.

Figure 5.1.2.1 d shows this so-called centre trace estimate. This is also the case where the overall width of the time windows is shortest if positive and negative moveout signals fall into the window. Galbraith and Wiggins (1968) showed that for the numerical solution of normal equations the filter length should always cover the total width of the time window. This ensures that the expected error (3.2.5.6) does not decrease any more essentially by increasing the filter length. The centre trace estimate therefore leads to the shortest filter operator and the shortest computation time. The normal equations for the centre trace estimate fulfil condition 3 of section 4.2, thus leading to centrosymmetric filters. This case also possesses simple phase characteristics as is shown in Chapter VI. The normal equations for a pass-reject filter with the time window of figure 5.1.2.1 d are

$$\sum_{i=1}^{N} A_i(f)\left[\mathrm{rec}(f)\frac{\sin 2\pi f\tau_c(i-j)}{\pi(i-j)\tau_c f} + \varrho R_{ij}^{1}(f) + \gamma\delta_{ij}\mathrm{rec}(f)\right] = G_j(f),(j=1,..,N)$$

where $R_{ij}^{1}(f)$ is given in (5.1.1.7) and $G_j(f)$ in (5.1.1.11). The computed filter could also be used in cases where the reject region falls to the right of figure 5.1.2.1 d. One would then only have to reverse the order of the input traces.

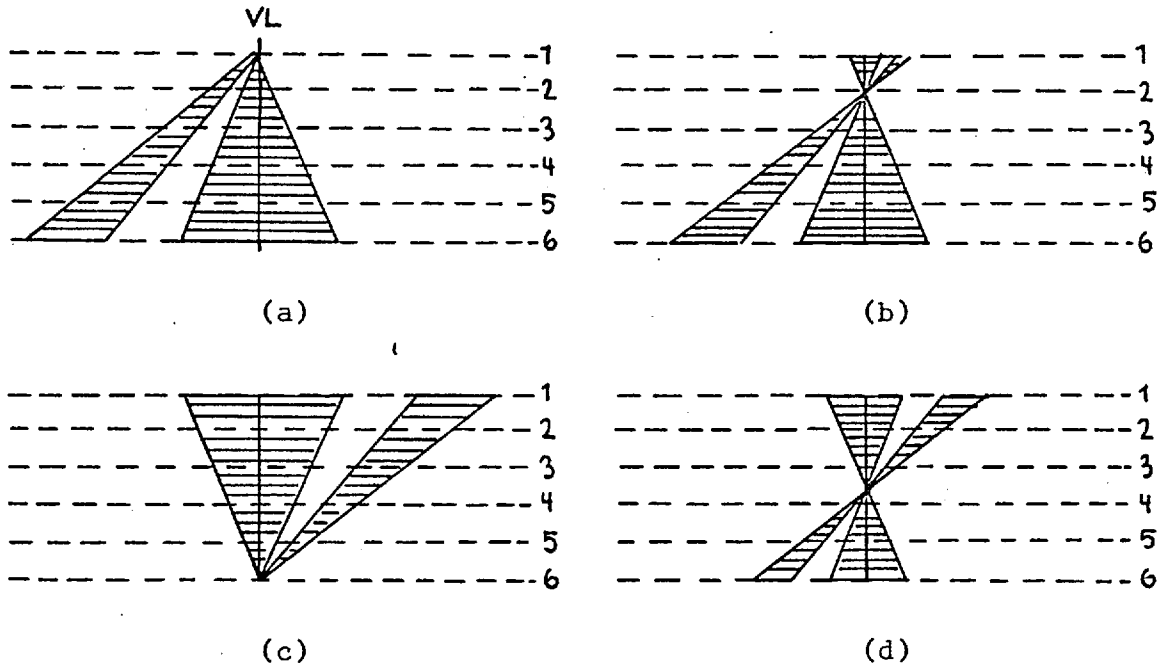

FIGURE 5.1.2.1 Time windows for velocity filters.

Multichannel velocity filters presented so far are only special cases of more general velocity filters, where any number of reject and pass regions for constant moveouts may be given. It is easy to specify in such a case the necessary normal equations with (4.2.4). To keep phase relations simple, one should however, in any case of a more complex time window, try to choose the centre trace estimate.

One may by no means expect that choosing certain pass and reject regions guarantees complete rejection or enhancement of signals in these regions. In Chapter VI the two-dimensional Fourier transform is applied for the characterisation of velocity filters. This shows in which way time windows approximately influence their transfer characteristics. It will also be shown that filters for a small number of narrow regions possess better characteristics than filters for a large number of broad regions.

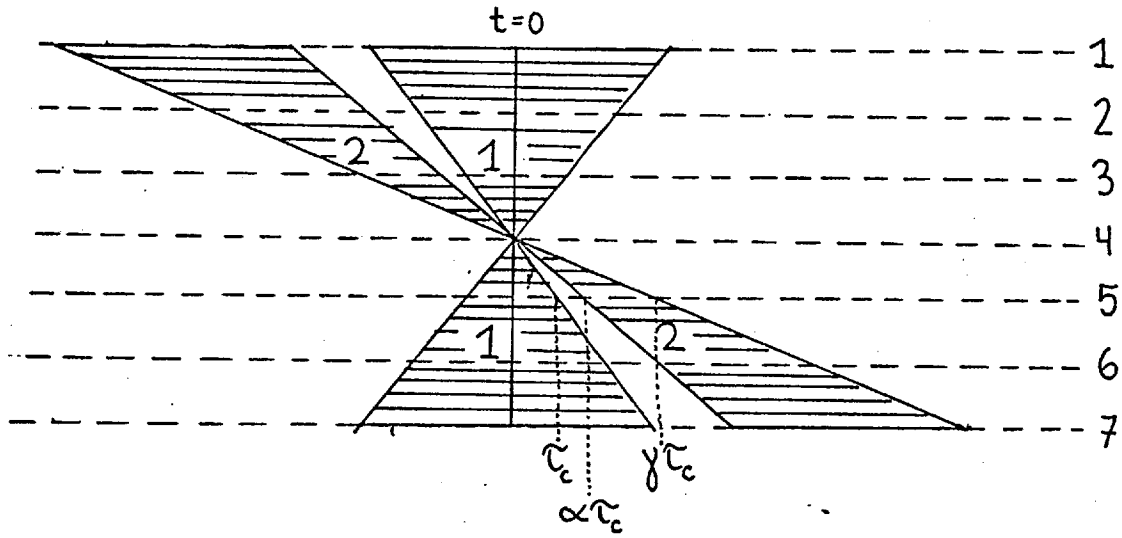

FIGURE 5.1.2.2 Centrosymmetric time window.

This window is obtained by inverting the order of the traces in figure 5.1.2.1 d. If region 1 is a pass region, then region 2 is a reject region (or vice versa). Note, whenever it is referred to a time window only the window shape (defined by τ_c, α, γ and the position of the centre trace) and not the actual number of traces involved is meant.

5.1.3 Three-dimensional multichannel velocity filters

It has already been emphasized that there are no restrictions to the spatial dimension in which the given class of filters can be applied. The common problem in reflection seismic is predominantly still a two-dimensional one. Application and research of three-dimensional velocity filters is therefore mainly confined to problems in earthquake seismology. Already there exist various approaches for the analysis of three-dimensional filtering and array problems (Carpenter, 1965; Binder, 1967 and Lacoss, et. al., 1969). Of special value as an introduction to three-dimensional filters is the work of Burg (1964). His approach is also based on the multichannel Wiener filter theory, and his assumption that signals and noise are uncorrelated, gives essentially the corresponding equations for (3.1.11). These are not further statistically averaged, as in this work, by making use of properly selected probability density functions in the time domain.

How to obtain special three-dimensional velocity filters with (4.2.4) is shown below. To avoid too much generality, the following treatment is applied to the processing of outputs of a two-dimensional array of seismometers. Figure 5.1.3.1 shows a horizontal plane, where $N_x \times N_y$ geophones may be placed on a rectangular grid. Their displacement in x-direction be one x-unit, in y-direction one y-unit. Two planes are given in the coordinate system which cut a wedge out of the lower semi-infinite space. These planes represent the upper and lower limit of a range in which plane wave arrivals are expected. As a further restriction, it is demanded that the waves are polarized. This means the normal vectors of the plane waves lie in a plane. It also corresponds to forcing the plane waves to divide $\Delta\tau_x$ and $\Delta\tau_y$ in the same ratio. The appropriate time window for figure 5.1.3.1 is given in figure 5.1.3.2. The window which specifies centrosymmetric filters is presented in figure 5.1.3.3. It is obtained by shifting the limits of the time window of figure 5.1.3.2 so that they cut

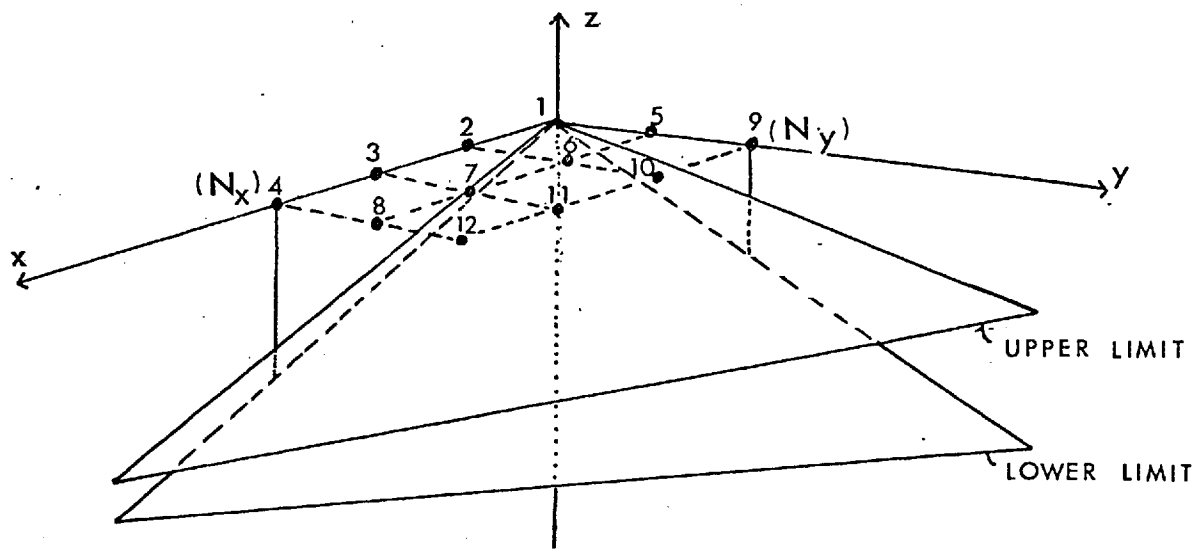

UPPER LIMIT : $z = \tau_x \cdot x - \tau_y \cdot y$

LOWER LIMIT: $z = -(\tau_x + \Delta\tau_x) \cdot x - (\tau_y + \Delta\tau_y)$

FIGURE 5.1.3.1 Two-dimensional recording array

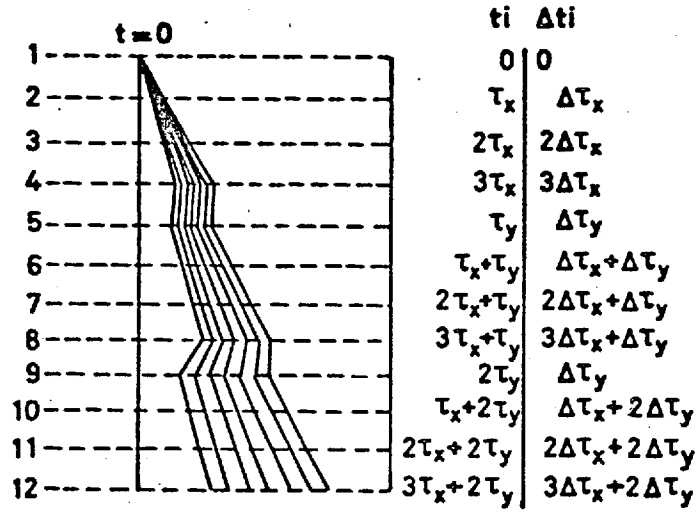

ti	Δti
0	0
τ_x	$\Delta\tau_x$
$2\tau_x$	$2\Delta\tau_x$
$3\tau_x$	$3\Delta\tau_x$
τ_y	$\Delta\tau_y$
$\tau_x+\tau_y$	$\Delta\tau_x+\Delta\tau_y$
$2\tau_x+\tau_y$	$2\Delta\tau_x+\Delta\tau_y$
$3\tau_x+\tau_y$	$3\Delta\tau_x+\Delta\tau_y$
$2\tau_y$	$\Delta\tau_y$
$\tau_x+2\tau_y$	$\Delta\tau_x+2\Delta\tau_y$
$2\tau_x+2\tau_y$	$2\Delta\tau_x+2\Delta\tau_y$
$3\tau_x+2\tau_y$	$3\Delta\tau_x+2\Delta\tau_y$

FIGURE 5.1.3.2 Time Window

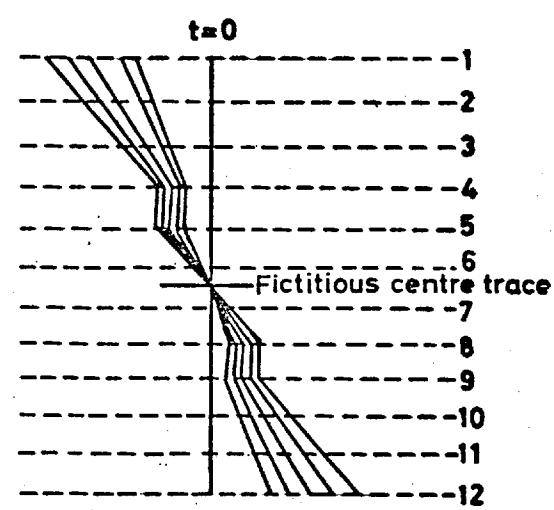

FIGURE 5.1.3.3 Centre trace estimate

each other at the centre trace. The normal equations (4.2.4) can now be used to obtain three-dimensional velocity filters with polarisation filter characteristics.

The probability density functions chosen in section 4.1 for the signals falling into the window of figure 4.1.1 have to be chosen slightly differently in the case of a multichannel velocity filter which does not restrict the normal vectors to lie in a plane. In appendix IV it is shown how multichannel normal equations for this case have to be specified. This certainly very interesting time domain approach for the computation of general three-dimensional velocity filters is however, not any further followed in this thesis. In section 7.3 examples are given for polarisation filters and the three-dimensional Fourier transform is applied for their characterisation.

5.2 Multichannel stacking filters for differential normal moveouts

The assumption that seismic signals arrive as plane waves, thus having constant moveout on traces recorded at equidistant array positions is certainly more valid in refraction or earthquake seismology than in reflection seismics. Three attempts (D'Hoeraene, 1966; Schneider, Prince and Giles, 1965 and Galbraith and Wiggins, 1968) are known where filters are designed for the rejection and enhancement of signals with differential normal moveout. All authors give design procedures which influenced the approach chosen in this work. However, they only describe a few properties of these filters. In section 7.4 transforms are given for some differential normal moveout filters which characterise them in a similar way as two- or three-dimensional Fourier transforms characterise velocity filters. Figures 5.2.1 and 5.2.2 give two typical examples for two- and three-dimensional problems where the given design is applicable. Each figure shows an equidistant recording array and a curved wave front at a fixed time.

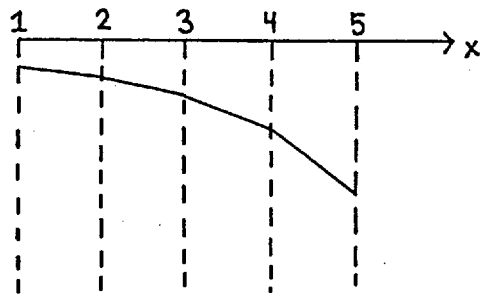

FIGURE 5.2.1 One-dimensional equidistant array and curved wave front.

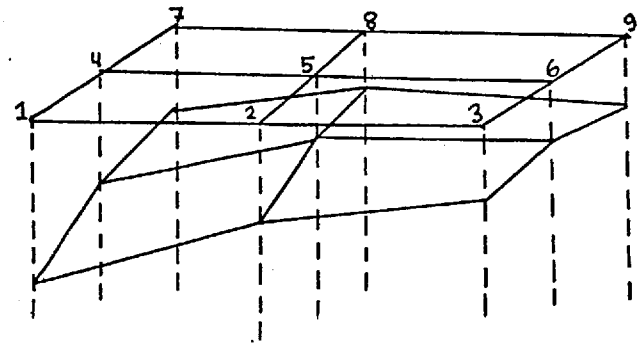

FIGURE 5.2.2 Two-dimensional array and curved wave front.

Detector positions do not necessarily have to be on a straight line or in a plane to specify time windows and to make use of equations (4.2.4.) These general cases are however not discussed in this work.

CHAPTER VI

INTERPRETATION OF THE TWO-DIMENSIONAL FOURIER TRANSFORM OF A TWO-DIMENSIONAL MULTICHANNEL STACKING FILTER

In Chapter III it was shown that two-dimensional convolution of N traces with an N-trace operator can be regarded as a multichannel filter process leading to 2N-1 output traces. The corresponding process in the (f-k) domain is multiplication of the two-dimensional Fourier transforms of both operators. The two-dimensional amplitude spectrum of the filter shows at once which regions in the (f-k) domain of the input traces are passed and which are rejected.

There is however, a big disadvantage connected with this kind of interpretation. This is that the product of the 2-D Fourier transforms of N input traces and an N-trace operator demands 2N-1 output traces in the time domain. Often as in our case, one is interested in only one output trace. For this purpose, the centre trace of the output is selected. By taking this trace out of the 2N-1 output traces, a single trace results, which no longer represents the product of the Fourier transforms of the input and the two-dimensional operator. It is therefore not immediately obvious that the application of the 2-D Fourier transform to a multichannel velocity filter is justified because the process of stacking differs from two-dimensional convolution. In this chapter it is shown how the 2-D Fourier transform of a stacking filter has to be interpreted to describe exactly the N-channel input one channel output relation.

In the case where velocity filters are designed in the frequency domain, the object of applying the 2-D Fourier transform to a computed filter is to show how much the transfer characteristics of the obtained filter approximate the desired ones. In the given case however, where the design is done in the time domain, it is possible to use the two-

dimensional Fourier transform of a filter as a tool of analysis to show how changes of parameters in the time domain influence characteristics in the frequency domain.

6.1 (f-k) - space

A plane wave front impinging on the detector array is given in figure 6.1.1. The velocity with which the wave front travels horizontally is $v = V/\sin\alpha$ where V is the propagation velocity, α the angle between the wave front and the horizontal and v is the apparent velocity. A travelling cosine wave along the x-axis may then be written in the form

$$f(x-vt) = A\cos 2\pi(kx-ft) = A\cos 2\pi k(x-vt)$$

where A is the amplitude, f the frequency and k the apparent wave number. The apparent velocity can be expressed as $v = f/k$. A travelling wave may therefore be described in either the time-distance (t-x) space or the frequency wave number (f-k) space. Hence a plane harmonic wave can be presented by a point in (f-k) space.

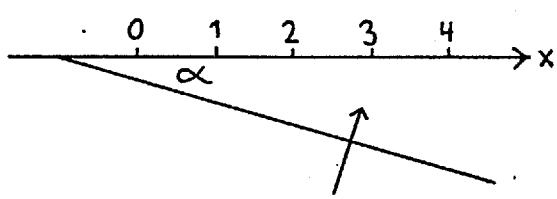

FIGURE 6.1.1 One-dimensional array with an arriving plane wave

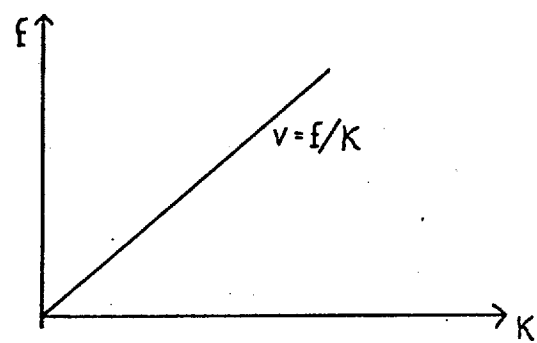

FIGURE 6.1.2 (f-k) domain and a line with constant velocity

An arbitrary function f(t,x) may be generally expressed by a complex function F(f,k) in (f-k) space. Both functions are connected by the two-dimensional Fourier transform pair.

$$F(f,k) = \int_{-\infty}^{+\infty}\int_{-\infty}^{+\infty} f(t,x)e^{-2\pi i(ft-kx)}dxdt \qquad (6.1.1)$$

$$f(t,x) = \int_{-\infty}^{+\infty}\int_{-\infty}^{+\infty} F(f,k)e^{2\pi i(ft-kx)}dfdk \qquad (6.1.2)$$

A digitized reflection seismogram can be regarded as a sampled function in both t- and x-domain. The Fourier transform of a one-dimensional operator is a periodic function. In a similar way, two-dimensional sampling results in a two-dimensional Fourier transform which is periodic in both frequency and wave number. If the time domain sampling interval is h, the spectral period is 1/h and the Nyquist frequency is 1/2h. If the distance between traces is Δ, the k-spectral period is $1/\Delta$ and the Nyquist wave number is $1/2\Delta$. The discrete version of the Fourier transform pair for a two-dimensional operator $f(jh,i\Delta)(i=-I1,I2;\ j=-J1,J2)$ is then

$$F(f,k)=h\Delta\sum_{i=-I1}^{I2}\sum_{j=-J1}^{J2} f(jh,i\Delta)e^{-2\pi i(fjh-ki\Delta)} \qquad (6.1.3)$$

$$f(jh,i\Delta)=\int_{-1/2h}^{+1/2h}\int_{-1/2\Delta}^{+1/2\Delta} F(f,k)e^{2\pi i(fjh-ki\Delta)}dfdk \qquad (6.1.4)$$

Without loss of generality h is used again as one time unit and Δ as one space unit. The relation $F(f,k) = F(-f,-k)^*$ holds for every real operator, which makes $|F(f,k)|$ a centrosymmetric function. $|F(f,k)|$ is therefore completely described in the sector $(0<k<1/\Delta\ ;\ 0<f<1/2h)$ of figure 6.1.3 . This region is called the basic section. Sengbush and Foster (1968) call the left half of this part the primary region.

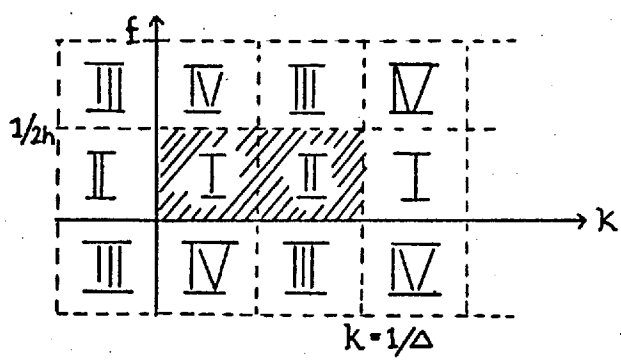

FIGURE 6.1.3 Periodic (f-k) diagram of a two-dimensional discrete operator

6.2 The transfer function of a multichannel stacking filter for signals with constant moveout

Let $a_i(t^*)$, $(-n \leq t^* \leq m;\ i=-N,..,N)$ be the operator of a discrete stacking filter as shown in figure 6.2.1. Without loss of generality an odd number 2N +1 of traces is chosen for the following considerations. The filter components are labelled from -N to +N. (For an even number see appendix 111).

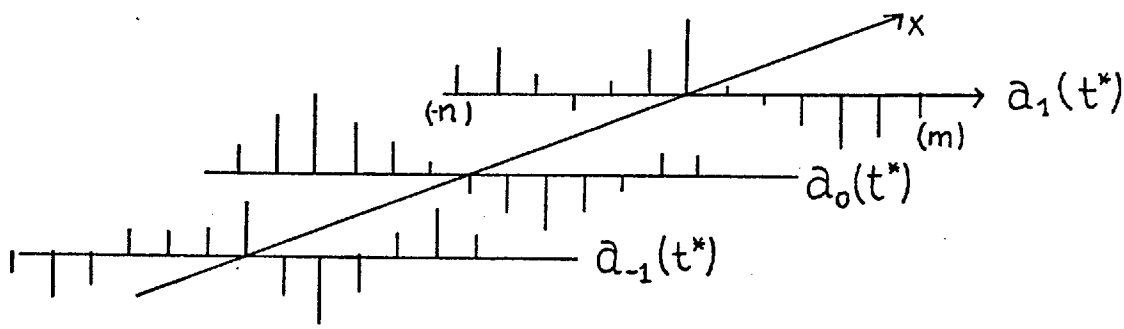

FIGURE 6.2.1 Discrete stacking filter

The discrete function

$$f_{\alpha}(t^*) = \sum_{i=-N}^{N} a_i(t^*) * \mathrm{sinc}(t^* - \alpha_i) \qquad (6.2.1)$$

is defined as the stacking filter response for broad band signals with the moveouts $\alpha_i (i=-N,N)$. The importance of this function becomes clear when 2N +1 inputs are given which have the form

$$x_i(t^*) = x(t^* - \alpha_i) = x(t^*) * \mathrm{sinc}(t^* - \alpha_i), \quad (i=-N,..,N) \qquad (6.2.2)$$

The output can then be written as

$$y(t^*) = x(t^*) * \sum_{i=-N}^{N} a_i(t^*) * \mathrm{sinc}(t^* - \alpha_i) \qquad (6.2.3)$$

$$y(t^*) = x(t^*) * f_{\alpha}(t^*) \qquad (6.2.4)$$

where $f_{\alpha}(t^*)$ takes the typical role of a unit impulse response. If

$f_{\alpha}(t^*)$ is known for all α_i the performance of the filter is known for all functions (6.2.2). In section 4.1 the stacking filters were designed in such a way that when the α_i (i=-N,...,N) fall on specified curves within a pass or reject region, $f_{\alpha}(t^*)$ should be ideally a unit spike or zero. The Fourier transform of $f_{\alpha}(t^*)$ is defined as the transfer function of the stacking filter:

$$F_{\alpha}(f) = \sum_{j=-N}^{N} A_j(f) e^{-2\pi i f \alpha_j}; |f| < 1/2 \qquad (6.2.5)$$

If signals in the input have constant moveout $\alpha_j = j\tau$, (j=-N,...,N), the transfer function

$$F(f,\tau) = \sum_{j=-N}^{N} A_j(f) e^{-2\pi i f \tau j} \qquad (6.2.6)$$

can be found with the help of the two-dimensional Fourier transform of the multichannel filter. This Fourier transform is

$$F(f,k) = \sum_{l=-n}^{m} \sum_{j=-N}^{N} a_j(l) e^{-2\pi i (fl-kj)} \qquad (6.2.7)$$

$$F(f,k) = \sum_{j=-N}^{N} e^{2\pi i k j} A_j(f) \qquad (6.2.8)$$

Taking the values of the transform along the line $k=-f\tau$ results again in expression (6.2.6). This very important result shows that the two-dimensional Fourier transform of a stacking filter includes all stacking filter transfer functions for signals with constant moveouts. If an additional filter B(f) is applied to the stacked output, the whole system possesses the transform

$$F^B(f,k) = B(f) \sum_{j=-N}^{N} e^{2\pi i k j} A_j(f) \qquad (6.2.9)$$

Applying B(f) on the stacked output is the same as applying it on each individual input before the stacking filter process.

At this point something has to be said about the phase characteristics of transfer functions. The usually complex function (6.2.6) for an arbitrary multichannel velocity filter becomes real and phase free for two important cases. For their discussion it is sufficient to know the amplitude spectra of the transfer functions only.

First Case

In section 4.2 it was shown that when a time window is centrosymmetric, the stacking filter is centrosymmetric as well. In this case $A_i(f) = A^*_{-i}(f)$, $(i=-N,..N)$ and $a_i(t^*)=a_{-i}(-t^*)$,$(i=-N,..N)$. By choosing the moveout of the input signals as $\alpha_j = \tau j$,$(j=-N,.,N)$ the transfer function becomes

$$F(f,\tau) = \sum_{j=-N}^{N} A_j(f)e^{-2\pi ifj\tau}$$

$$= A_0(f) + \sum_{j=1}^{N} (A_j(f)e^{-2\pi ifj\tau} + A_j^*(f)e^{2\pi ifj\tau})$$

Because $A_0(f)$ is real and every term has its complex conjugate in the sum, the transfer function is real and phase free.

Second Case

This case is actually included in the first one, but because of its importance it is discussed separately. When the time window is symmetric, the stacking filter fulfills the conditions

$$a_i(t^*) = a_i(-t^*) = a_{-i}(t^*), \quad (i=-N,\ldots,N)$$

and

$$A_i(f) = A_{-i}(f) = A_i^*(f), \quad (i=-N,\ldots,N)$$

With $\alpha_j = j\tau$,$(j=-N,N)$ in this case the transfer function becomes

$$F(f,\tau) = \sum_{j=-N}^{N} A_j(f) e^{-2\pi i f j \tau}$$

$$= A_0(f) + 2\sum_{j=1}^{N} A_j(f) \cos 2\pi f j \tau$$

Because all $A_j(f),(j=-N,..,N)$ are real the transfer function is real as well.

In actual fact, both formulations are contained in the following simple statement:

Let $A_i(f) = A^*_{-i}(f)$ and $\alpha_i = -\alpha_{-i}$, $(i=-N,..,N)$

then the transfer function is real.

This is seen immediately by writing $F_\alpha(f)$ in the following way

$$F_\alpha(f) = \sum_{j=-N}^{N} A_j(f) e^{-2\pi i f \alpha_j} \qquad (6.2.10)$$

$$= A_0(f) + \sum_{j=1}^{N} (A_j(f) e^{-2\pi i f \alpha_j} + A^*_j(f) e^{2\pi i f \alpha_j})$$

It is this more general case which is to be considered in section 7.3 where transfer functions of polarisation filters are investigated. In the second case all components of the highly symmetric stacking filter are phase free. It is therefore not surprising that transfer functions are also phase free. Phase free components alone do not necessarily guarantee phase free transfer functions. In section 4.2 it was shown that trace symmetric time windows of the form of figure 4.2.1 or figure 4.2.2 always specify phase free components. Transfer functions in this case are however, only phase free for $\tau=0$. Alternatively the first case shows that filter components do not have to be necessarily phase free to give zero phase transfer functions.

So far it was shown how to interpret the two-dimensional Fourier transform of a stacking filter. The function of this two-dimensional

Fourier transform along the line $k=-f\tau$ for $|f| \leq \frac{1}{2}$ gives the transfer function for the case where input signals have the same waveform and constant moveout on each trace. It therefore provides an ideal transform of the stacking filter, if these kind of input signals are expected. It is however of little value for signals which have changing waveform and non-constant moveout from trace to trace. In section 7.4 it is shown how to transform a stacking filter to obtain transfer functions, which belong to signals with certain differential normal moveouts.

In case of the two-dimensional Fourier transform of a stacking filter one should also note, that if the aperiodic functions $x_i(t^*)=\mathrm{sinc}(t^*-i\tau)$ $(i=-N,\ldots,N)$ are chosen as input to the filter, then the inverse of the transfer function for constant moveout corresponds to the response of the filter for this special input.

It can be also easily verified, that if the (f-k) diagram is computed from $A_{-j}(f),(j=-N,\ldots,N)$ instead of from $A_j(f),(j=-N,..,N)$ one obtains

$$\tilde{F}(f,k) = \sum_{j=-N}^{N} e^{2\pi ikj} A_{-j}(f) = \sum_{j=-N}^{N} e^{-2\pi ikj} A_j(f) \qquad (6.2.11)$$

where $\tilde{F}(f,k)=F(f,-k)$. The transfer function for constant moveout is now obtained by taking the values of $\tilde{F}(f,k)$ along the line $k=f\tau$ in the range $|f|\leq\frac{1}{2}$. Because of this reason the (f-k) diagram of a stacking filter is, throughout this thesis, presented in form of formula (6.2.11). Note, that formula (6.2.11) and (6.2.8) are identical for symmetric filters.

Another reason for inverting the stacking filter components is the following one: If the input traces have the Fourier transforms $X_i(f),(i=-N,..,N)$ the Fourier transform of the stacked output can be written as

$$Y(f)= \sum_{i=-N}^{N} A_i(f)X_i(f)$$

The same expression is also obtained by doing a two-dimensional convolution of the filter $A_{-i}(f)$, $(i=-N,..,N)$ with the same input and taking the centre trace of the convolution as shown in section 3.2.2.

Example Number 1

To make the above theoretical considerations more clear, an example is given. A multichannel filter was designed which passes signals falling into region 1 and rejects signals falling into region 2 of figure 5.1.2.2.

The design parameters are:

number of traces: $N = 6$

length of filter: $LF = 17$

uncorrelated noise: $\nu = 0.08$

chatter: $t_c = 0.01$

region parameter: $\alpha = 2.0$

region parameter: $\gamma = 4.0$

region parameter: $\tau_c = 0.8$

correlated noise: $\varrho = 30$

The six responses of the computed optimum filter are given in figure 6.2.1 and as expected, it is a centrosymmetric filter. Its two-dimensional amplitude spectrum is shown in figure 6.2.2. This figure presents the basic region of figure 6.1.3. All contours and isometric plots in this thesis show the amplitude spectrum $|\tilde{F}(f,k)|$ in decibels

$$\tilde{\tilde{F}}(f,k) = 20\log_{10}\frac{|\tilde{F}(f,k)|}{|A_{max}|}$$

within the range from 0dB to -30dB. $|A_{max}|$ is the maximum amplitude encountered in the basic range.

In figure 6.2.2 the τ-lines are shown for τ=-0.8;0.8;1.6;3.2. The line τ=3.2 cuts the line k=1 at f=5/16 and therefore can be thought to continue from (k=0; f= 5/16)in the same direction to the right to cut the

horizontal line f=0.5 at k=1.2 With formula (6.2.11) the transfer functions for constant moveout signals are found along these lines between f=0 and f=0.5. Figure 6.2.3 shows the amplitude spectra of some transfer functions for the above filter. They were obtained by passing broad band signals with the given constant moveout through the stacking filter and taking the Fourier transform of the output. They can however, be easily obtained by taking the values along the corresponding τ-lines of figure 6.2.2. For τ= 4.0 the filter again has good pass characteristics for the range around half the Nyquist frequency. All transfer functions have zero phase.

By making use of the concept of the transfer function along the τ-lines, the characteristics of the two-dimensional amplitude spectrum (figure 6.2.2) also find an easy explanation. Due to the design procedure of Chapter IV, transfer functions along all lines falling into pass region 1 of figure 6.2.4 should ideally equal one; while all transfer functions falling into sector 2 of figure 6.2.5 should ideally equal zero. Both of these conditions have to be fulfilled simultaneously by the stacking filter. Figure 6.2.6 shows which regions of the filter are supposed to be pass regions (+) and which reject regions(-). In figure 6.2.6 there are two regions which should both be pass and reject regions at one time. One expects in such a case, that the least squares principle makes a compromise between both. Comparing figure 6.2.6 with figure 6.2.2 shows at once the described similarities. On region A and B there are no constraints.

With the above example, it is obvious that the defined concept of the stacking filter transfer function is of great help for the analysis of the characteristics of a multichannel velocity filter. Transfer functions for signals with constant moveout can be found for any kind of stacking filter in the way described above. In figure 6.2.7 (f-k)-plots of a 6-trace and 12-trace straightforward stack are given. These

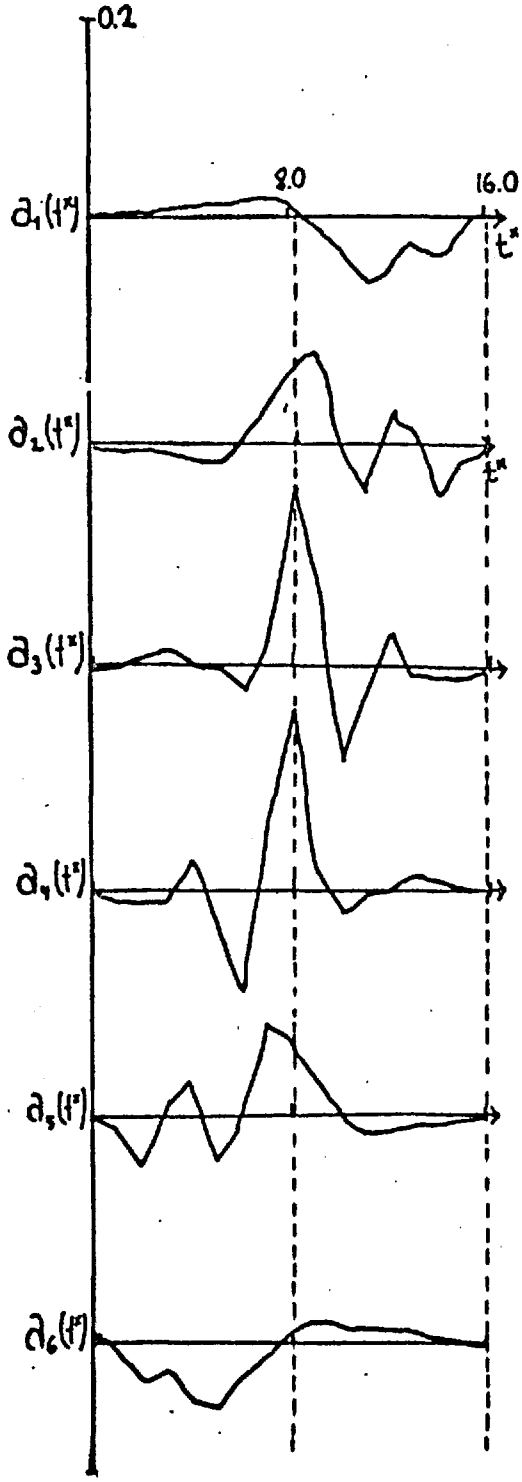

FIGURE 6.2.1

Filter number 1
Six components in the time domain

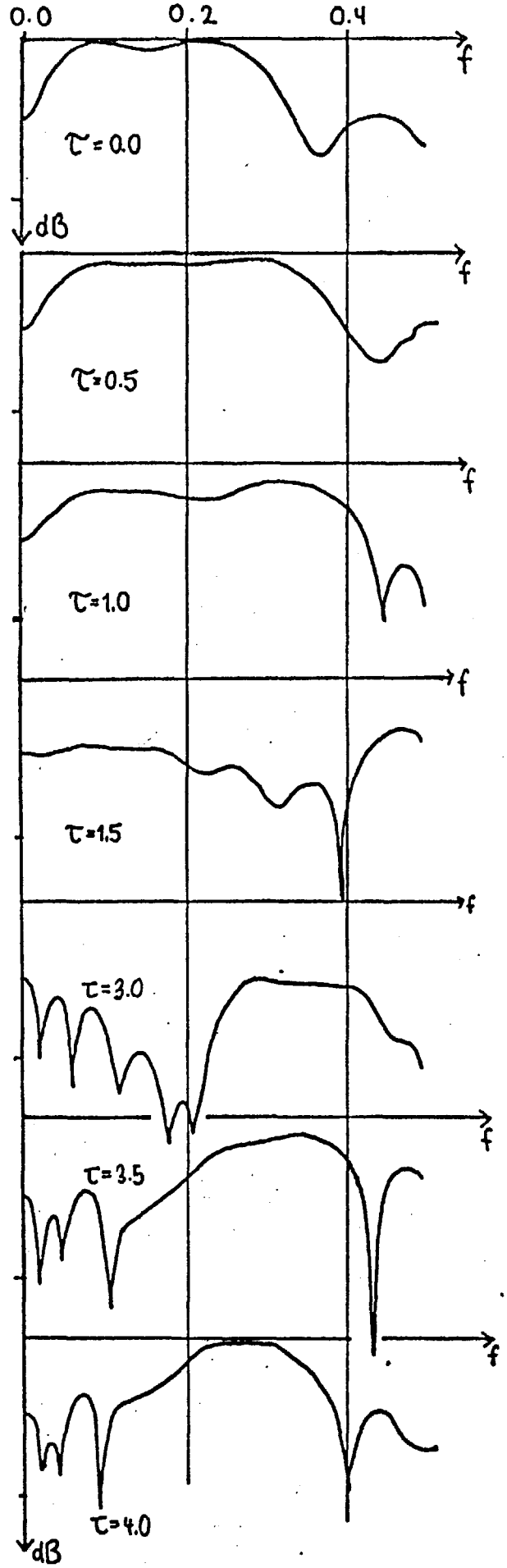

FIGURE 6.2.3

Filter number 1
Stacking filter transfer functions

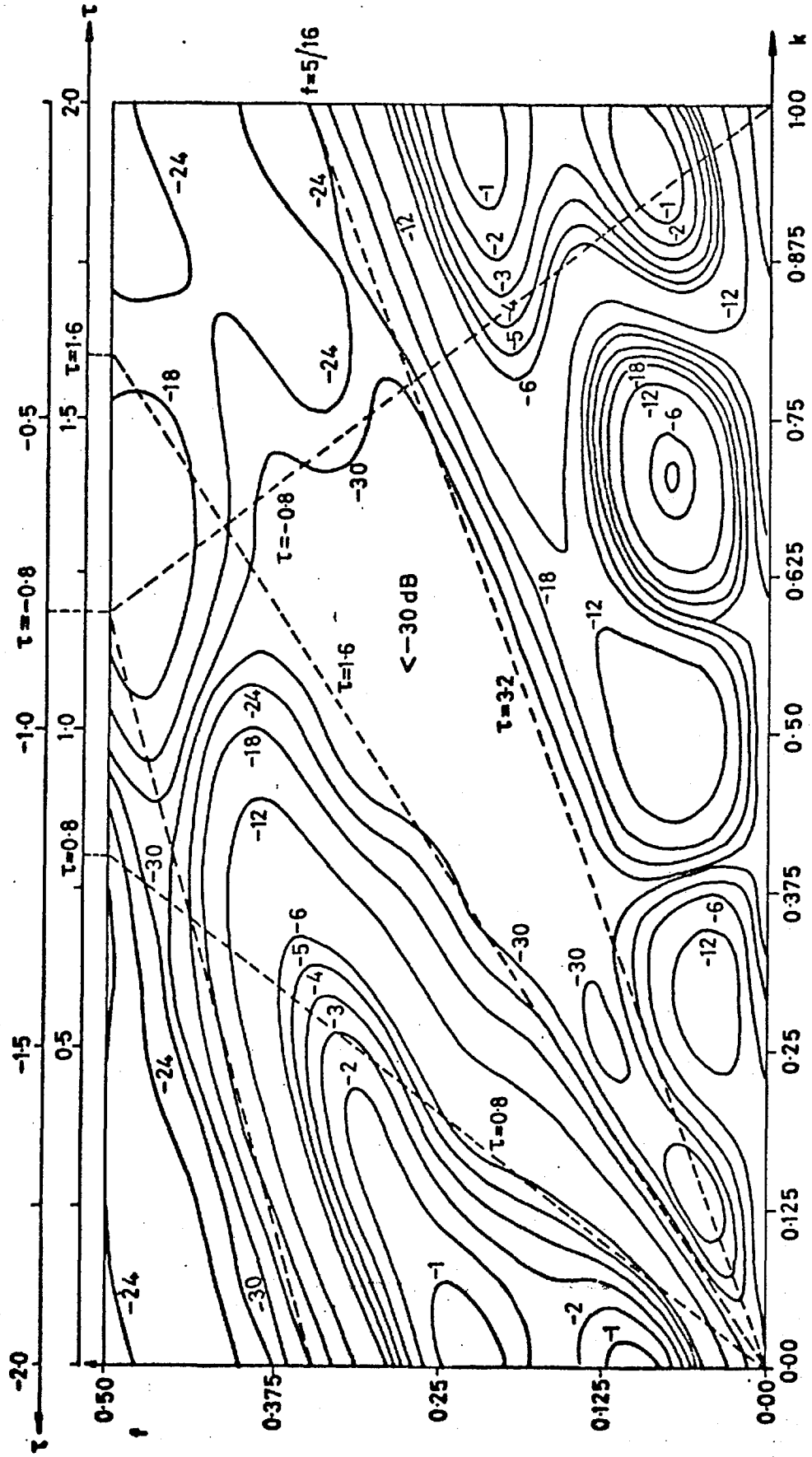

FIGURE 6.2.2 Filter number 1 (f-k) plot

τ_c=0.8 ; α=2.0 ; γ=4.0 ; N=6 ; LF=17; ν=0.08 ; ρ=30.0 ; t_c=0.01

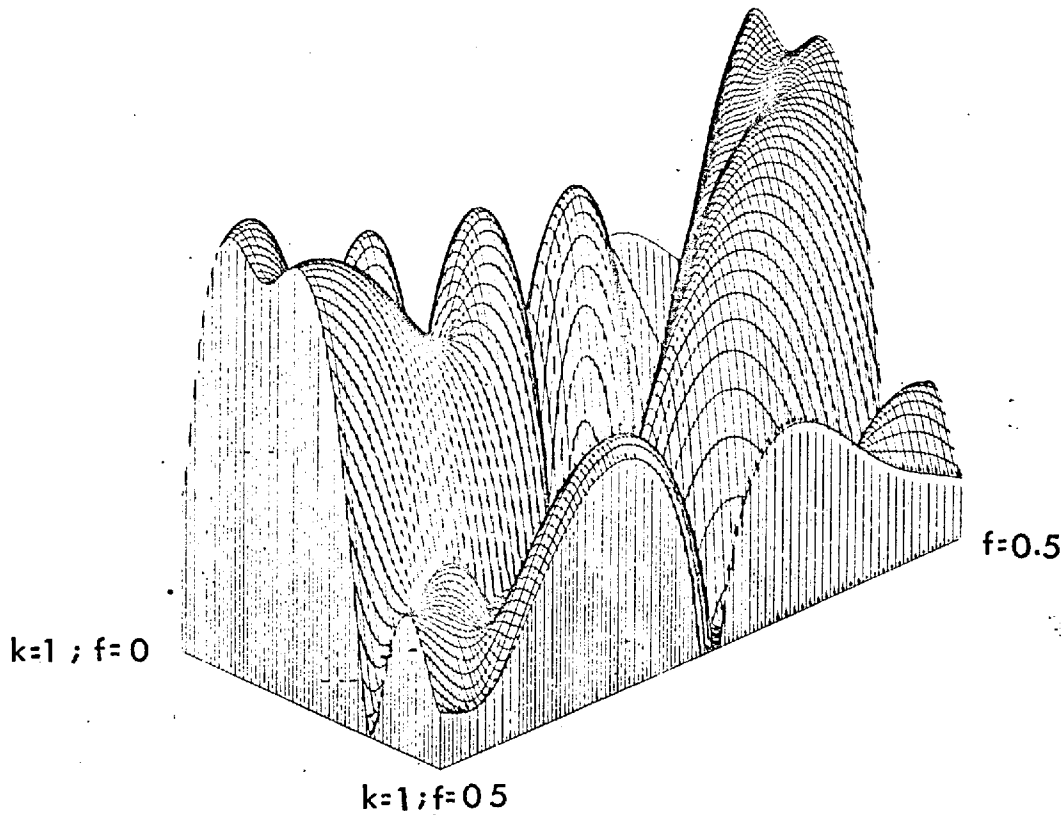

FIGURE 6.2.2 a Filter number 1

Isometric plot of figure 6.2.2 viewed from (k=1 ; f=0.5)

stacking filter components are zero-delay unit spikes. Transfer functions may again be obtained along radial lines from the origin. The straightforward stack has an ideal response for zero-moveout signals. Transfer functions however, change enormously for small deviations from the moveout zero.

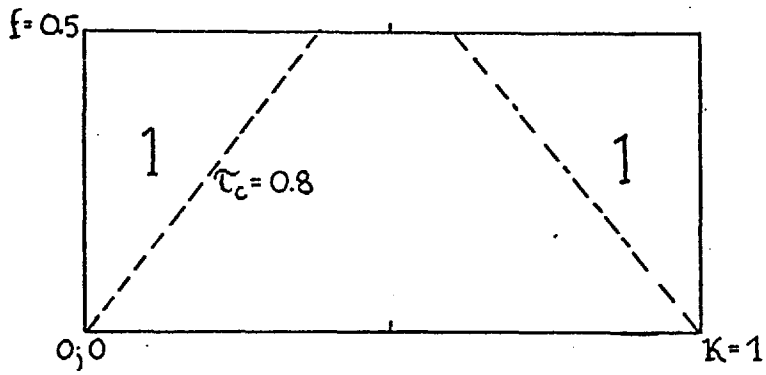

FIGURE 6.2.4 Pass-region for filter number 1

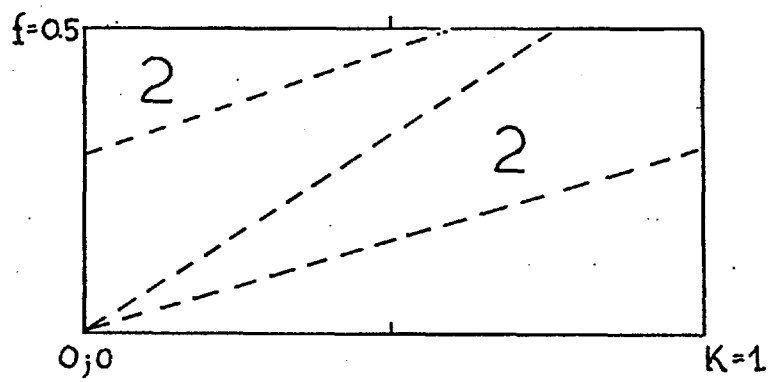

FIGURE 6.2.5 Reject region for filter number 1

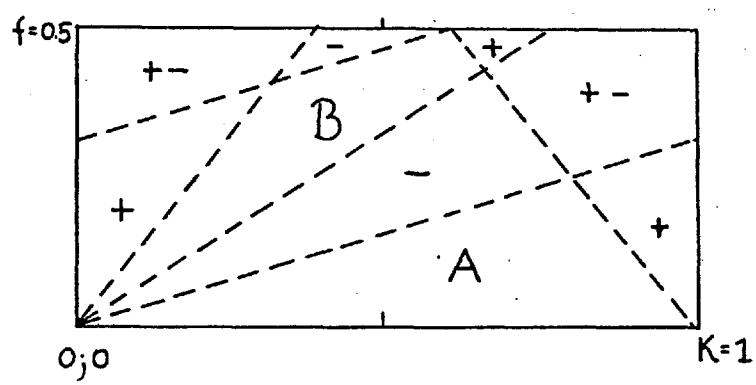

FIGURE 6.2.6 Pass and reject region for filter number 1

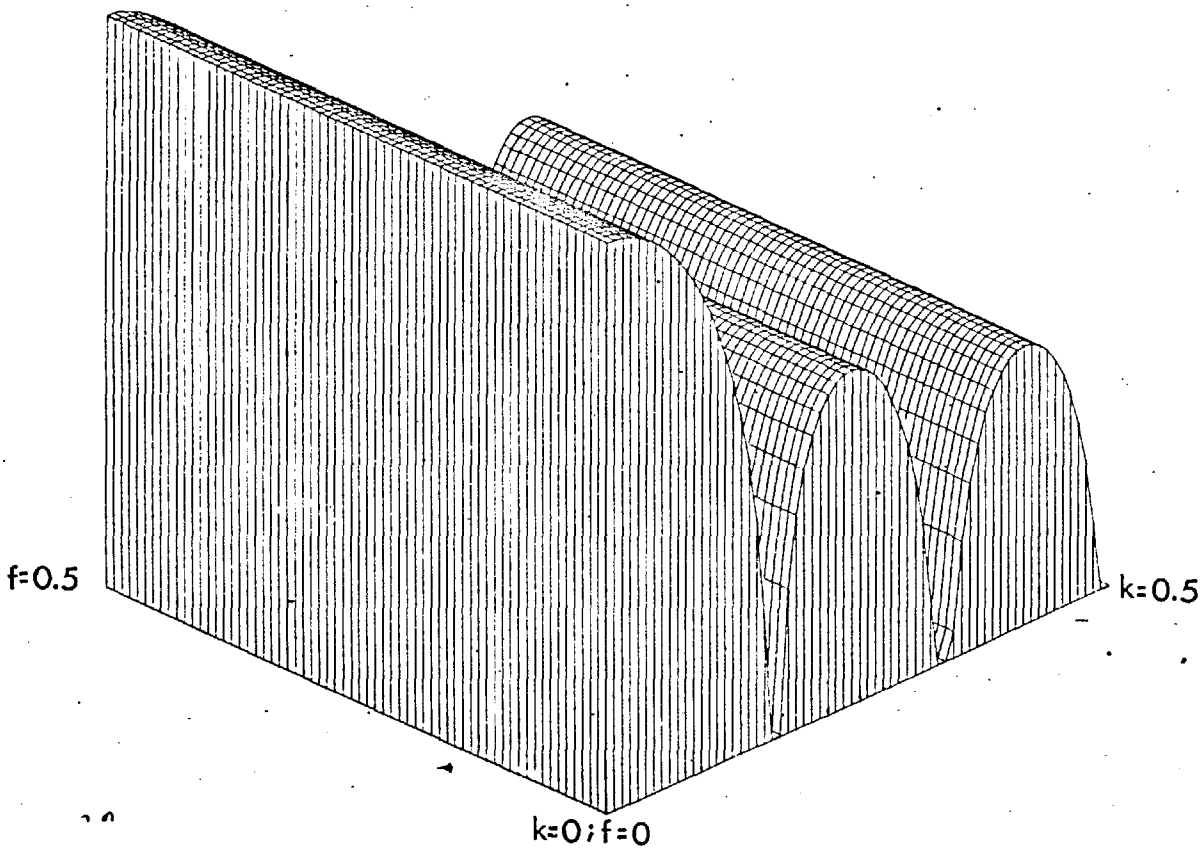

6-trace stack

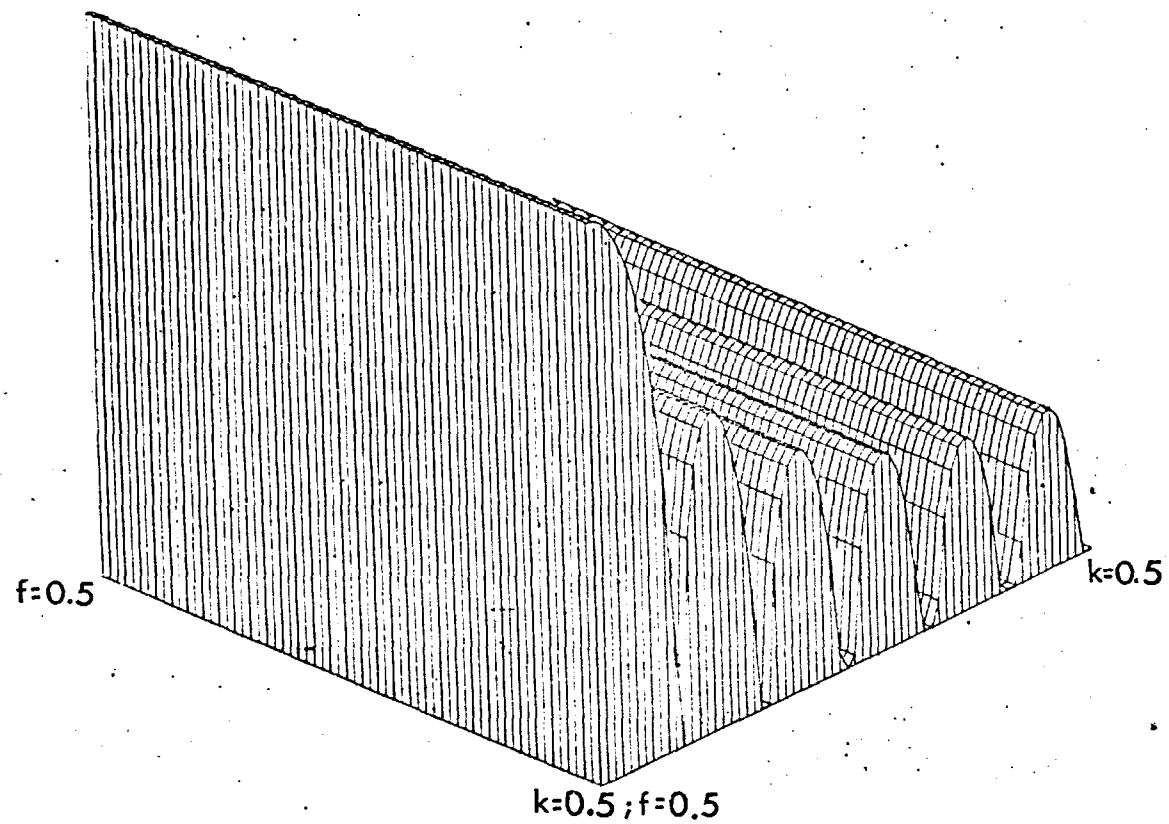

12-trace stack

FIGURE 6.2.7 Isometric plot of 6-trace and 12-trace straight forward stack

CHAPTER VII

COMPUTATIONAL EXPERIMENTS AND FILTER CHARACTERISTICS

The basic aim in previous chapters was to emphasize the generality of the normal equations (4.2.4) and to discuss their application for various two-dimensional and three-dimensional filtering problems. Computed filters alone however show little about their performance. Characterising a filter is therefore as important as its design procedure. Filters reveal their inherent properties by applying them to properly selected signal traces. Compared with the characterisation by a transform from which responses for a broad class of test signals can be obtained simultaneously(see example number 1)this approach is, however, very simple. The aim in this chapter is therefore to characterise the given stacking filters with appropriate transforms, which give a deep insight into their general performance. Before doing so, the salient points of previous chapters are summarized below.

1. The analog normal equations (4.2.4) are designed with the least squares principle for random stationary processes.
2. 'Approximate' solutions for the analog normal equations are obtained with the discrete equations (3.2.5.5). They are solved with the fast multichannel Levinson algorithm.
3. Stacking filters can be computed for two-and three-dimensional problems where signals have constant or differential normal moveout.
4. Time windows for a given problem are not unique. Symmetries of windows are reflected in symmetries of computed stacking filter components.

5. The transfer function of a stacking filter as defined by the output for broad band signals with constant moveout is helpful concept for the characterisation of a filter. Phase properties of transfer functions depend strongly on the shape of a time window. Symmetric and centrosymmetric windows have zero-phase transfer functions for all signals with constant moveout. Transfer functions can be obtained from the two-dimensional Fourier transform of a filter.

In this chapter some characteristics of two-dimensional velocity filters are presented. In section 7.2 symmetric and centrosymmetric velocity filters are compared. In section 7.3 an introduction to the three-dimensional Fourier transform is given and a stacking filter transfer function for the three-dimensional case is defined. Also some characteristics of three-dimensional polarisation filters are discussed. In section 7.4 suitable transforms are derived for the characterisation of filters designed for differential normal moveout signals.

Not all inherent properties of a filter can be obtained from Fourier transforms. For the characterisation of filters in the presence of uncorrelated noise other functions are presented in section 7.6 which are also important. A good insight into characteristics of two-dimensional multichannel velocity filters is helpful for the understanding of the total class of filters. For practical reasons, two-dimensional velocity filters are only computed for either six or twelve traces.

7.1 Optimum multichannel velocity filters

Filters for symmetric regions, as given in figure 5.1.1.1, designed without provision for chatter, are discussed by Foster and Sengbush (1968). The value of their treatment is of special importance since they compare optimum multichannel velocity filters with doublet and 'pie-slice' filters and show the superiority of the former in many aspects. Although they describe the observed foldings along the line k=0.5, they give little explanation for them. It is with the help of the concept of the transfer function for signals with constant moveout and the periodicity of the (f-k)domain that a deeper insight into the numerous foldings is gained. Using periodicity one realizes that in the case of filters with symmetric regions the (f-k)plot has to be symmetric about k=0.5 and consequently folding of the τ-lines will take place along this line . The transfer characteristics are therefore entirely contained in the square ($0<f<0.5$; $0<k<0.5$) of the two-dimensional Fourier transform. This, however, is an unnecessary restriction. There is more freedom for the design of filters available in the total basic region of the (f-k) domain. Non-symmetric filters can make use of this.

So far, it seems that it is possible to predict approximately the features of an (f-k) diagram for a two-dimensional multichannel velocity filter with the sole knowledge of the form of the time window. There is, however, one more inherent feature common to optimum multichannel velocity filters; that is the suppression of the amplitude spectrum for overlapping pass regions in the (f-k) domain. To show this effect, various 12-trace pass filters were computed with equation (5.1.1.13). The time window for this case is given in figure 4.2.4. The only parameter that was varied was τ_c, which took on the values τ_c = 0.5; 1.0; 1.5; 2.0. The factor ν was chosen as ν= 0.08. (f-k) plots are given in figure 7.1.1 to figure 7.1.4. For $\tau_c<1$ it is seen that the amplitude characteristics

approximate well with the desired response in the pass region. The approximation around the Nyquist frequency $f_N = 0.5$ however, becomes worse as τ_c reaches the value $\tau_c = 1$. For $\tau_c > 1$ it is observed that the pass region becomes narrower instead of wider for high frequencies. For this reason, Foster and Sengbush discussed (f-k) diagrams almost exclusively in the region ($0<k<0.5$; $0<f<f_c$), where they defined f_c as the folding frequency. It was decided in this thesis to show generally the whole basic region. For symmetric filters however, only the sector ($0<k<0.5$; $0<f<0.5$) is shown.

For all problems, where there is no overlapping of pass- with pass regions or reject with pass regions, one has the heuristic feeling that the expected error (3.2.5.6) as a function of the filter length should tend to zero. One may however, never expect that the error approaches zero for filters where time window configurations possèss overlapping regions. This is because the desired transfer functions cannot be completely approximated anymore in the specified range. For the above sequence of filters the expected errors are shown in figure 7.1.5. Each curve has a different length because for broader windows longer filters were chosen. Optimum delay is always in the middle of each filter. The curves show that expected errors increase with increased overlapping of pass regions. If the overlapping of regions occurs more than once, the relation between a time window and its (f-k) plot is even more complex. A filter designed for $\tau_c = 4$ will approximate an (f-k) diagram as shown in figure 7.1.6.

All symmetric filters for an even number 2N of traces have one thing in common: i.e. their two-dimensional amplitude spectrum equals zero along the line k = 0.5. From equation (6.2.8 A) (appendix lll) it can be shown that the two-dimensional transform

$$F(f,k) = \sum_{n=-m}^{m} \sum_{j=-(\frac{2N-1}{2})}^{(\frac{2N-1}{2})} a_j(n) e^{-2\pi i(fn-kj)}$$

or

$$F(f,k)=\sum_{j=\frac{2N-1}{2}}^{\frac{2N-1}{2}} e^{2\pi ikj}A_j(f) = \sum_{j=\frac{1}{2}}^{\frac{2N-1}{2}} A_j(f)\cos 2\pi kj$$

equals zero for k = 0.5

$$F(f,0.5) = \sum_{j=\frac{1}{2}}^{\frac{2N-1}{2}} A_j(f)\cos \pi j = 0$$

This equation does not hold for a symmetric stacking filter with an odd number 2N +1 of components. In such a case, the two-dimensional Fourier transform along the line k = 0.5 becomes

$$F(f,k)=\sum_{j=-N}^{N} e^{2\pi ikj}A_j(f)=A_0(f)+\sum_{j=1}^{N} A_j(f)\left[e^{2\pi ikj}+e^{-2\pi ikj}\right]$$

$$=A_0(f)+2\sum_{j=1}^{N} A_j(f)\cos 2\pi kj$$

or

$$F(f,0.5)=A_0(f)+\sum_{j=1}^{N}(-1)^j A_j(f)$$

An example of a symmetric filter with an odd number of components (filter number 6) is given in figure 7.1.7 which shows the contours of an 11-trace filter where all other parameters are the same as for filter number 3.

From figure 7.1.1 to figure 7.1.4 one can conclude that the plateaux are very flat for narrow time windows and become continuously rippled by increasing the window width. The height of the hills in the reject region decreases with increasing τ_c, and the escarpment becomes steeper as well. All transfer functions approximate the value 0dB for near zero frequencies. This is a typical feature of optimum multichannel velocity filters which is not obtained by any other velocity filters. It will be observed again in a similar form in section 7.3 where corresponding three-dimensional velocity filters are investigated. For narrow pass regions, the contours of the escarpment become increasingly more parallel to

the f-axis for low frequencies. Apart from minor changes it may appear that filter number 2 to number 4 (figure 7.1.1 to figure 7.1.3) represent a scaled section (scaled in f-direction) of filter number 5 . (Figure 7.1.4)

This is justified in the discussion in Chapter VIII where a deeper insight into the relation between time windows and (f-k) plots will be obtained. To complete this short treatment about optimum multichannel velocity filters, their most important characteristics are repeated -

1. Decreasing the width of reject regions or increasing the amount of correlated noise results in increased rejection within these regions.
2. Increasing the uncorrelated noise in the design results in a loss of high frequency content in the signal region.

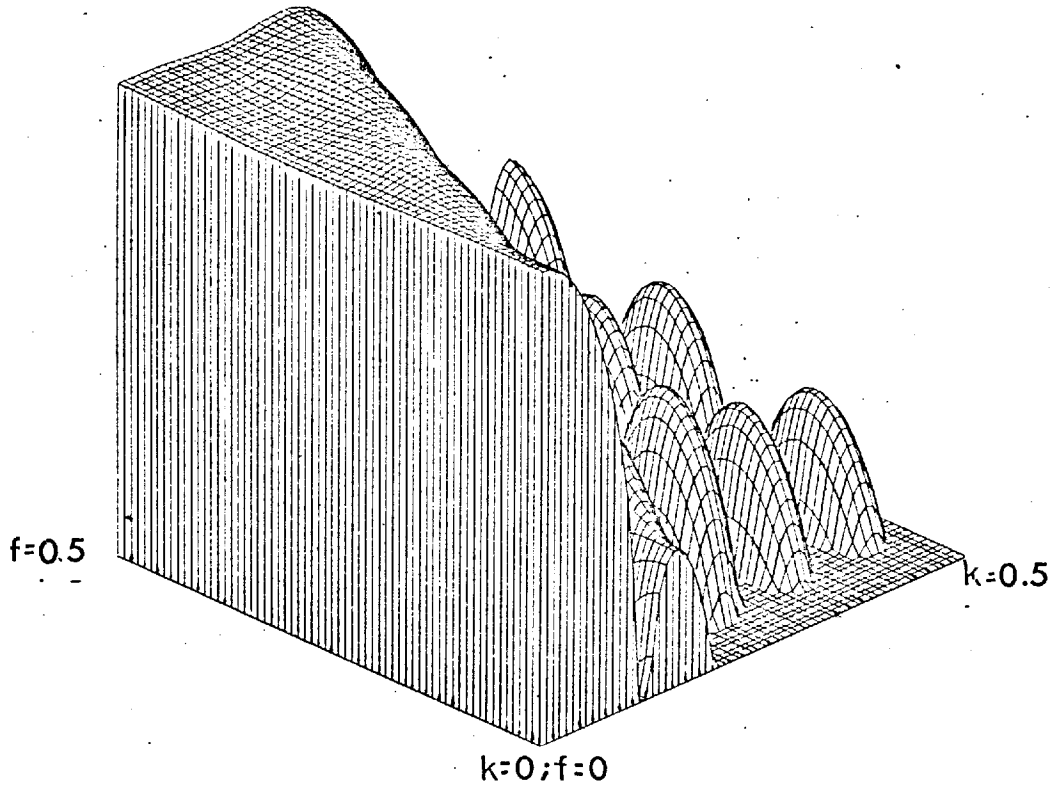

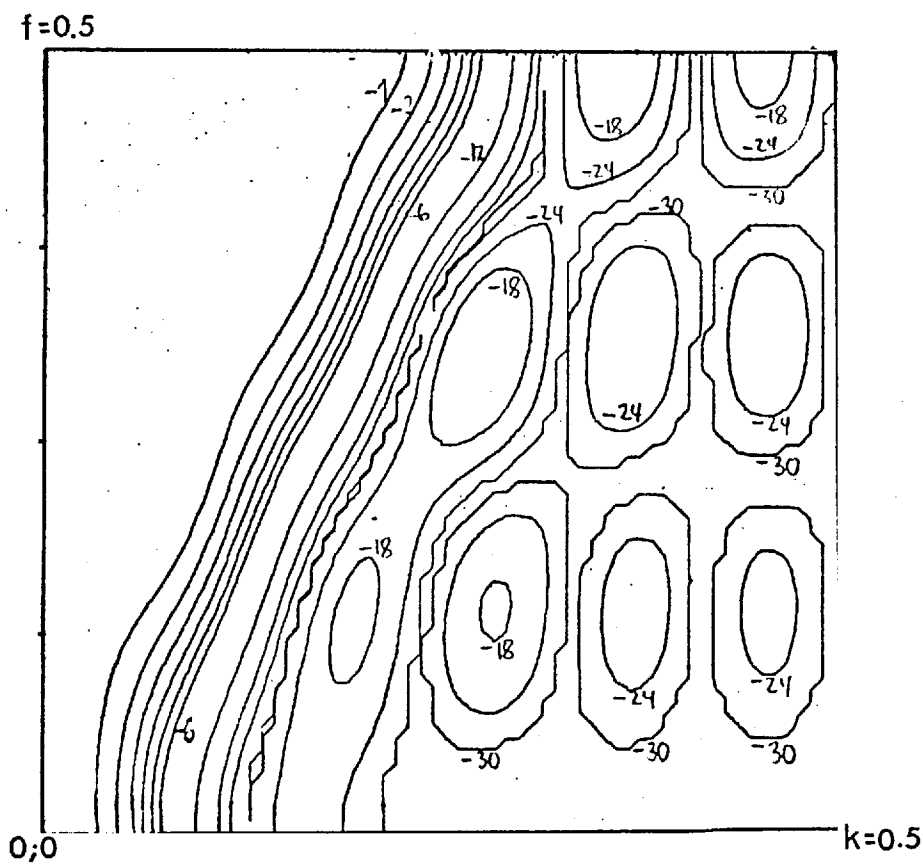

FIGURE 7.1.1 Filter number 2
(f-k) diagram and isometric plot
τ_c= 0.5 ; N=12 ; LF=7 ; ν=0.08 ; t_c= 0.01

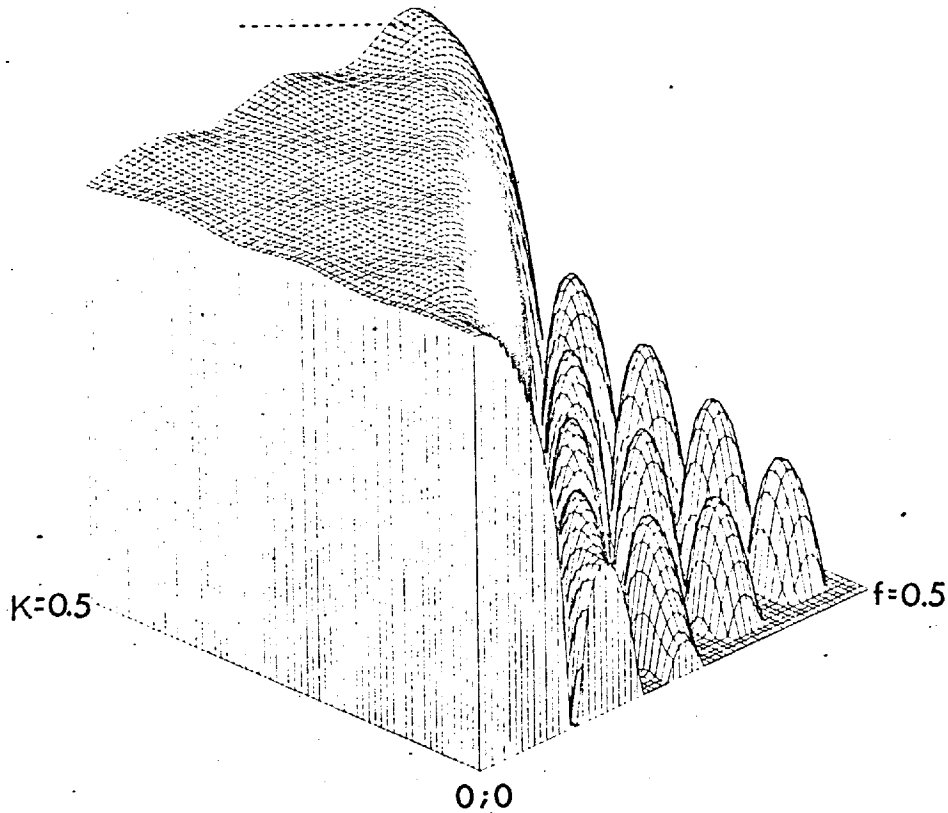

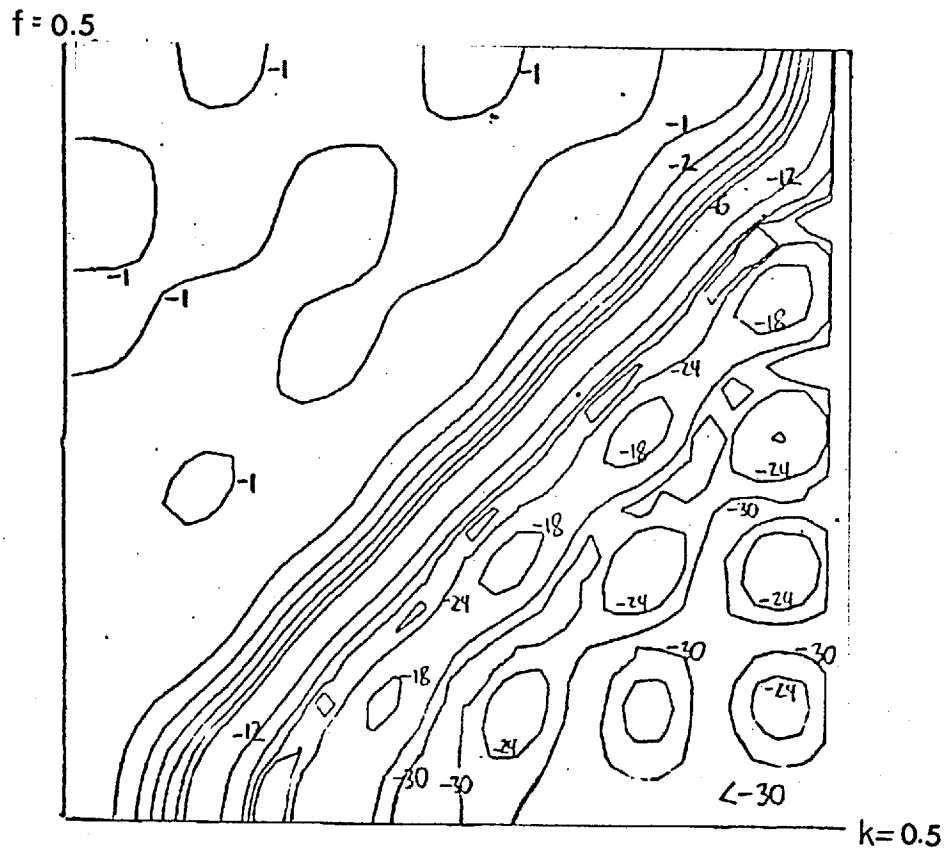

FIGURE 7.1.2 Filter number 3

(f-k) diagram and isometric plot
τ_c= 1.0 ; N=12 ; LF=13 ; ν=0.08 ; t_c=0.01

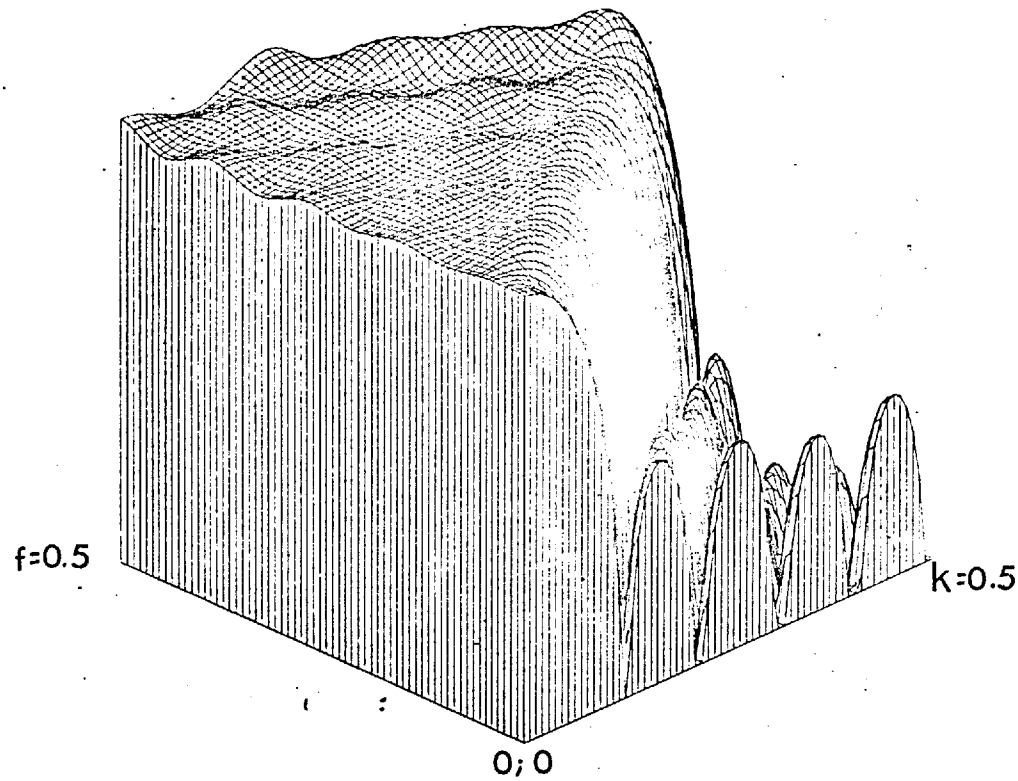

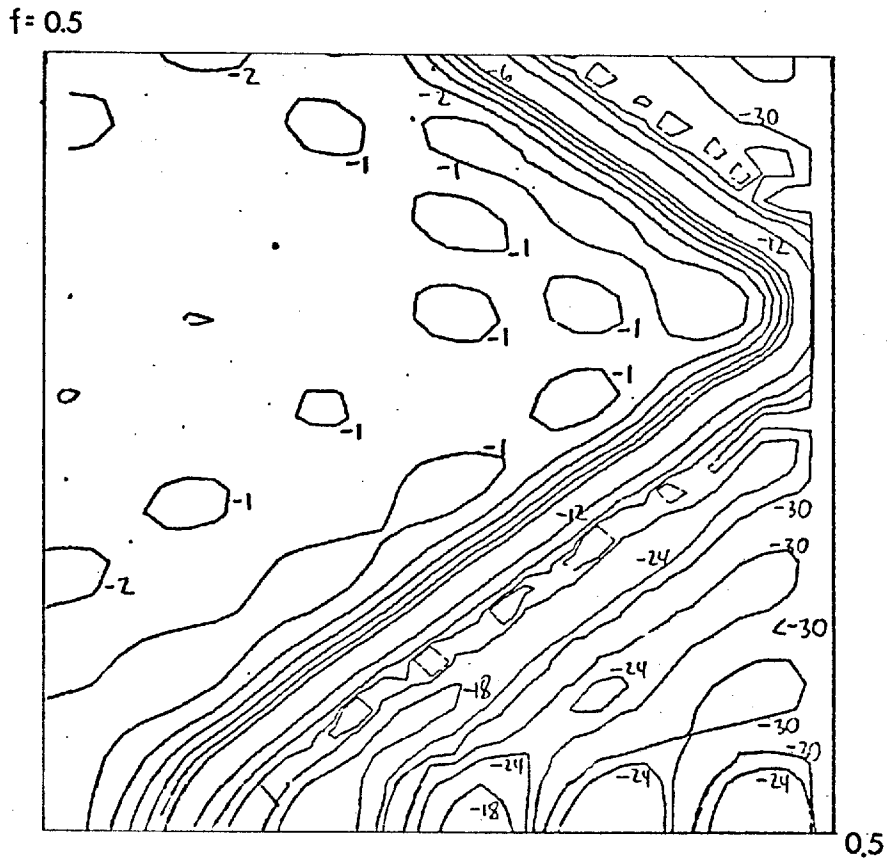

FIGURE 7.1.3 Filter number 4

(f-k) diagram and isometric plot

τ_c=1.5 ; N=12 ; LF=19 ; γ=0.08 ; t_c=0.01

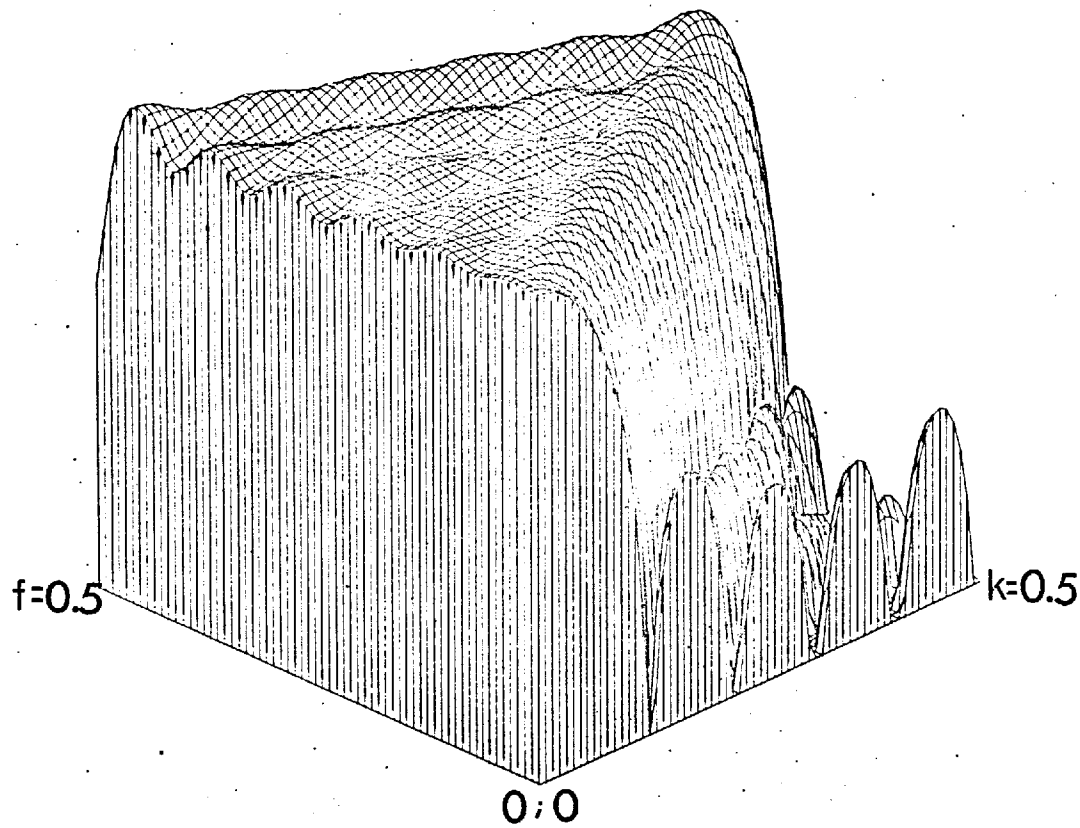

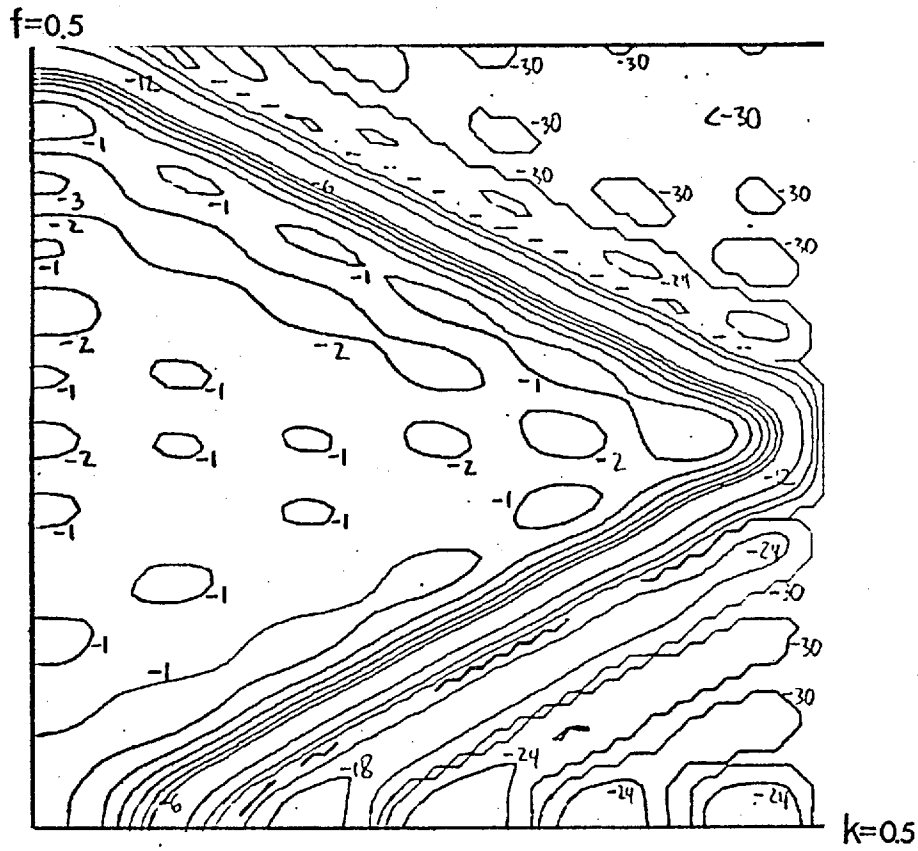

FIGURE 7.1.4 Filter number 5

(f-k) diagram and isometric plot

τ_c=2.0 ; N=12 ; LF=25 ; γ=0.08 ; t_c=0.01

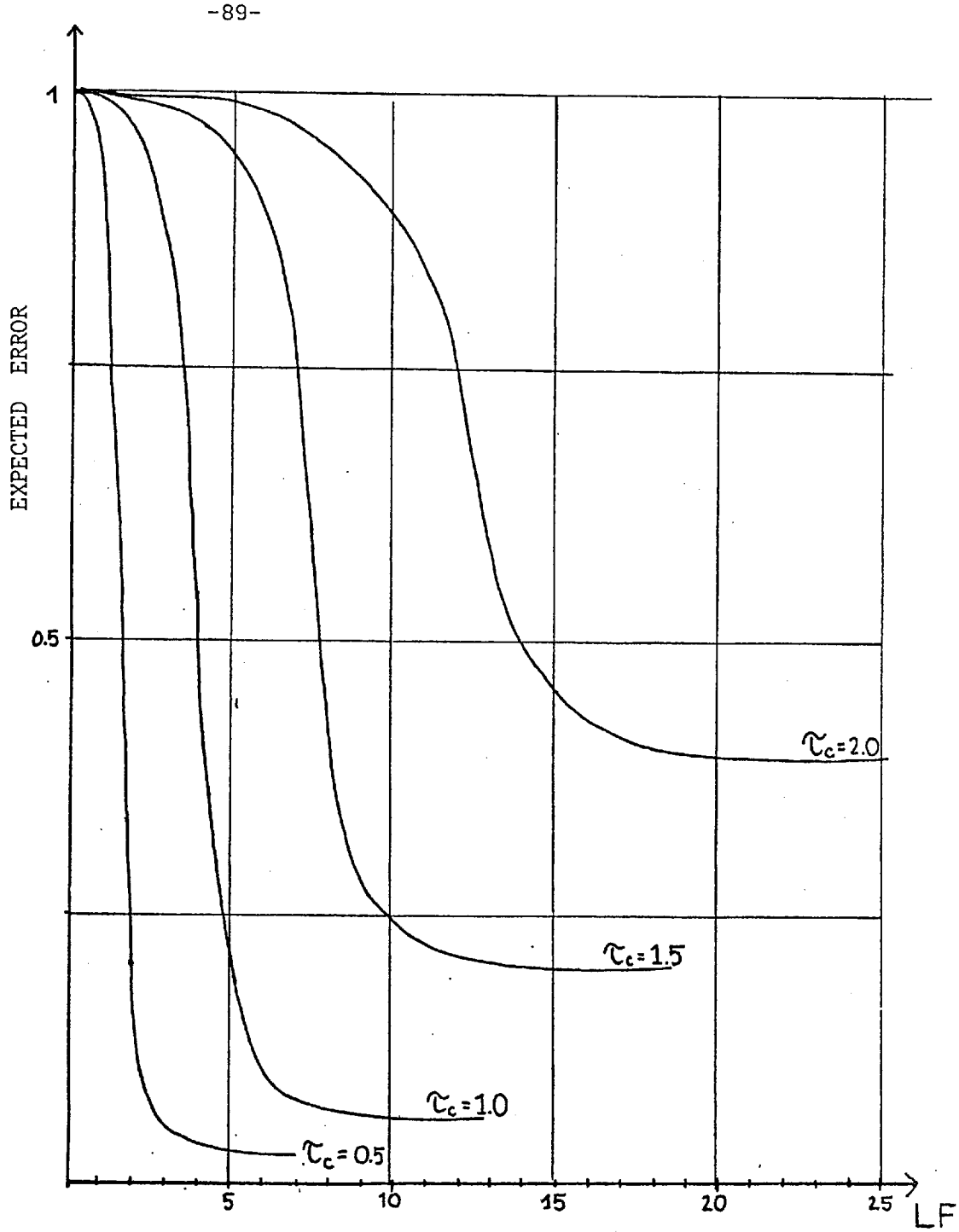

FIGURE 7.1.5 Expected Errors as a function of the filter length

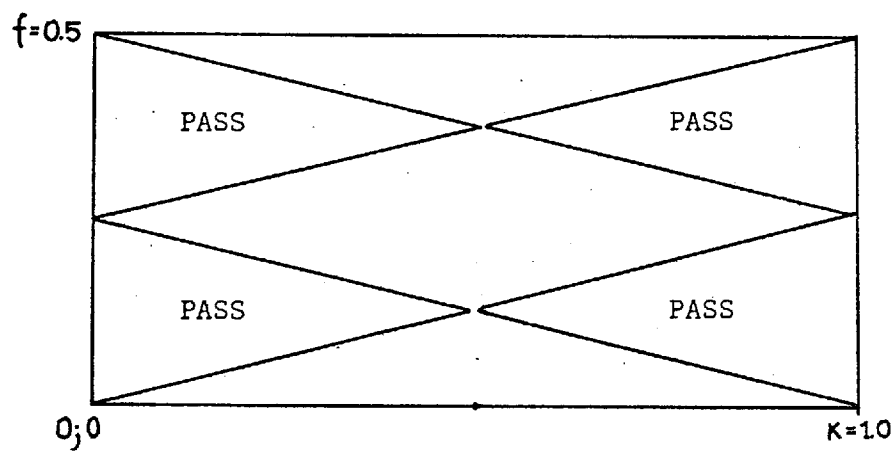

FIGURE 7.1.6 (f-k) diagram for a pass filter with τ_c = 4.

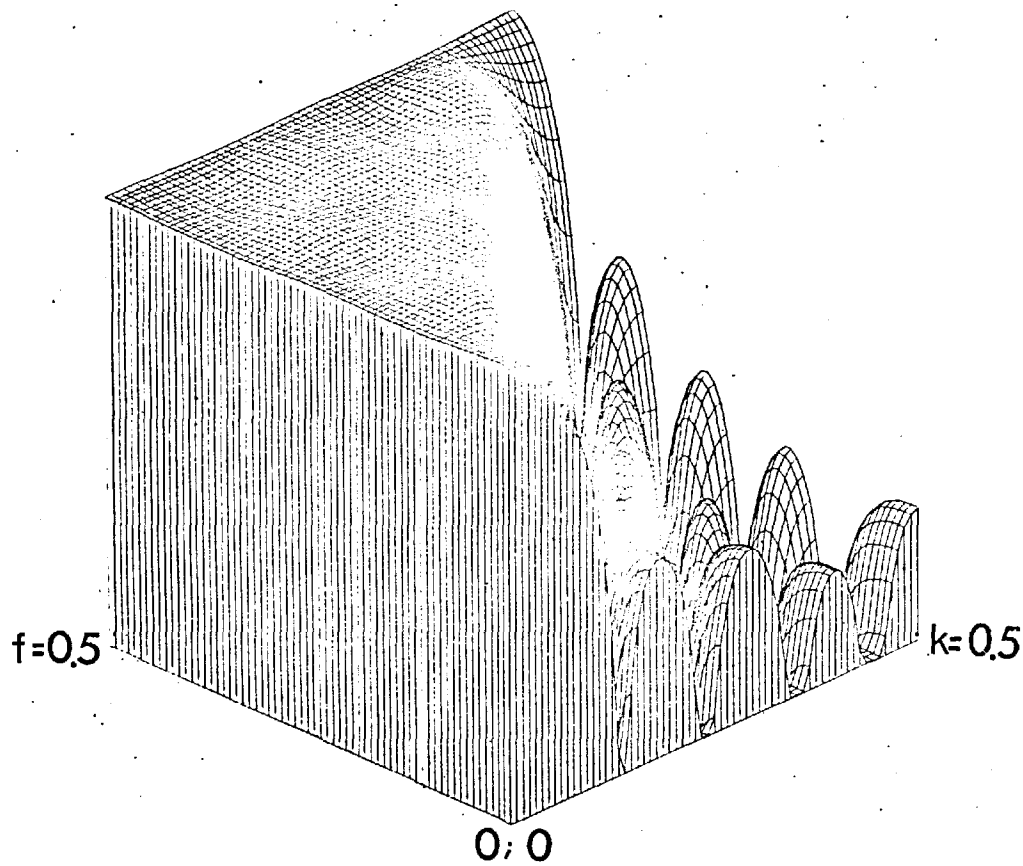

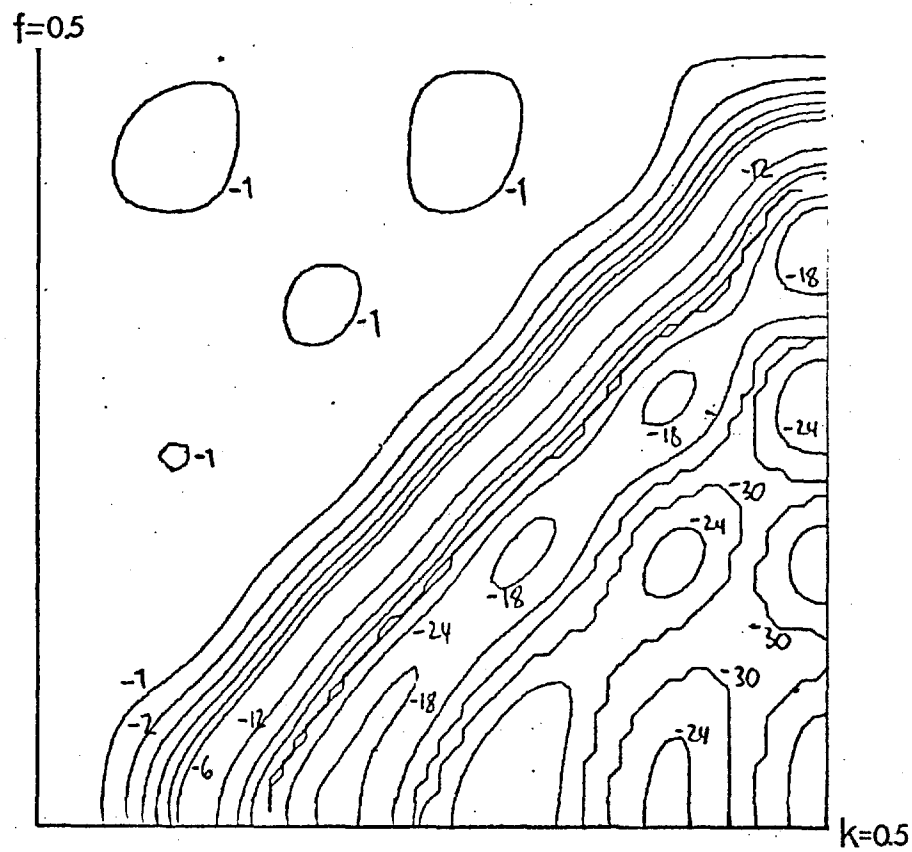

FIGURE 7.1.7 Filter number 6

(f-k) digaram and isometric plot

τ_c=1.0; N=11 ; LF=13 ; ν=0.08 ; t_c=0.01

7.2 A comparative study of symmetric and centro-symmetric velocity filters

By making use of the above rules which relate time windows with the characteristics of the (f-k) diagram, it is easy to give examples which show the superiority of centro-symmetric filters (designed for two regions) over symmetric filters (optimum multichannel velocity filters designed for three regions). Both types have the same essential attribute; they show minimum distortion since all transfer functions for signals with constant moveout have zero phase. Three different examples are discussed below. They are selected to emphasize three different features which are responsible for the fact that centro-symmetric filters generally possess superior characteristics over symmetric filters.

1. Example number 2 (filter number 7) gives the corresponding symmetric filter for filter number 1. It shows how much of the pass region of example number 1 is lost by admitting an additional symmetric reject region in the design.
2. In example number 3, a centro-symmetric reject pass filter is compared with its corresponding symmetric version. In the symmetric version pass regions overlap, thus showing rejection in a region where centro-symmetric filters still approximate fairly well the desired pass region.
3. One may easily get the impression that due only to fewer overlappings of regions in the (f-k) diagram, do filters, designed for two regions, possess superior characteristics over the ones designed for three regions. Example number 4 shows that even when little or no overlapping occurs, then two reject regions have a stronger negative influence on a pass region than one reject region.

Example Number 2

The symmetric version for filter number 1 is computed with (5.1.1.12). Figure 7.2.1 shows the six computed components of filter number 7 and figure 7.2.1 a shows the contours of its two-dimensional amplitude spectrum. The contours should be compared with filter number 1. (figure 6.2.2.) The pass region in the left half of figure 7.2.1 a, shows a considerable loss if compared with the characteristics of figure 6.2.2. Even in regions which remain pure pass regions in both cases the approximation is better for the centrosymmetric filter. Figure 7.2.1 b gives an isometric plot of filter number 7, viewed from the upper right-hand corner. It can be compared with the plot of figure 6.2.2 a.

Example Number 3

A symmetric reject-pass filter for the time window of figure 5.1.1.1 and its centro-symmetric version for the window of figure 4.2.6 were computed with the following design parameters :

τ_c=0.5; N=12; LF=19; ν=1.0; t_c=0.2; α=1; γ=3; ρ=30

The contours of the amplitude spectrum for the symmetric filter are given in figure 7.2.4 and they show the expected suppression where pass regions overlap. An isometric plot of half the basic region viewed from the origin is given in figure 7.2.4 a. Figure 7.2.5 gives the contours of the corresponding centro-symmetric version and figure 7.2.5 a, shows its isometric plot viewed from (k = 1; f = 0). Most of the contours in this case, follow the typical trend of the pass region. The right half of the reject region seems to still influence the pass region for high frequencies by depressing the contours by about 6dB. The approximation of the desired pass region is still good if compared with the symmetric case where an approximation is impossible. This is especially shown by the isometric plot of figure 7.2.5 b, which gives a view from the point (k = 1; f = 0.5). Both the symmetric and centro-symmetric filter favour the transfer

characteristics of the reject region for frequencies in the specified parts. The contours of the pass region obtained for low frequencies are in both cases strongly bent towards the k-axis where pass regions occupy a fairly wide range. This feature is especially strong for the symmetric filter and it may be heuristically explained by the fact that no restrictions were imposed on the internal regions of the (f-k) diagram. Pass regions may therefore deviate into this part without violating any specified conditions.

Example Number 4

One may argue that the interference of design regions in the (f-k) diagram effects predominantly high frequencies in a range where, due to the usual sampling of seismograms, hardly any arrivals are expected.

Each additional design region however, influences the whole (f-k) plot in every point, thus showing the strong inter-dependence of all values with each other. A number of computational experiments showed that with fewer design regions values in non-overlapping regions are also better approximated. To show this effect, a symmetric and centro-symmetric pass-reject filter were computed for the following design parameters:

N=12; LF=13; ν=0.08; t_c=0.01; α=1; γ=1.1; τ_c=1.0; ϱ=1

The (f-k) diagrams of the symmetric and centro-symmetric filter are given in figure 7.2.6 and figure 7.2.7. Both diagrams may be compared with the one of filter number 3 which has the same design parameters without reject regions. It is seen that although there is increased rejection and a steeper escarpment for low frequencies, there is also an increased ripple in the plateaux of the pass region. Very high values are on the opposite side of the pass region across the reject region. Reject regions are in both cases nearly entirely depressed to -30dB. The ripple in the pass region of the symmetric filter falls into a range of 5dB, while the ripple for the centro-symmetric filter covers only a range of 3dB. All transfer functions for zero frequency are, for the symmetric case, about 6dB further

down than for the centro-symmetric.

Altogether the three examples were selected to emphasize that whenever two regions are sufficient for the design, centro-symmetric filters should be computed. They have superior characteristics over optimum multichannel velocity filters. Three different effects mainly account for this:

1. Less possible overlapping of pass with reject regions (example number 2).
2. Less possible overlapping of pass with pass regions (example number 3).
3. Less influence of one region on other regions which generally occurs without any overlapping (example number 4).

Computational experiments further show that approximations of expected pass and reject regions increase with the number of traces and the filter length. To give an example, in figure 7.2.8 the (f-k) plot of a six-trace filter with the design parameters of filter number 3 is shown. The contours should be compared with the ones of figure 7.1.2. The escarpment is in this case less steep and fewer hills in the reject region are higher. Nevertheless, the pass-regions in both cases are nearly equally good.

With the help of the above examples, it is seen how a more complex time window will influence the (f-k) plot. The more regions that are chosen in the time domain, the more they will interfere with each other in the (f-k) domain. One more feature of multichannel velocity filters which was constantly observed in the (f-k) diagram is worthwhile mentioning and is described as follows: Whenever reject regions with a high value for ϱ lie next to a pass region, they 'push' the pass region into parts of the (f-k)-diagram with fewer restrictions. This has already been seen with filter

number 8 and number 9, where the 'pushing effect' is especially strong for low frequencies. Figure 7.2.9 shows the (f-k) diagram of another centro-symmetric pass-reject filter. Here this effect may be well observed in the lower right corner of the basic section.

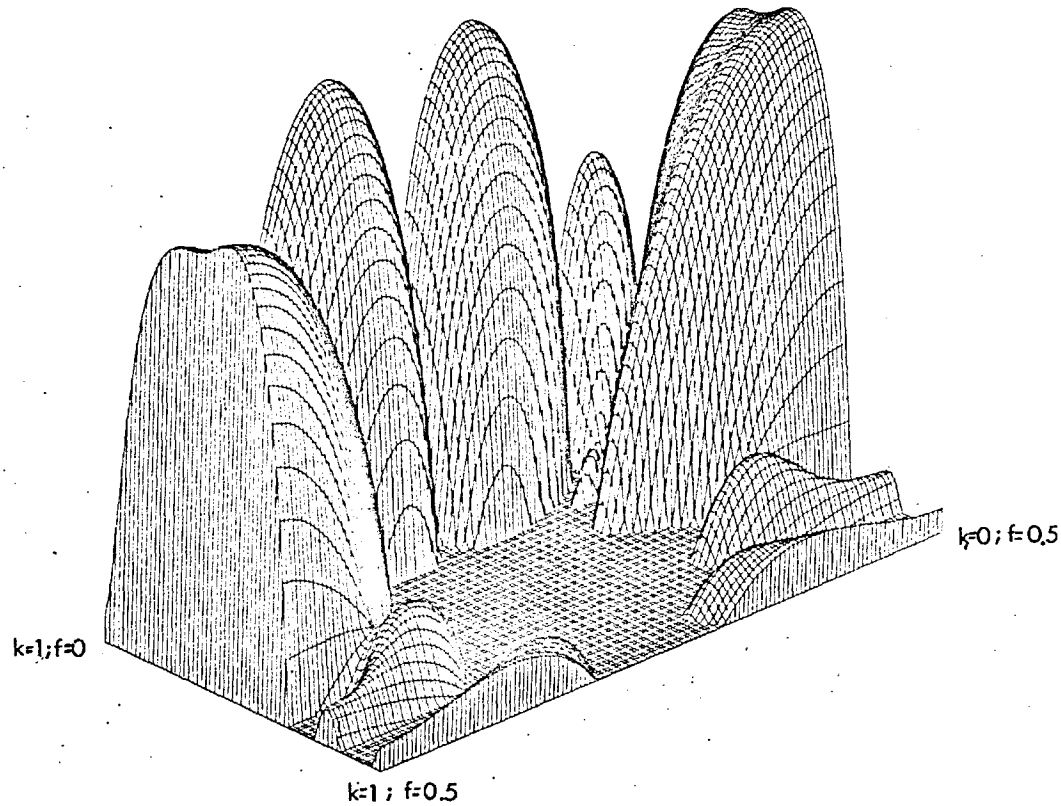

FIGURE 7.2.1 b Filter number 7

Isometric plot viewed from (f=0.5 ; k=1.0)

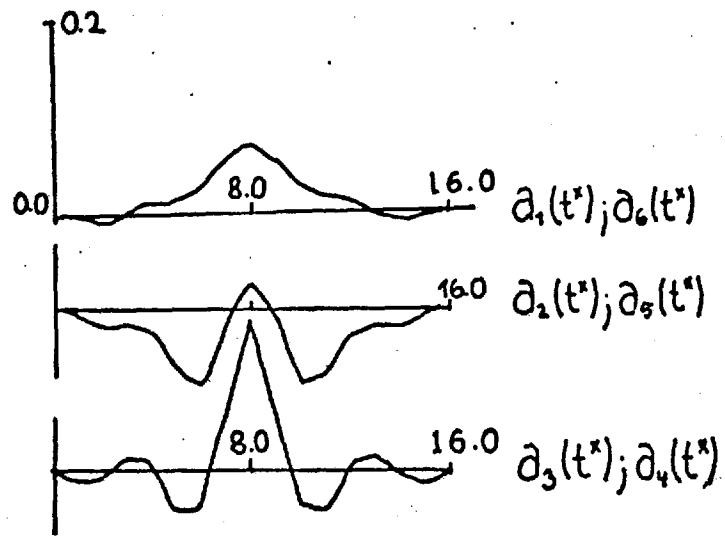

FIGURE 7.2.1 Filter number 7

Components of the stacking filter

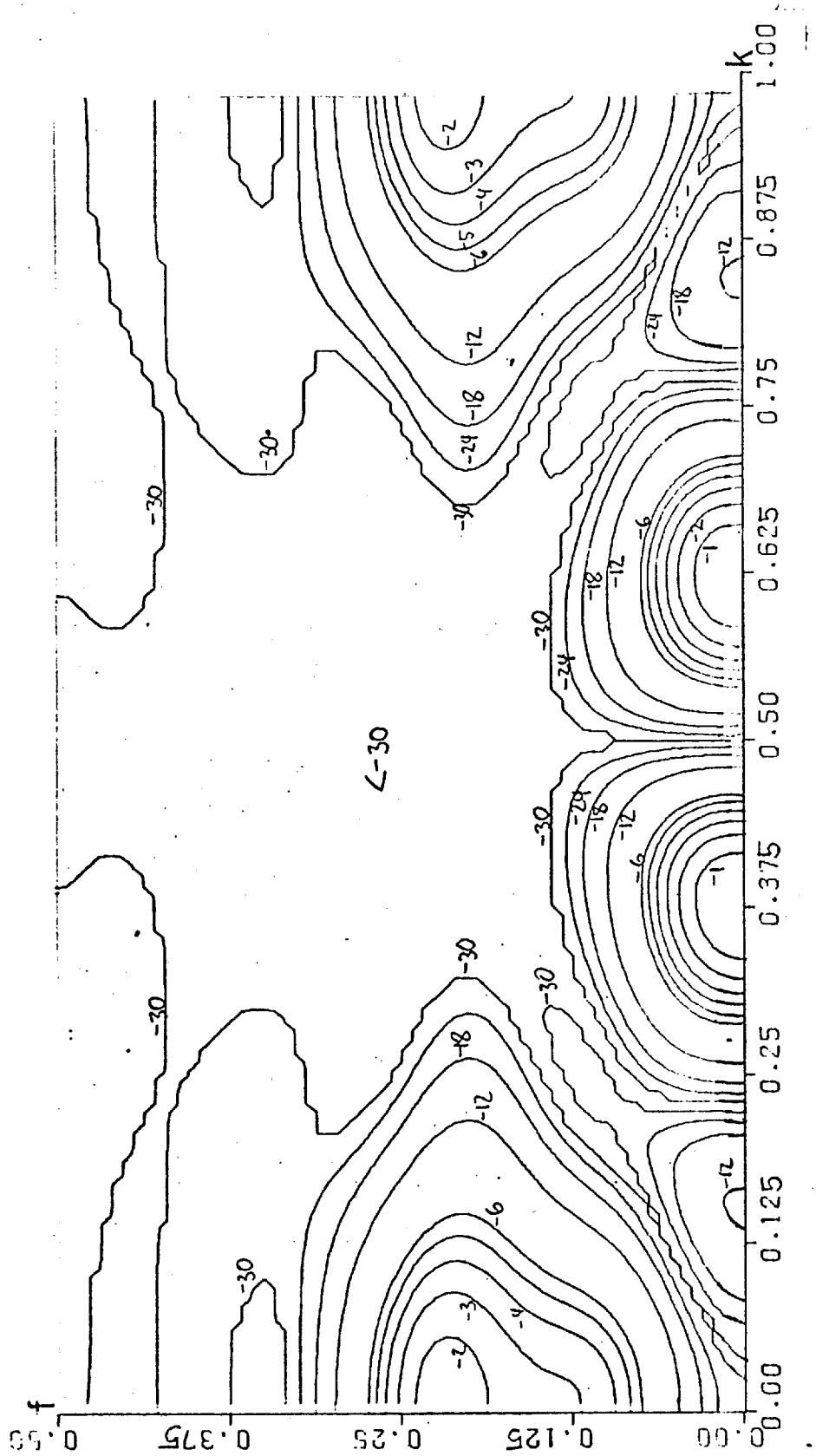

FIGURE 7.2.1. a Filter number 7:(f-k) plot

τ_c=0.8 ; α=2 ; γ=4 ; N=6 ; LF=17 ; ν=0.08 ; ϱ=30 ; t_c=0.01

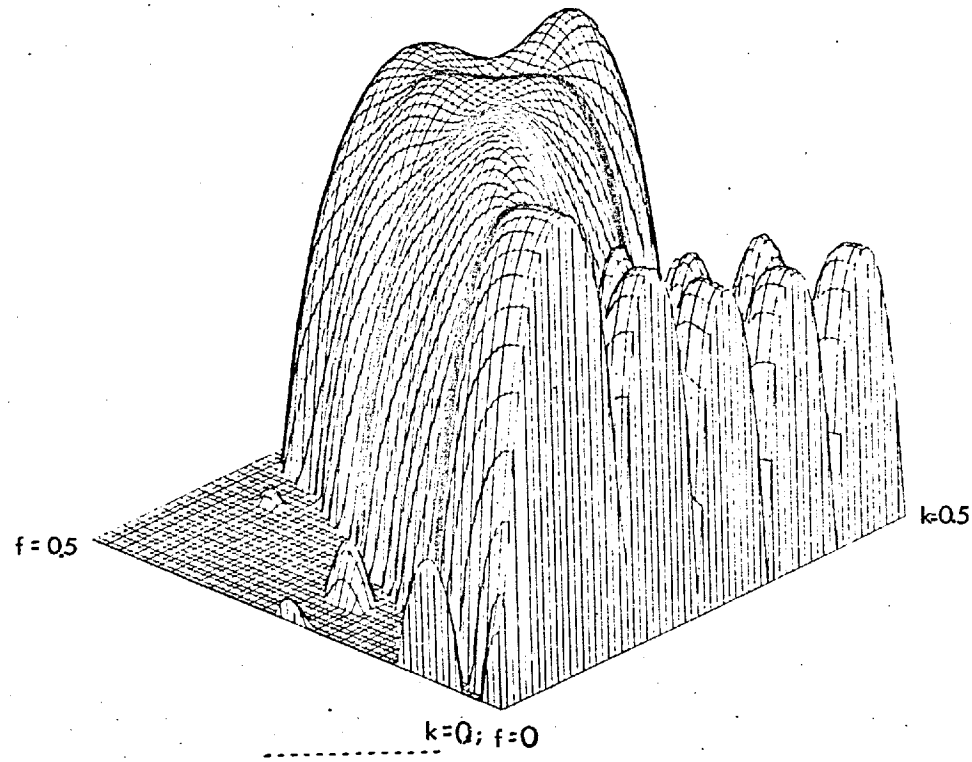

FIGURE 7.2.4 a Isometric plot

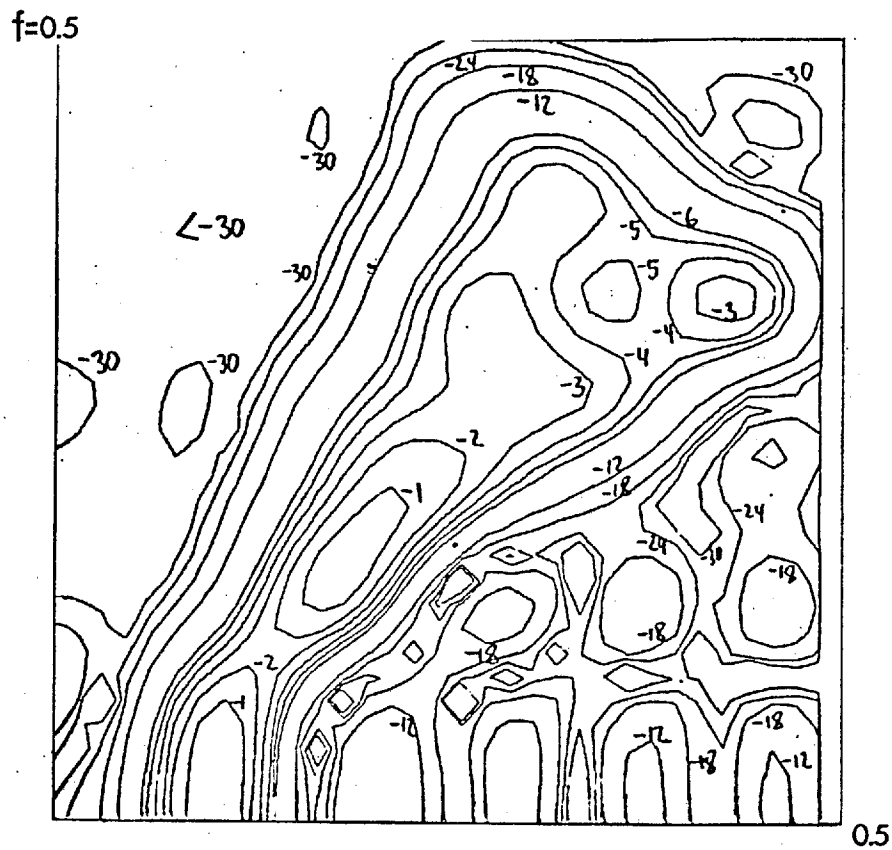

FIGURE 7.2.4 Filter number 8

(f-k) diagram τ_c=0.5 ; α=1.0 ; γ=3.0 ;

N=12 ; LF=19 ; ν=1.0 ; t_c=0.2; ϱ=30.

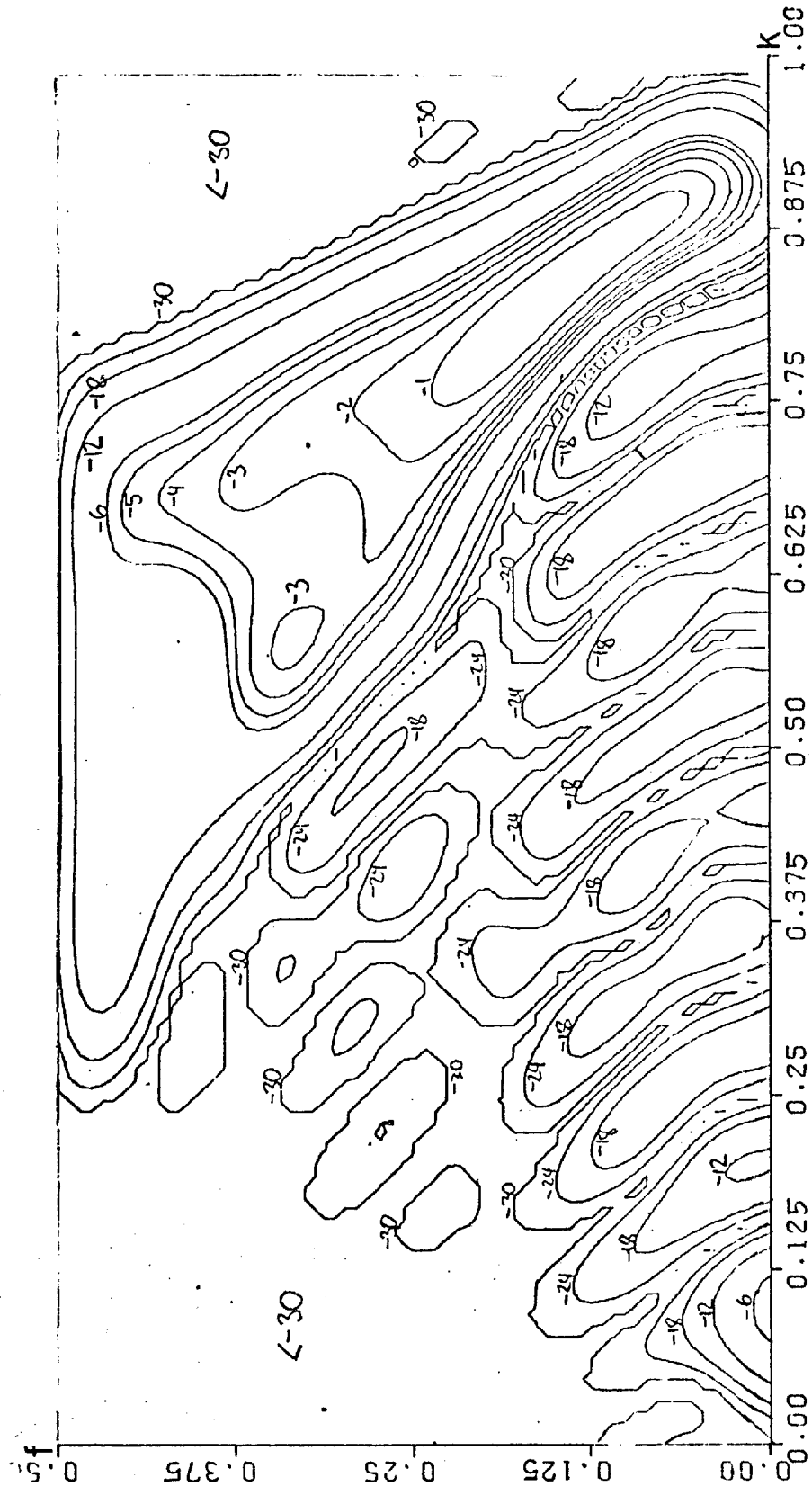

FIGURE 7.2.5 Filter number 9

(f-k) diagram

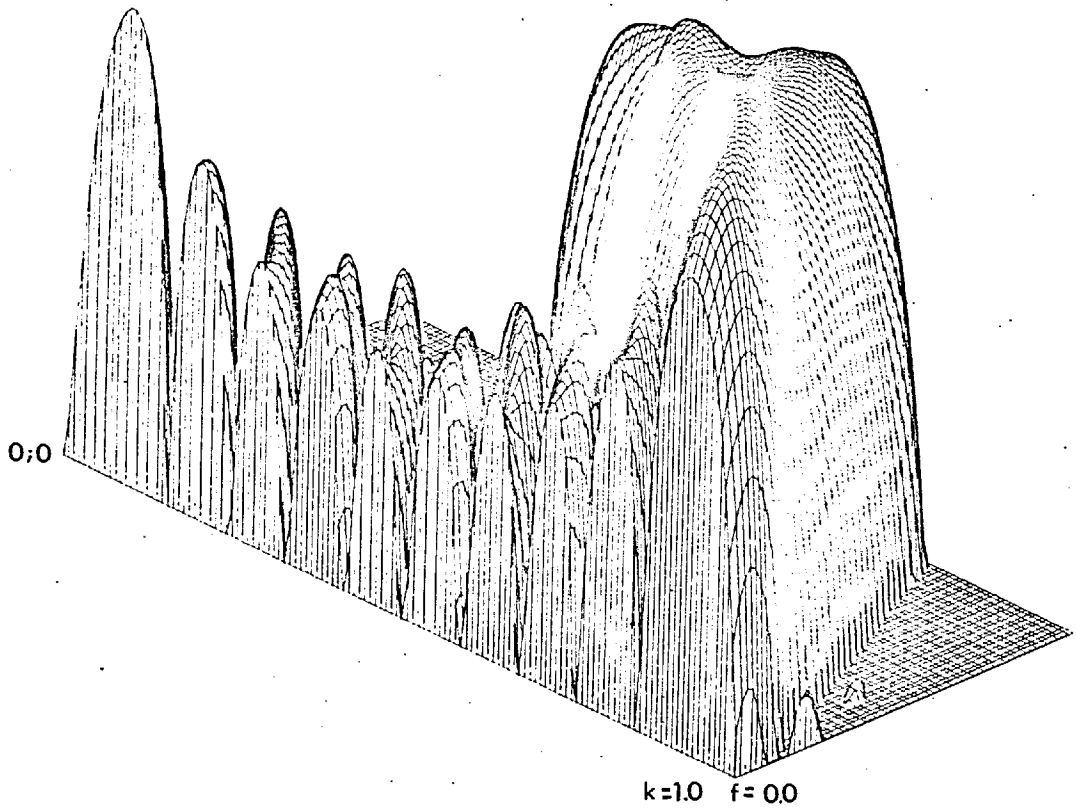

FIGURE 7.2.5 a Filter number 9

Isometric plot viewed from (k=1.0 ; f=0.0)

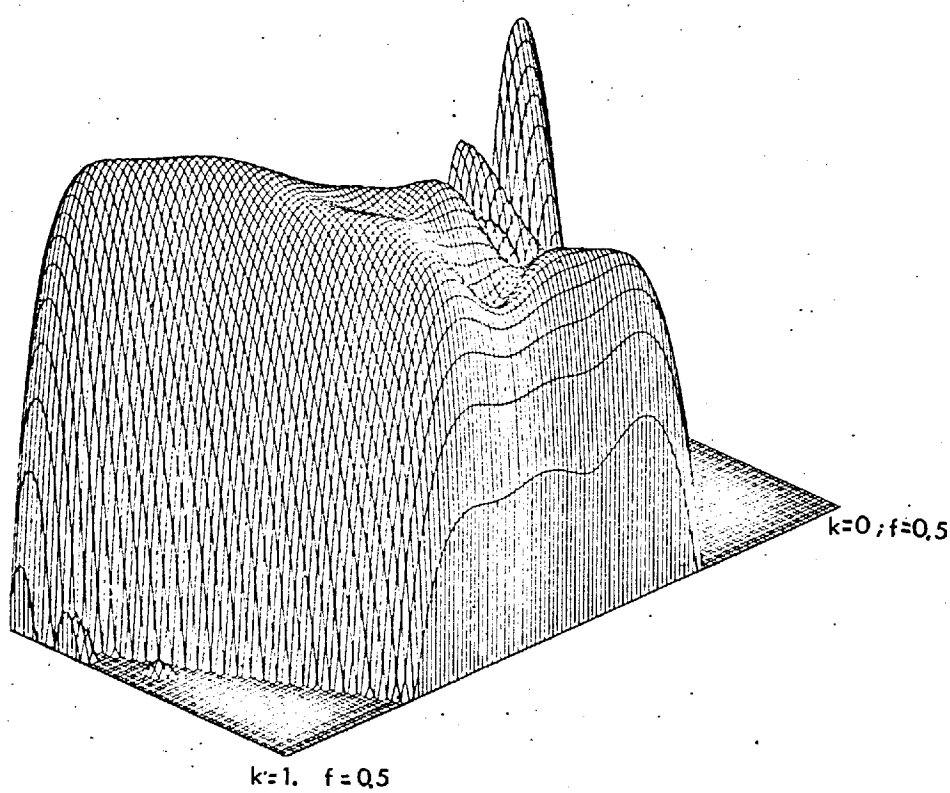

FIGURE 7.2.5. b Filter number 9

Isometric plot viewed from (k=1.0 ; f=0.5)

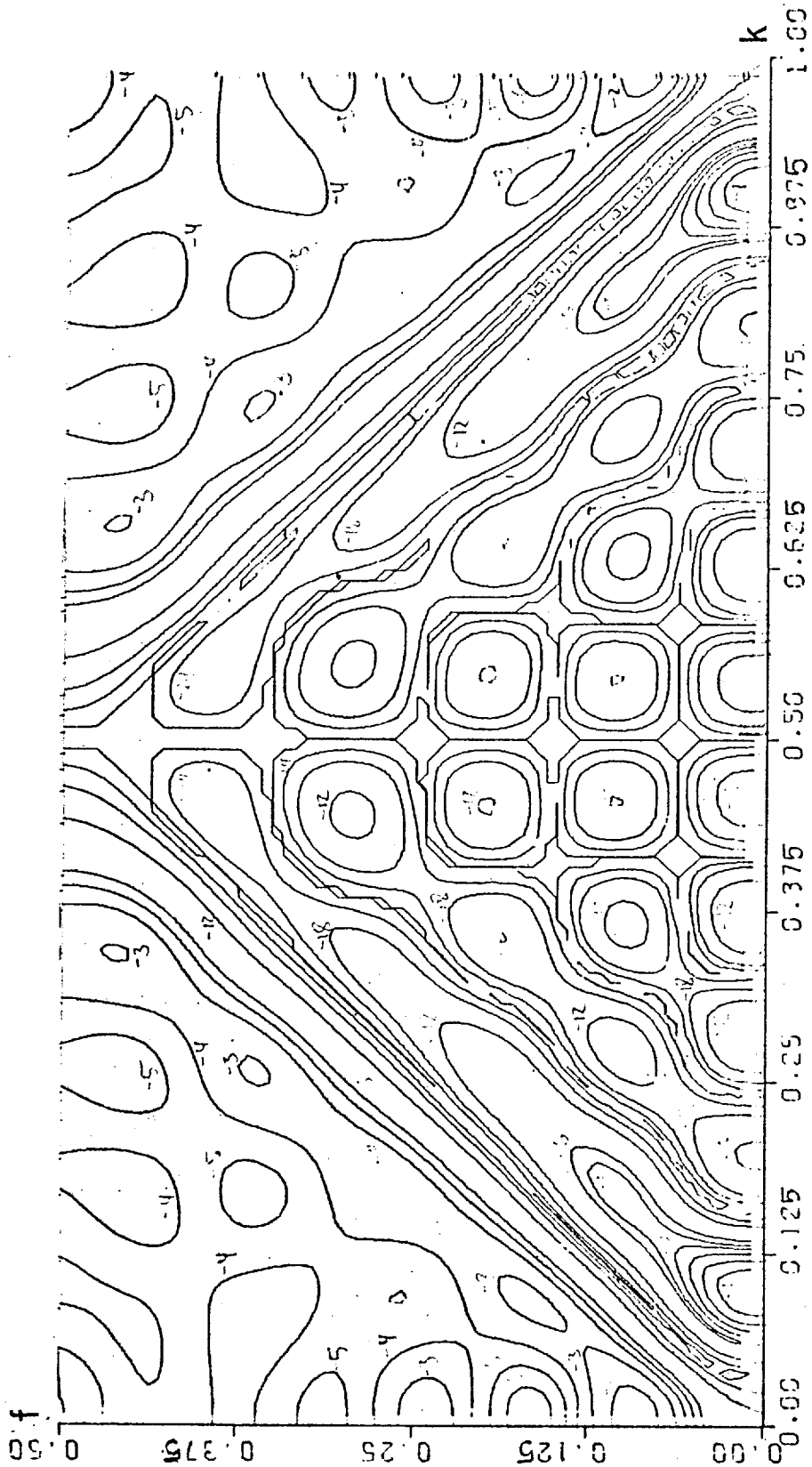

FIGURE 7.2.6 Filter number 10
(f-k) diagram

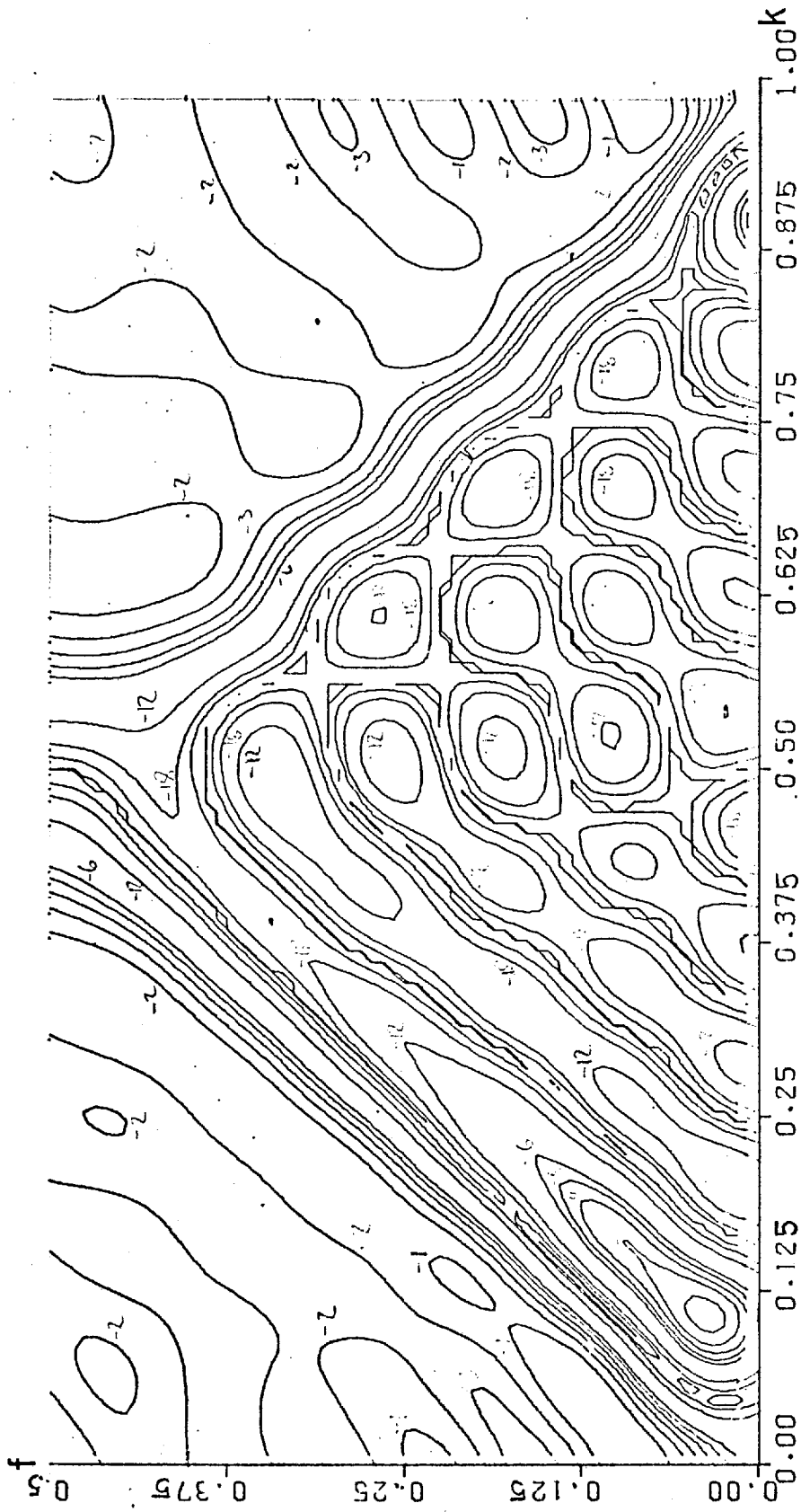

FIGURE 7.2.7 Filter number 11 (f-k) diagram

τ_c=1.0 ; N=12 ; LF=13 ; α=1.0 ; γ=1.1 ; ν=0.08 ; ρ=1.0 ; t_c=0.01

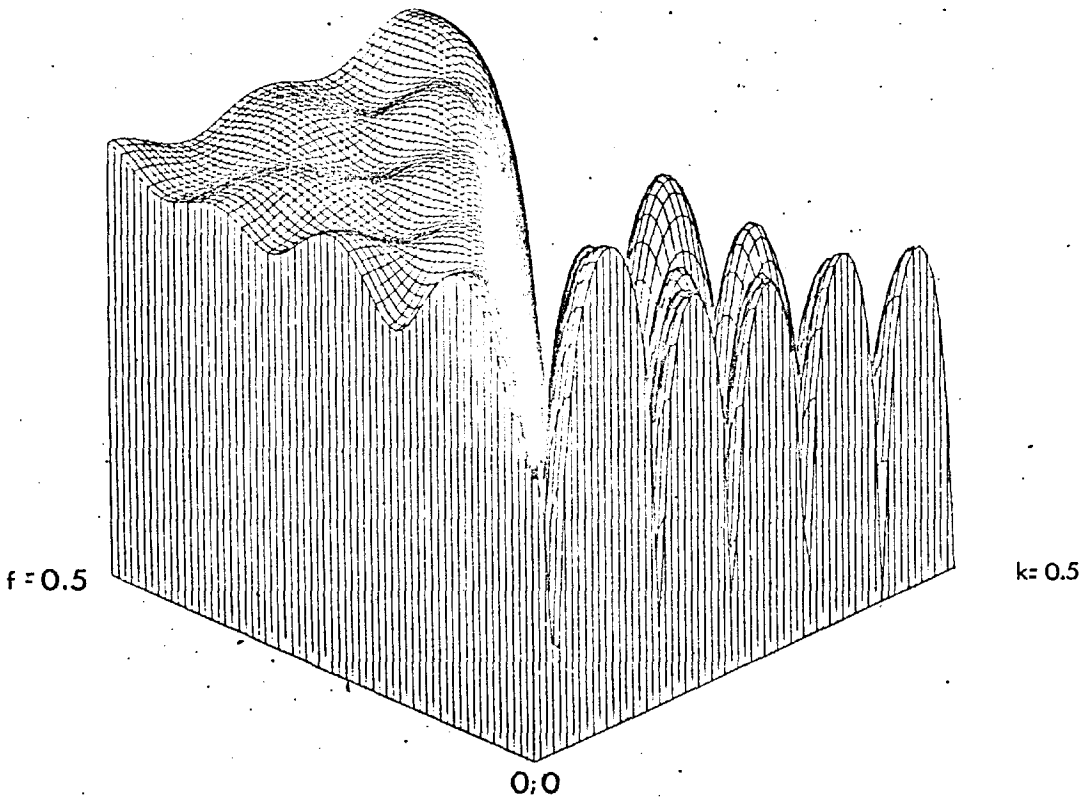

FIGURE 7.2.6 a Filter number 10
Isometric plot

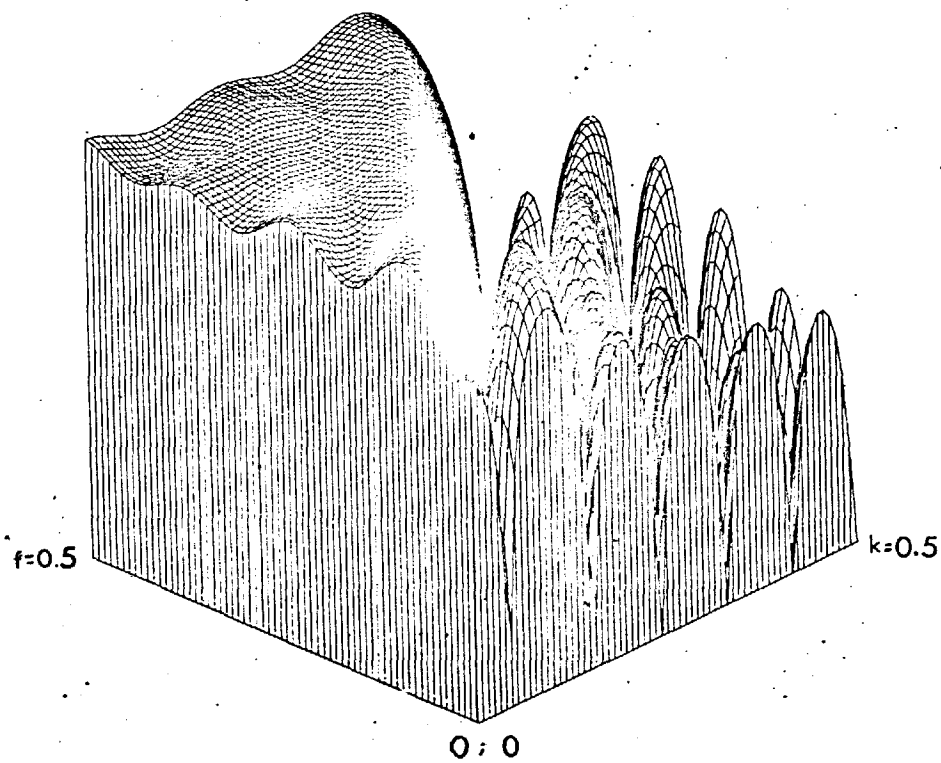

FIGURE 7.2.7. a Filter number 11
Isometric plot

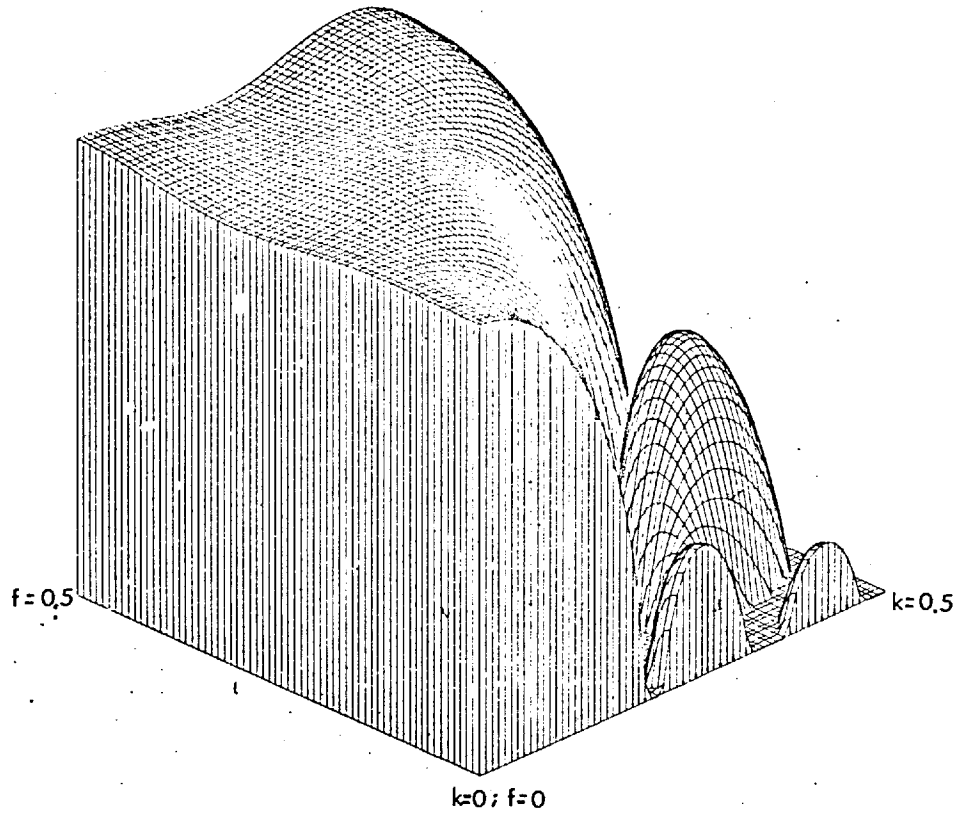

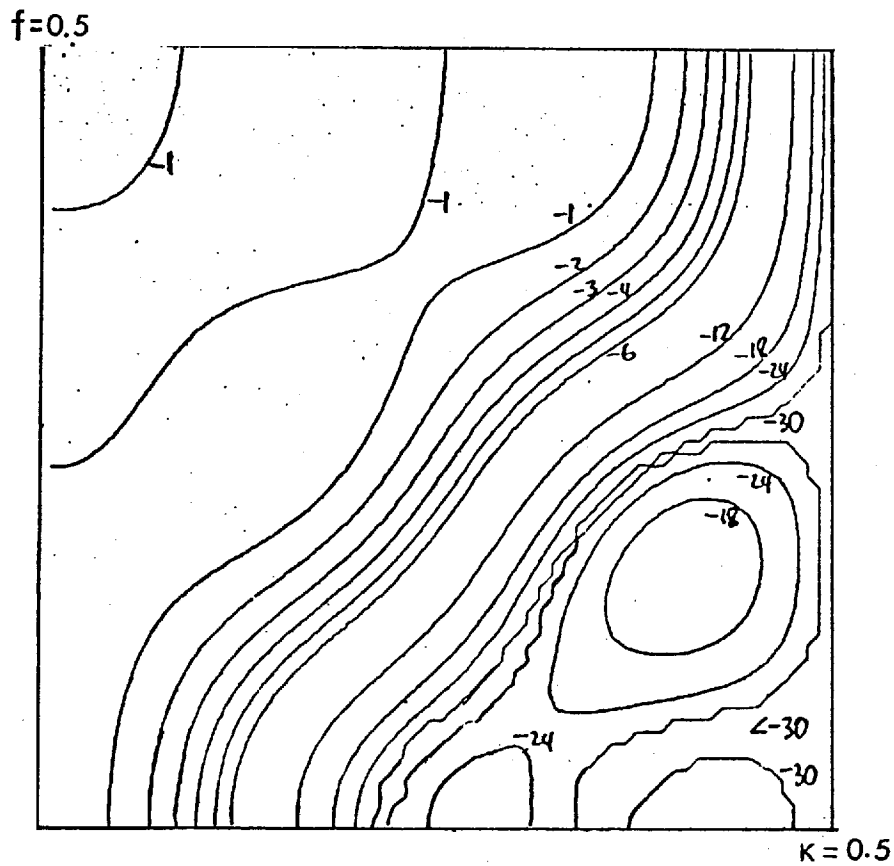

FIGURE 7.2.8 Filter number 12

(f-k) diagram and isometric plot

τ_c=1.0 ; N=6 ; LF=7 ; ν=0.08

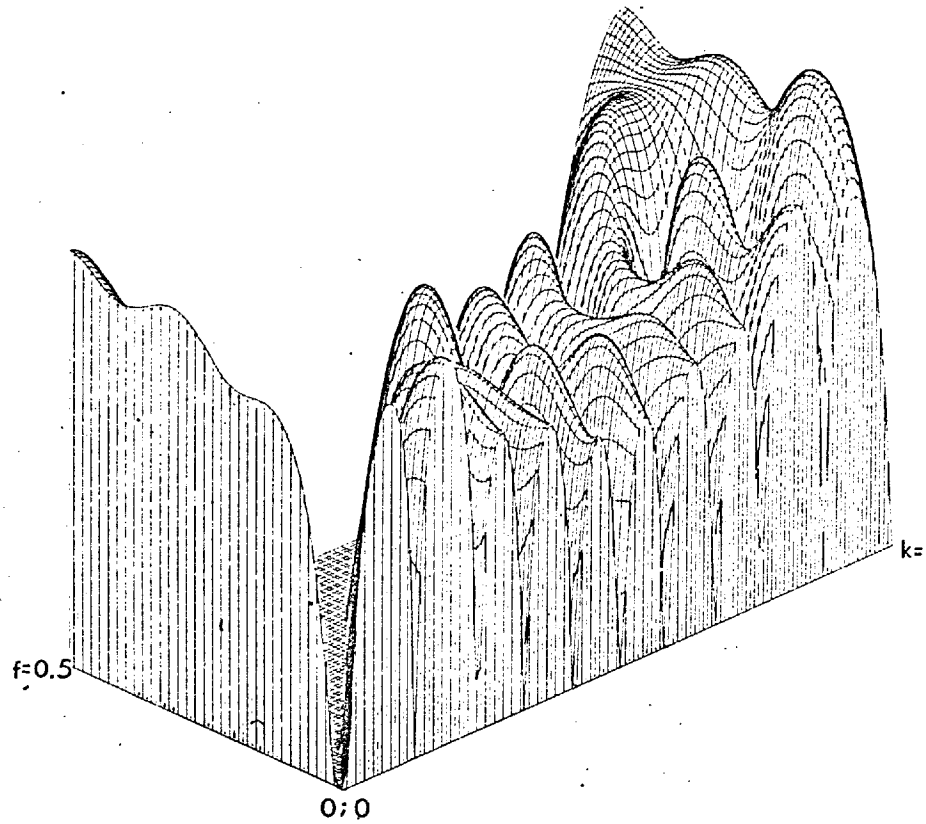

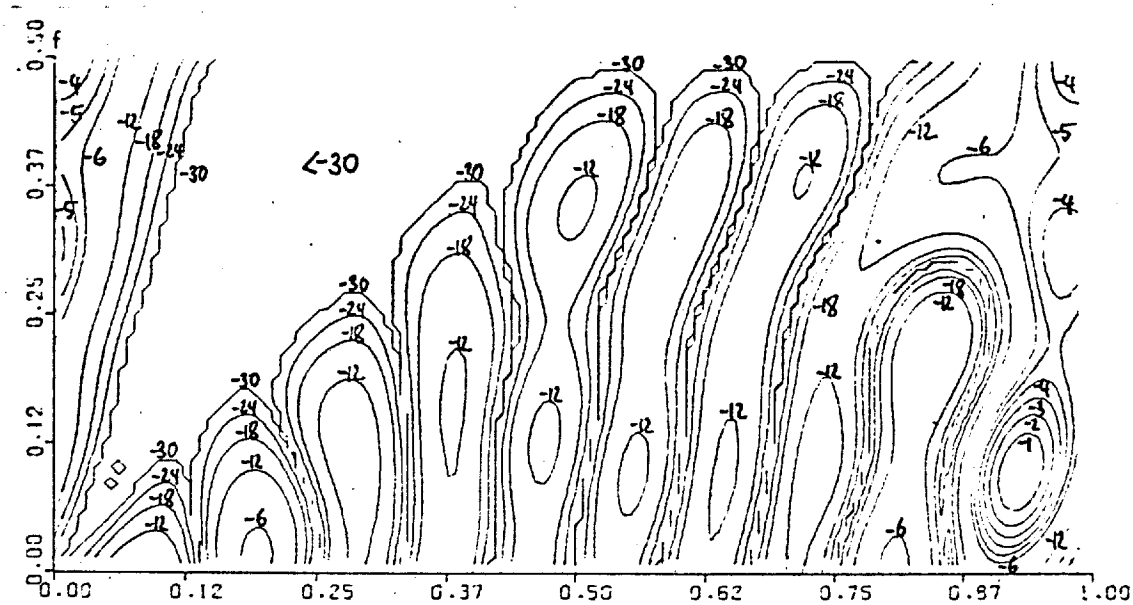

FIGURE 7.2.9 Filter number 13

(f-k) diagram of a pass- reject filter to show the pushing effect.

τ_c=0.25 ; α=1.0 ; γ=4.0 ; N=12 ; LF=11 ; ν=0.08 ; ρ=20 ; t_c=0.01

7.3 Characteristics of three-dimensional multichannel velocity filters

In section 5.1.3 it was shown how to specify certain time windows for traces recorded with a two-dimensional array. With these windows and the normal equations (4.2.4) three-dimensional stacking filters can be computed which will enhance or reject plane waves falling into a certain range (figure 5.1.3.1) with normal vectors lying in a plane. In this section some of these filters are computed and characterised. The three-dimensional Fourier transform is the appropriate tool for the characterisation of the filters. Transfer functions for three-dimensional filters are defined similar to the two-dimensional case.They are contained in the three-dimensional Fourier transform.Their phases depend on the window shape and centro-symmetric or symmetric windows should again be chosen to keep phase properties simple. These time windows are the ones which, due to the shortest possible length of all corresponding time windows, also lead to the fastest convergence of filters.

Let $a_i(t^*)(i=1,..,N_xN_y;-n\leq t^*\leq m)$ be the components of the stacking filter for the two-dimensional recording array of figure 5.1.3.1. Without loss of generality N_x and N_y are chosen to be odd so that the centre of the recording array falls together with the recording position of the centre trace. For reasons of simplicity, the traces and filter components are re-numbered by giving each detector position the two indices i, j. With $N1 = (N_x-1)/2$ and $M1 = (N_y-1)/2$ one may write

$$a_{-N1,-M1}(t^*)=a_1(t^*);\quad a_{-N1+1,-M1}(t^*)=a_2(t^*);\quad \ldots\ a_{0,0}(t^*)=a_{(N_xN_y+1)/2}(t^*)$$

$$\ldots\ a_{N1,M1}(t^*) = a_{N_xN_y}(t^*)\ .$$

Let
$$f_\alpha(t^*) = \sum_{i=-N1}^{N1}\sum_{j=-M1}^{M1} a_{ij}(t^*)*\mathrm{sinc}(t^*-\alpha_{ij}) \qquad (7.3.1)$$

be the response and $$F_{\alpha}(f) = \sum_{i=-N1}^{N1} \sum_{j=-M1}^{M1} A_{ij}(f) e^{-2\pi i f \alpha_{ij}} \qquad (7.3.2)$$

the transfer function for broad band signals with moveout α_{ij}. If the moveout belongs to a plane wave

$$\alpha_{ij} = \tau_x i + \tau_y j, \quad (|i| \leq N1; \quad |j| \leq M1)$$

the transfer function becomes

$$F(f,\tau_x,\tau_y) = \sum_{i=-N1}^{N1} \sum_{j=-M1}^{M1} A_{ij}(f) e^{-2\pi i f(\tau_x i + \tau_y j)} \qquad (7.3.3)$$

Because the three-dimensional Fourier transform can be expressed as

$$F(f,k_x,k_y) = \sum_{\tilde{l}=-n}^{m} \sum_{i=-N1}^{N1} \sum_{j=-M1}^{M1} a_{ij}(\tilde{l}) e^{-2\pi i(f\tilde{l} - k_x i - k_y j)}$$

$$= \sum_{i=-N1}^{N1} \sum_{j=-M1}^{M1} A_{ij}(f) e^{2\pi i(k_x i + k_y j)} \qquad (7.3.4)$$

one may find the transfer function (7.3.3) from it along the line: $k_x = -f\tau_x$; $k_y = -f\tau_y$ in the range $|f| \leq \frac{1}{2}$. k_x, k_y is known as the vector wave number (Burg, 1964). One may again reverse the order of the filter (see (6.2.13)) to obtain the transfer function along $k_x = f\tau_x$; $k_y = f\tau_y$ For symmetric and centro-symmetric time windows the transfer functions for all possible plane waves have zero phase due to equation (6.2.10). The basic region of the three-dimensional Fourier transform of a real sampled three-dimensional operator is given in figure 7.3.1. The transfer function of the stacking filter for a plane wave characterised by $\tau_x = a$ and $\tau_y = b$ is obtained along the line A. In the case where $a>1$ or $b>1$, the line $k_x = fa$; $k_y = fb$ runs through additional blocks of the same basic type which repeat periodically in the k_x and k_y direction.

In the rest of this section some examples are discussed. The recording pattern of figure 7.3.3 is given with $N_x=5$ and $N_y=4$.

For a three-dimensional pass filter the parameters $\tau_x=1, \Delta\tau_x=-2, \tau_y=1, \Delta\tau_y=-2$ are chosen for the pass region. The additional design parameters are specified as LF = 7, ν = 0.08 and t_c = 0.01. The resulting symmetric time window for the twenty traces is shown in figure 7.3.2. Due to the high symmetry of this window the computed stacking filter contains only four different responses. These are given in table 7.3.1. Figure 7.3.2 shows the traces to which they have to be applied. Figure 7.3.5 gives the expected response of the polarisation filter in the basic range of the three-dimensional Fourier transform. Both figure 7.3.2 and figure 7.3.5 are again logically connected with the help of the defined concept of the stacking filter transfer function. Figure 7.3.4 shows the three-dimensional Fourier transform of the computed stacking filter. To simplify the presentation, horizontal layers (for fixed frequencies) of this transform are given. The contours of a filter (number 15) with the above parameters, however, with N_x = 4 and N_y = 3 are shown in figure 7.3.8. The pass regions are broader in this second case. This example was selected to show that the approximation of the desired characteristics increases with the size of the array. All transfer functions also start with no rejection for zero frequency, a feature already observed for two-dimensional optimum multichannel velocity pass filters.

A straight forward three-dimensional stack (all traces of the two-dimensional array are added) has also a three-dimensional Fourier transform. It is independent of the frequency. Any horizontal cut through the basic region of a 5x4 recording array is given in figure 7.3.9, one for a 11 x 11 array in figure 7.3.10. The straight forward three-dimensional stack passes perfectly plane waves, which fall perpendicularly on the array from below. The selection of these waves from others coming in with certain angles increases with the number of detectors in the array.

One might think that detectors should be placed on all grid points of a rectangular array, but this is not necessary . The given time domain design is very flexible to compute filter components for any kind of array. It must be generally emphasized that detector positions can have arbitrary spacing among each other. It is only necessary for the characterisation of the filter with the discrete Fourier transform that their coordinates should fall on grid inter-sections. Below is the design of filter number 16, which is expected to have the desired pass characteristic of figure 7.3.5 where however, detectors are placed on the cross of figure 7.3.6. The time window for this array has to be specified as shown in figure 7.3.7. The obtained stacking filter components $a_1(t^*)$ to $a_5(t^*)$ and $a_{10}(t^*)$ are given in table 7.3.2 and the three-dimensional Fourier transform is shown in figure 7.3.11. Filter number 16 no longer acts as a polarisation filter for the selected direction. The characteristics approximate very well to what one would expect for a general three-dimensional velocity filter where plane waves are to be passed with normal vectors falling within an inverted pyramid instead of on a plane.

The desired polarisation filter characteristics of the cross-shaped array are far better approximated if plane waves are to be selected whose direction of propagation falls together with the direction of one branch of the cross. To give an example for this case, again the detector positions of figure 7.3.6 are used. This time, however, plane waves are to be filtered whose three-dimensional transfer diagram is given in figure 7.3.12. The time window is shown in figure 7.3.13. The three-dimensional transform of the stacking filter (number 17) obtained is presented in figure 7.3.18. Transfer characteristics for this case approximate very well the desired ones.

It is clear from the last two examples that an array may have good polarisation properties in one direction and less good characteristics in another direction. Optimizing a three-dimensional filter for a

given design region and fixed detector positions does still not result in an absolute optimum for a given number of detectors where their position has to be included in the design as well. It is generally possible to minimize the mean square error with respect to both filters and seismometer locations (Burg, 1964) . This leads to non-linear equations which are difficult to solve. A semi-practical approach, where responses are computed for various detector positions would however, be very helpful. This certainly very interesting line of further research is not followed in this work.

To complete this section two more examples of polarisation filters are discussed. The recording array for both cases is given in figure 7.3.15. This array has the advantage that due to its high symmetry, a computed filter can be applied four times by simply interchanging the filter components in a circular way. Four directions can then be easily scanned with only one set of filters. For the first example the desired transfer characteristic in the (f,k_x,k_y) domain is the one of figure 7.3.5. The time window of the pass region is given in figure 7.3.16 . Additional design parameters are N = 21; LF = 11; ν = 0.5. The three-dimensional Fourier transform is shown in figure 7.3.19. Characteristics are comparable approximately with filter number 14 (fig.7.3.4). There are, however, high values throughout the middle of the basic region. Filter number 19 provides the second example where filter number 18 is supplemented by allowing an additional reject region (figure 7.3.14) in the design. The weighting factor for the correlated noise is ϱ = 1. The time window for the reject region is given in figure 7.3.17. In the (f,k_x,k_y) space there is both a pass and reject region simultaneously along the line $k_x = k_y = 0$. The pass region in figure 7.3.20 is shifted into a region with no constraints. This typical feature was already observed with two-dimensional multichannel velocity filters. One may also notice that high values may be encountered in regions which were not included in the design. Rejection increases with

increasing the weighting factor ϱ of the noise. Figure 7.3.21 shows the characteristics for the last example (filter number 20), where ϱ =20.

One may generally conclude, that features of two-dimensional multichannel velocity filters can be observed in a similar way in the three-dimensional case. Uncorrelated noise in the design depresses the high frequency content. Overlapping of regions may occur. The more regions that are used in the design, the greater may be their interference in the (f, k_x, k_y) domain.

a_1 (t*)	a_2 (t*)	a_3 (t*)	a_4 (t*)
0.0097	0.0054	-0.0041	-0.0023
-0.0214	0.0239	-0.0054	-0.0022
0.0063	-0.0128	0.0344	-0.0200
-0.0060	-0.0023	0.0022	0.1247
0.0063	-0.0128	0.0344	-0.0200
-0.0214	0.0239	-0.0054	-0.0022
0.0097	0.0054	-0.0041	-0.0023

TABLE 7.3.1 Stacking filter components of filter number 14

a_1 (t*)	a_2 (t*)	a_3 (t*)	a_4 (t*)	a_5 (t*)	a_{10}(t*)
0.0086	0.0022	-0.0062	0.0097	-0.0219	0.0409
-0.0046	0.0134	-0.0013	-0.0058	-0.0073	0.0236
-0.0150	0.0080	0.0181	-0.0159	-0.0096	0.0201
0.0003	-0.0055	0.0145	0.0193	-0.0344	0.0263
0.0046	-0.0047	-0.0028	0.0249	0.0423	-0.0227
0.0044	-0.0044	-0.0015	-0.0031	0.1323	0.0466
0.0046	-0.0047	-0.0028	0.0249	0.0423	-0.0227
0.0003	-0.0055	0.0145	0.0193	-0.0344	0.0263
-0.0150	0.0080	0.0181	-0.0159	-0.0096	0.0201
-0.0046	0.0134	-0.0013	-0.0058	-0.0073	0.0236
0.0086	0.0022	-0.0062	0.0097	-0.0219	0.0409

TABLE 7.3.2 Stacking filter components for filter number 16

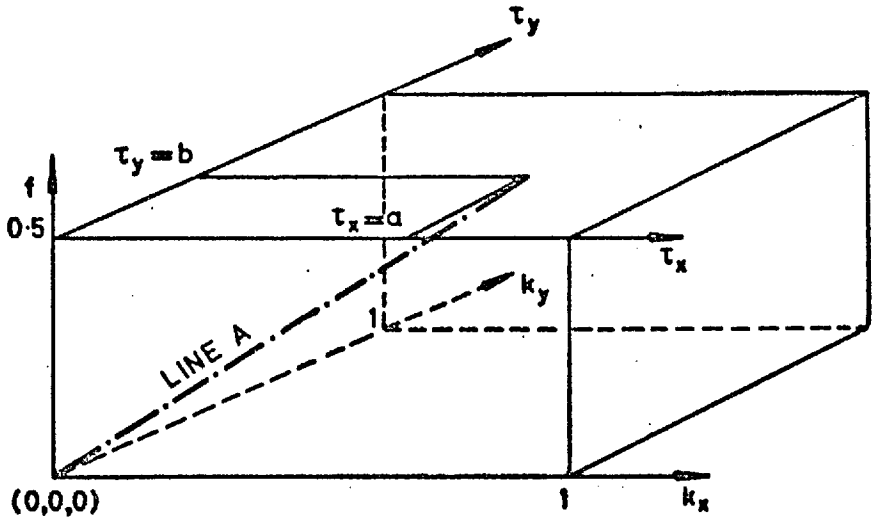

FIGURE 7.3.1 Basic region of the three-dimensional discrete Fourier transform

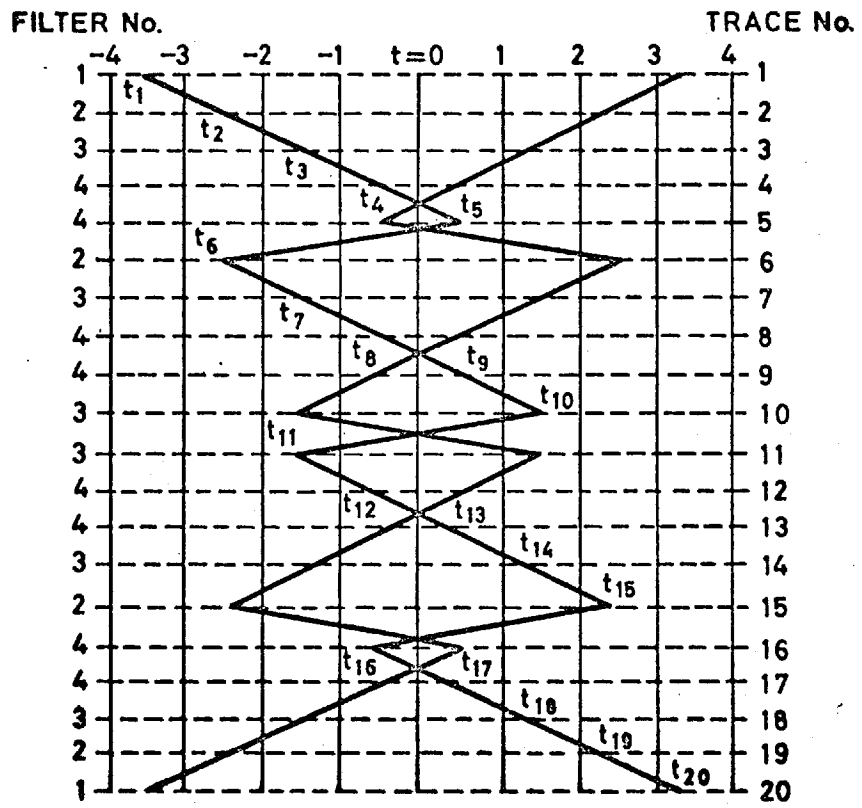

FIGURE 7.3.2 Filter number 14 Time window

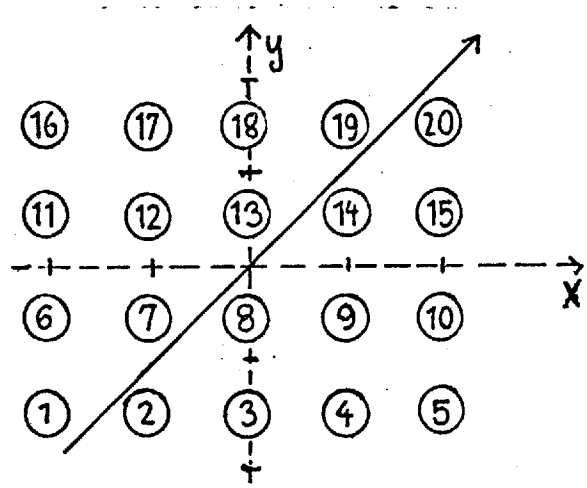

FIGURE 7.3.3 Recording array for filter number 14

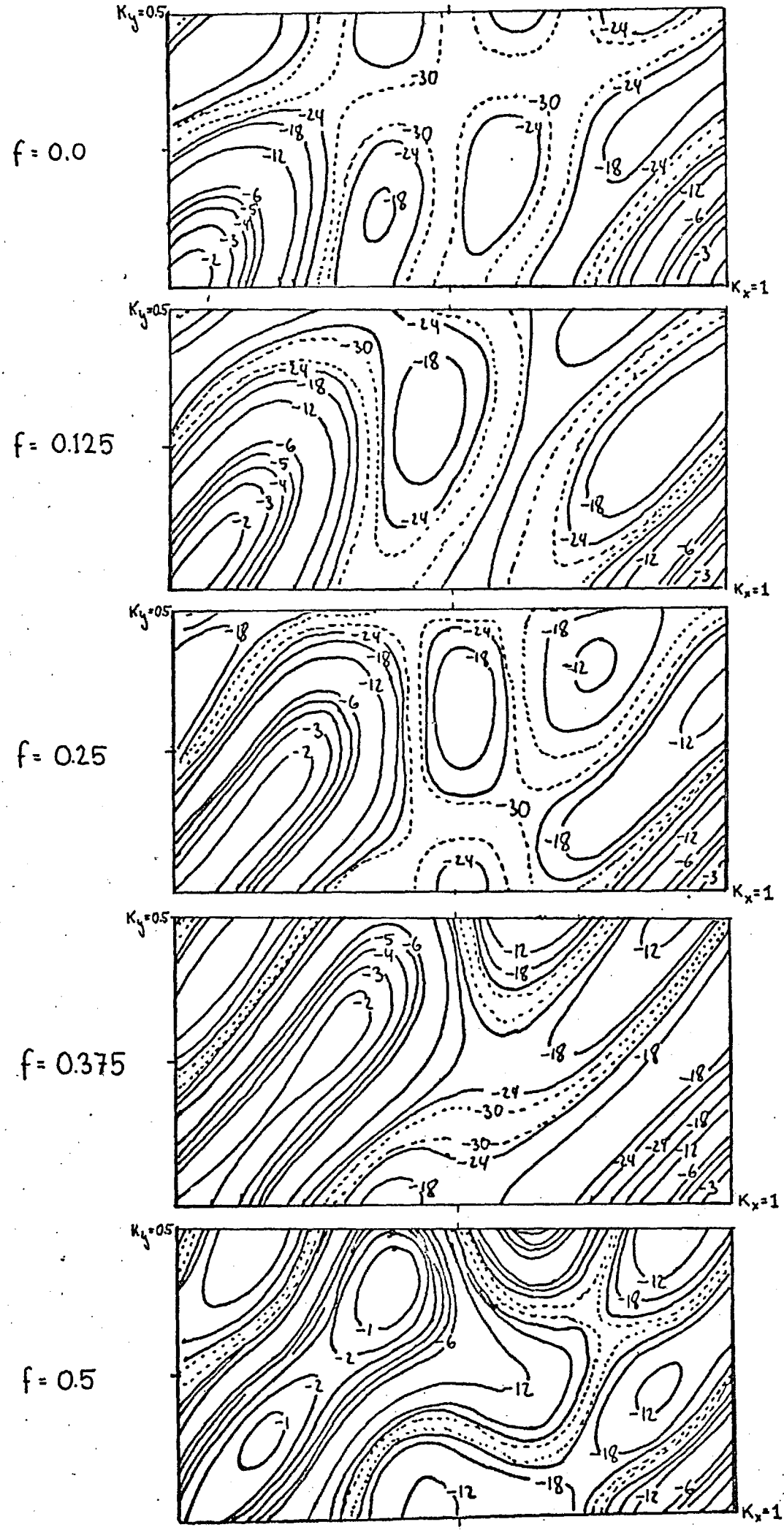

FIGURE 7.3.4 Filter number 14 (f,k_x,k_y) diagram

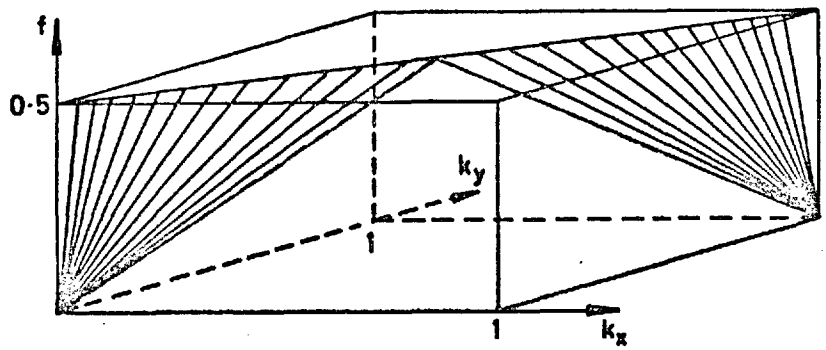

FIGURE 7.3.5 (f,k_x,k_y) diagram

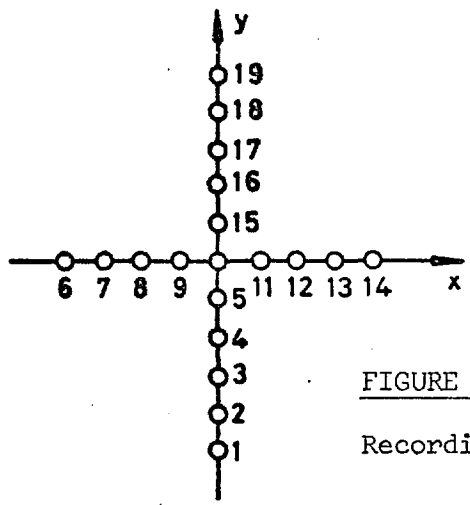

FIGURE 7.3.6

Recording array

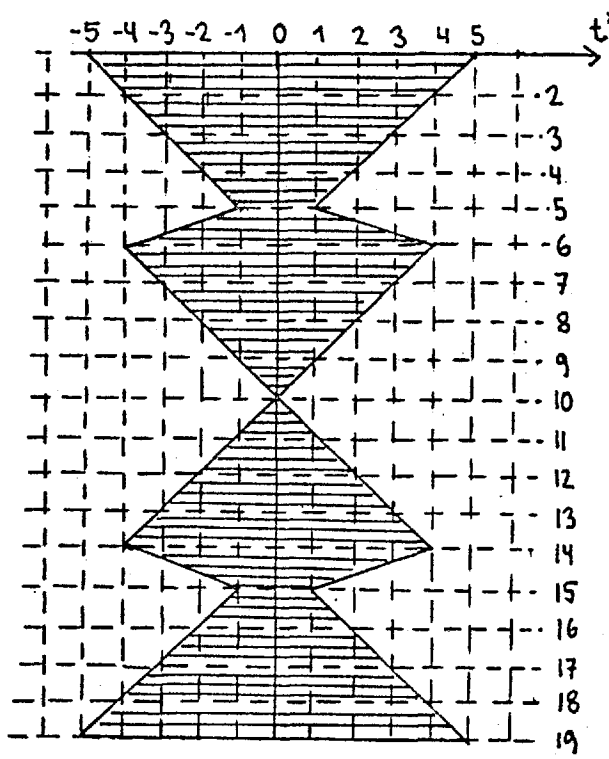

FIGURE 7.3.7

Time window

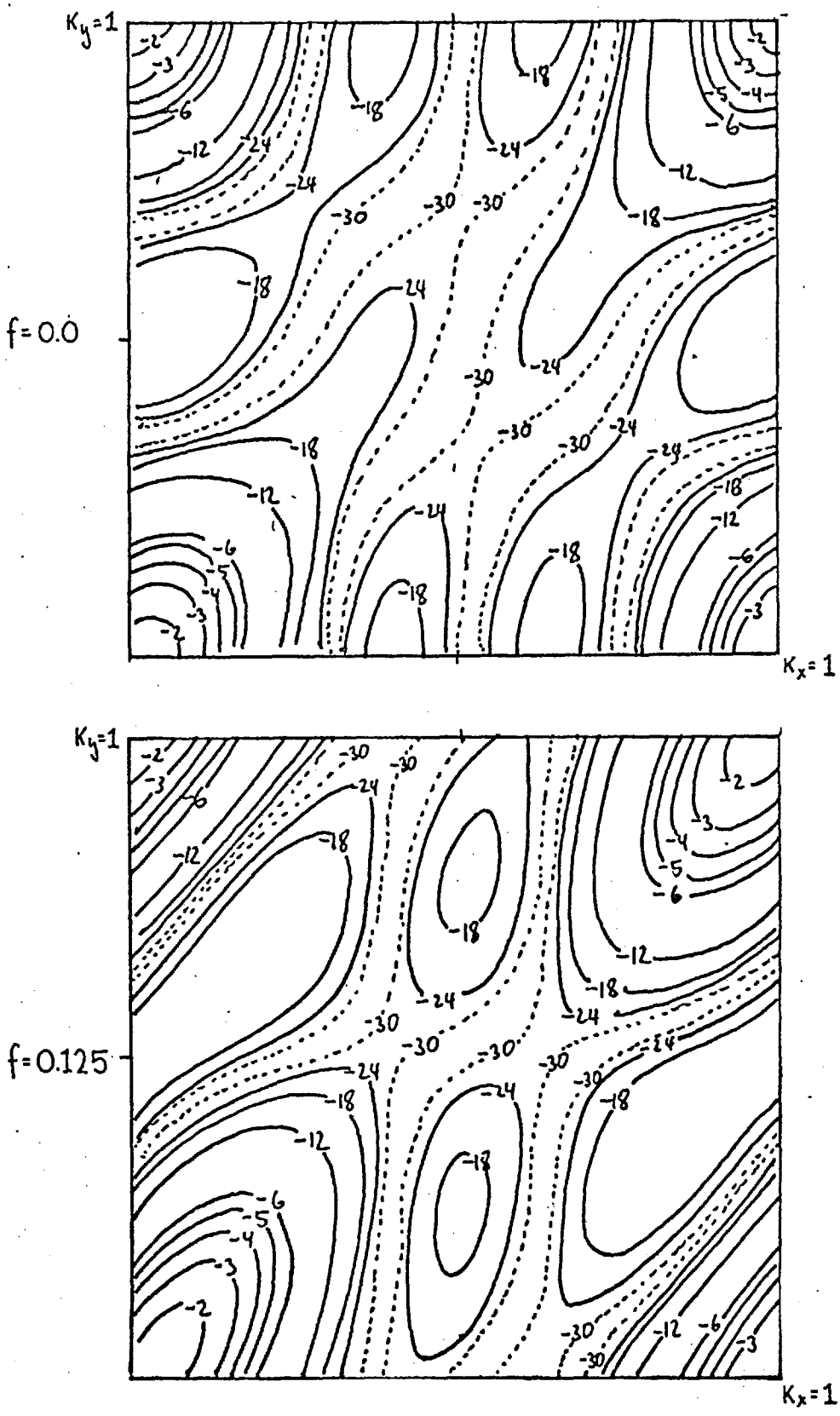

FIGURE 7.3.8 Filter number 15

(f,k_x,k_y) diagram (continued on next page)

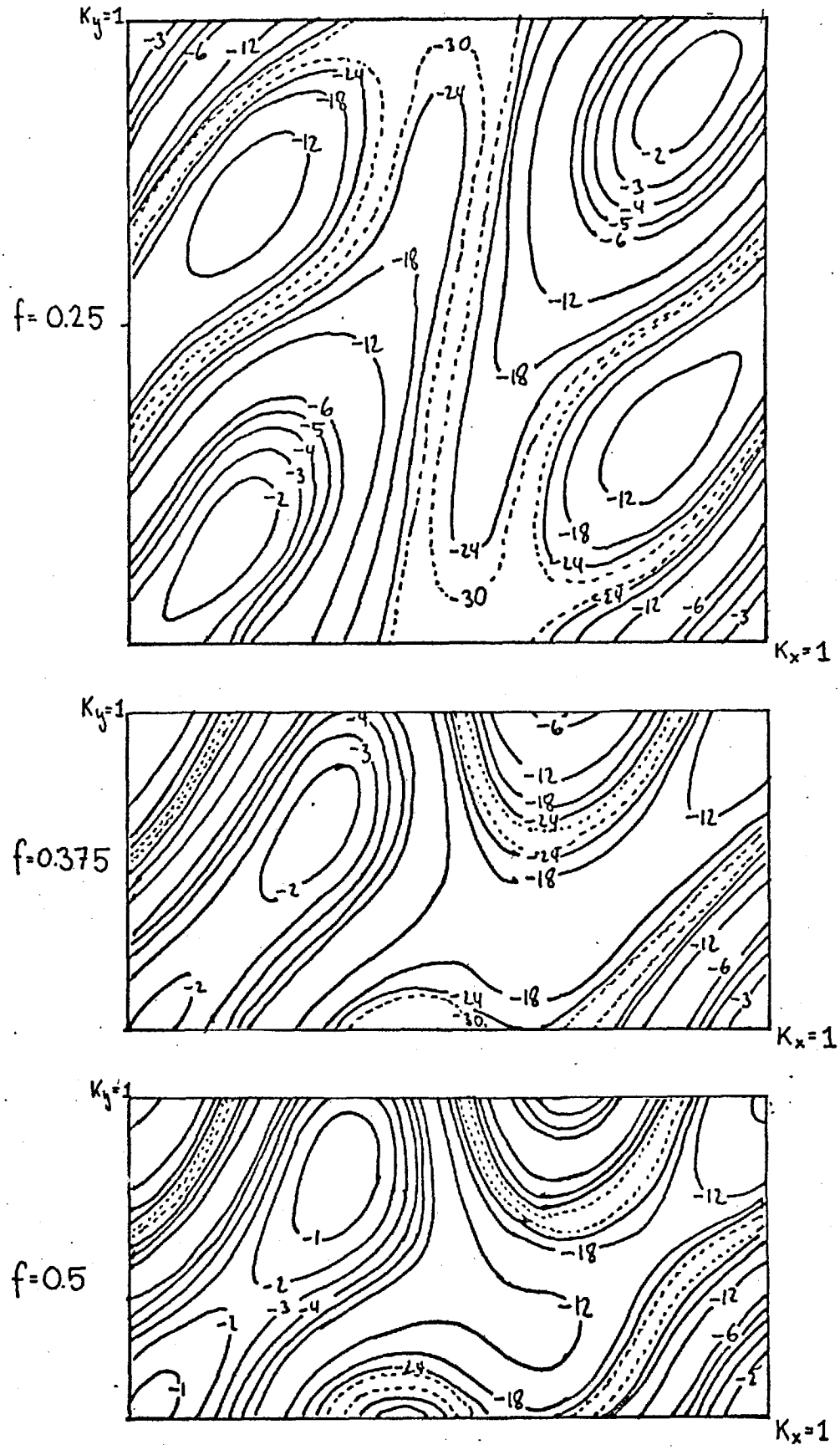

FIGURE 7.3.8 Filter number 15

(f,k_x,k_y) diagram (continuation from previous page)

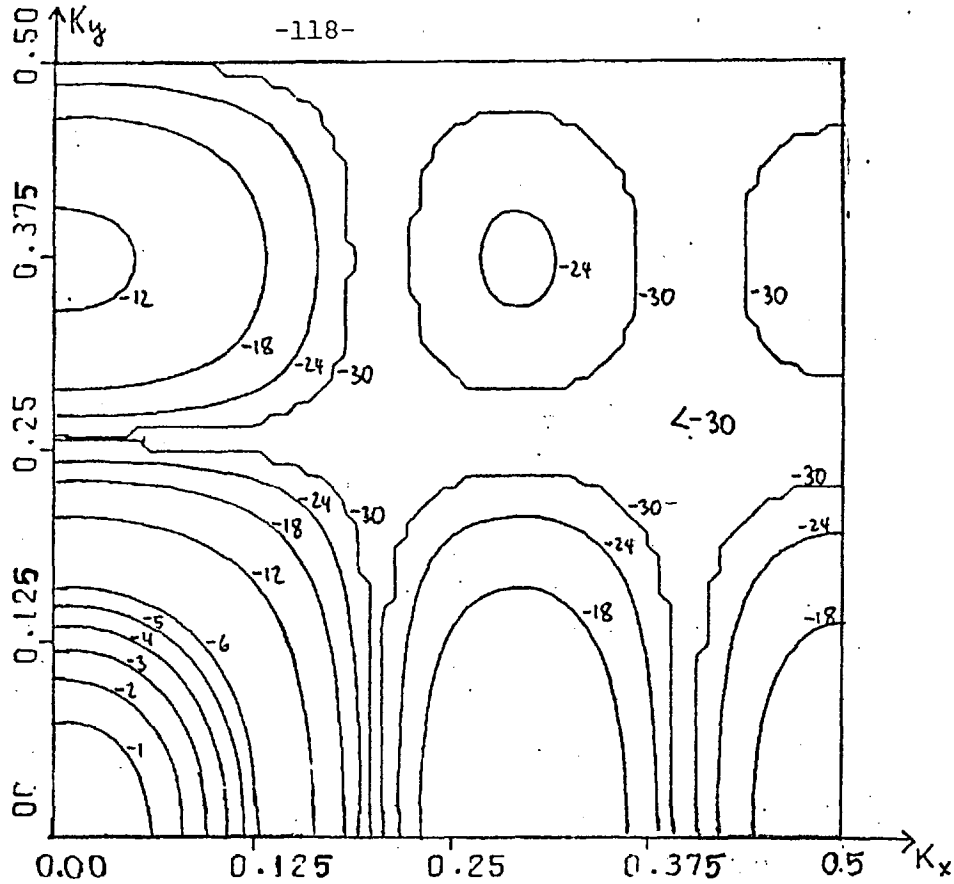

FIGURE 7.3.9 (k_x-k_y) plane for a 5x4 recording array

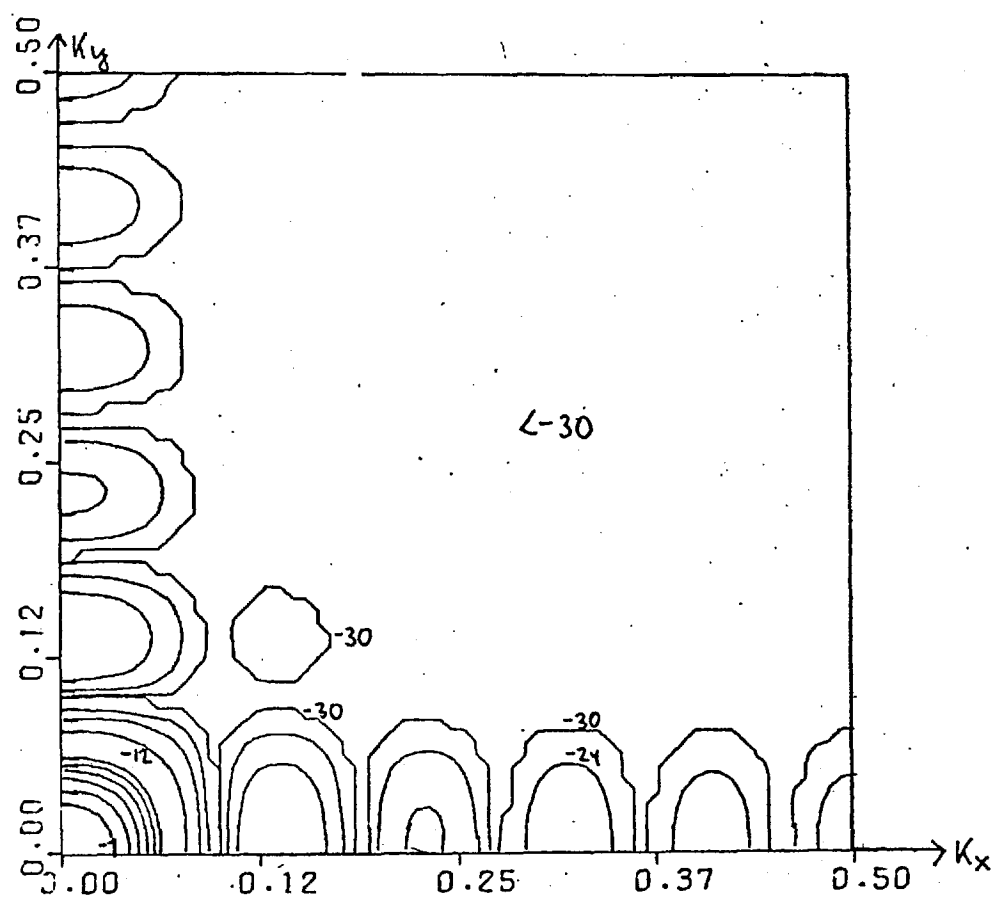

FIGURE 7.3.10 (k_x-k_y) plane for a 11x11 recording array

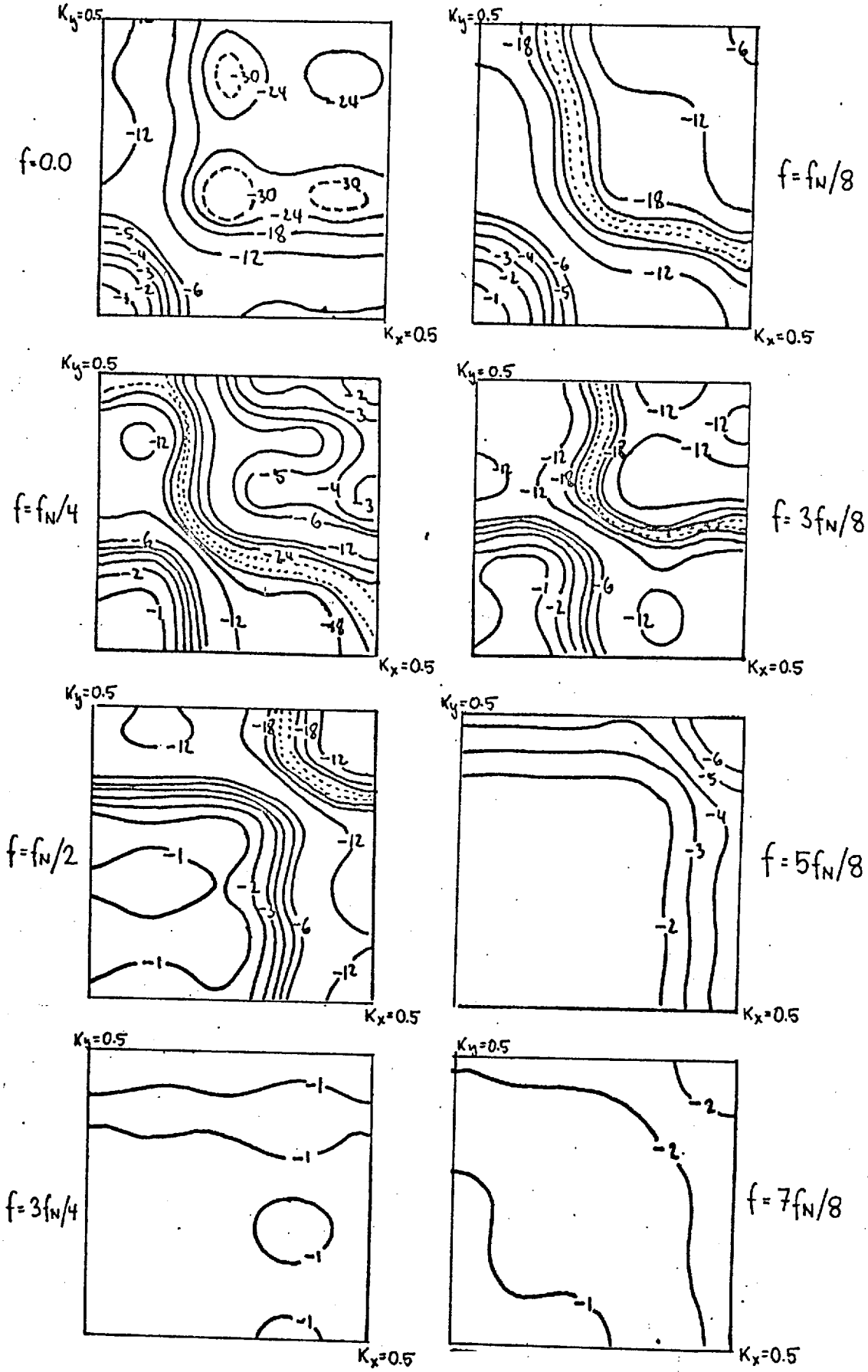

FIGURE 7.3.11 Filter number 16; (f,k_x,k_y) diagram

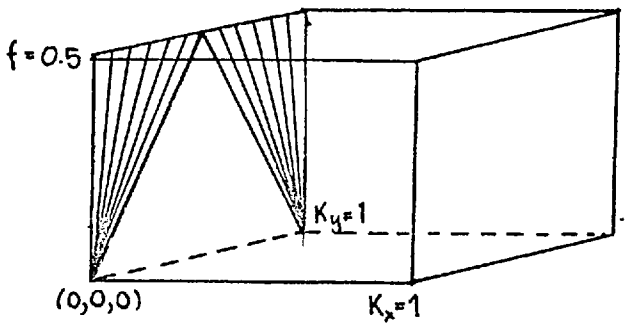

FIGURE 7.3.12 (f,k_x,k_y) diagram

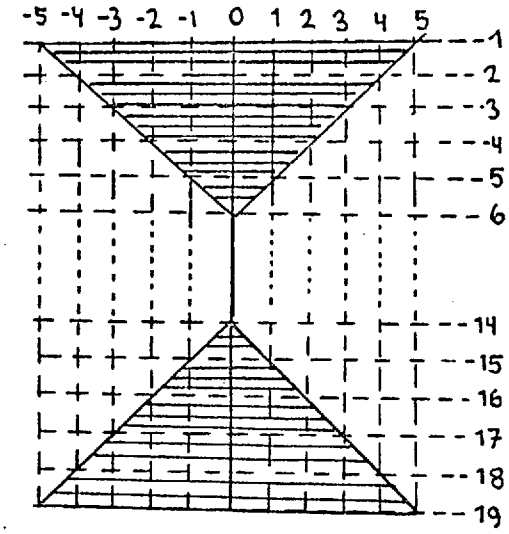

Figure 7.3.13 Time window

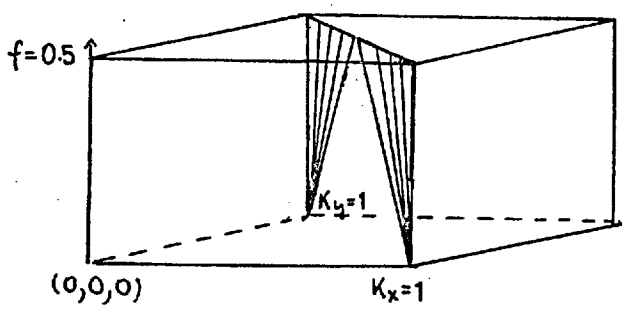

FIGURE 7.3.14 (f,k_x,k_y) diagram

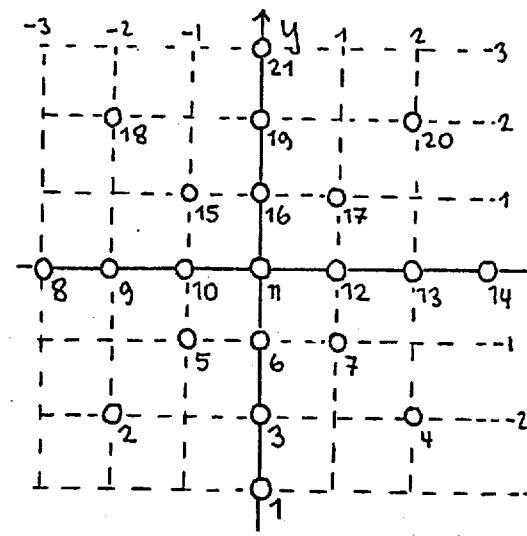

FIGURE 7.3.15 Recording array

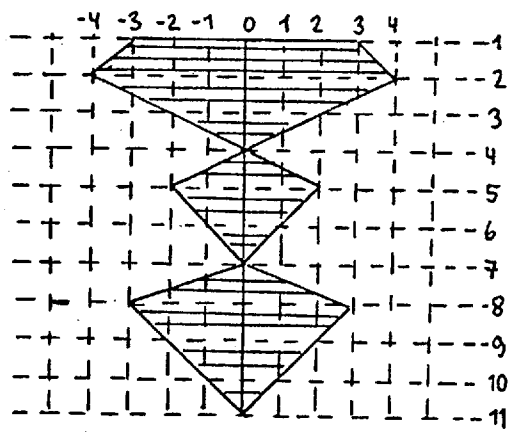

FIGURE 7.3.16 Upper part of a symmetric time window

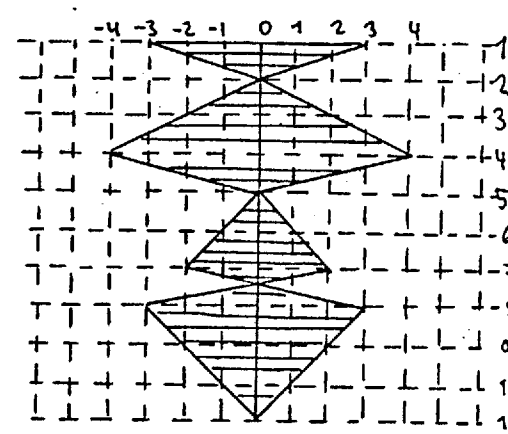

FIGURE 7.3.17 Upper part of a symmetric time window

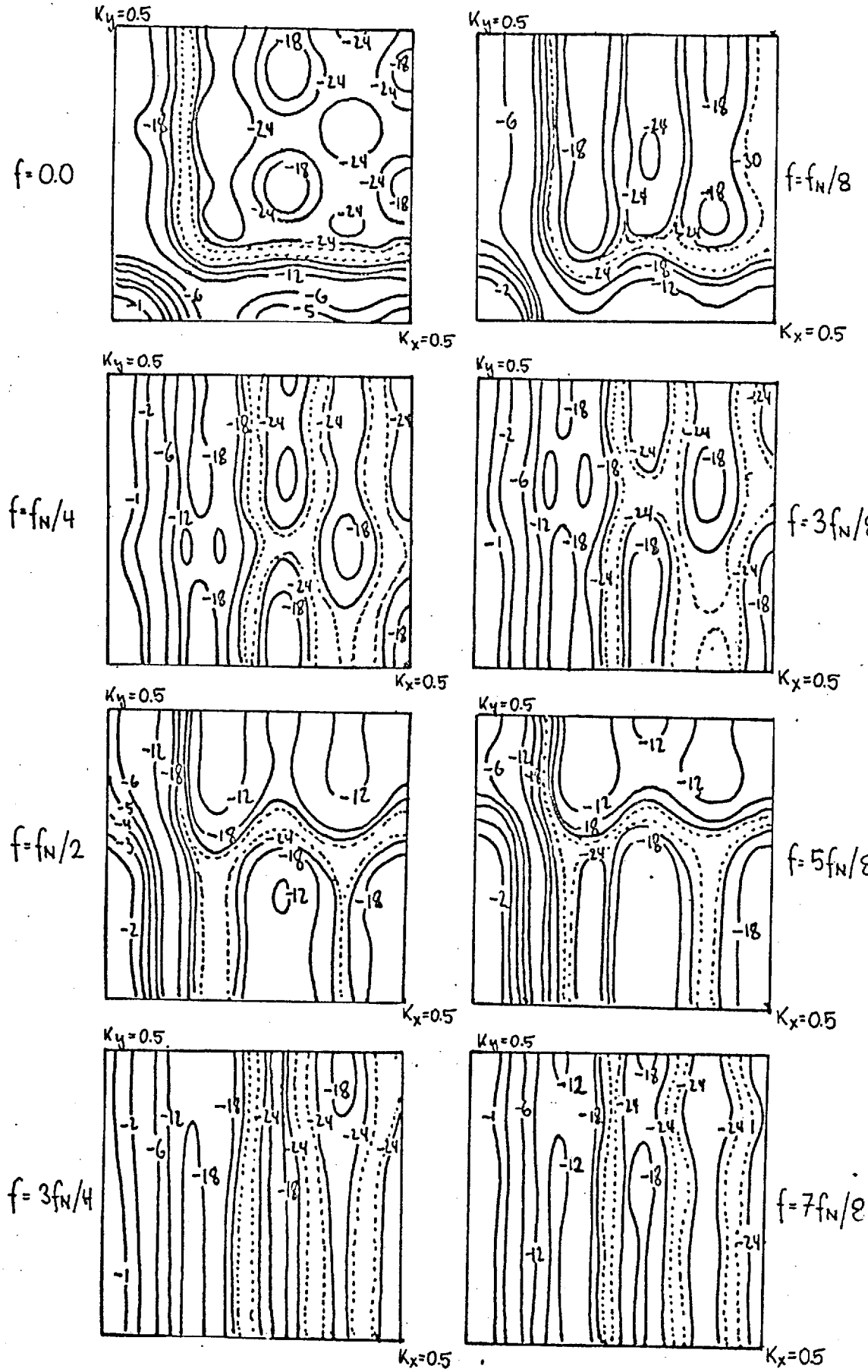

FIGURE 7.3.18 Filter number 17; (f,k_x,k_y) diagram

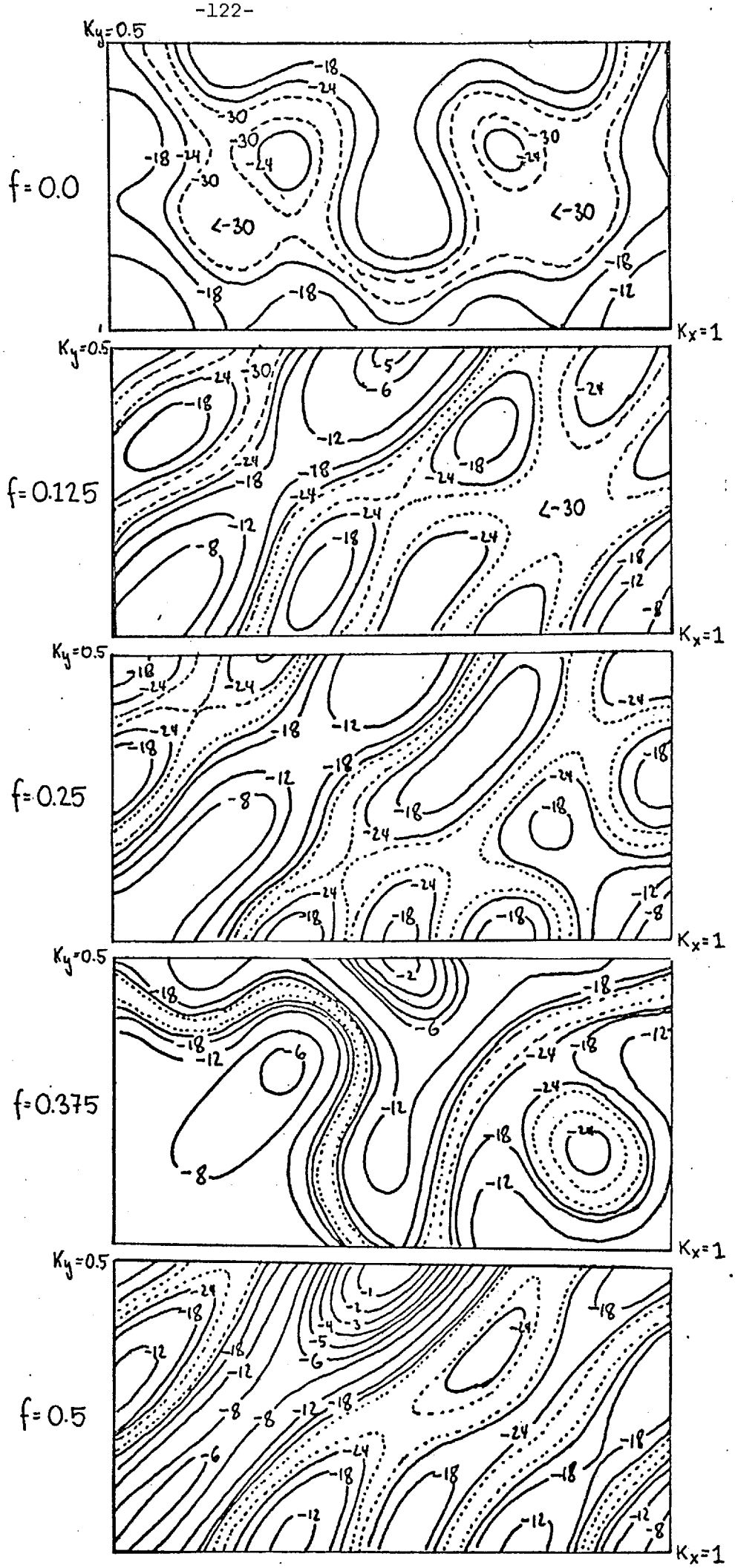

FIGURE 7.3.19 Filter number 18; (f,k_x,k_y) diagram

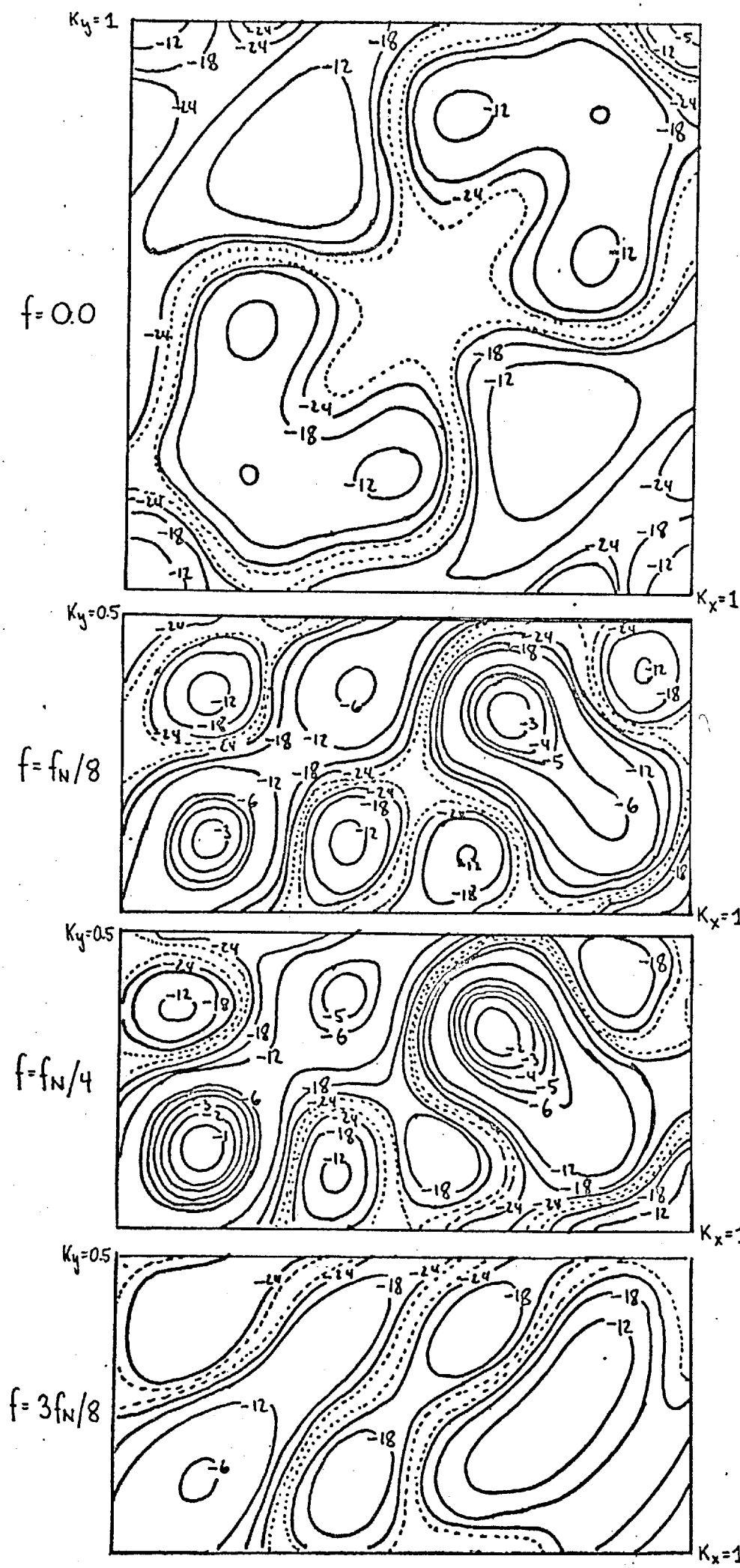

FIGURE 7.3.20 Filter number 19; (continued on next page)

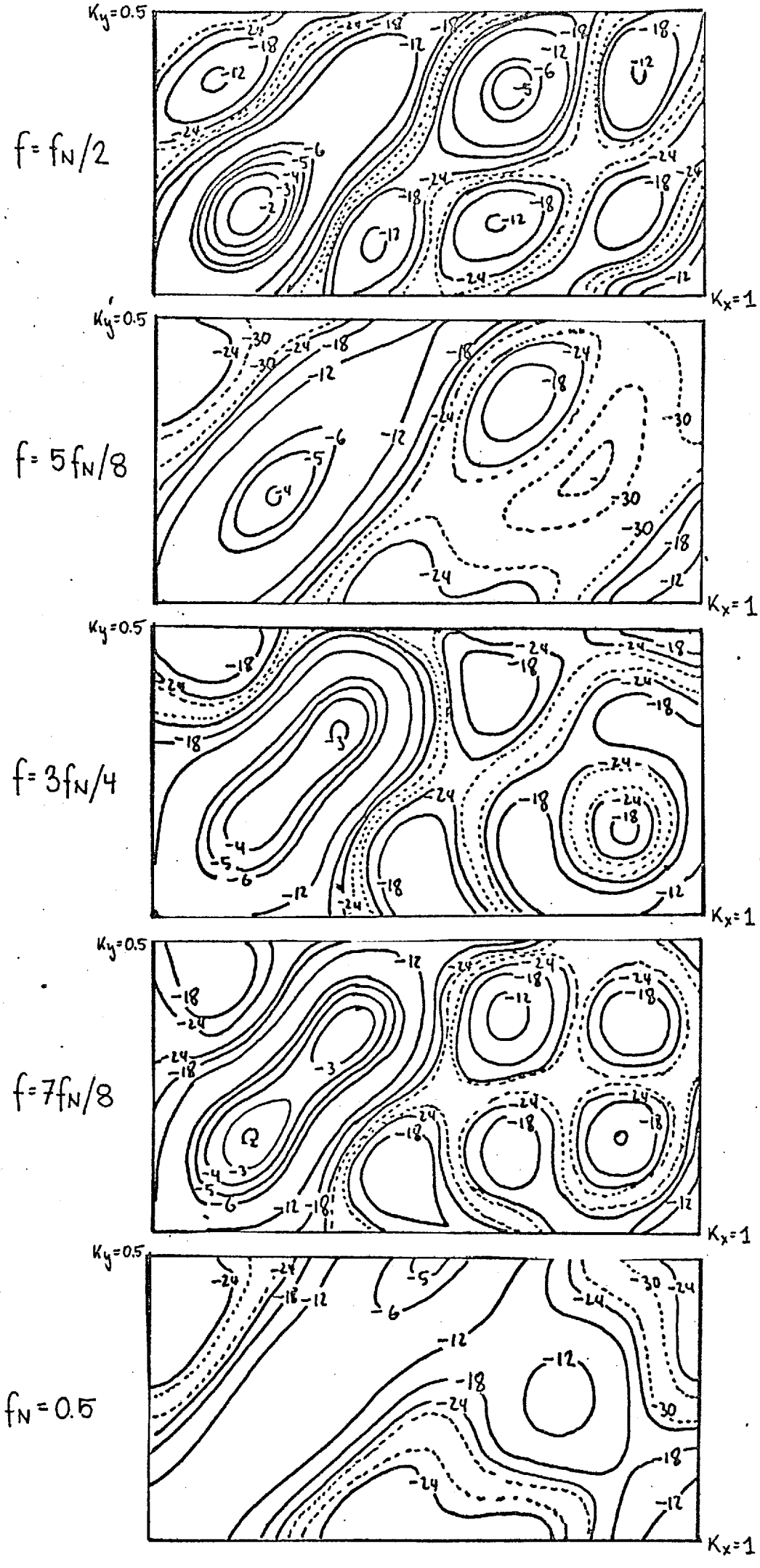

FIGURE 7.3.20 Filter number 19 (continuation from previous page)

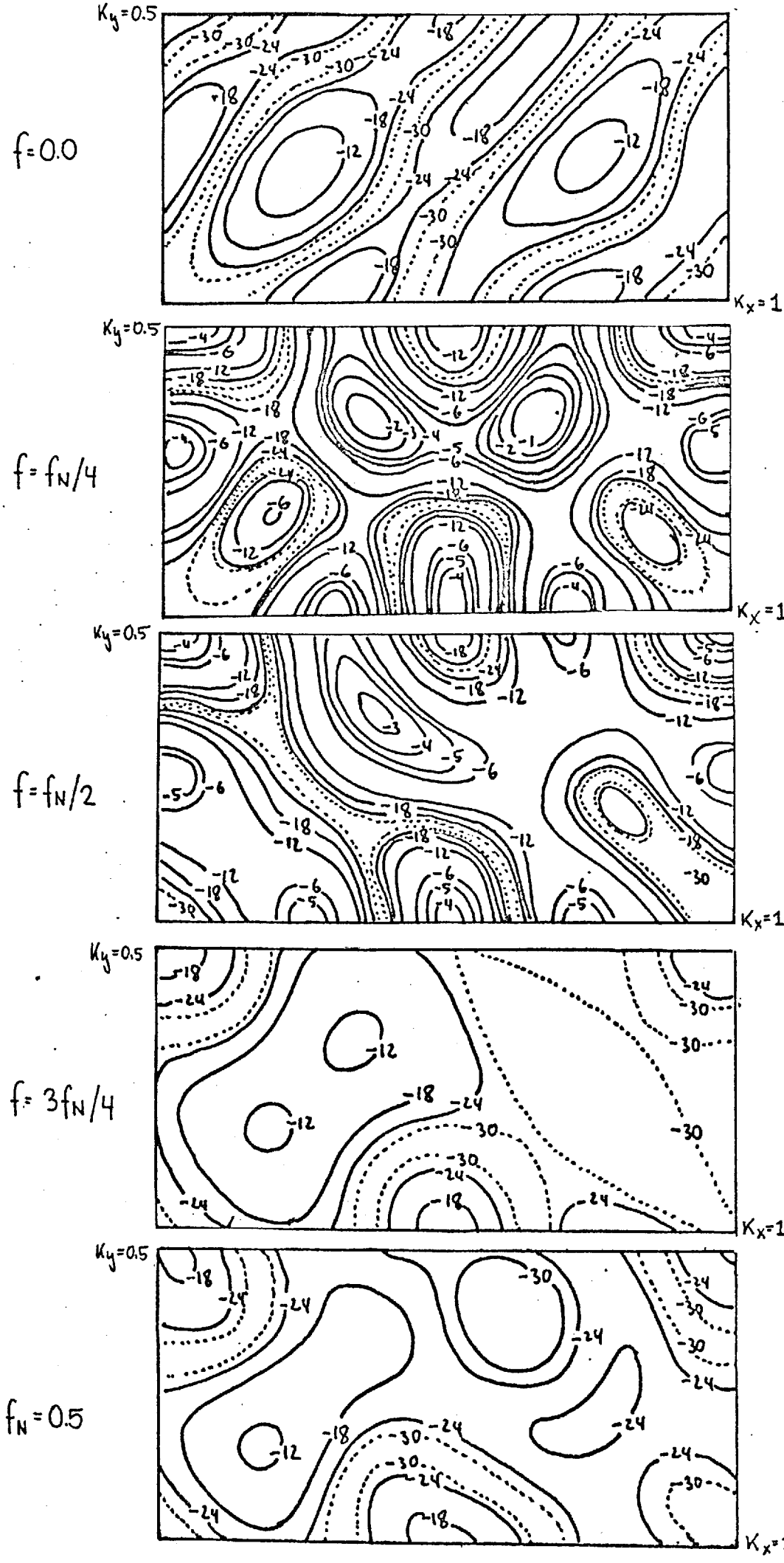

FIGURE 7.3.21 Filter number 20

7.4 Characteristics of differential normal moveout filters

By specifying various types of time windows, the normal equations (4.2.4) have been used for the design of two- and three-dimensional velocity filters. The two- or three-dimensional Fourier transform of the filters contains all transfer functions for signals with constant moveout. It is therefore the most appropriate tool for the filter characterisation. If, however, signals pass through a velocity filter which have differential instead of constant moveout then the (f-k) plot of a filter is of no further help. Equally it generally makes little sense to apply a two-dimensional Fourier transform to a filter which was designed for differential normal moveout. One would then obtain the transfer functions for signals with constant moveout from it.
For differential normal moveout filters, one has to look for other transforms, which include all transfer functions for the differential normal moveout signals used in the design.

In this section it is shown how with simple manipulations, a diagram for a stacking filter may be computed from which the transfer functions for signals belonging to a specified family of differential normal moveout curves can be obtained. It is also shown that for a special class of filters, such a transform is again the most appropriate tool of characterisation. The technique is explained with the help of the following examples.

Example Number 6

The problem is to characterise filter number 12 (designed for signals with contant moveout) for signals having the following moveout:

$$\begin{aligned}
\alpha_1 &= 0 \quad \text{on trace } 1 \\
\alpha_2 &= \tau \quad " \quad " \quad 2 \\
\alpha_3 &= 2\tau \quad " \quad " \quad 3 \quad (-\infty < \tau < +\infty) \\
\alpha_4 &= 4\tau \quad " \quad " \quad 4 \\
\alpha_5 &= 6\tau \quad " \quad " \quad 5 \\
\alpha_6 &= 9\,\tau \quad " \quad " \quad 6
\end{aligned} \tag{7.4.1}$$

For this purpose, a new stacking filter ($B_j(f)$, $j = 1,..,10$) is defined from the six components of filter number 12 as shown in table 7.4.1.

$B_1(f)$	$B_2(f)$	$B_3(f)$	$B_4(f)$	$B_5(f)$	$B_6(f)$	$B_7(f)$	$B_8(f)$	$B_9(f)$	$B_{10}(f)$
$A_1(f)$	$A_2(f)$	$A_3(f)$	0	$A_4(f)$	0	$A_5(f)$	0	0	$A_6(f)$

TABLE 7.4.1

In this way, the transfer function for the given moveout (7.4.1)

$$F_{\alpha}(f) = \sum_{j=1}^{6} A_j(f)\, e^{-2\pi i f \alpha_j} \tag{7.4.2}$$

is expressed as

$$F(f,\tau) = F_{\alpha}(f) = \sum_{j=1}^{10} B_j(f) e^{-2\pi i f j \tau}$$

This formula can be obtained from the two-dimensional Fourier transform of $B_j(f)$, $(j = 1,..,10)$

$$F(f,k) = \sum_{j=1}^{10} B_j(f) e^{+2\pi i j k} \tag{7.4.3}$$

along the line $k = -f\tau$

The function (7.4.3) is called the transfer diagram of filter number 12 for the family of curves (7.4.1). For the above example the two-dimensional amplitude spectrum of this diagram is given in figure 7.4.1. It contains all amplitude spectra of the transfer functions for any given τ of the family of curves (7.4.1) and has to be interpreted as follows; Each transfer

function for a value τ is obtained along the line which connects the origin with that value on the τ-axis. The given diagram should be compared with the contours of figure 7.2.8. Both plots have the same transfer function for $\tau = 0$.

From the above example it is obvious that the described technique is of value if the moveout has the form $\alpha_j = k\tau$, where k is an integer number. If the moveout is $\alpha_j = k\tau + \beta_j$, where β_j may be a real number, the same procedure has to be done with $A_j(f)e^{2\pi i f \beta_j}$ instead of $A_j(f)$. The greater the curvature of the test curves, the more zero components have to be introduced in the newly defined vector.

The transfer diagram of filter number 12 for the family of curves

$$\begin{aligned} \alpha_1 &= 5/2 + \tau & \alpha_4 &= -1/2 + \tau \\ \alpha_2 &= 3/2 + \tau & \alpha_5 &= -3/2 + \tau \\ \alpha_3 &= 1/2 + \tau & \alpha_6 &= -5/2 + \tau \end{aligned} \qquad (-\infty < \tau < +\infty) \qquad (7.4.4)$$

is correspondingly obtained by transforming $B_j(f)=A_j(f)\, e^{\beta_j 2\pi i f}$, $(j=1,..,6)$ into the (f - k) domain . The amplitude spectrum of this transform is given in figure 7.4.2. This example shows in addition, how to derive a useful filter in a quick way from a given stacking filter by simply shifting the stacking filter components for constant amounts on each trace. This observation may be generalized in the following way:

Let $A_j(f)$, $(j=-N,..,N)$ be the components of a stacking filter and $\tilde{F}(f,k)$ be the two-dimensional Fourier transform as defined with formula (6.2.11 Shifting each component by the contant amount $j\delta$ leads to the stacking filter

$$B_j(f)=A_j(f)e^{-2\pi i \delta j f}, \quad (j=-N,\ldots,N)$$

whose corresponding transform $\tilde{F}^B(f,k)$ is related to $\tilde{F}(f,k)$ by the formula $\tilde{F}^B(f,k)=\tilde{F}(f,k+\delta f)$, $|f| \leq \frac{1}{2}$. Any line $k=f\tau_0$ with $|f| \leq \frac{1}{2}$ in $\tilde{F}(f,k)$ maps into the line $k=f(\tau_0+\delta)$ in $\tilde{F}^B(f,k)$.

If a filter has to be computed for the time window of figure 7.4.9 b, one may make use of the stacking filter for the time window of figure 7.4.9 a without solving again the normal equations. The stacking filter components need only be delayed by constant amounts on each trace .The filter obtained by this process is the optimum filter for a window,where the window limits have the same shift as the filter components. In this way it is possible to derive may useful filters from a computed one.

In the following part of this section differential normal moveout filters are characterised. Transforms for some of these filters are given from which all transfer functions for the differential normal moveout signals can be obtained which were assumed in the filter design. An appropriate example for such a time window is shown in figure 7.4.3. Filters with these kind of windows are important for two-dimensional problems encountered in the filtering of CDP-data. The centre point is selected in such a way that the overall length of the window is short. The family of curves which is inherently assumed in the design of a filter for the given window is

$$\begin{array}{lll} \alpha_1 = 0 & \alpha_5 = 5\tau & \alpha_9 = 15\tau \\ \alpha_2 = \tau & \alpha_6 = 7\tau & \alpha_{10} = 18\tau \\ \alpha_3 = 2\tau & \alpha_7 = 9\tau & \alpha_{11} = 22\tau \\ \alpha_4 = 3\tau & \alpha_8 = 12\tau & \alpha_{12} = 26\tau \end{array} \qquad (-\infty < \tau < \infty) \qquad (7.4.5)$$

From the twelve filter components obtained in this case, a 27-trace filter has to be defined in the way described above. The two-dimensional Fourier transform of it contains all transfer functions for signals belonging to the family of curves (7.4.5) Three examples are given below:

Example Number 7.

A stacking filter for the time window of figure 7.4.3 without reject region was computed for the following design parameters(filter no.21)

$N = 12$; $LF = 27$; $\varrho = 0$; $\nu = 0.08$; $\tau_p = 1$; $\tau_R = 0$; $t_d = 13$

τ_p and τ_R is defined in figure 7.4.3.

The trace-symmetric stacking filter components are given in table 7.4.2. The amplitude-spectrum of the transfer diagram is shown in figure 7.4.4 . Signals belonging to the curves (7.4.5) with any value $|\tau|<1$ pass with hardly any change in their amplitude characteristics. However, for frequencies below f = 0.16 the filter rejects very well those signals which fall into the reject region close to the escarpment. Frequencies higher than f = 0.25 pass for every value of τ.

This is no longer the case for filter number 22 with the above parameters, where however, τ_p = 1/3. Contours and isometric plot for this case are given in figure 7.4.5. Note that again for the scaled time windows transfer diagrams seem to be scaled versions of each other. (This effect is explained in Chapter VIII). The two-dimensional Fourier transform for the last differential normal moveout filter is shown in figure 7.4.6. It characterises the performance of the filter for signals with constant moveout. One may conclude that when constant moveout signals fall into the pass region of figure 7.4.3 they pass nearly undistorted. A rejection of constant moveout signals outside this range is worse than the rejection of differential normal moveout signals which fall into the curved reject region. A good knowledge of the actual moveout incorporated into the filter design is therefore of great help to obtain optimum rejection. It was generally found that the escarpment has maximum steepness if the filtered signals were the same ones as used in the filter design.

Example Number 8

A stacking filter for the window of figure 7.4.3 was computed with the following design parameters (filter number 23)

N = 12; LF = 11; t_d = 6; ν = 0.08; ϱ = 2.0; τ_p = 0.5; τ_R = 0.25

The amplitude spectrum of the transfer diagram is shown in figure 7.4.7. Apart from depressions for high frequencies, pass and reject regions are

fairly well approximated. For signals falling on curves outside the specified range, the filter becomes very selective for certain frequencies and certain values τ. An application of these filters has therefore to be done with extreme care. Figure 7.4.8 shows the amplitude spectrum of the transfer diagram for filter number 24 , which has the above design parameters, where however, $\tau_R = 0.05$. As expected, the narrower reject region is better approximated in this case. Apart from the strong selectivity of the filter outside specified regions, observed features are very similar to multichannel velocity filters. For instance one may easily predict the values τ_p and τ_R of the above filter type, for which pass and reject regions will overlap in the transfer diagram.

The technique described for the characterisation of differential normal moveout filters is very useful, because properties of these filters are revealed which cannot be found otherwise. The given examples in this section were based on seismic considerations. Although these examples show the complexity of the problem, further research on this subject is certainly useful. It was generally found that reject and pass regions are well approximated. It is, however, difficult to predict characteristics outside specified regions. These may sometimes even exceed the height of pass regions.

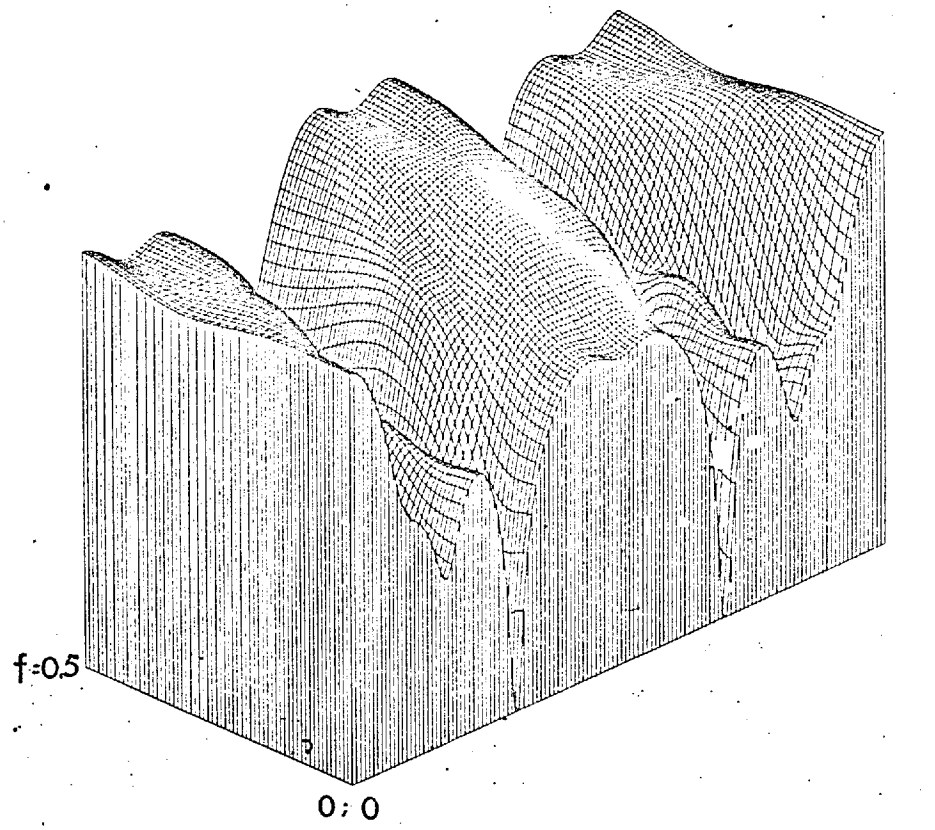

Isometric plot of the transfer diagram

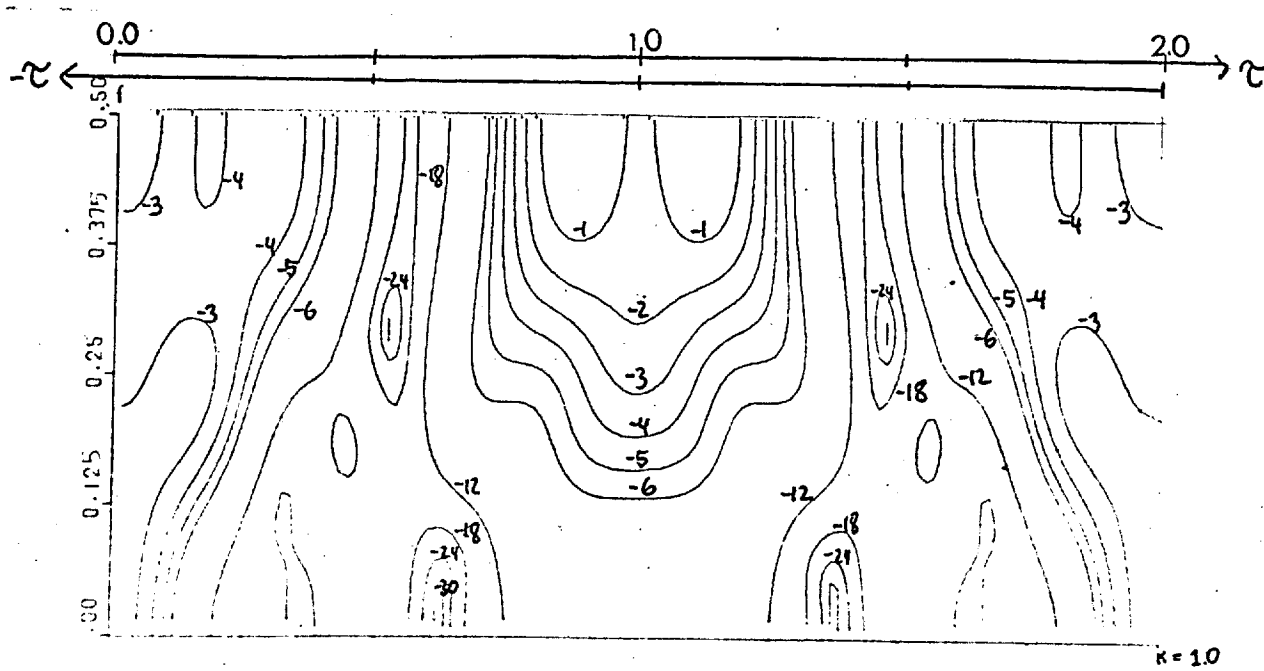

FIGURE 7.4.1 Transfer diagram of filter number 12 for the family of curves (7.4.1)

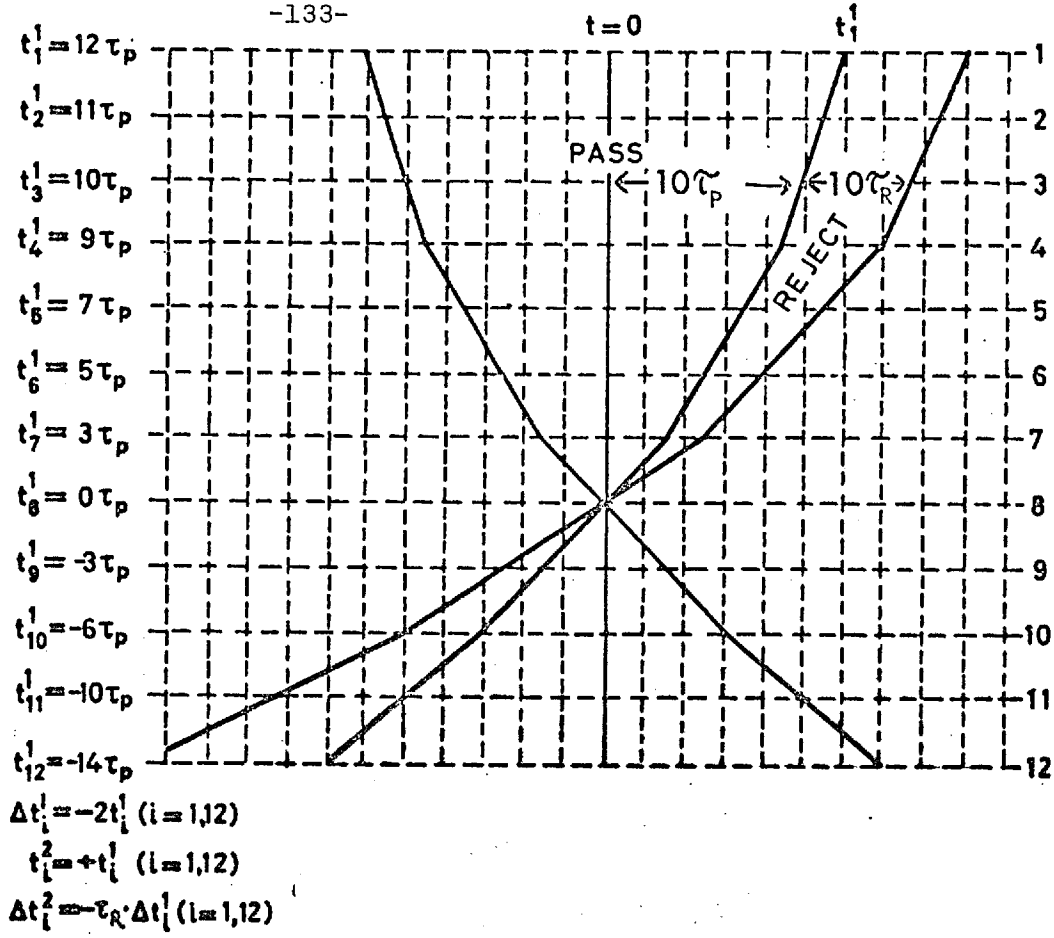

FIGURE 7.4.3 Time window for a differential normal moveout filter

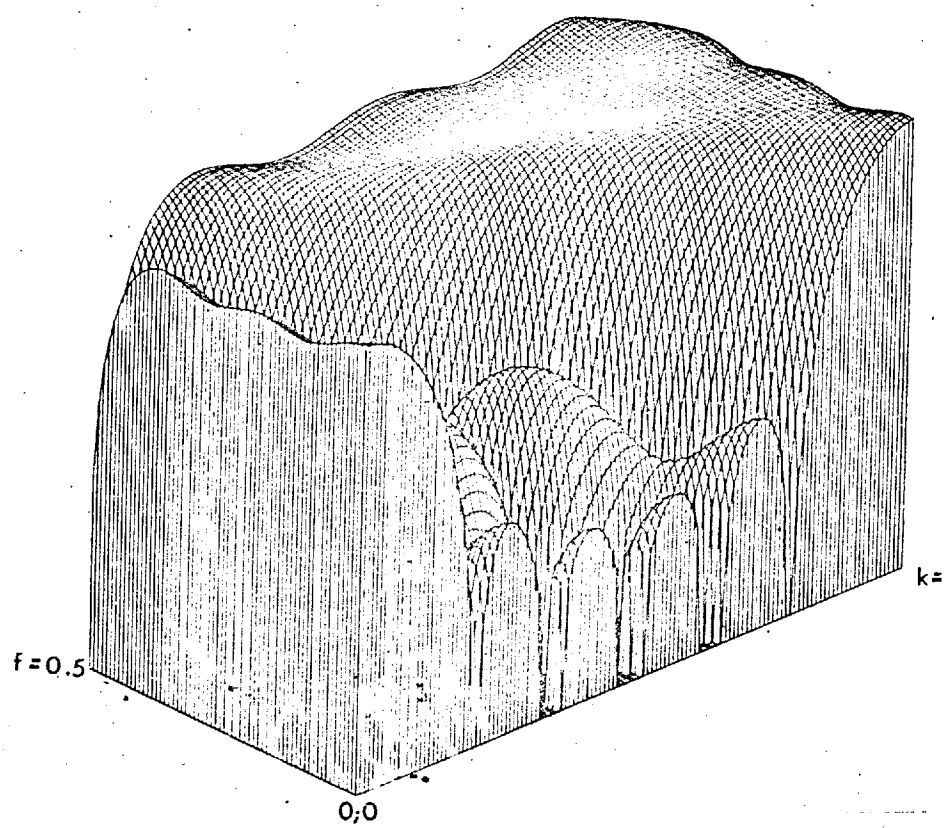

FIGURE 7.4.2 Isometric plot of the transfer diagram of filter number 12 for the curves (7.4.4)

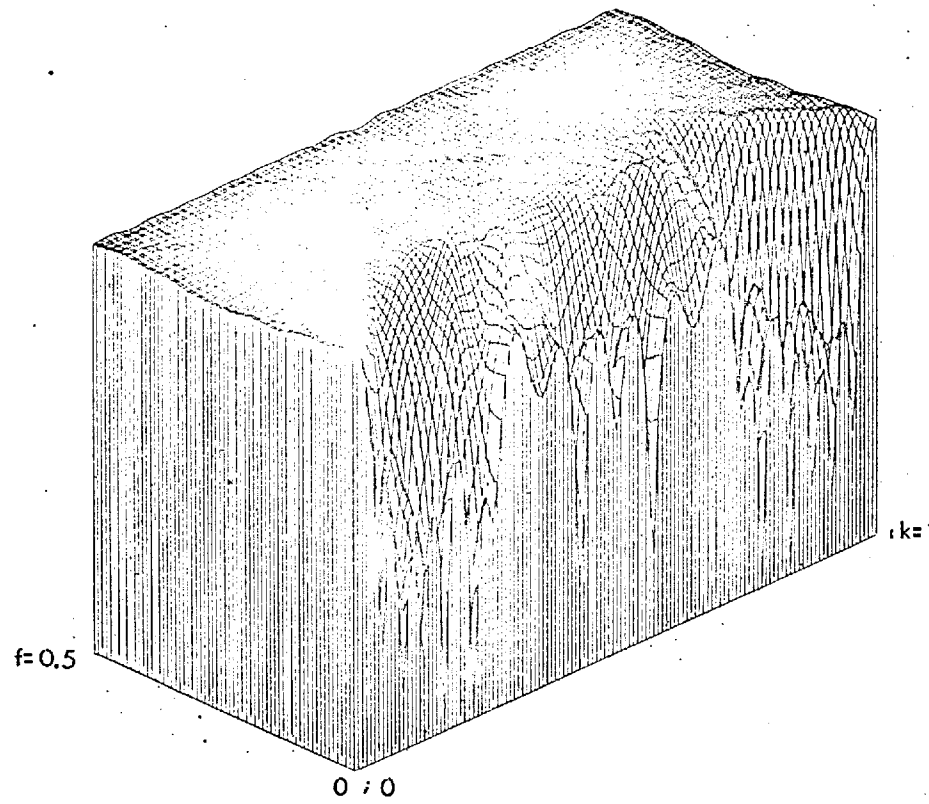

Isometric plot

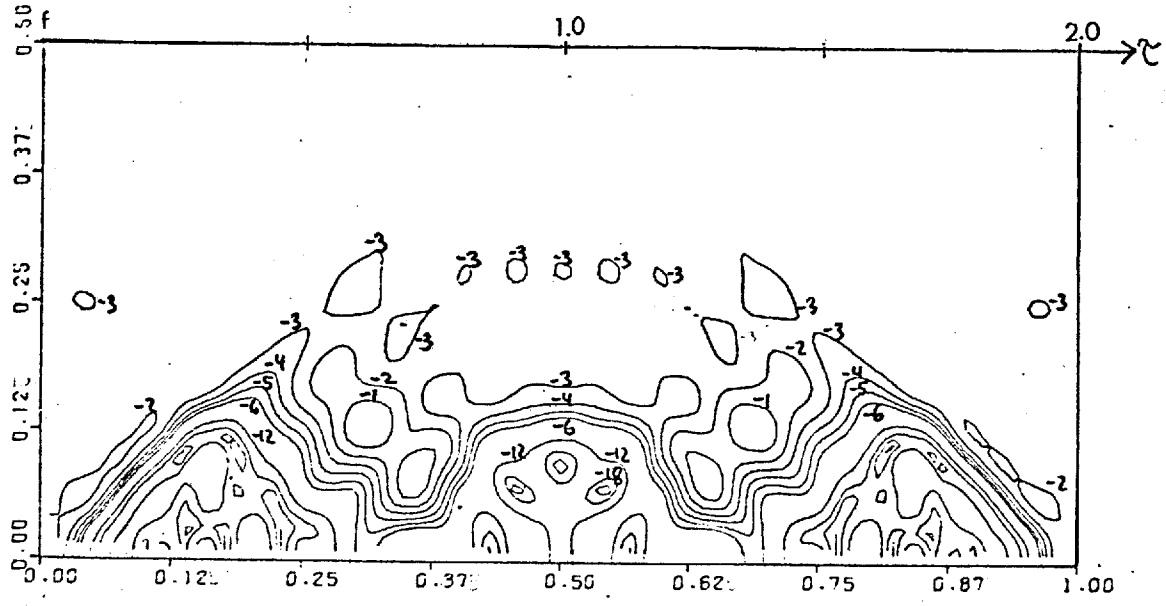

FIGURE 7.4.4 Filter number 21

Amplitude spectrum of the transfer diagram for the curves (7.4.5)

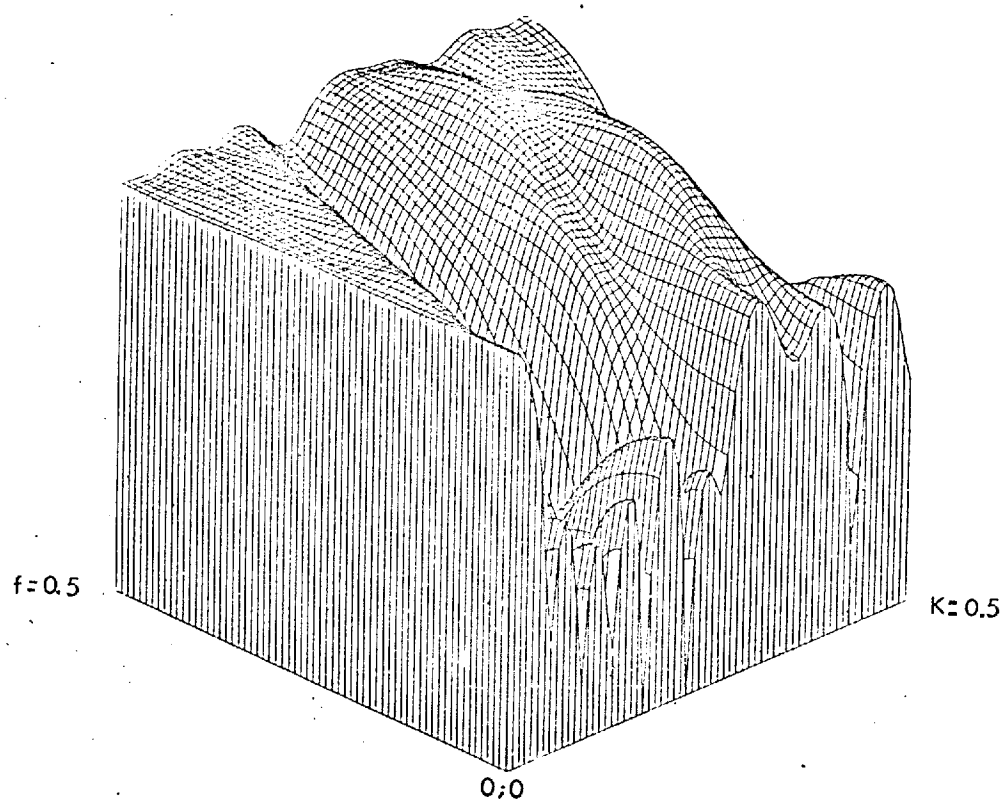

Isometric plot

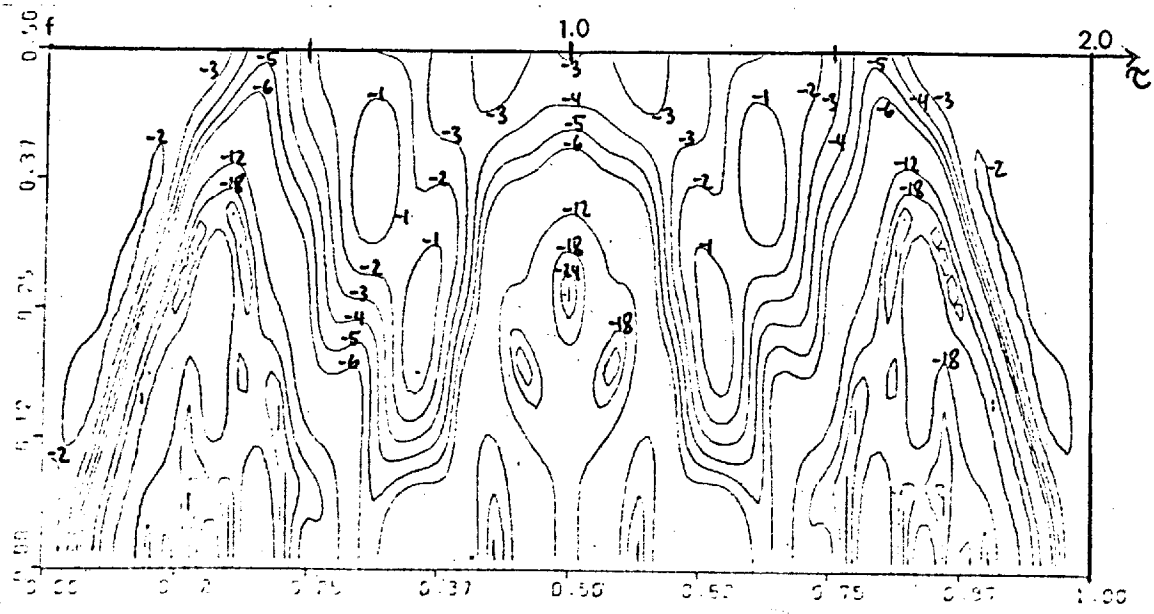

FIGURE 7.4.5 Filter number 22

Amplitude spectrum of the transfer diagram for the curves (7.4.5)

$a_1(t^*)$	$a_2(t^*)$	$a_3(t^*)$	$a_4(t^*)$
.39605986E-02	.18528000E-03	.41511356E-03	-.20914340E-02
.44760574E-02	.18791995E-02	.19973804E-02	-.19042706E-02
-.93270522E-03	.78796904E-02	.20015003E-02	.72681975E-03
-.54918890E-02	.62108495E-02	.83088194E-02	.15215123E-02
-.51301991E-02	-.29108407E-03	.10620171E-01	.74004230E-02
-.52911068E-02	-.14156254E-02	.39269813E-02	.13839116E-01
-.41298549E-02	-.24110071E-02	.94959516E-03	.10802602E-01
-.32562704E-02	-.28277320E-02	.95696903E-03	.44392271E-02
-.26164861E-02	-.17899649E-02	-.21768343E-04	.15306412E-03
-.24444591E-02	-.45419197E-03	-.21614005E-02	.39040968E-03
-.16197869E-02	-.17268916E-02	-.11224825E-02	.32524405E-03
-.15766798E-02	-.23400018E-02	-.89600450E-05	.25206942E-03
-.18732843E-02	-.12778698E-02	-.38428111E-03	-.33764818E-03
-.23850548E-02	.72211152E-05	-.14838971E-02	-.35803595E-04
-.18732838E-02	-.12778703E-02	-.38428113E-03	-.33784817E-03
-.15766793E-02	-.23400020E-02	-.89604063E-05	.25206946E-03
-.16197865E-02	-.17268916E-02	-.11224829E-02	.32524393E-03
-.24444586E-02	-.45419199E-03	-.21614007E-02	.39040944E-03
-.26164857E-02	-.17899646E-02	-.21768661E-04	.15306397E-03
-.32562707E-02	-.28277312E-02	.95696902E-03	.44392267E-02
-.41298554E-02	-.24110064E-02	.94959600E-03	.10802601E-01
-.52911080E-02	-.14156241E-02	.39269820E-02	.13839119E-01
-.51302004E-02	-.29108344E-03	.10620172E-01	.74004227E-02
-.54918898E-02	.62108495E-02	.83088205E-02	.15215125E-02
-.93270580E-03	.78796903E-02	.20015011E-02	.72682036E-03
.44760570E-02	.18791989E-02	.19973809E-02	-.19042705E-02
.39605995E-02	.18527832E-03	.41511463E-03	-.20914342E-02

$a_5(t^*)$	$a_6(t^*)$	$a_7(t^*)$	$a_8(t^*)$
-.16974060E-02	.75587746E-04	-.18586974E-02	-.13632270E-02
-.37865141E-02	.53791838E-03	-.11679524E-02	-.24444852E-02
-.51685779E-02	-.29626446E-03	.45161666E-03	-.32557156E-02
-.59378630E-02	-.32247696E-02	.11020672E-02	-.37693584E-02
-.32757010E-02	-.59561854E-02	.68550144E-03	-.39020336E-02
.12310785E-02	-.89445443E-02	-.27592770E-02	-.11188491E-02
.11366198E-01	-.75674364E-02	-.77218951E-02	.20025726E-02
.19242584E-01	-.24591481E-02	-.15182382E-01	.97016185E-03
.16659204E-01	.11758446E-01	-.18329459E-01	-.89649394E-02
.10473923E-01	.25235738E-01	-.15499567E-01	-.29120803E-01
.37306909E-02	.25325031E-01	.60976572E-02	-.57496641E-01
.18436806E-02	.19047564E-01	.38022168E-01	-.89008781E-01
.16782608E-02	.86765030E-02	.56871973E-01	-.11626519E+00
.27594387E-02	.54693282E-02	.66660952E-01	.79662696E+00
.16782609E-02	.86785030E-02	.56871973E-01	-.11626519E+00
.18436806E-02	.19047564E-01	.38022168E-01	-.89008781E-01
.37306910E-02	.25325031E-01	.60976572E-02	-.57496641E-01
.10473923E-01	.25235738E-01	-.15499567E-01	-.29120803E-01
.16659204E-01	.11758447E-01	-.18329459E-01	-.89649394E-02
.19242584E-01	-.24591480E-02	-.15182382E-01	.97016190E-03
.11366198E-01	-.75674365E-02	-.77218951E-02	.20025727E-02
.12310782E-02	-.89445443E-02	-.27592769E-02	-.11188490E-02
-.32757016E-02	-.59561854E-02	.68550120E-03	-.39020336E-02
-.59378632E-02	-.32247699E-02	.11020675E-02	-.37693585E-02
-.51685781E-02	-.29626542E-03	.45161734E-03	-.32557156E-02
-.37865135E-02	.53791780E-03	-.11679518E-02	-.24444852E-02
-.16974055E-02	.75587033E-04	-.18586976E-02	-.13632269E-02

TABLE 7.4.2 Filter number 21

Stacking filter components (continued on next page)

$a_9(t^*)$	$a_{10}(t^*)$	$a_{11}(t^*)$	$a_{12}(t^*)$
-.23423390E-03	-.32963206E-02	.45874679E-03	.44785853E-02
.89900492E-03	-.49925502E-02	.27719745E-02	.31178877E-02
.20427275E-02	-.68708127E-02	.49270305E-02	.13690514E-02
.15239537E-02	-.72796865E-02	.95039349E-02	-.11930350E-02
-.94372101E-03	-.60969926E-02	.13201530E-01	-.31992524E-02
-.69128727E-02	-.17189838E-02	.12363387E-01	-.44254333E-02
-.13151406E-01	.36532012E-02	.10243217E-01	-.41225311E-02
-.17968580E-01	.13815983E-01	.62637977E-02	-.33554925E-02
-.16339714E-01	.22690312E-01	.26476414E-02	-.21218794E-02
-.90554443E-02	.22795694E-01	-.56968915E-04	-.15351086E-02
.13610487E-01	.19457739E-01	-.44950270E-03	-.14124789E-02
.42140302E-01	.12018291E-01	-.10971467E-03	-.18792632E-02
.56855910E-01	.54419929E-02	.12227174E-02	-.20648204E-02
.64730754E-01	.15290744E-02	.16552376E-02	-.22552385E-02
.56855910E-01	.54419930E-02	.12227174E-02	-.20648208E-02
.42140302E-01	.12018291E-01	-.10971468E-03	-.18792630E-02
.13610487E-01	.19457739E-01	-.44950287E-03	-.14124790E-02
-.90554442E-02	.22795694E-01	-.56969193E-04	-.15351085E-02
-.16339714E-01	.22690312E-01	.26476412E-02	-.21218794E-02
-.17968580E-01	.13815983E-01	.62637976E-02	-.33554923E-02
-.13151406E-01	.36532012E-02	.10243217E-01	-.41225309E-02
-.69128726E-02	-.17189841E-02	.12363387E-01	-.44254331E-02
-.94372047E-03	-.60969929E-02	.13201529E-01	-.31992524E-02
.15239540E-02	-.72796866E-02	.95039350E-02	-.11930347E-02
.20427275E-02	-.68708132E-02	.49270308E-02	.13690511E-02
.89900491E-03	-.49925503E-02	.27719748E-02	.31178877E-02
-.23423357E-03	-.32963210E-02	.45874685E-03	.44785849E-02

TABLE 7.4.2 Stacking filter components

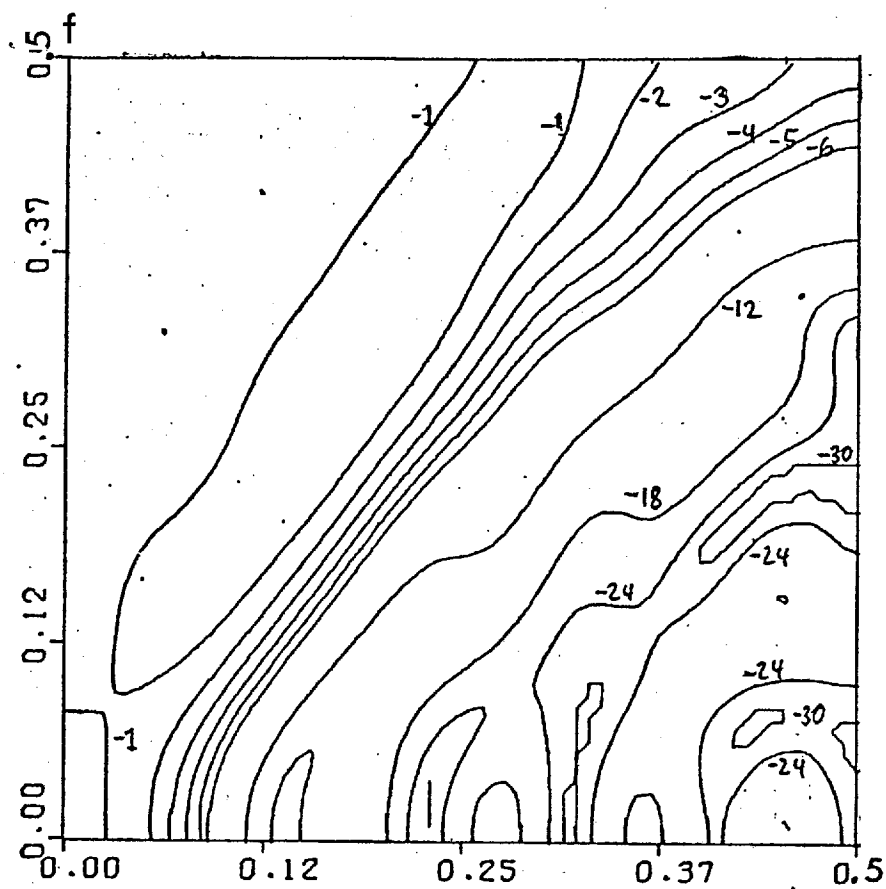

FIGURE 7.4.6 (f-k) diagram of the differential normal moveout filter number 22

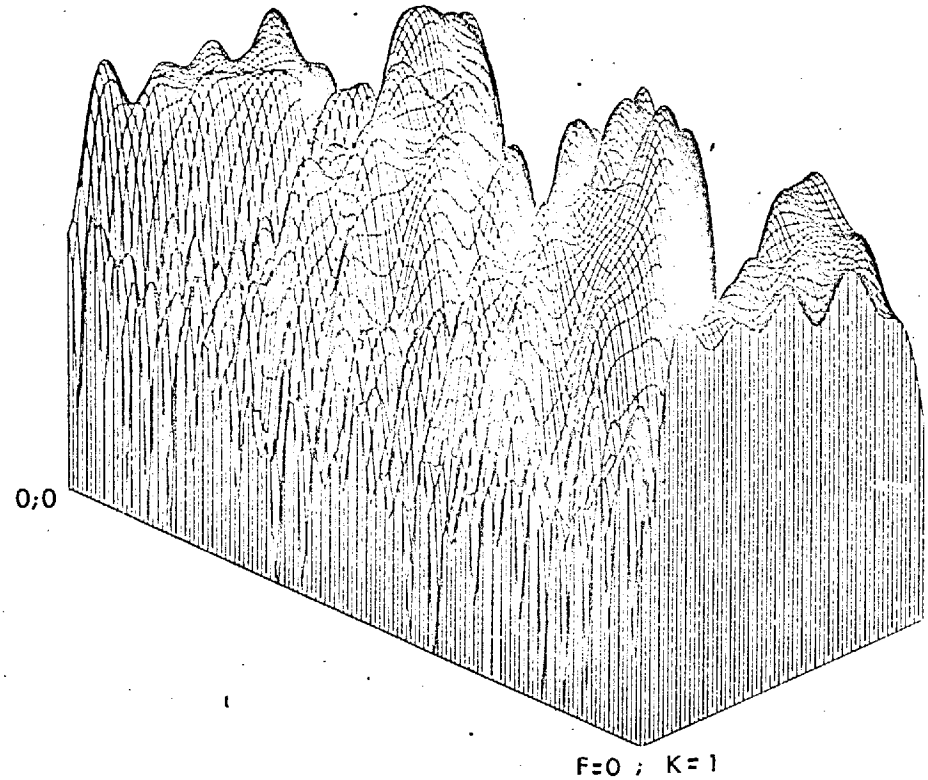

Isometric plot

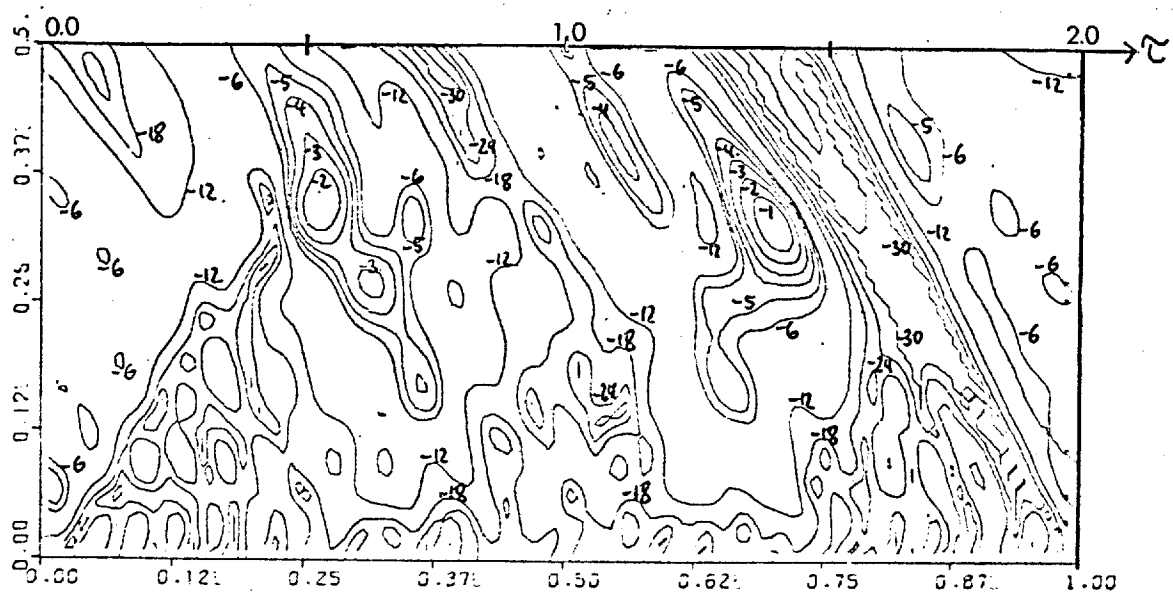

FIGURE 7.4.7 Filter number 23

Amplitude spectrum of the transfer diagram for the curves (7.4.5)

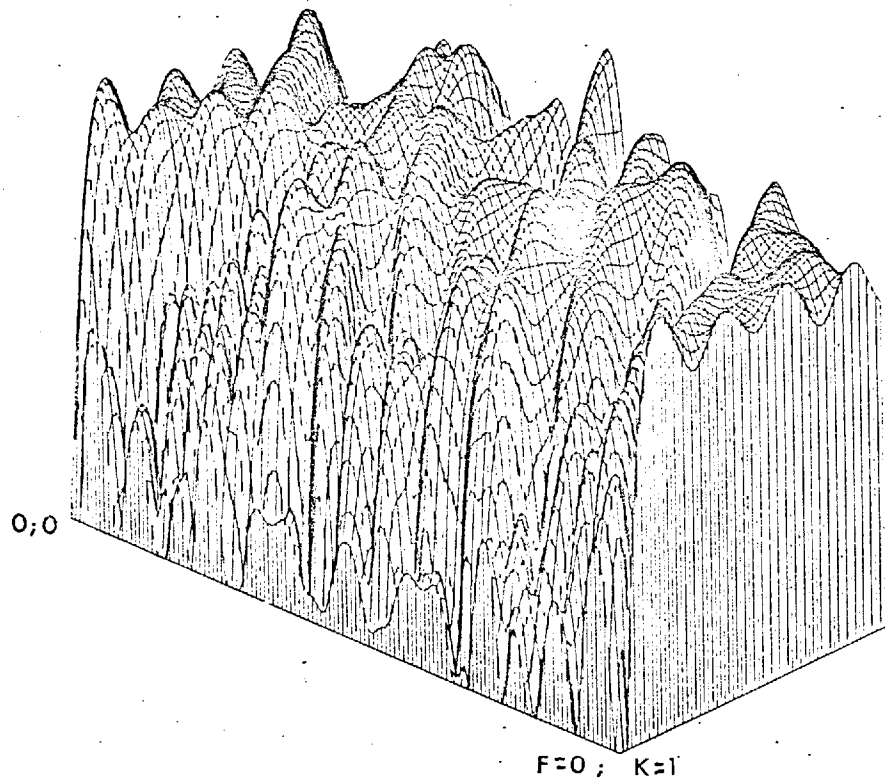

Isometric plot

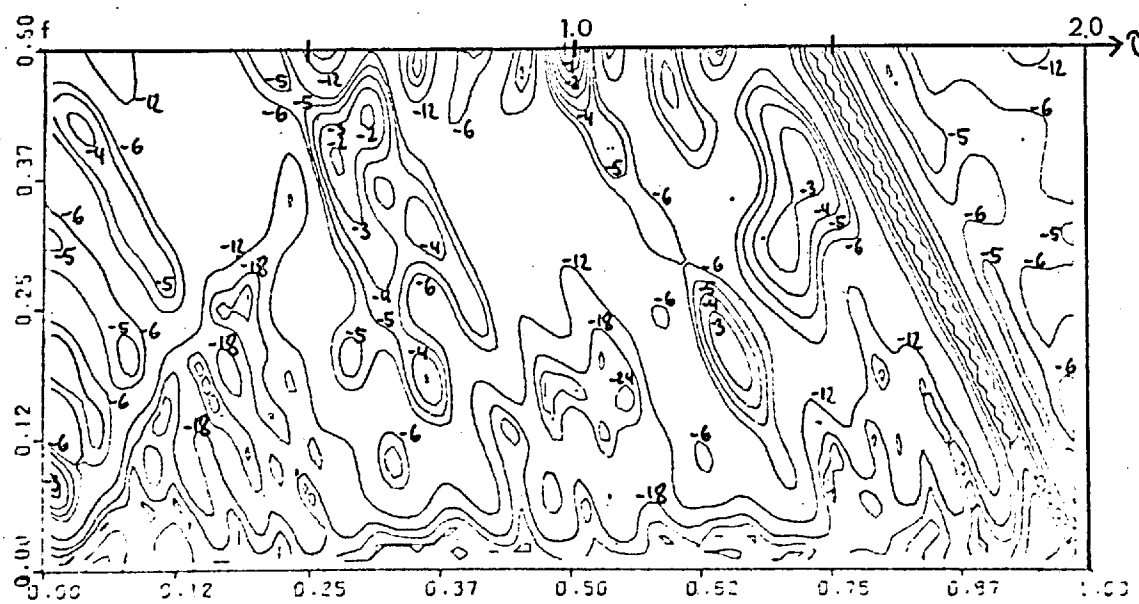

FIGURE 7.4.8 Filter number 24

Amplitude spectrum of the transfer diagram for the curves (7.4.5)

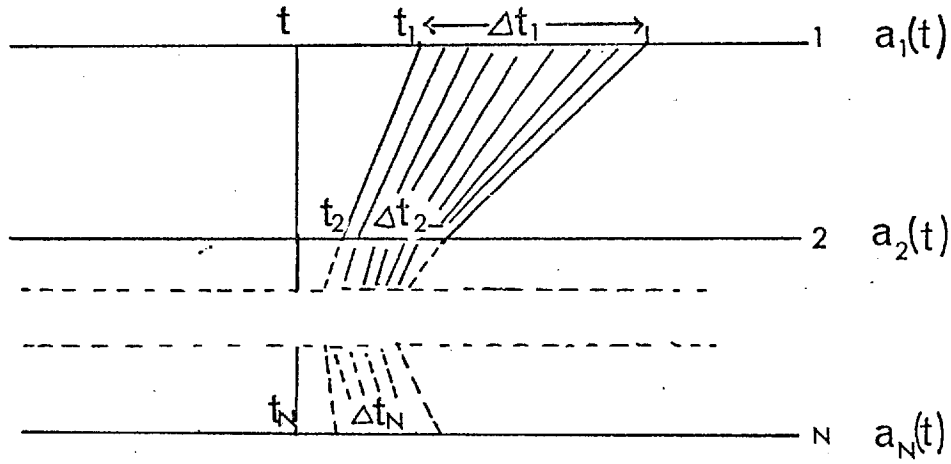

FIGURE 7.4.9 a

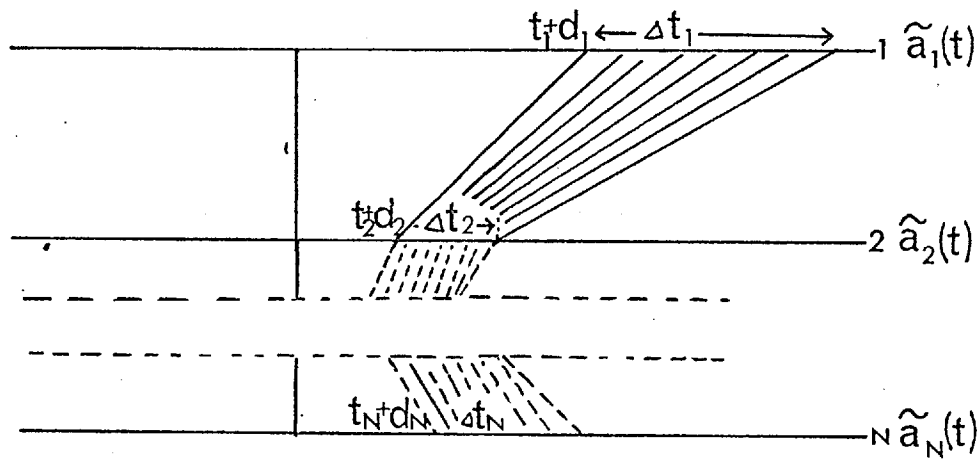

FIGURE 7.4.9 b

FIGURE 7.4.9 Relationship between shifted stacking filter components and time windows .

If the normal equations for the upper window are

$$\sum_{i=1}^{N} A_i(f)R_{ij}(f) = G_j(f) \quad , (j=1,\ldots,N)$$

where $R_{ij}(f)$ and $G_j(f)$ is given in (4.2.5) and (4.2.6), then the ones for the lower window are obtained by replacing t_i with $\tilde{t}_i=t_i+d_i$ in the upper ones.

This leads to the following normal equations:

$$\sum_{i=1}^{N} (\tilde{A}_i(f)e^{2\pi i d_i f}) R_{ij}(f) = G_j(f) \quad , (j=1,..,N)$$

The solutions of these are in the time domain $\tilde{a}_i(t)=a_i(t-d_i),(i=1,.N)$ and therefore can be expressed with the solutions of the filter for the upper window.

7.5 The influence of chatter

The aim in previous sections of this chapter was to characterise various stacking filters with their most appropriate transforms. These transforms revealed various properties which are common to all filters. In the rest of this chapter some more design parameters are described. In this section, in particular, the influence of the chatter parameter t_c is discussed. It is shown that for small values t_c it is not necessary to provide for chatter in the filter design. The same purpose is achieved by applying a special filter to the stacked output. Below, some computational experiments were done with pass-velocity filters to show how various values of t_c influence the (f-k) plot.

The design parameters of filter number 3 were chosen and some (f-k) plots for filters with various values of t_c were computed. Figure 7.5.1 shows the (f-k) plots of some of these filters. The contours should be compared with the ones of figure 7.1.2 . One sees immediately that t_c influences only the frequency content of the (f-k) diagram. The transfer characteristics stay very much the same for low frequencies. In figure 7.5.2 some zero moveout transfer functions for the given filter type are shown. By increasing t_c higher frequencies are increasingly rejected. This seems obvious because a certain value for t_c means a bigger distortion for high frequency signals than for low ones. It is therefore quite logical that (f-k) diagrams of multichannel velocity filters designed for high values t_c show suppressed characteristics for high frequencies.

The fact that only the frequency content is changed by t_c leads to the idea of applying a filter to the output which has a similar effect as the incorporation of t_c into the normal equations. These equations give a hint towards the selection of such a filter. It is assumed, expression (4.2.3) has the factor $\mathrm{sinc}^2(t_c f)$ instead of $\mathrm{sinc}(t_c f)$. Both functions are very similar for small values of t_c and $|f| < \frac{1}{2}$.

With the condition that $\gamma = 0$ these slightly changed normal equations correspond to a problem where, for the filtered signals rec(f) sinc (t_cf) instead of rec (f), a corresponding filter is designed with no chatter at all. Filtering the broad band signals in the input with sinc (t_cf) is the same as filtering the output with B(f) = rec (f) sinc (t_cf). In this way there is no need for incorporating t_c in any filter design at all. B(f) is the filter which takes care of the influence of t_c. Some amplitude spectra of B(f) for various values t_c were computed. They were very similar to the zero moveout transfer functions of figure 7.5.2. as long as γ and t_c were less than one.

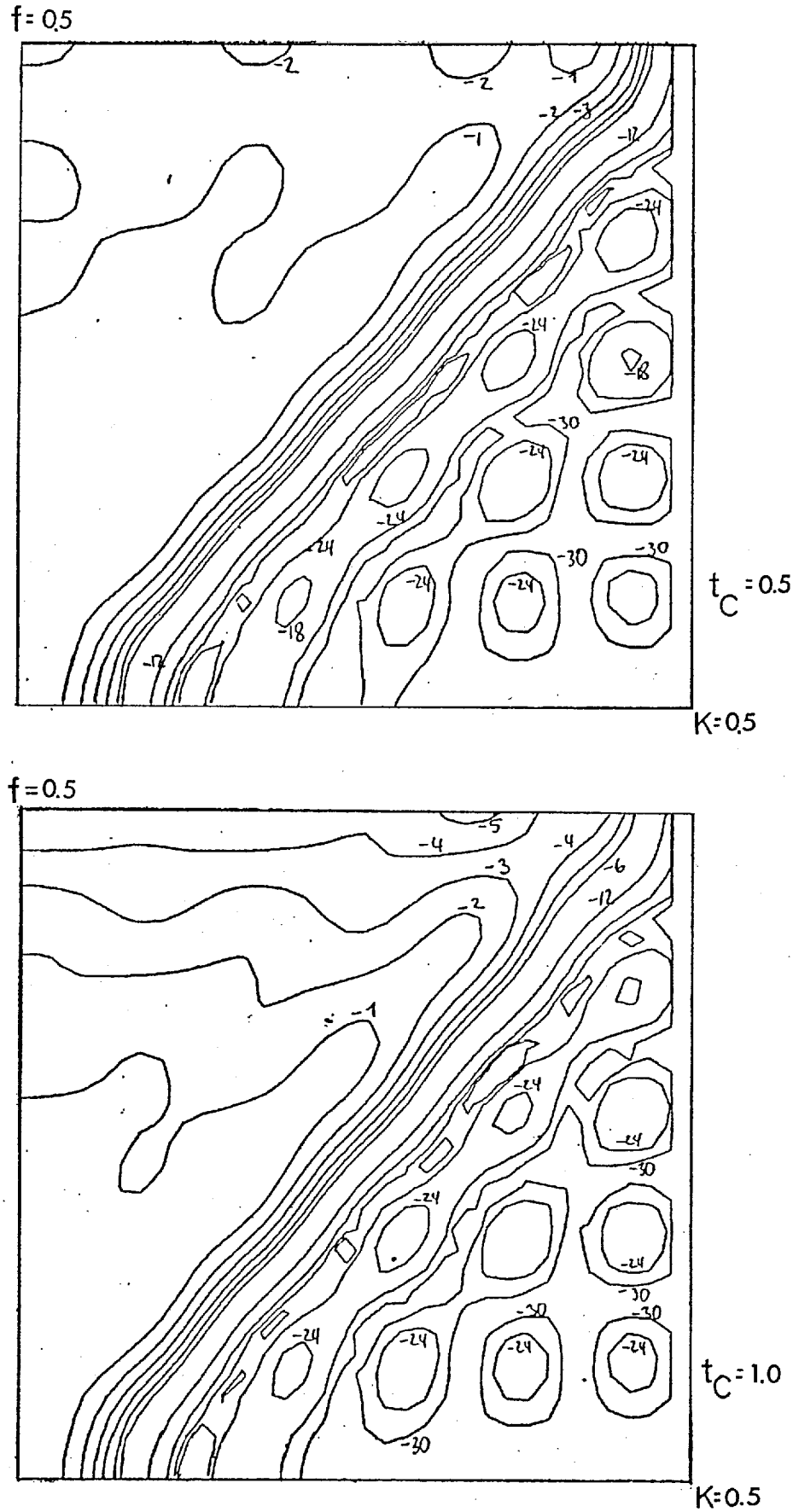

FIGURE 7.5.1 (f-k) diagrams (continued on next page)

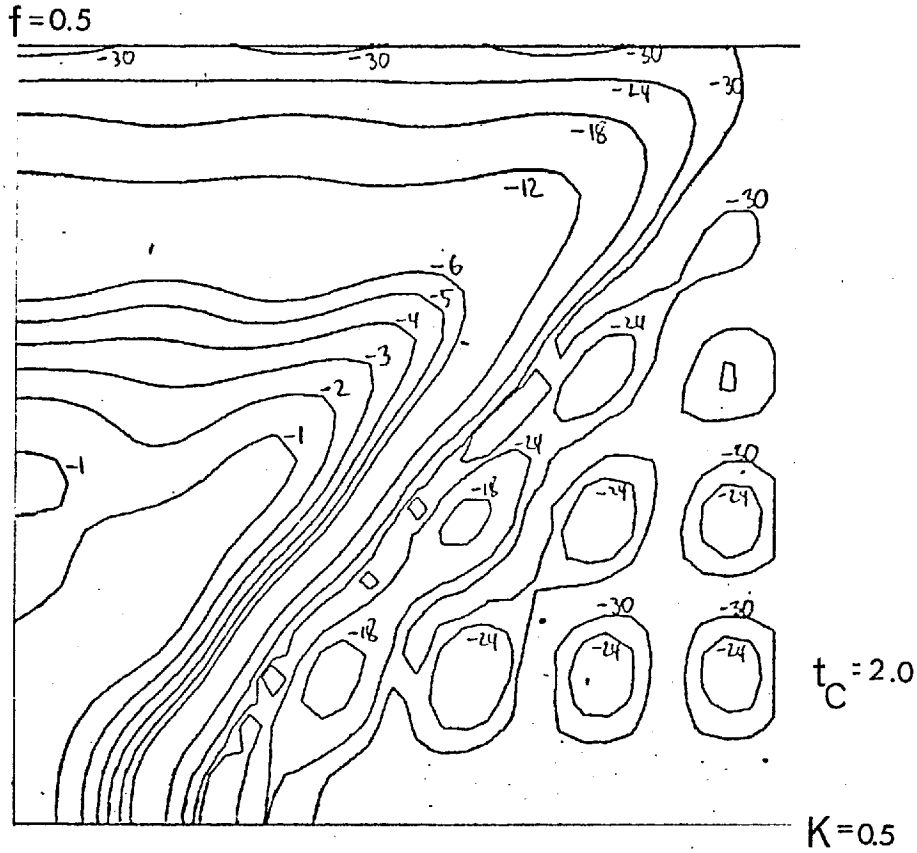

FIGURE 7.5.1 (f-k) diagram

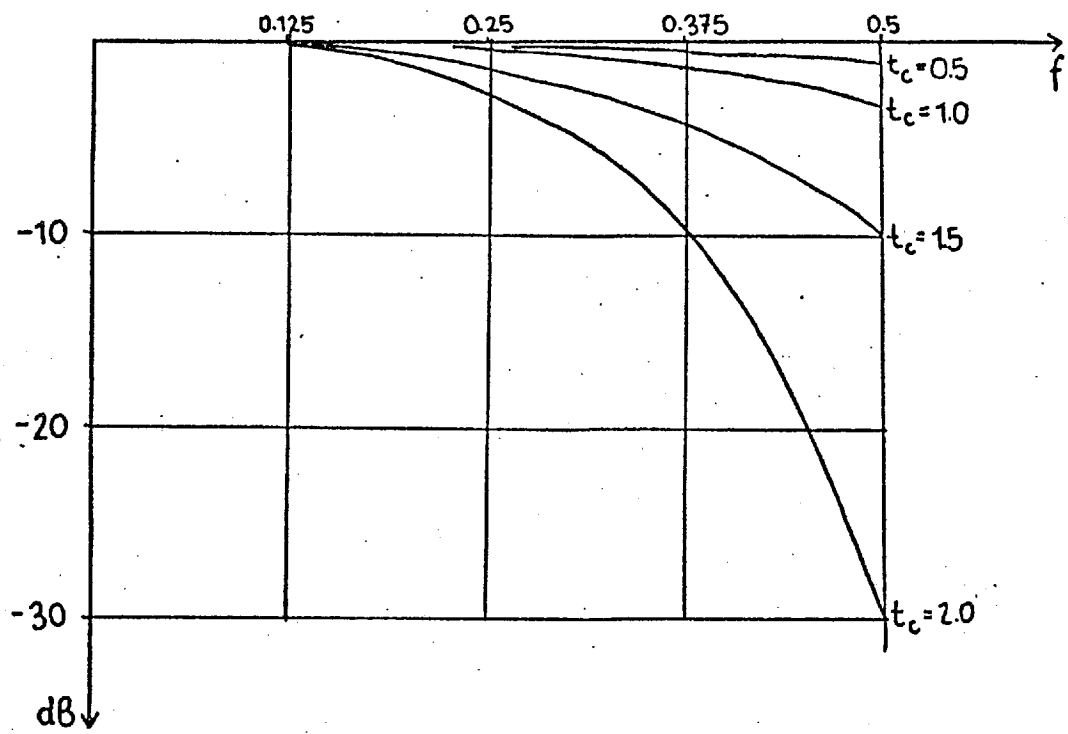

FIGURE 7.5.2 Zero moveout transfer functions

7.6 Influence of the weighting factor for correlated and uncorrelated noise

In this section some computational experiments are discussed which were done in connection with the parameters ϱ and ν. For reasons of simplicity the following treatment is confined to two-dimensional velocity filters. Results may however be generalized.

In previous sections stacking filters were characterised with certain transforms, from which transfer functions for given moveouts could be obtained. Using Parsevals theorem, the output energy for broad band signals for a particular moveout τ becomes:

$$E(\tau)=\int_{-\frac{1}{2}}^{+\frac{1}{2}}\left|F(f,\tau)\right|^2 df=2\int_{0}^{\frac{1}{2}}\left|\sum_{j=1}^{N}A_j(f)e^{-2\pi ijf\tau}\right|^2 df \qquad (7.6.1)$$

This function can usually be quite well estimated by simply looking at the two-dimensional Fourier transform. If, for instance, signals have the moveout τ_s and correlated noise the moveout τ_r the signal to correlated noise ratio for this case can be expressed as

$$S_r = E(\tau_s)/E(\tau_r) \qquad (7.6.2)$$

If signals have the rectangular band width rec (f/η); $(\eta<1)$ then their passed energy is obtained as

$$E(\tau) = 2\int_{0}^{1/2\eta}\left|F(f,\tau)\right|^2 df \qquad (7.6.3)$$

If K broad band noise families uncorrelated to each other with the constant moveouts τ_i, $(i=1,..,K)$ are present, their total energy in the output is

$$E = \sum_{i=1}^{K} E(\tau_i)$$

$E(\tau)$ was computed for filter number 12 with $\eta = 1$ and also for the 6-trace straightforward stack(see figure 6.2.7). Both functions are shown in figure 7.6.1. If the constant moveouts for broad band signals and noise

are known, one may read their appropriate energy values from the graph and obtain the signal to correlated noise ratio by simple division. The straightforward stack leads to good ratios, if the signals have more or less exact zero moveout. However, for fairly small deviations from this the ratios are more favourable in the case of filter number 12. Increasing ϱ may considerably improve the signal to correlated noise ratio. Figure 7.6.2 shows some functions $E(\tau)$ for filter number 1, where ϱ takes on various values. In figure 7.6.4 some corresponding (f-k) plots are given. The influence of ϱ on transfer characteristics can often be quite well predicted by recalling the relation between time windows and (f-k) plots and remembering the fact that high values of ϱ depress reject regions. Note that both pass and reject region are generally effected when ϱ is increased.

So far, little attention has been given to transfer characteristics of stacking filters to uncorrelated noise. Characteristics related to signals and correlated noise can be derived from the two-dimensional Fourier transform. This transform, however, gives no information about the response of the filter to uncorrelated noise. The presence of this noise is often quite considerable and by increasing it in the design (or the weighting factor ν of the error) considerable improvement of the signal to total noise ratio can be obtained. Let $n_i(t^*)$, $(i=1,..,N)$ be the uncorrelated noise components in the input and $a_i(t^*)$, $(i=1,.,N; -n \leq t^* \leq m)$ the components of the stacking filter. The corresponding noise in the output is then

$$n(t^*) = \sum_{i=1}^{N} a_i(t^*) * n_i(t^*)$$

whose autocorrelation is

$$\varphi_{nn}(\tau^*) = \sum_{i=1}^{N} \varphi_{a_i a_i}(\tau^*) * \varphi_{n_i n_i}(\tau^*),$$

from which the noise power is obtained as

$$E_{\bar{n}} = \varphi_{nn}(0)$$

By making, therefore, a further assumption that

$$\varphi_{n_i n_i}(\tau^*) = a \operatorname{sinc}(\tau^*)$$

one sees that

$$E_n = a\sum_{i=1}^{N} \varphi_{a_i a_i}(0) = a\sum_{\hat{t}^*=-n}^{m} \sum_{i=1}^{N} a_i^2(\hat{t}^*) \qquad (7.6.4)$$

The sum of the squared stacking filter components therefore is a good criterion to investigate the performance of a filter on uncorrelated noise. Especially for the straight forward stack, where the filter components are zero delay spikes of a height 1/N the power of the passed noise is $E_n = a/N$. It is well known, that if noise events are randomly distributed, then simple addition of traces represents the best possible technique for its suppression (Burg, 1964). Ideally therefore, what is desired is a stacking filter which approximates well the specified pass and reject regions and shows also optimally the same characteristics in relation to uncorrelated noise as a straight forward stack. For optimum multichannel velocity filters it is known that increasing uncorrelated noise in the design results in a depression of the pass regions of the (f-k) diagram. This property was observed for all filters belonging to the class treated in this thesis. From this observation one may still not conclude in which way the response for uncorrelated noise is changed. If special attention is therefore to be given to the improvement of the signal to uncorrelated noise ratio in the output, the following function can be used to characterise a filter for broad band signals.

$$S(\tau) = E(\tau)/E_n \qquad (7.6.5)$$

$E(\tau)$ is given in (7.6.3) and E_n is used as in (7.6.4) with a = 1.

For instance if broad band signals and noise with the same power in the traces and the constant moveouts τ_s and τ_r are given, the signal to total noise ratio becomes with (7.6.5)

$$\frac{S(\tau_s)}{S(\tau_r) + 1} = \frac{E(\tau_s)}{E(\tau_r) + E_n}$$

A number of functions $S(\tau)$ for a series of filters was computed where the design parameters are the ones of filter number 12 except for the value ν, which was increased steadily. The functions are shown in figure 7.6.3. The dotted line belongs to the straight forward stack. There is no doubt that for low values ν, the signal to uncorrelated noise ratio can be fairly poor. This is certainly one of the reasons why velocity filters with good pass and reject characteristics applied to real seismograms may still show bad results. By increasing ν, the signal to noise ratio may, however, be improved. It was generally found that for about $\nu = 100$, a limiting curve $S(\tau)$ is obtained. For $\nu > 100$ no further essential improvement of the signal to noise ratio is possible. Figure 7.6.5 shows some (f-k) diagrams for filter number 12 and various values ν. These characteristics stay nearly unchanged for $\nu > 100$. A good signal to total noise ratio for the output trace is generally achieved by giving both ϱ and ν a value of approximately 40. By doing this, one should however be aware of the changes caused in the (f-k) diagram. All computational experiments show that the improvement of one filter property has to be paid for with a deterioration of other filter characteristics. These experiments also emphasize the importance of the time domain design. By designing a filter in the (f-k) domain it would be difficult to influence the signal to noise ratio.

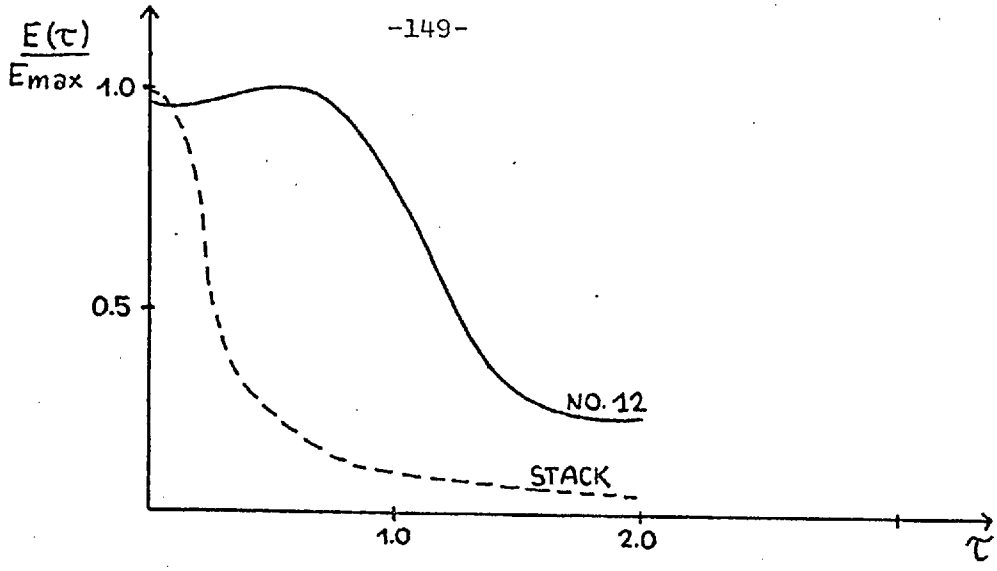

FIGURE 7.6.1

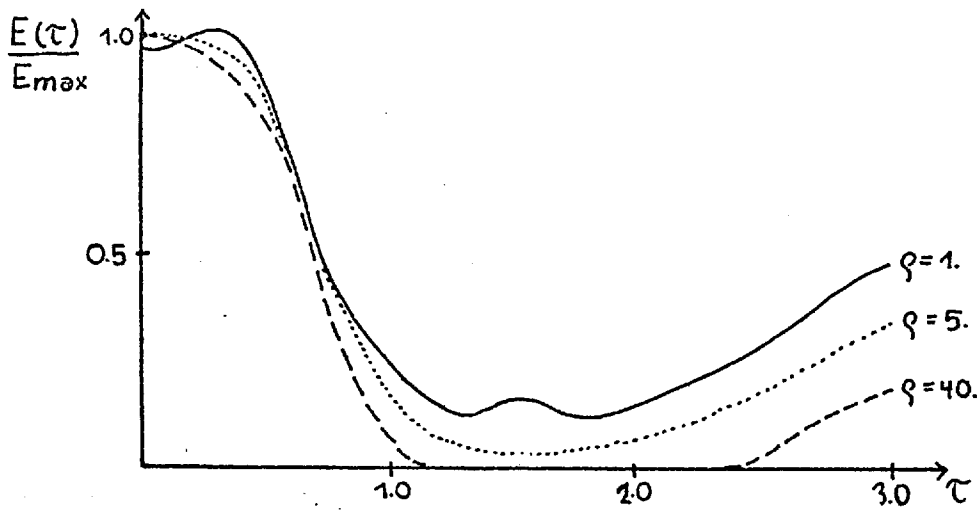

FIGURE 7.6.2

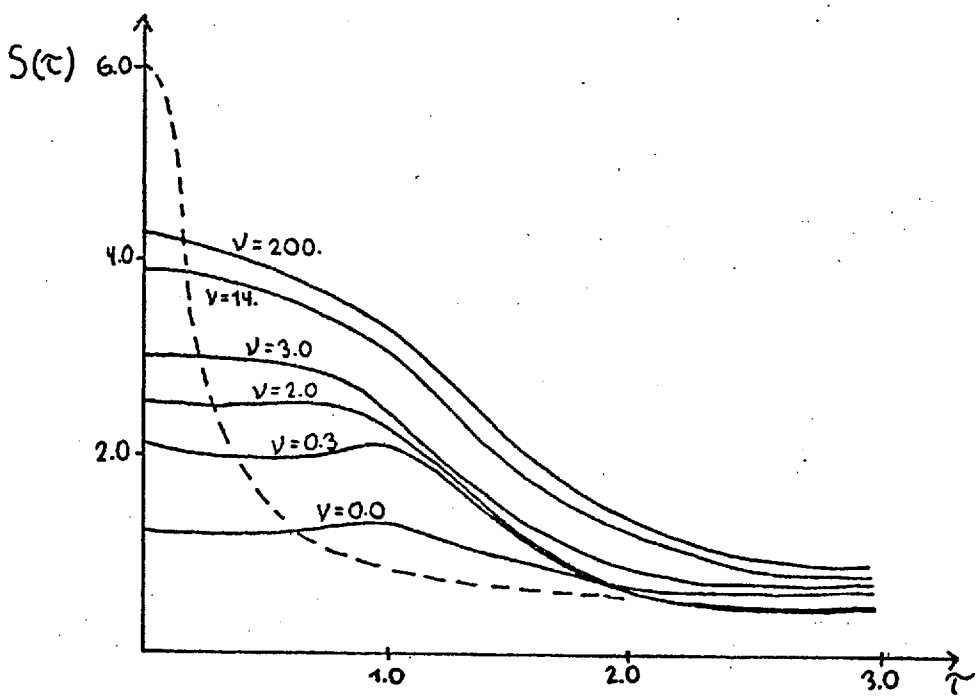

FIGURE 7.6.3

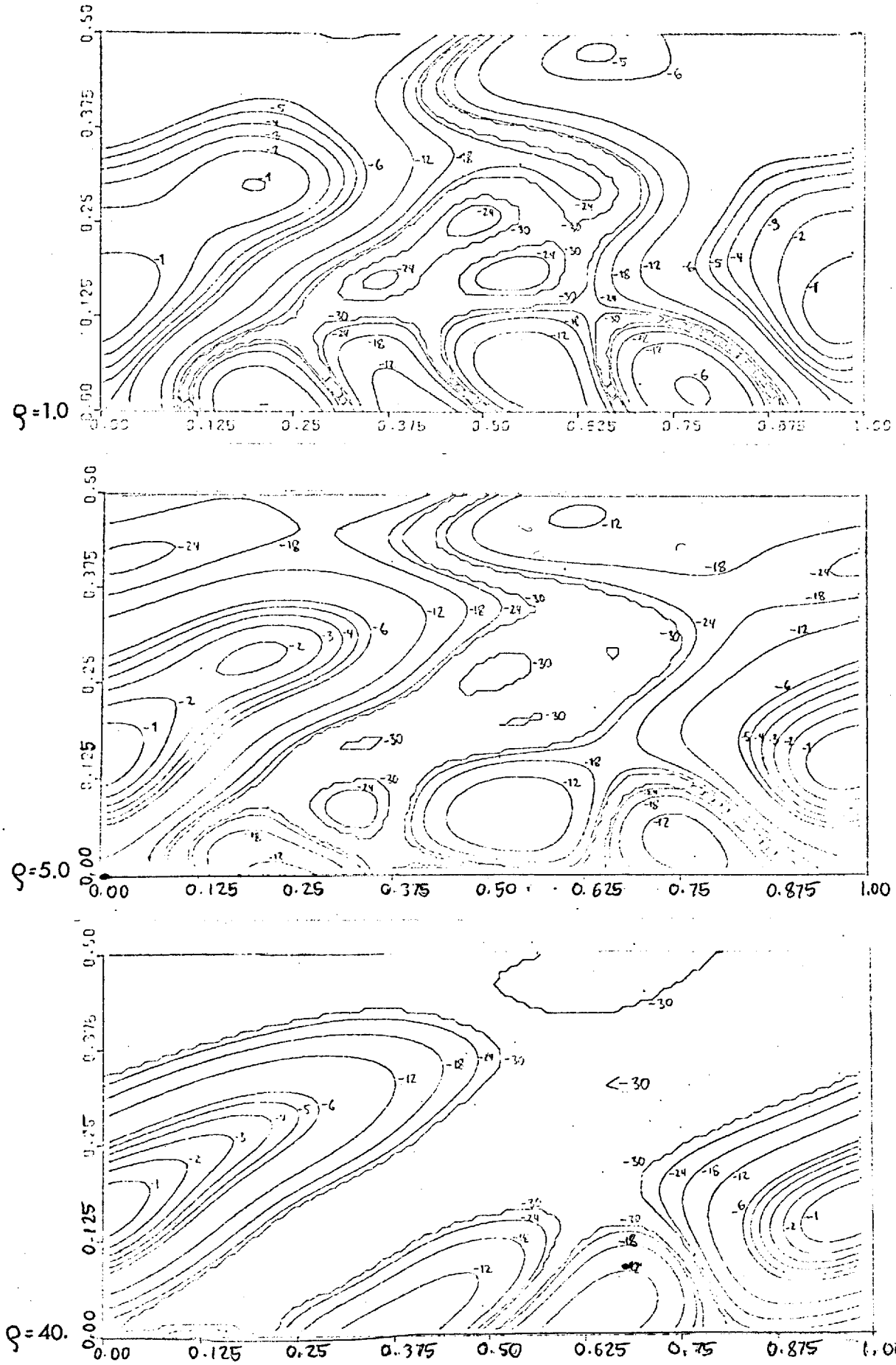

FIGURE 7.6.4 (f-k) diagrams to demonstrate the influence of ρ

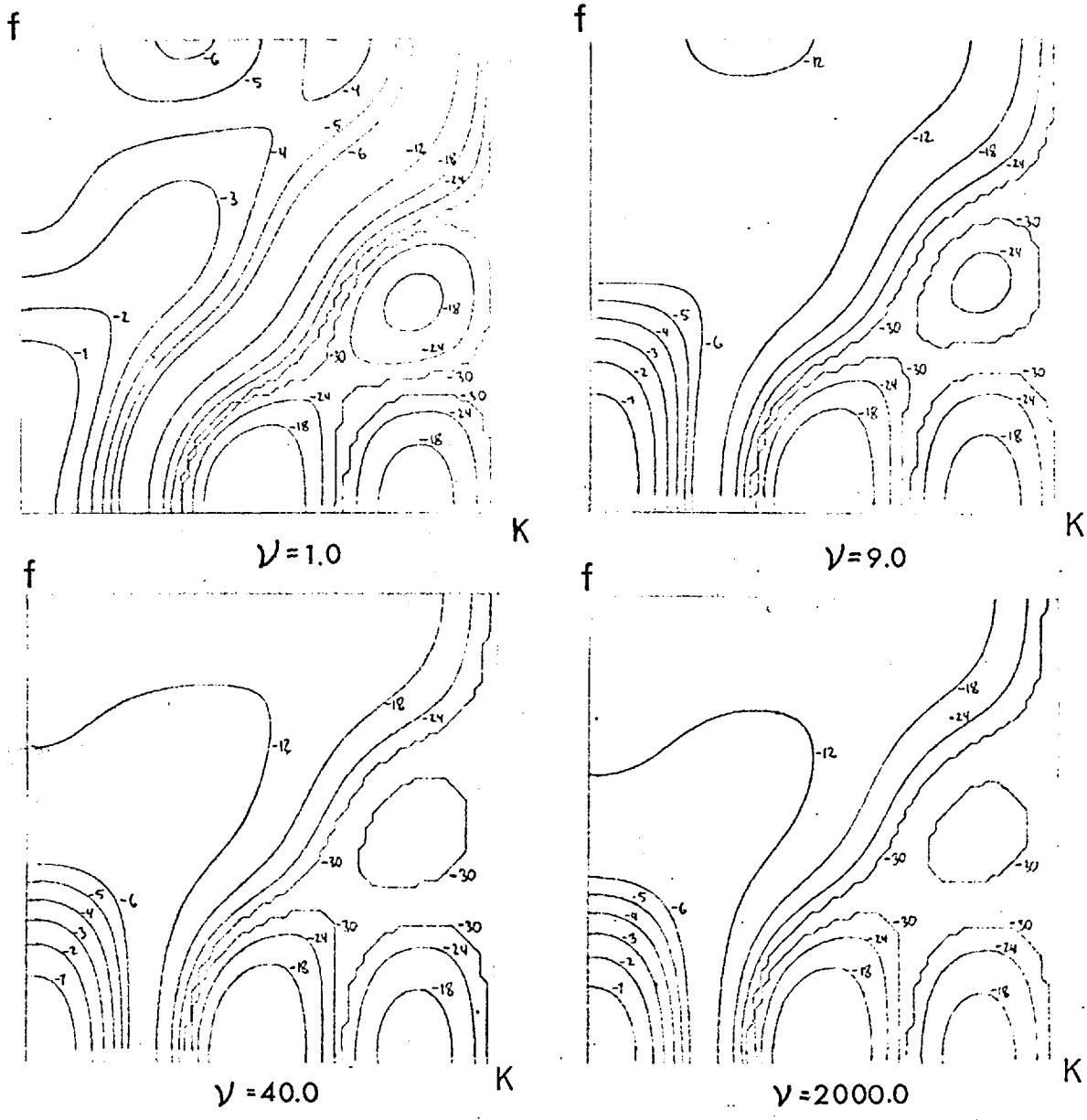

FIGURE 7.6.5 (f-k) diagrams for filter number 12 for various values of ν

7.7 Design of suboptimum stacking filters

In this section some methods of obtaining filters for large arrays from optimum stacking filters designed for small arrays are shown. The characteristics of these filters are not as good as the ones of the optimum stacking filters. They are therefore called suboptimum. Note that this term is used here in a different sense as by Foster, Sengbush, Watson (1964). Suboptimum filters need less computation time and computer space for the design. Three different approaches for the filter computation are given below. For reasons of simplicity the treatment is confined to the case of two-dimensional velocity filters. Most ideas can be logically extended to the whole class of filters.

1. The two-dimensional convolution technique.

In chapter VI it was shown that two-dimensional convolution of an N-trace operator with a M-trace operator leads to an (N + M - 1) trace operator. The two-dimensional Fourier transform of the (N + M - 1) trace operator is the product of the transforms of the N- and M-trace operators. In this way one may obtain a stacking filter for N + M - 1 traces from two stacking filters designed for N and M traces. If N- and M-trace operators have similar characteristics in the (f-k) domain, the response of the (N + M -1)-trace filter is better than either of the smaller filters, because the product of the Fourier transforms enhances pass- and depresses reject regions (dB values in the given (f-k) plots have to be added). If N and M trace operator are both symmetric or centro-symmetric, the (N + M -1) trace filter is also symmetric or centro-symmetric.

2. Cascade filter technique.

Let 2M traces be given where signals arrive with the constant moveout τ. A 2M-trace filter for a certain window is desired, however only an M-trace filter $a_j(t^*)$, (j=1,.M)for the same window shape is available.

It is shown below how to use two of the given filters on all 2M traces. By applying the filter to traces 1 to M and again to traces M +1 to 2M, two output signals result with moveout $M\tau$. After filtering these two output traces with a stacking filter $b_i(t^*)$,(i = 1,2) where the time window is M times broader than the given one, one obtains again a single trace filtered output. Because of the broad design region for the 2-channel filter numerous foldings in its (f-k) diagram may occur. This technique therefore, should be only used for narrow design regions. Instead of applying these stacking filters in cascade, one may use the stacking filter $c_i(t^*)$,(i = 1,..,2M)

$$c_i(t^*) = a_i(t^*)*b_1(t^*), \quad (i=1,..,M)$$

$$c_{i+M}(t^*) = a_i(t^*)*b_2(t^*), \quad (i=1,..,M)$$

3. Supplementing of time windows

When a time window for M + N traces is given each filter component obtained depends on the total shape of the window and on all traces. Nevertheless, it seems logical that if for M and N subsequent traces of the window two stacking filters $a_i(t^*)$for i=1,.,M and i=M+1,.,M+N are individually computed, the stacking filter $a_i(t^*)$ (i=1,M+N) should show suboptimum characteristics if applied to all M+N traces simultaneously. The experiments carried out were generally successful, especially when a given time window was separated at a centre point. To give an example, a 6-trace filter for the time window of figure 7.7.1 was computed. The filter components are given in table 7.7.1. With these components the following 11-trace filter was defined: $c_i(t^*) = a_i(t^*)$,(i=1,..,5) $c_{i+5}(t^*) = a_{7-i}(t^*)$,(i=1,..,6). The stacking filter is now a suboptimum filter for the time window of figure 4.2.4. The two-dimensional Fourier transform of $c_i(t^*)$,(i=1,11) is given in figure 7.7.2. It shows that the characteristics are the ones of the desired time window. When compared with the characteristics of filter number 6 (see figure 7.1.7) one may

easily see that the specified regions are less well approximated. Also the reject region of the suboptimum filter is higher and the escarpment is less steep. The essential difference lies however, in the computation time. The suboptimum filter was computed in 2.5 sec, while the optimum filter needed 12 sec. The described method therefore, is of special value, for very large arrays.

The technique is also useful to obtain filters for less traces from filters designed for many traces. Whenever time windows were reduced by taking various traces out, the remaining components usually showed reasonably well characteristics which corresponded to the expected characteristics of the left time window. This approach is purely practical. To be certain that the method works, the two-dimensional Fourier transform should be applied to the resulting filter to check its characteristics.

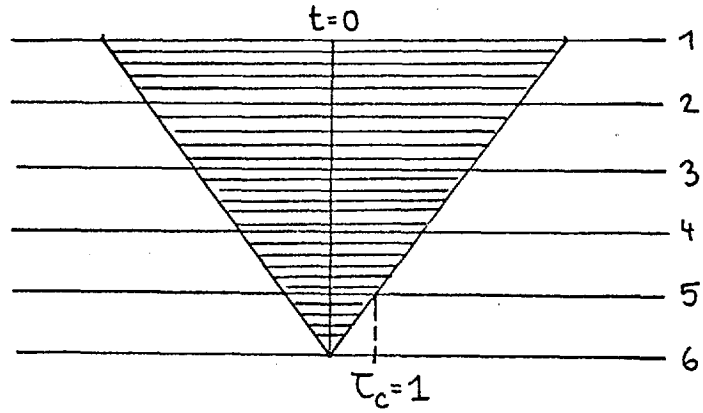

FIGURE 7.7.1 Time window for a pass filter (end trace estimate)

$a_1(t^*)$	$a_2(t^*)$	$a_3(t^*)$
.64936139E-02	.13543963E-02	.42121275E-02
.66728768E-04	.12205933E-01	.38795549E-02
-.18454900E-01	.22437790E-01	.12722552E-01
-.15747459E-01	-.40144179E-02	.39113787E-01
-.87068792E-02	-.12676570E-01	.14274044E-01
-.12404779E-01	-.22020857E-02	-.99609271E-02
-.71472265E-02	-.10705509E-01	.74001271E-02
-.12404779E-01	-.22020858E-02	-.99609270E-02
-.87068793E-02	-.12676570E-01	.14274044E-01
-.15747459E-01	-.40144162E-02	.39113787E-01
-.18454900E-01	.22437790E-01	.12722551E-01
.66728797E-04	.12205933E-01	.38795546E-02
.64936139E-02	.13543962E-02	.42121275E-02

$a_4(t^*)$	$a_5(t^*)$	$a_6(t^*)$
-.93947895E-03	-.58549519E-03	-.49701414E-02
.13954026E-02	-.26703299E-02	-.74324095E-02
.39635419E-02	-.54971276E-02	-.11090605E-01
.99023043E-02	-.45939103E-02	-.21550710E-01
.56752353E-01	-.57695972E-02	-.37040202E-01
.45063079E-01	.04026227E-01	-.10411501E+00
-.70702361E-02	.17985853E+00	.76310295E+00
.45630950E-01	.04026227E-01	-.10411501E+00
.56752354E-01	-.57695970E-02	-.37040201E-01
.99023043E-02	-.45939100E-02	-.21550711E-01
.39635421E-02	-.54971274E-02	-.11090605E-01
.13954031E-02	-.26703295E-02	-.74324095E-02
-.93947705E-03	-.58549434E-03	-.49701412E-02

TABLE 7.7.1 Stacking filter components for the filter with the time window of figure 7.7.1; N=6 ; τ_c=1.0 ; ν=0.08

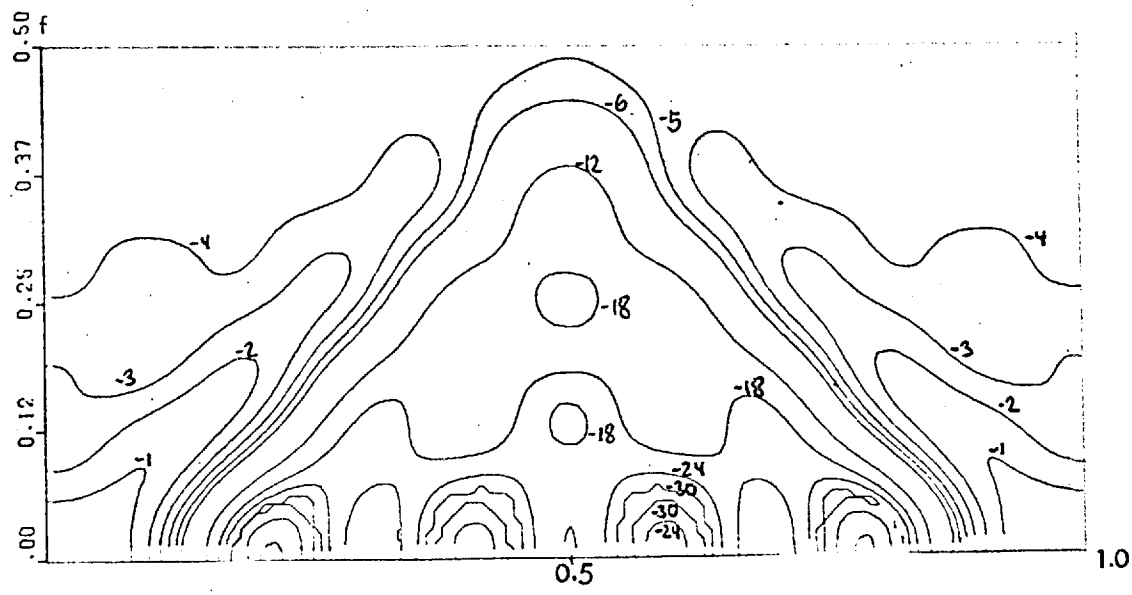

FIGURE 7.7.2 (f-k) diagram of a 11-trace suboptimum filter

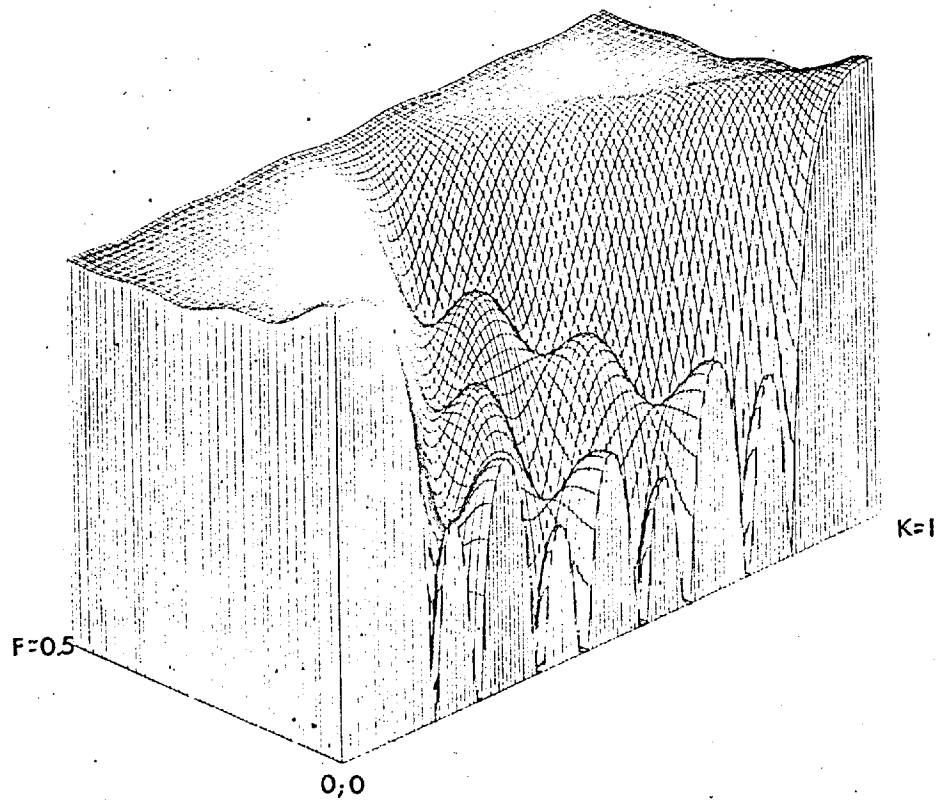

Isometric plot of 7.7.2

CHAPTER VIII

THE SCALING EFFECT

From the normal equations (4.2.4) a number of conclusions could be drawn about the symmetries of the stacking filters. These symmetries are important to find the phase responses of transfer functions for special cases as discussed in Chapter VI.

There is however, one more important property revealed by the normal equations which is discussed in this chapter separately because it gives deep insight into multichannel stacking filters. This property is also of great economical value for the design of stacking filters and makes their application therefore even more attractive. By making full use of the described effect, it is possible to derive a number of stacking filters from a computed one by scaling the filter responses. In this way a tremendous amount of computer time for the filter design can be saved. Scaled filters have approximately the same characteristics as the ones which are directly computed from the normal equations.

Let t_j^k and $\Delta t_j^k (j=1,..,N;k=1,..,L)$ be the design parameters for L time windows designed for the signals, while $\bar{t}_j^k$ and $\overline{\Delta t}_j^k (j=1,N;k=1,K)$ are the corresponding design parameters for K regions of correlated noise. The continuous version of the normal equations for the most general case in the frequency domain is

$$\sum_{i=1}^{N} A_i(f)\,\mathrm{rec}(f)\left[R_{ij}(f)+\nu\delta_{ij}\right] = \mathrm{rec}(f)G_j(f),(j=1,.N) \quad (8.1)$$

where $R_{ij}(f)$ is given in (4.2.5) and $G_j(f)$ in (4.2.6) however for the following considerations without the factor rec(f) and $\nu = 0$. One realizes that by replacing the design parameters with the scaled ones (with η as scaling factor) such as,

$$\tilde{t}_j^{\,k} = \frac{1}{\eta} t_j^{\,k}; \quad \Delta\tilde{t}_j^{\,k} = \frac{1}{\eta}\Delta t_j^{\,k}; \quad \tilde{\bar{t}}_j = \frac{1}{\eta}\bar{t}_j^{\,k}; \quad \Delta\tilde{\bar{t}}_j^{\,k} = \frac{1}{\eta}\Delta\bar{t}_j^{\,k}; \quad \tilde{t}_c = \frac{1}{\eta} t_c$$

the following normal equations are obtained

$$\sum_{i=1}^{N} \tilde{A}_i(f)\,\mathrm{rec}(f)\left[\tilde{R}_{ij}(f) + \nu\delta_{ij}\right] = \mathrm{rec}(f)\,\tilde{G}_j(f), \quad (j=1,..,N) \qquad (8.2)$$

where $\tilde{R}_{ij}(f) = R_{ij}(f/\eta)$ and $\tilde{G}_j(f) = G_j(f/\eta)$

A comparison between the normal equations (8.2) and (8.1) shows that replacing rec(f) with rec(f/η) in (8.2) gives

$$\mathrm{rec}(f/\eta)\sum_{i=1}^{N} \hat{A}_i(f)\left[\tilde{R}_{ij}(f) + \nu\delta_{ij}\right] = \mathrm{rec}(f/\eta)\,\tilde{G}_j(f), \quad (j=1,..,N) \qquad (8.3)$$

and leads to the solution $\hat{A}_j(f) = A_j(f/\eta)$, (j=1,.N). This means the knowledge of the solution of (8.1) includes the knowledge of all other problems, where signals and regions are a scaled version of (8.1). In the special case where $\eta > 1$ even the solution of (8.2) is included in (8.1). Since solutions of the above normal equations for a fixed value of f cannot be influenced by other frequencies they have to be

$$\tilde{A}_j(f) = A_j(f/\eta)\,\mathrm{rec}(f), \quad (j=1,..,N) \qquad (8.4)$$

This important property of the continuous frequency domain version of the normal equations is also valid to a certain degree for the discrete approximate solutions. If $a_j^{\,n}(t^*)$ $(-n \le t^* \le n,\ j=1,.N)$ are the discrete solutions, an approximate solution for (8.1) would be in the time domain

$$a_j^{\,n}(t) = \sum_{i=-n}^{n} a_j^n(i)\,\mathrm{sinc}(t-i), \quad (j=1,..,N) \qquad (8.5)$$

The continuous functions

$$\hat{a}_j^{\,n}(t) = \eta a_j^{\,n}(\eta t) = \eta\sum_{i=-n}^{n} a_j^n(i)\,\mathrm{sinc}\,(\eta t-i), \quad (j=1,..,N) \qquad (8.6)$$

should therefore be an 'approximate' solution for (8.3).

The Fourier transform of (8.6) is confined to the range $|f| < 1/2\eta$. If η is less than one, sampling of (8.6) can be done without aliasing

$$\hat{a}_j^n(t^*) = \eta \sum_{i=-n}^{n} a_j^n(i) \text{ sinc } (\eta t^* - i), \quad (j=1,..,N) \qquad (8.7)$$

This expression represents an approximate discrete solution which could be obtained by computing the stacking filter for a broader scaled design region, using however, the narrower band signal rec (f/η). Because (8.7) is generally an infinitely long operator it has to be truncated. These scaled discrete filters were always given a fairly short length of the width of the time window and the results obtained were found to be satisfactory.

To give some examples, the response of filter number 4 was scaled with $\eta = 3/4$ using the above described scaling procedure. The two dimensional Fourier transform of the scaled filter is given in figure 8.1. It has about the same (f-k) diagram as filter number 5, however, confined to the range $|f| \leq 3/8$. In the same way, filter number 2 was scaled with $\eta = 1/2$ and $\eta = 1/4$. Contours and isometric presentations for the scaled responses are given in figure 8.2 and figure 8.3. Comparing the (f-k) plots of filter number 3 (Fig. 7.1.2) and number 5 (Figure 7.1.4) with Fig. 8.2 and 8.3 it could be noticed that characteristics of the scaled responses are about as good in the expected frequency range as the ones of the directly computed filters.

If $\eta<1$ the gain in width of the time window obtained by simply scaling the responses of filters has to be paid for with a loss of the high frequency content in the scaled responses. This loss is often acceptable (may even be desirable), because the seismic frequency content is usually expected in the low part of the basic region. The lowest limit of η for scaling is therefore given by the highest frequency which is to be filtered by the scaled stacking filter. A look at the computer time

(CDC 6600) for the differently designed filters as given in table 8.1 reveals the importance of the scaling effect. The computer time for the scaling process itself took in all cases less than 0.5 sec. for a stacking filter. Designing a filter for a broader time window by scaling the responses for a narrower window may mean a tremendous saving of computing time. From each filter one may derive any number of scaled versions. To make an a priori broad band assumption for the signals is therefore useful in getting the optimum out of the scaling procedure.

So far the scaling effect was treated only for $\eta<1$. This corresponds to broadening the time windows. Choosing $\eta>1$ corresponds to narrowing the time windows. The computation time involved in the filter design for broad time windows is longer than that for narrow windows. It would not be justified in this case to suffer also a loss in the characteristics of the scaled responses. As a matter of fact, it can be shown that a filter designed for a broad time window already includes all filter responses for $\eta>1$ (see formula 8.4).

To show the scaling effect for $\eta>1$ the discrete filter number 4 was scaled with $\eta = 3/2$ by making use of formula (8.7) again. The two-dimensional Fourier transform of the scaled filter is given in figure 8.4. It is essentially the expected one of filter number 3. There is, however, a step of around 6 dB at f = 0.25. The difference in height from the lower plateau to the reject region is the same as in filter number 3. This filter could be used in the same way as long as the frequency content is confined to $|f|<0.25$. The step in the plateau is due to aliasing, because the Fourier transform of each component (8.6) exceeds the range $|f|\leq 1/2$ and the frequencies $1/2<|f|<1/2\eta$ have to be folded back in the scaled and sampled filter. For the case $\eta = 3/2$ the aliased frequencies lie in the range $0.25<|f|<0.5$. The fact that the step between the two plateaux is about 6 dB, shows that the amplitude spectrum of the Fourier

transform in the upper pass region is twice as high. It may be recalled that the sampled function of sinc (ηt) for $1>\eta>1/2$ has the Fourier transform

$$S(f) = \begin{cases} 1 \text{ for } f < \frac{1}{2}-\frac{1}{2}\eta \\ 2 \text{ for } \frac{1}{2}-\frac{1}{2}\eta < |f| < \frac{1}{2} \end{cases} \qquad (8.8)$$

The amplitude ratio at the step is two and the dB value is therefore $20 \log_{10} 2 \approx 6.02$. The fact that the corners of the step are not sharp is due to truncation of the discrete scaled responses.

To prevent aliasing, one therefore has to antialias the responses for $\eta>1$ as given in formula (8.4). This means equation (8.6) has to be convolved with sinc(t)

$$\tilde{a}_j^n(t) = \eta a_j^n(\eta t) * \text{sinc}(t) = \eta \int_{-\infty}^{+\infty} \sum_{i=-n}^{n} a_j^n(i)\,\text{sinc}(\eta\tau - i)\,\text{sinc}(t-\tau)\, d\tau \qquad (8.9)$$

$$\tilde{a}_j^n(t) = \eta \sum_{i=-n}^{n} a_j^n(i)\,\text{sinc}(t - i/\eta), \quad (j=1,..,N) \qquad (8.10)$$

and sampled again

$$\tilde{a}_j^n(t^*) = \eta \sum_{i=-n}^{n} a_j^n(i)\,\text{sinc}(t^* - i/\eta), \quad (j=1,..,N) \qquad (8.11)$$

Formula (8.10) is an 'approximate' solution of (8.2) in the time domain. It has to be used instead of (8.6) whenever a scaled version of a discrete filter for $\eta>1$ is desired. Using equation (8.11), the time responses of filter number 4 were again scaled with $\eta = 3/2$. The two-dimensional Fourier transform is given in figure 8.5. As can be seen the (f-k) plot corresponds to the expected one of filter number 3.

The above examples to describe the scaling effect were selected from two-dimensional multichannel velocity filters. This was done to use the two-dimensional Fourier transform as a tool to compare the differently designed filters. It must, however, strongly be emphasized that the scaling effect applies to the total class of the given stacking

filters. Formula (8.6) and (8.11) can be used in every case.

Apart from the enormous amount of computer time which may be saved by making full use of the scaling effect, it also explains other observations which so far, have no mathematical explanation. When designing a pass-reject filter one has the heuristic feeling that the stepout between signal and correlated noise must increase as the dominant wave length of signal and noise increases. Various experiments were done where broad band signals were filtered with one stacking filter and low-passed signals filtered with half the Nyquist frequency and twice the moveout were filtered with another filter where the window was twice as wide. The responses for several signal stepouts agreed to within one percent. This observation which applies to all stacking filters is explained below, both for a multichannel velocity filter and a general stacking filter.

If the two dimensional Fourier transform for an exact solution of (8.1) is

$$F(f,k) = \sum_{j=1}^{N} e^{2\pi i k j} A_j(f) \text{ rec } (f) \qquad (8.12)$$

then the transform for the exact solution of (8.2) for a scaled region is a scaled version

$$F(f/\eta,k) = \sum_{j=1}^{N} e^{2\pi i k j} A_j(f/\eta) \text{ rec } (f) \qquad (8.13)$$

The best one can hope for is that the (f-k) plots of finite length filters, designed for time windows, which are scaled versions of each other, satisfy the relation between (8.12) and (8.13) approximately. Comparing the (f-k) diagrams of filter number 2 to number 4 shows that these transforms have the general character of being scaled. The hills in the reject region, which should have the same height for the exact solutions may however, show great changes.

It is assumed that the exact solution of a velocity filter is given. Figure 8.6 a, may contain its two-dimensional Fourier transform. The inverse Fourier transform along the line A is the stacking filter response $f_0(t)$ for broad band signals with constant moveout τ_0. Owing to (8.12) and (8.13) the values along the line A will appear along line B of figure 8.6 b, which may contain the two-dimensional Fourier transform of the filter designed for the scaled region with $\eta = \frac{1}{2}$. This line B is now the transfer function for the signals rec $(f/\frac{1}{2})$ (low-passed with half the Nyquist-frequency) having twice the moveout. The inverse Fourier transform of the function along the line B is $\frac{1}{2}f_0(\frac{1}{2}t)$ and is therefore a scaled version of $f_0(t)$.

With the help of the scaling effect a deep insight is gained into the relation between (f-k) diagrams and time windows of multichannel velocity filters. These rules may be extended to three-dimensional multichannel velocity, polarisation or differential normal moveout filters. For the most general case of a stacking filter one may express therefore, the following rule (which applies exactly only for the 'exact' solutions).

Let $A_j(f)$, $(j=1,..,N)$ be the components of a stacking filter which was designed for broad band signals and a certain time window .

$$F_{\alpha}(f) = \sum_{j=1}^{N} A_j(f) e^{-2\pi i f \alpha_j} \operatorname{rec}(f)$$

is the transfer function of the filter for broad band signals with arbitrary moveout $\alpha_i (i=1,..,N)$. Scaling the time window by a factor $\eta<1$ and again using broad band signals in the design leads to the solutions

$$\tilde{A}_j(f) = A_j(f/\eta), \ (j=1,..,N), \ |f| \leq \tfrac{1}{2}\eta$$

The transfer function of this scaled stacking filter for signals $\operatorname{rec}(f/\eta)$ with moveout $\tilde{\alpha}_j = \alpha_j/\eta$ becomes

$$\tilde{F}_{\tilde{\alpha}}(f) = \sum_{j=1}^{N} A_j(f/\eta)\, e^{-2\pi i \alpha_j (f/\eta)}\, \mathrm{rec}\,(f/\eta)$$

thus showing that the equation

$$\tilde{F}_{\tilde{\alpha}}(f) = F_{\alpha}(f/\eta) \quad ; |f| \leq \tfrac{1}{2}\eta$$

holds. From this it is seen that the responses are scaled versions of each other.

Traces N	Filter length L F	Window Sections	Time (sec)
6	11	1	2.50
6	13	1	3.06
11	11	1	11.77
12	7	1	7.40
12	11	3	21.62
12	17	2	35.22
12	21	1	48.88
12	27	1	64.34
19	11	1	50.43
20	7	1	26.84
20	7	3	39.45
21	15	1	101.75

TABLE 8.1 Computation time for various optimum multichannel stacking filters

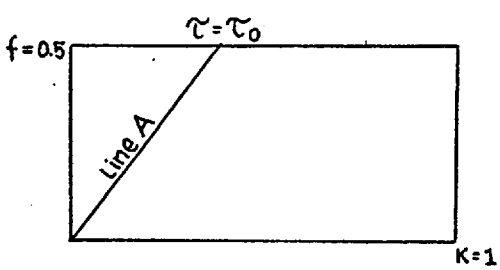

FIGURE 8.6 a

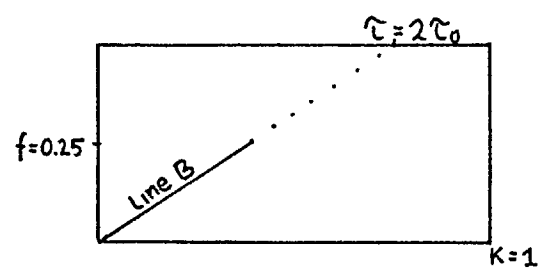

FIGURE 8.6 b

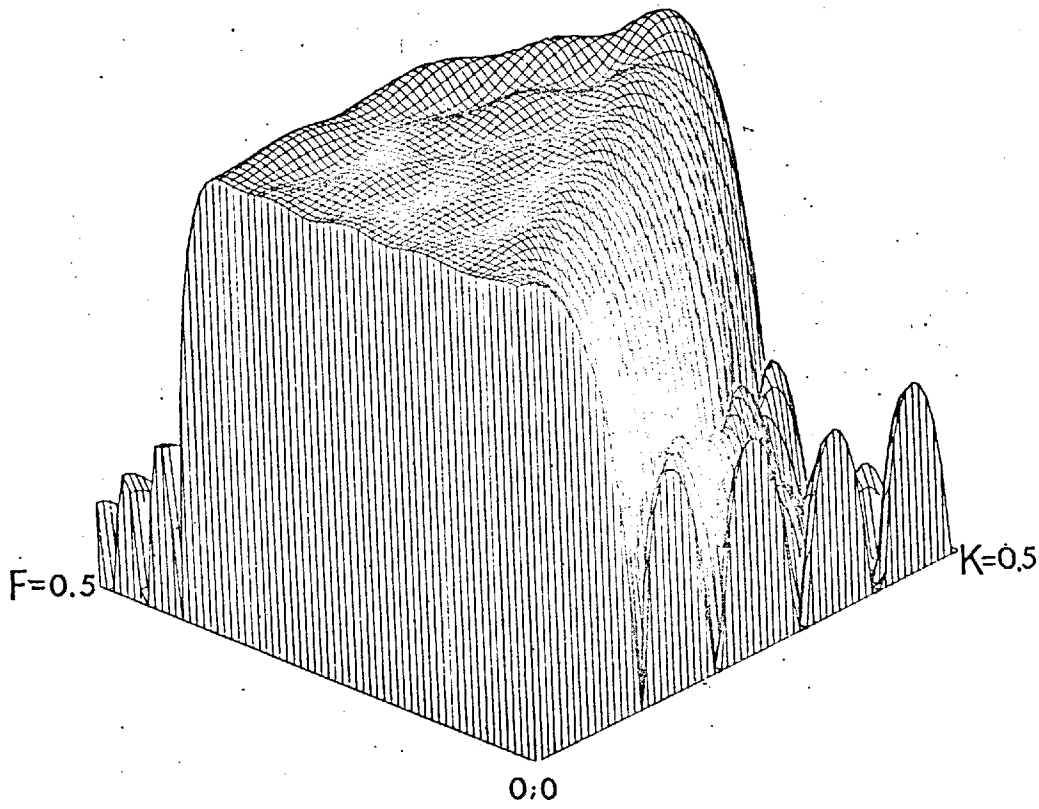

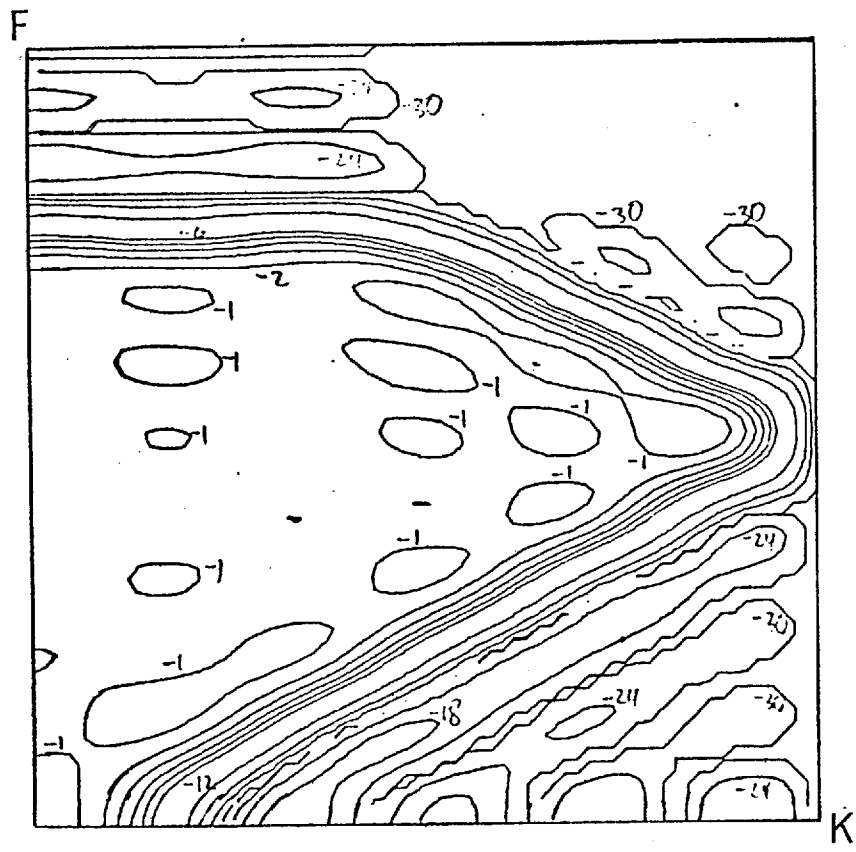

FIGURE 8.1 (f-k) diagram and isometric plot

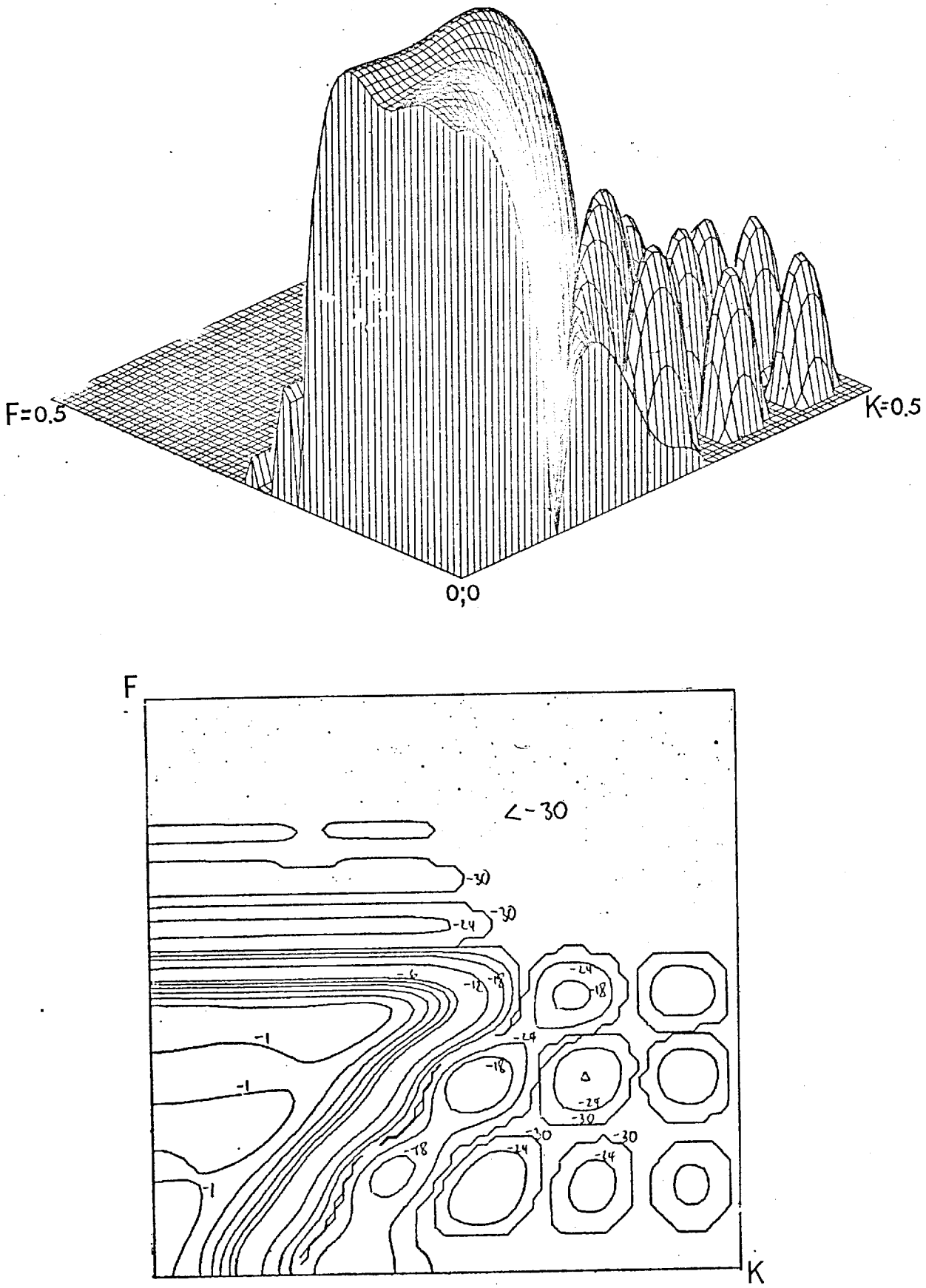

FIGURE 8.2 (f-k) diagram and isometric plot

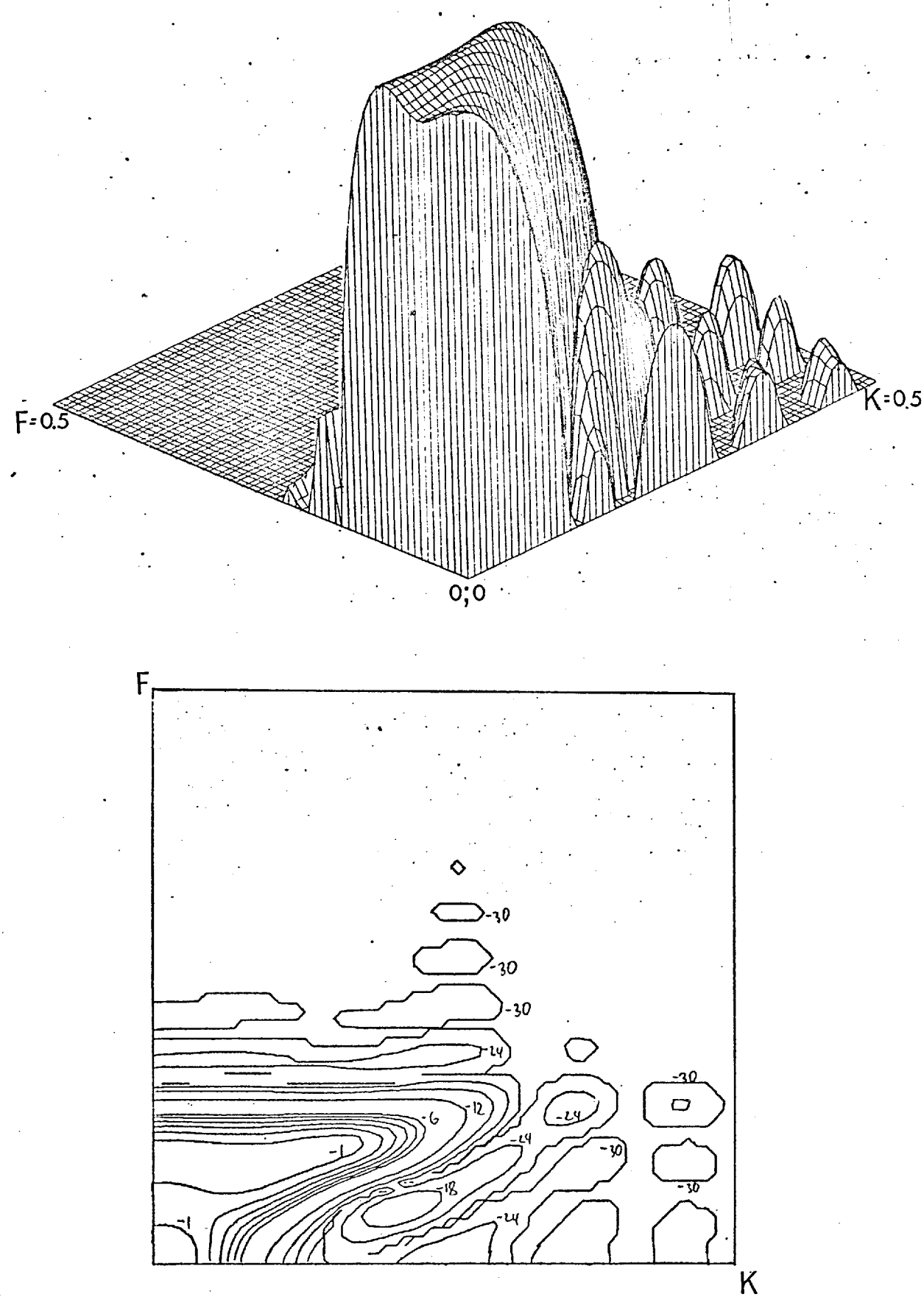

FIGURE 8.3 (f-k) diagram and isometric plot

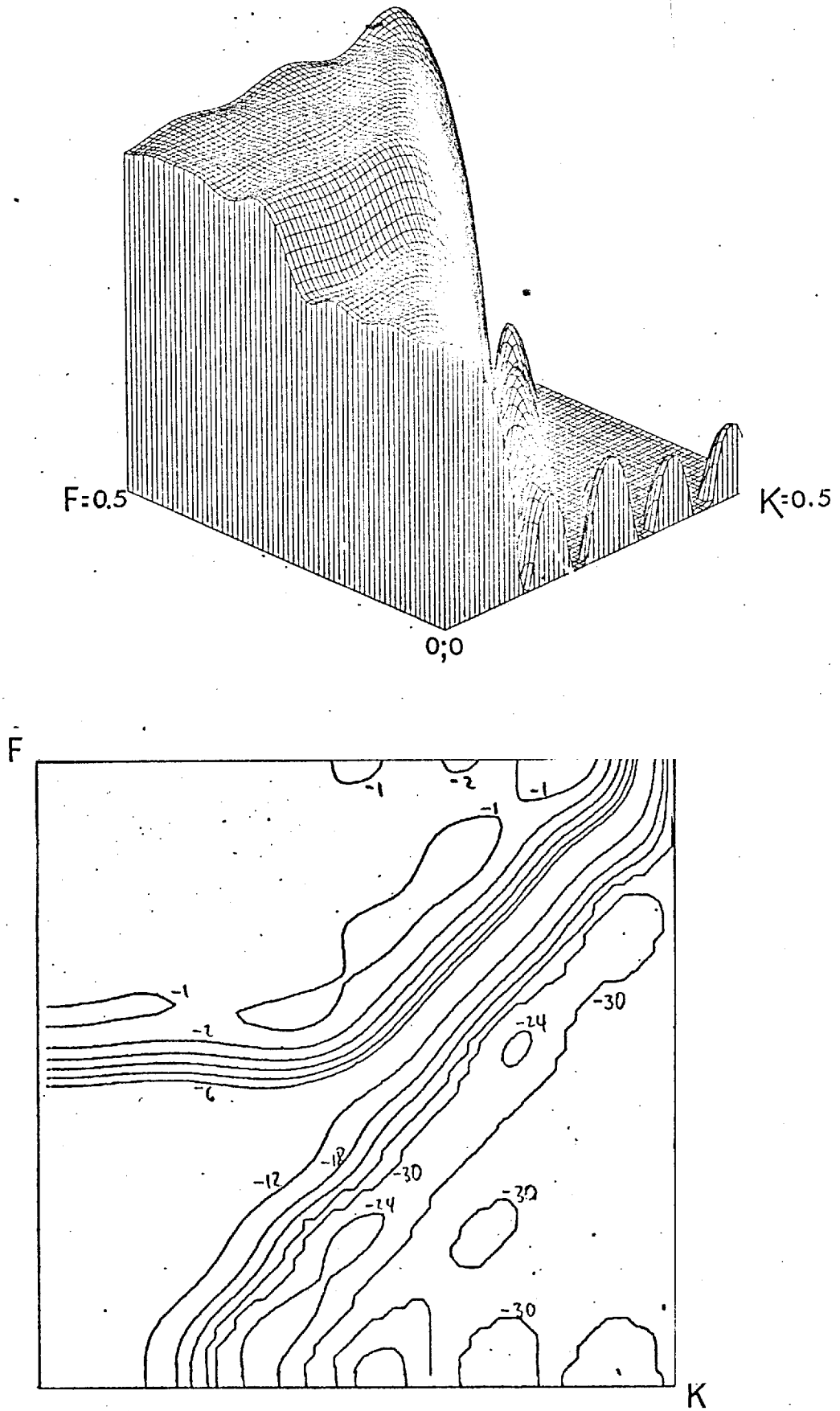

FIGURE 8.4 (f-k) diagram and isometric plot

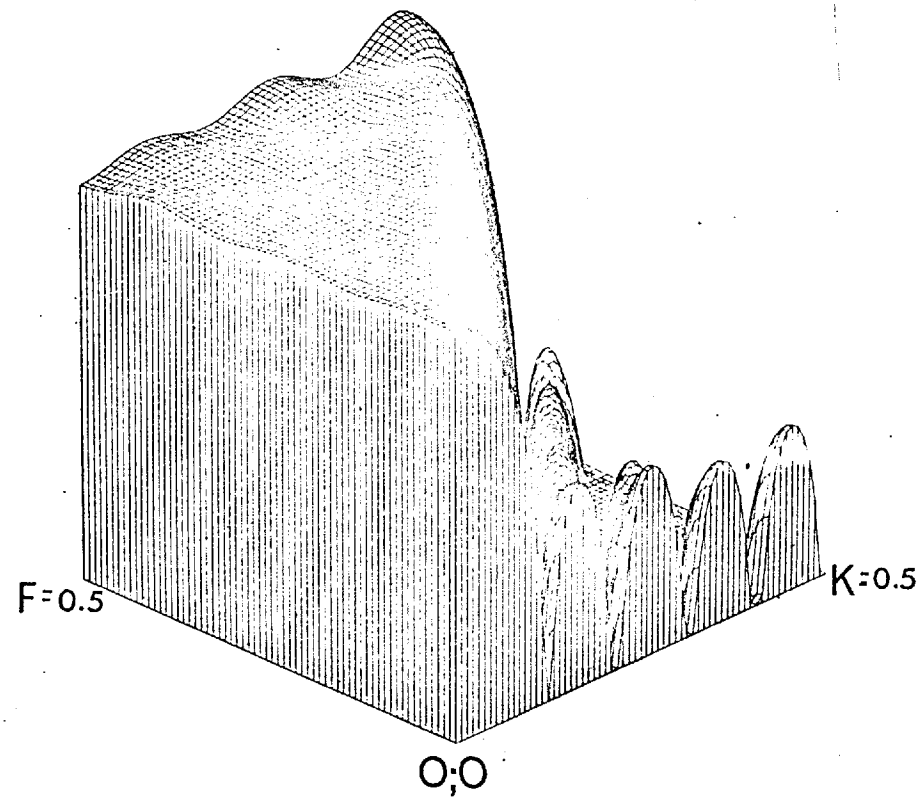

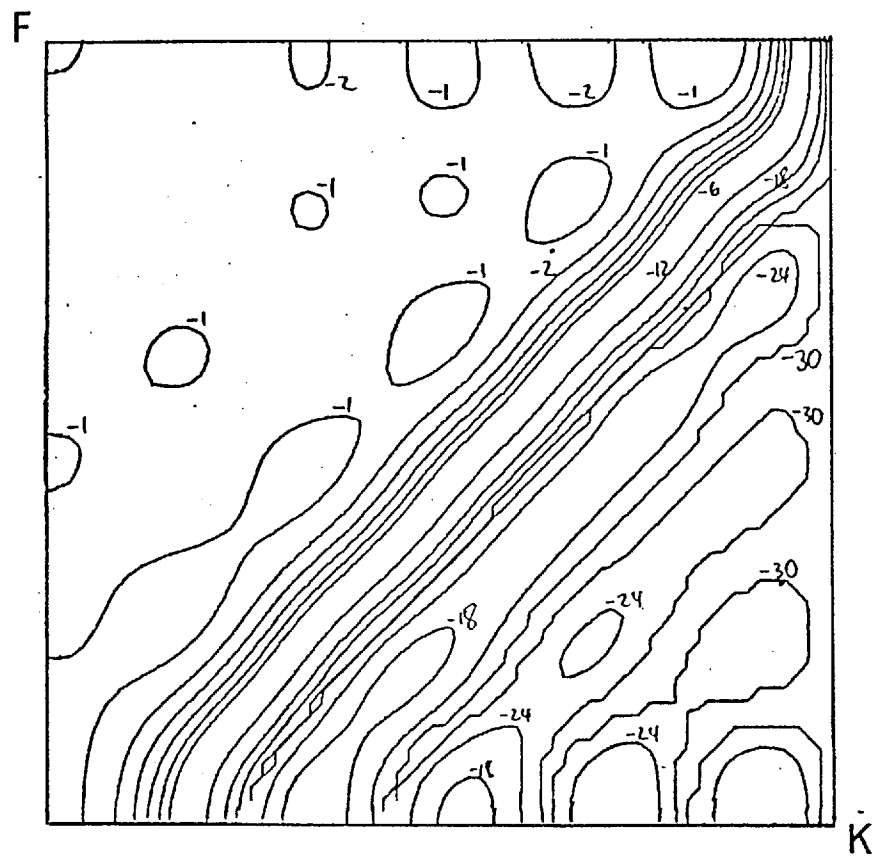

FIGURE 8.5 (f-k) diagram and isometric plot

CHAPTER IX

THE CORRELATION TECHNIQUE

The following stochastic models could be used for the multichannel stacking filter design in previous chapters.

$$x_i(t) = s(t-\tau_i) + r(t-\tilde{\tau}_i) + n(t) \quad (i=1,..,N)$$

Signals s(t), correlated noise r(t) and uncorrelated noise n(t) are uncorrelated to each other. To simplify computations, the components were always assumed to be broad band signals. This is justified on the following grounds:

1. Filters are usually computed to be kept in a library with the intention to apply them for various similar problems where autocorrelations of signals and noise may vary in each case.
2. The broad band assumption corresponds to minimizing or maximizing transfer functions of the stacking filter for certain time window regions.
3. The broad band assumption is the most economical, if filters for scaled windows are to be derived from computed ones.
4. The characteristics of multichannel velocity filters designed with the broad band assumption are still superior to other known velocity filters.

The knowledge of the shape of time windows, in which signals are either to be enhanced or rejected, is also assumed. This assumption is justified because stacking filters may be applied to actual seismic traces in an 'indirect' way. This means that various filters may be applied to a multitrace section as in the computation of velocity spectra (Taner

and Koehler,1969). Traces showing the most convincing results will imply that the chosen filter parameters fit the actual case best. This indirect approach has to be done systematically.

If, however, a more 'direct' approach is to be chosen, then moveouts as well as autocorrelations of the trace components should be estimated prior to the filter design. Below a technique is described from which arbitrary moveouts as well as the autocorrelations $\varphi_{ss}(\tau^*)$; $\varphi_{rr}(\tau^*)$ and $\varphi_{nn}(\tau^*)$ may be approximately obtained from the stochastic model. The technique is similar to the single channel approach given by Ostrander (1966) and the multichannel approach of Schneider and Backus (1968). It is in actual fact based on a study of the autocorrelation matrix of the traces which gives a deep insight into the problem. This may already reveal most of the desired properties. Below an example is given. It is assumed that the organized noise on three traces is given by the white noise series $r_i(t^*) = r(t^* - \tilde{\tau}_i)$ where the relative moveout is $\tilde{\tau}_i = (i-3)^2$ and the power on each trace equals one. The moveout is shown in figure 9.1. The crosscorrelation function $\varphi_{r_1 r_2}(\tau^*)$ for instance is then represented by a spike at position $t^* = 3$. The autocorrelation matrix is shown in figure 9.2.

The moveout as shown in figure 9.1 is obtained three times and appears in a shifted way in all three columns (or rows) of the autocorrelation matrix. The shift from column one to two equals $\tilde{\tau}_1 - \tilde{\tau}_2$, from one to three $\tilde{\tau}_1 - \tilde{\tau}_3$ and from two to three $\tilde{\tau}_2 - \tilde{\tau}_3$. Generally one may conclude that for n traces the relative moveout is obtained n times. It would therefore have been only necessary to compute any column or row of the autocorrelation matrix to recover the moveout. Note that if signal and correlated noise are uncorrelated, their autocorrelation matrices are simply added. If organized noise or signals are not white the moveout in the autocorrelation matrix stays unchanged. Each spike however, has now to be

convolved with the corresponding autocorrelation function of the signal or noise.

If the traces are given as

$$x_i(t^*) = s(t^*-\tau_i) + n(t^*) \quad \text{or} \quad x_i(t^*) = r(t^* - \tilde{\tau}_i) + n(t^*), (i=1,..,N)$$

it is theoretically always possible to obtain (Ostrander, 1966) φ_{nn}, τ_i and φ_{ss} or $\tilde{\tau}_i$ and φ_{rr}. This is not any longer the case if organized noise and signals are present (with or without uncorrelated noise). To show this, the autocorrelation matrix of five synthetic traces was computed. These traces are described by the following stochastic model

$$x_i(t^*) = s(t^*) + r(t^* - (i - 5)^2), \ (i=1,..,5)$$

The minimum delay wavelet of the random process s (t*) is given in figure 9.3 and the minimum delay wavelet of r (t*) in figure 9.4. The autocorrelation matrix of the five traces is shown in figure 9.5. It reveals some basic features which can be expressed as follows:

1. The best chances for detecting moveouts and autocorrelations are by analysing the first or the last column (or row) of the autocorrelation matrix. In this case the correlation functions of signal and noise have the largest separation from each other.
2. The crosscorrelation between the two extreme traces gives the best estimation of the autocorrelation functions.
3. After the relative moveout of the correlated noise with respect to the signal is approximately determined, it is immediately clear, which side of the two-sided autocorrelation functions is more accurate. (In the above example it is the left

side for the correlated noise and the right side for the signal in the first column).

It may be argued that the chosen model for an actual 'real life' seismogram is far too simple to compute the desired components in the way described above. For a more complicated model it is believed that a better estimation of moveouts is obtained with an average over all columns of the matrix. The averaging concept can be employed as follows:

Columns i and j of the matrix are each stored term by term into a one-dimensional array and the crosscorrelation $\hat{\varphi}_{ij}(\tau^*)$ between both is computed. The position of a maximum value of this function obtained with respect to the moveout origin reveals the shift between autocorrelation moveouts from column i to j. To give an example, each column of the computed autocorrelation matrix of figure 9.5 was stored into one array and $\hat{\varphi}_{ij}(\tau^*)$ was computed. Some functions $\hat{\varphi}_{ij}(\tau^*)$ are shown in figure 9.6. They reveal the shift of the autocorrelations from column to column in a very distinct way. It was generally found that the resolution obtained in this case was better than the resolution already obtained with the autocorrelation matrix, in particular when signals changed their form from trace to trace. The outcome of results depends however, very much on the band width and moveouts of signals and may strongly vary from case to case. It is ultimately only an extensive application of the described technique on actual traces which will show its practical value.

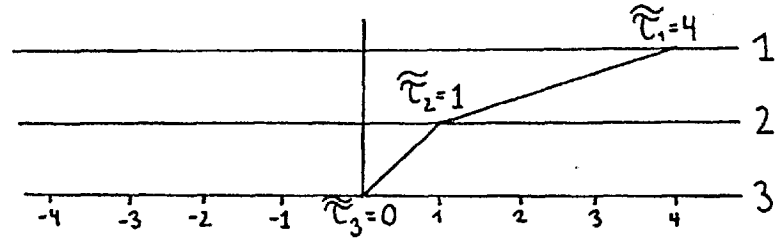

FIGURE 9.1 Relative Moveout

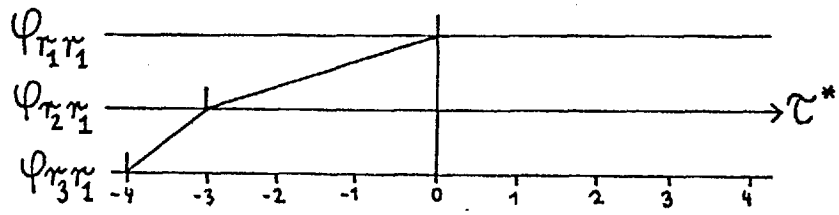

First column

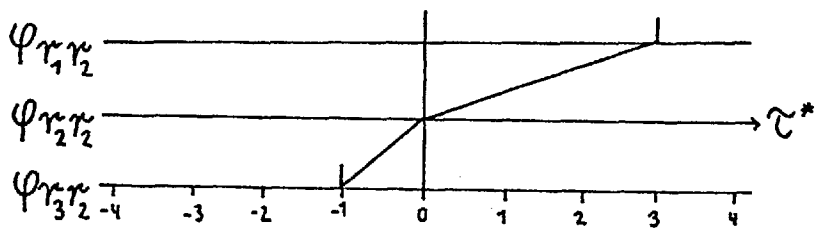

Second column

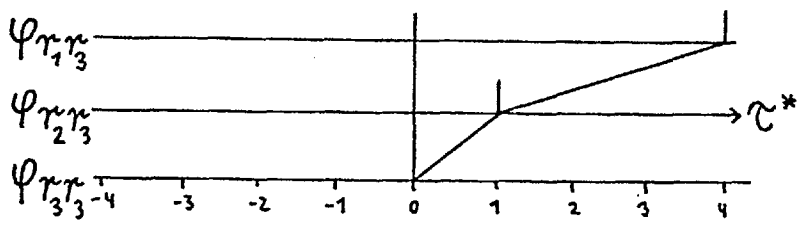

Third column

FIGURE 9.2 Autocorrelation matrix

First Column

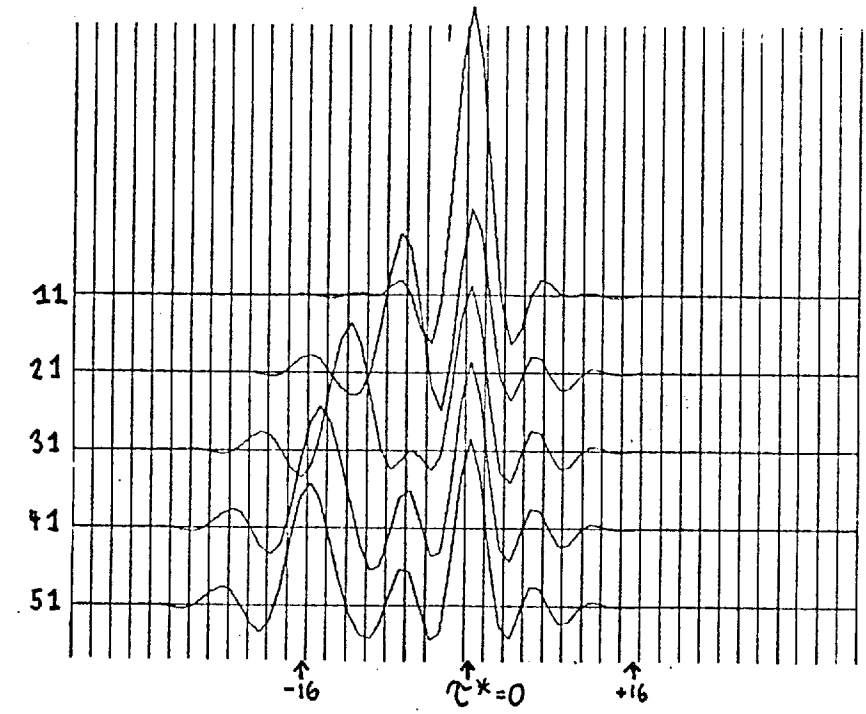

Second Column

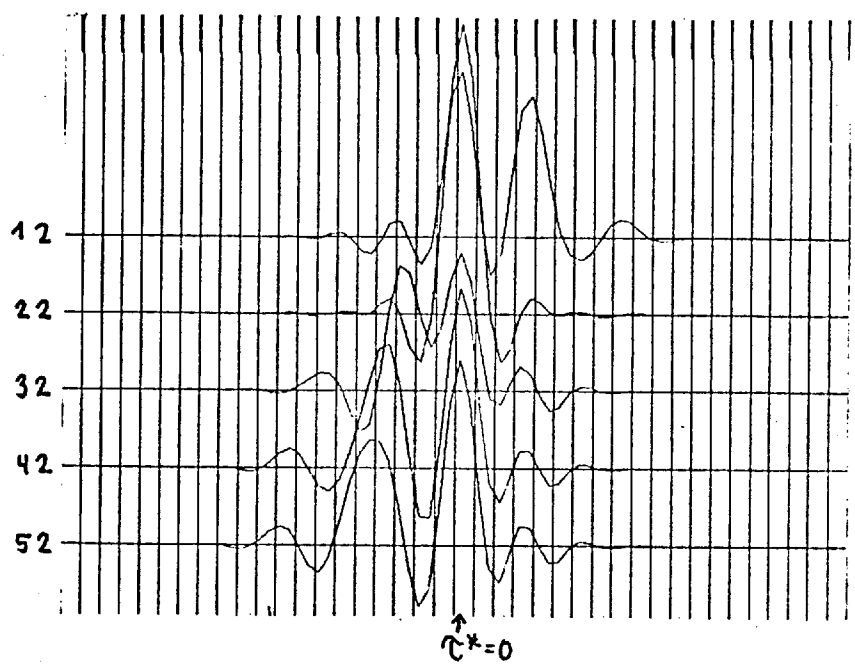

Third Column

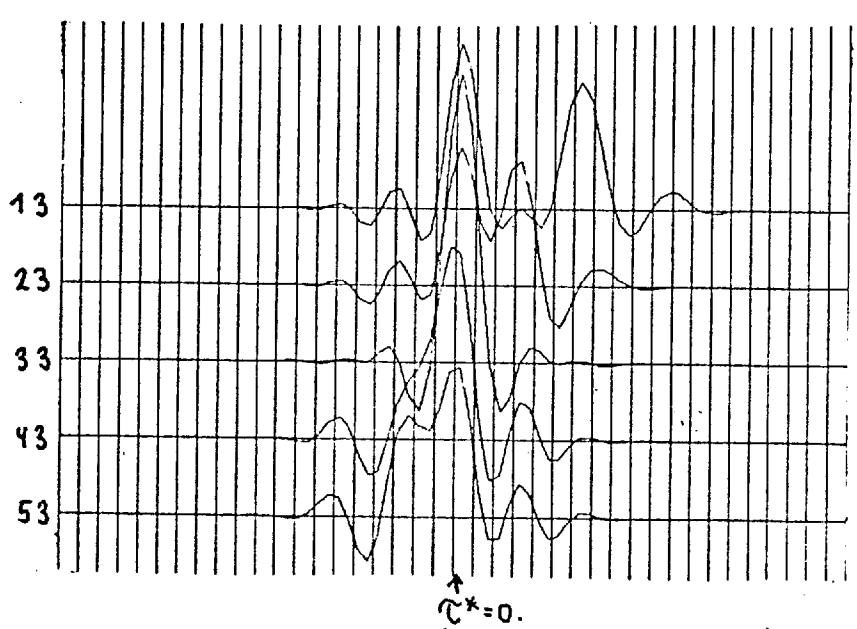

FIGURE 9.5 Autocorrelation matrix (continued next page)

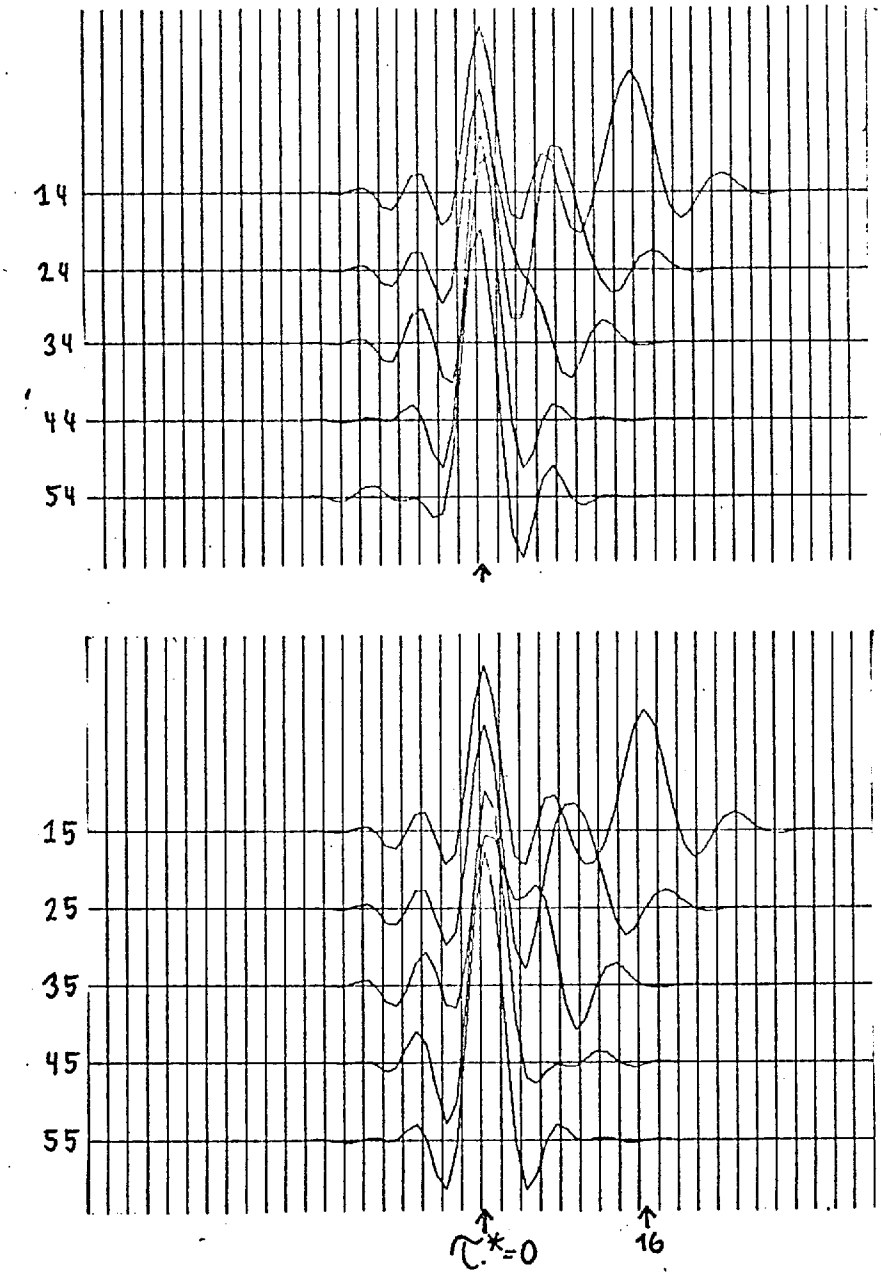

FIGURE 9.5 Autocorrelation matrix

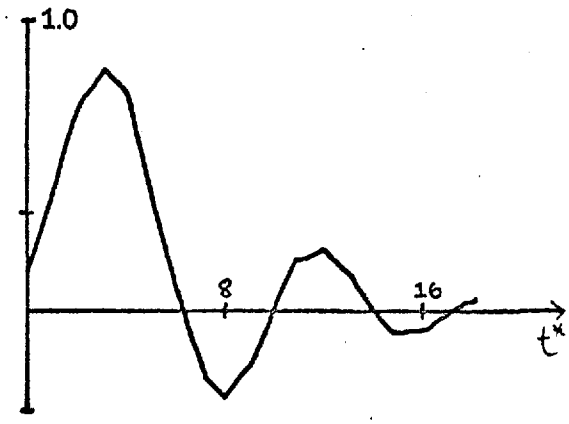

FIGURE 9.4 Minimum delay wavelet for the random correlated noise r(t*).

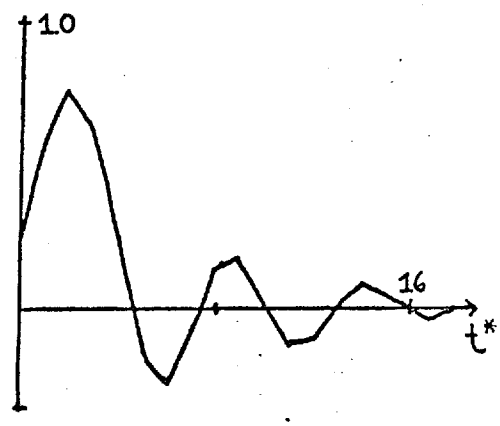

FIGURE 9.3 Minimum wavelet for the random signal s(t*)

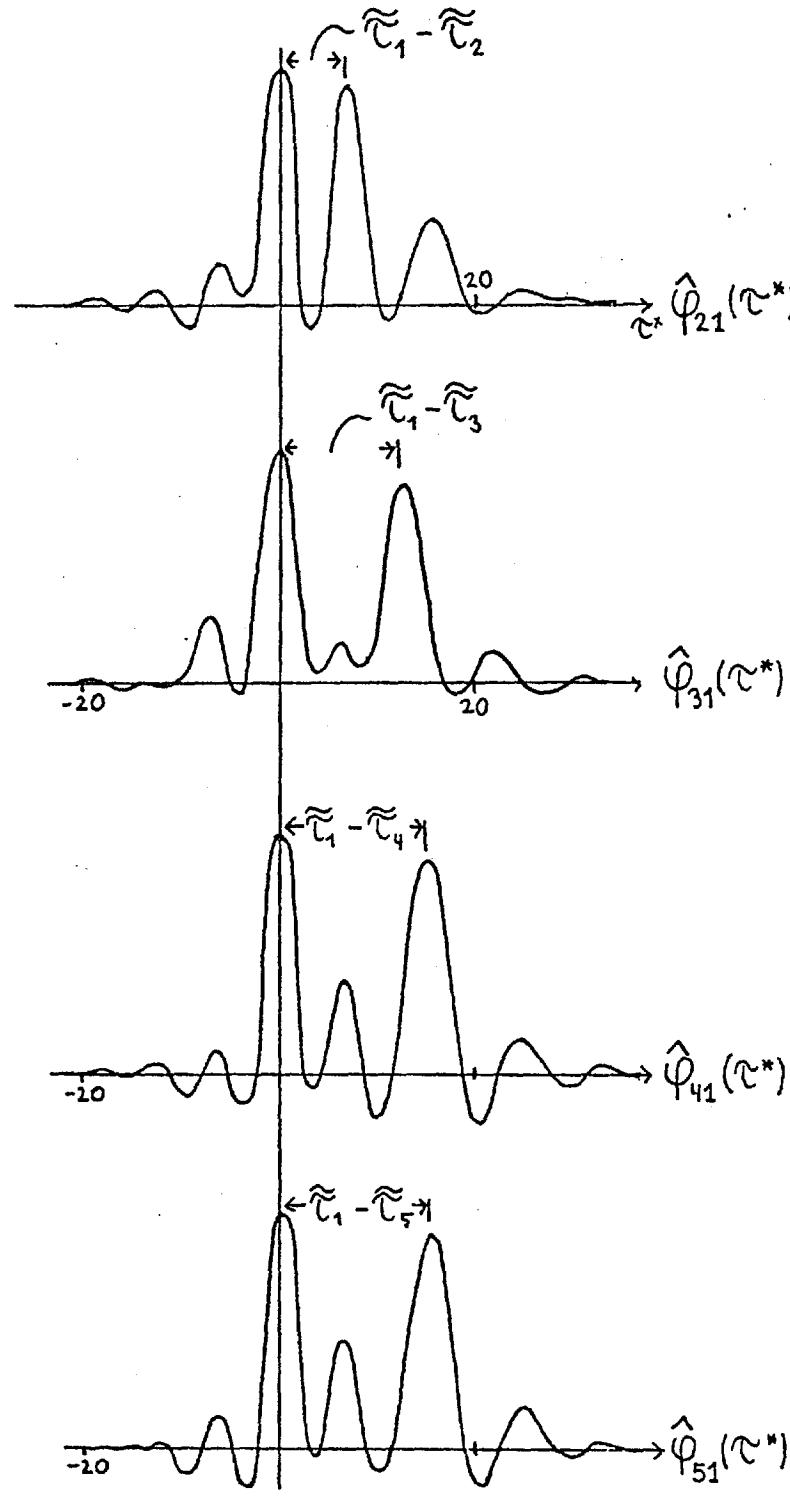

FIGURE 9.6 Crosscorrelations between columns of the autocorrelation matrix of figure 9.5.

CHAPTER X

CONCLUSIONS

1. Discrete two-dimensional filters can be formulated as discrete multichannel filters.

2. Under the assumption that signals and noise are uncorrelated, a least squares criterion for multichannel filters can be chosen which gives different weights to errors caused by signals or noise.

3. Continuous multichannel normal equations can be solved with the discrete normal equations if all correlation functions are band limited. Approximate continuous solutions are obtained.

4. A general purpose stacking filter can be designed which may be used as a

   (a) two-dimensional velocity filter

   (b) three-dimensional velocity filter

   (c) polarisation filter

   (d) differential normal moveout filter

5. Symmetries of the stacking filter depend on the choice of a time window

   (a) Time windows which are symmetric on each trace specify phase-free components.

   (b) Centro-symmetric time windows specify centro-symmetric stacking filters

   (c) Symmetric time windows specify symmetric stacking filters

   (d) If design parameters of a window are the same on two different traces, the computed stacking filter components are also the same for these traces

(e) Stacking filters whose time windows may be obtained from each other by rearranging the traces have identical filter components for corresponding traces

6. Optimum multichannel velocity filters are included in the class of filters discussed in this thesis.

7. The two-dimensional Fourier transform of a stacking filter has to be interpreted in a way which differs from the interpretation of a two-dimensional convolution filter.

8. The concept of the defined transfer function of a stacking filter is of great use for the characterisation of filters due to the following reasons:

(a) It provides an appropriate means of describing the N input one output channel relation of a stacking filter.

(b) It explains the characteristics of the two or three-dimensional Fourier transform of multichannel stacking filters.

(c) For signals with constant moveout it can be obtained from the two- or three-dimensional Fourier transform along straight lines corresponding to the moveout.

9. The phase properties of a stacking filter transfer function for constant moveout signals depend on the symmetries of the stacking filter components.

(a) Symmetric and centro-symmetric filters have phase-free transfer functions for signals with constant moveout.

(b) Trace symmetric stacking filters have a phase-free transfer function for zero-moveout signals.

10. Characteristics of centro-symmetric multichannel velocity filters are superior over the ones of symmetric filters because

(a) less overlapping of pass with pass or reject with pass regions is possible;

(b) additional design regions have a negative influence on other regions.

Both filter types have zero phase transfer functions for constant moveout signals.

11. Reject regions with a large weighting factor 'push' pass regions in the frequency wave number domain into regions with fewer restrictions.

12. Polarisation filters can be designed for arbitrary detector positions.

(a) Characteristics for a certain direction depend strongly on the shape of the array.

(b) Features are similar to two-dimensional velocity filters.

13. Transfer characteristics of stacking filters for certain families of differential normal moveout signals can be obtained with special transforms.

14. Some differential normal moveout filters can be exactly characterised with certain transforms.

(a) Pass and reject regions are generally well approximated.

(b) Characteristics in unspecified regions are difficult to predict.

(c) Filters are generally very selective in unspecified regions.

15. Constant moveout signals falling into a curved pass region or differential normal moveout signals falling into a velocity filter pass region are generally passed without distortion in their amplitude spectra. For optimum rejection the moveout of filtered signals should however match the moveout of the signals used in the filter design.

16. The allowance for chatter in the design depresses the transfer characteristics for high frequencies. For small chatter values t_c a moving average filter $B(f) = \text{sinc}\,(t_c f)$ applied to the output trace achieves the same purpose as the incorporation of chatter in the design.

17. Suboptimum filters can be derived from optimum filters in various ways.

18. Increasing the weighting factor ϱ and ν improves the signal to noise ratio, but leads to greater signal distortion.

19. The scaling effect is helpful for the filter design.

(a) With this effect the computation time can be tremendously reduced.

(b) Various scaled filter versions can be obtained from a computed filter.

(c) Broadening a time window by scaling the components results in a high frequency loss of the scaled filter.

(d) For narrowing the time window by scaling, the stacking filter components have to be antialiased.

(e) The effect gives a deep insight into the characteristics and performance of filters with scaled regions.

20. Autocorrelations of signals and noise can be included into the filter design. Differential normal moveouts and autocorrelations

can often be estimated with the correlation technique.

SUGGESTIONS FOR FURTHER RESEARCH

The studies made so far have opened the venue of subsequent and further investigations, in particular on the following topics:

1. The necessity of obtaining more characteristics of polarisation filters for various detector positions. These could be tabulated in a form convenient to find optimum characteristics as a function of detector positions.

2. A comparative study of the given three-dimensional velocity and polarisation filters with other known filters.

3. In the process of the present investigation another design of a three-dimensional filter evolved, the description of which is given in Appendix IV. Further studies on this subject could be carried out.

4. Three-dimensional filters could be designed in the time domain, where plane wave normal vectors fall

   (a) within an inverted cone

   (b) on the surface of an inverted cone.

5. Further characteristics of differential normal moveout filters.

6. The application of the given filters and the correlation technique on actual seismograms.

ACKNOWLEDGEMENTS

The author wishes to express his thanks to Dr B. P. Dash for supervision, encouragement and the final reading of the manuscript.

His thanks are due to Mr J. W. J. Hosken and Mr S. Deregowski of British Petroleum Research Centre for the stimulating discussions, suggestions and helpful criticism throughout the study.

Thanks are expressed to the author's colleague, Dr K. O. Ahmed, for helpful discussions.

His thanks are due to Dr M. R. Foster and Dr R. L. Sengbush of Mobil Oil Corporation, Dallas, Texas, for providing the Calcomp-subroutine for the isometric plots.

The author gratefully acknowledges the excellent computing facilities of Imperial College Centre of Computing and Automation. The Research work was supported by a Research Bursary made available at the Imperial College by the British Petroleum Company, without which the present study would not have been possible. The author gratefully wishes to acknowledge this.

REFERENCES

Anstey, N.A., 1964. "Correlation Techniques". Geophys. Prospecting. V. 12, No. 4, December, 1964.

Baldwin, R., 1964. "Array research multichannel filter systems for Tonto Forest Observatory". Special Report No. 3 AFTAC Project VT/4053, Contract AF 33 (657) - 12747.

Binder, F.H., 1967. "Large-array signal and noise analysis". Special report No. 12 - Analysis of long period noise: Texas Instrument Special Report No. 12.

Black, D.I. and Scollar, I., 1969. "Spatial filtering in the wave-vector domain". Geophysics, V. 34, p. 916 - 923

Blackman, R.B. and Tukey , I.W., 1968. "The Measurement of Power spectra from the point of view of Communication Engineering". The Dover Press, New York.

Broding, R.A., Bentley-Llewellyn, N.J. and Hearn, D.P., 1964. "A study of a three-dimensional seismic detection system". Geophysics, V. 29, p. 221.

Bryan, J.G., 1967. "Statistical test of the hypothesis that a time series is stationary". Geophysics, V. 32, p. 499 - 511.

Burg, I.P., 1964. "Three-dimensional filtering with an array of seismometers". Geophysics V. 29, p. 693 - 713.

Carpenter, F.W., 1965. "A historical review of large aperture seismometer arrays". Proc. I.E.E.E.

Cheng, D.K., 1963. "Analysis of Linear Systems". Addison-Wesley Publishing Co. Inc., Reading Massachusetts.

Clay, C.S., 1966. "Wave guides, arrays and filters". Geophysics, V. 31, p. 501 - 505.

Cook, E.E. and Taner, M.T., 1969 "Velocity Spectra and their use in Stratigraphic and Lithographic Differentiation". Geophys. Prosp. V. 27, p. 433 -448.

Cooley, I.W. and Tukey, I.W., 1965. "An Algorithm for the Machine calculation of Complex Fourier Series". Mathematics of Computation. Vol. 19, p. 297 - 301.

Darby, E.K. and Davies, E.B., 1967. "The analysis and design of two-dimensional filters for two-dimensional data". Geophys. Prosp. V. 15, p. 383 - 406.

Davies, E.B. and Mercado, E.J., 1968. "Multichannel deconvolution filtering of field recorded data". Geophysics, V. 33, p. 711 - 722.

D'Hoeraene, J., 1966. "Filtrage spatio temporel des courbures". Geophys. Prosp., V. 14, p. 27 - 44.

Dobrin, M.B., Ingalls, A.L. and Long, J.A., 1965. "Velocity and frequency filtering of seismic data using laser light". Geophysics, V. 30, p. 1144 - 1178.

Doetsch, G., 1961. "Anleitung zum praktischen Gebrauch der Laplace Transformierten". München.

Embree, P., Burg, J.B. and Backus, M.M., 1963. "Wideband filtering - the 'pie-slice' process". Geophysics, V. 28, p. 948 - 974.

Fail, J.P. and Grau, G., 1963. "Les filtres en eventail". Geophys. Prosp. V 11, p. 131 - 163.

Foster, M.R., Sengbush, R.L. and Watson, R.J., 1964. "Design of suboptimum filter systems for multitrace seismic data processing". Geophys. Prosp., V. 12, p. 173 - 191.

Frazer, R.A., Duncan W.J. and Collar, A.R., 1963. "Elementary Matrices". Cambridge Univ. Press, Cambridge.

Gantmacher, F.R., 1959. "The Theory of Matrices".Vol. 1, Chelsea, New York, 1959.

Galbraith, J.N. and Wiggins, R.A., 1968. "Characteristics of optimum multichannel stacking filters". Geophysics, V. 33, p. 36 - 48.

Jury, E.I., 1958. "Sampled-Data Control Systems". New York, John Wiley and Sons, Inc.

Jury, E.I., 1967. "Theory and application of the z-transform method". Wiley, New York.

Khintchine,A., 1934. "Korrelationstheorie der stationären stochastischen Prozesse": Math.Ann., V.109, p.604-615.

Kolmogorov,A., 1941. "Interpolation and Extrapolation von stationären zufälligen Folgen"; Bull.Acad.Sci.U.S.S.R.,Ser.Math.,V.5, p.3-14.

Kolmogorov,A, 1939. "Sur l'interpolation et extrapolation des suites stationaires": C.R.Acad.Sci.Paris. V.208, p.2043-2045.

Lacoss, R.T., Kelly, E.J. and Toksoz, M.N., 1969. "Estimation of seismic noise structure using arrays". Geophysics, V. 34, p. 21 - 38.

Lanczos, C., 1966. "Discourse on Fourier series". Univ. Mathematical Monographs, London.

Lee, Y.W., 1960. "Statistical Theory of Communication". John Wiley and Sons, Inc., New York.

Lighthill, M.J., 1966. "Einführung in die Theorie der Fourier-Analysis und der verallgemeinerten Funktionen". Mannheim

Mayne, W.H., 1962. "Common Reflection point horizontal data stacking techniques". Geophysics, V. 27, p. 927 - 938.

Mayne, W.H., 1965. "Common Reflection Point Techniques in Highly Explored Areas". Paper presented at SEG, Dallas, Texas.

Meyerhoff, H.J., 1966. "Horizontal Stacking and Multichannel Filtering applied to Common Depth Point Seismic Data". Geophys. Prosp. V. 24, p. 441 - 454.

Mesko, C.A., 1966. "Two-dimensional filter theory and the second derivative method". Geophysics, V. 31, p. 606 - 617.

Ostrander, J., 1966. "Spectral Estimation of signal and noise power and power ratios for Reflection Seismograms". M.Sc. Thesis, Pennsylvania State University.

Papoulis, A., 1962. "The Fourier integral and its applications". Mc Graw - Hill Book Company, Inc.

Papoulis, A., 1965. "Probability, random variables and stochastic processes". New York, Mc Graw - Hill Book Co. Inc., p. 583.

Ricker,N., 1953 . "The form and laws of propagation of propagation of seismic wavelets": Geophys. V.18, p.10-40.

Robinson, E.A., 1954. "Predictive decomposition of time series with applications to seismic exploration". M.I.T. Geophysical Analysis Group, Report No. 7, M.I.T., Chapter 5.

Robinson, E.A., 1962. "Random wavelets and cybernetic systems". London, Charles Griffin and Co. Ltd.

Robinson, E.A., 1963. "Multichannel z-transforms and minimum delay". Geophysics, V. 31, p. 482-500.

Robinson, E.A., 1964. "Seismic arrays for the detection of nuclear explosions". Scientific Report No. 8, ARPA Project Vela Uniform Contract AF 19 (604) 7378, (AD 608-275).

Robinson, E.A. and Treitel, S., 1967. "Principles of Digital Wiener Filterin Geophys. Prosp., V. 15, p. 309 - 333.

Robinson, E.A., 1967 (a). "Statistical Communication and Detection with special reference to Digital Data processing of Radar and seismic signals". Griffins of London.

Robinson, E.A., 1967 (b). "Multichannel Time Series Analysis with Digital Computer Programs". Holden Day, Inc.

Schneider, W.A., Larner, K.L., Burg, J.P. and Backus, M.M., 1964. "A new data-processing technique for the elimination of ghost arrivals on reflection seismograms". Geophysics, V. 29, p. 783 - 805.

Schneider, W.A., Prince, Jr., E.R. and Giles, B.F., 1965. "A new data-processing technique for multiple attenuation exploiting differential normal moveout". Geophysics, V. 30, p. 348 - 362.

Schneider, W.A. and Backus, M., 1968. "Dynamic correlation analysis". Geophysics, V. 33, p. 105 - 126.

Sengbush, R.L. and Foster, M.R., 1968. "Optimum multichannel velocity filters". Geophysics, V. 33, p. 11-35.

Shanks, J.L., 1967. "Recursive filters for digital processing". Geophysics, V. 32, p. 33 - 51.

Simpson, J.K., 1967. "Travelling signal-to-noise ratio and signal power estimates". Geophysics, V. 32, p. 485 - 493.

Smith, M.K., 1954. "The directional filtering properties of multiple seismometer groups". MIT Geophysical Analysis Group Report N. 6, Section 5, MIT, Cambridge, Mass.

Smith, M.K., 1956. "Noise analysis and multiple seismometer theory". Geophysics, V. 21, p. 342.

Treitel, S. and Robinson, E.A., 1969. "Optimum Digital Filters for Signal to Noise Ratio Enhancement". Geophys. Prosp., V. 27, p. 248 - 293.

Taner, M.T. and Koehler, F., 1969. "Velocity spectra - digital computer derivation and applications of velocity functions". Geophysics, V. 34, p. 859 - 881.

Wadsworth,G.P.,Robinson,E.A,Bryan,J.G.,and Hurley,P.M.,1953, "Detection of reflections on seismic records by linear operators": Geophysics,V.18., p.539-586.

Wold,H,1938. "A study in the analysis of stationary time series": Uppsala, Almquist and Wisksells.

Wiggins, R.A. and Robinson, E.A., 1965. "Recursive Solution to the multi-channel filtering problem". Jour. of Geophys. Res., V. 70, p. 1885 - 1891.

Wiggins, R.A., 1966. "ω- k Filter Design". Geophys. Prosp. V. 24, p. 427 - 440.

Wiener, N., 194 9 "Extrapolation, interpolation, and smoothing of stationary time series". The Technology Press of M.I.T., Cambridge, Mass.

Yule,G.U., 1921 , "On the time-correlation problem with special reference to the variate-difference correlation method: J.Roy.Stat.Soc., V.84, p.497-526.

Yule,G.U., 1927 . "On a method of investigating periodicities in disturbed series, with special reference to Wolfer 's sunspot numbers: Phil. Trans. Roy. Soc., V.226,p.267-298.

APPENDIX 1

The integral (4.1.15) can be reduced to expressions containing sines, cosines and integrals of the form

$$\int_{-\infty}^{x} \left(\frac{\sin x}{x}\right) dx$$

All three types of functions are standard programs in the computer. Generally any integral of the form

$$\int_{-\gamma}^{\gamma} \text{sinc}^2 (af) \text{ sinc } (bf) \cos (\pi cf)\, df$$

may be expressed as

$$\frac{1}{8\pi^4 a^2 b} \int_{-\gamma}^{\gamma} \left(\frac{F_1(f)}{(b + c) f^3} + \frac{F_2(f)}{(b - c) f^3} \right) df$$

where

$$F_1(f) = \sin \pi f \cdot (2a-(b+c)) + 2 \sin f\pi(b+c) - \sin f\pi(2a+(b+c))$$

$$F_2(f) = \sin \pi f \cdot (2a-(b-c)) + 2 \sin f\pi(b-c) - \sin f\pi(2a+(b-c))$$

The integral

$$\int \frac{\sin Af}{f^3}\, df$$

can be further simplified to give

$$\int \frac{\sin Af}{f^3}\, df = -\tfrac{1}{2} \frac{\sin Af}{f^2} - \frac{A}{2} \left[\frac{\cos Af}{f} + A \int \frac{\sin Af}{f}\, df \right]$$

APPENDIX II

OPTIMUM FILTER FOR VARYING BAND WIDTH OF THE INPUT SIGNALS

In the design of the general purpose stacking filter in section 4.1 it was shown how to provide for uncertainties in the arrival times, chatter and variable gain of the input traces.

The basic idea of design consisted in the proper computation of expectation values of the power and crosspower spectra for the stacking filter normal equations.

The following expressions were initially obtained for the expectations of the power and crosspower spectra.

$$E\left\{\Phi_{ii}(f)\right\} = \tilde{\tilde{\Phi}}_{s\,s}(f) \tag{II.1}$$

$$E\left\{\Phi_{ij}(f)\right\} = \tilde{\tilde{\Phi}}_{s\,s}(f)\,\mathrm{sinc}^2(t_c f)\,\mathrm{sinc}(\tau_{ij} f)\,e^{2\pi i t_{ij} f} \tag{II.2}$$

$$E\left\{\Phi_{j}(f)\right\} = \tilde{\tilde{\Phi}}_{s\,s}(f)\,\mathrm{sinc}(t_c f)\,\mathrm{sinc}(\Delta t_j f)\,e^{2\pi i f \tau_j} \tag{II.3}$$

It would have been also possible to allow for varying band width of the input signals.

In the sequel it is shown, how to obtain corresponding expressions for (II.1) to (II.3) in the case such variations are permitted.

For the following discussion it is therefore assumed that the input signals can be expressed as

$$s_i(t) = s_{\varrho_i}(t) * \varepsilon(t-\alpha_i) \tag{II.4}$$

where the Fourier transform of the aperiodic function $s_{\varrho_i}(t)$ is given as $S_{\varrho_i}(f) = \mathrm{rec}(f/\varrho_i)/\varrho_i$ and the power spectrum of the stationary process $\varepsilon(t)$ is $\mathrm{rec}(f)$.

It is assumed that the band widths of the input signals are independent of each other and vary randomly over the ensemble of all possible input signals

in a manner such that each channel has the following ensemble probability density function for the band width:

$$p_4(\varrho) = \frac{1}{2b}\ \mathrm{rec}\ \left(\frac{\varrho - a}{2b}\right) \quad ; \ (a+b \leq \tfrac{1}{2}) \tag{II.5}$$

As desired output the following trace is taken: $s_o(t) = s_a(t) * \mathcal{E}(t)$. $s_a(t)$ has the average band width of the input signals, so that its Fourier transform is $S_a(f) = \mathrm{rec}(f/a)/a$.

By taking one special realization of the input signals in form of (II.4) one would have obtained the following expectation values for the power and crosspower spectra of the general purpose stacking filter.

$$E\left\{\Phi_{ii}(f)\right\} = \Phi_{s_{\varrho_i} s_{\varrho_i}}(f) \tag{II.6}$$

$$E\left\{\Phi_{ij}(f)\right\} = \Phi_{s_{\varrho_i} s_{\varrho_j}}(f)\,\mathrm{sinc}^2(t_c f)\,\mathrm{sinc}(\tau_{ij} f)\,e^{2\pi i t_{ij} f} \tag{II.7}$$

$$E\left\{\Phi_{j}(f)\right\} = \Phi_{s_a\, s_{\varrho_j}}(f)\,\mathrm{sinc}\,(t_c f)\,\mathrm{sinc}(\Delta t_j f)\,e^{2\pi i f \tau_j} \tag{II.8}$$

where

$$\Phi_{s_{\varrho_i} s_{\varrho_i}}(f) = \mathrm{rec}(f/\varrho_i)/\varrho_i^2 \tag{II.9}$$

$$\Phi_{s_{\varrho_i} s_{\varrho_j}}(f) = \mathrm{rec}(f/\varrho_i)\,\mathrm{rec}(f/\varrho_j)/\varrho_i \varrho_j \tag{II.10}$$

$$\Phi_{s_a\, s_{\varrho_j}}(f) = \mathrm{rec}(f/a)\,\mathrm{rec}(f/\varrho_j)/a\varrho_j \tag{II.11}$$

By making use of the probability density funtion (II.5) the expressions (II.9) to (II.11) in formulae (II.6) to (II.8) have to be replaced by the following ensemble averages.

Determination of the power spectra

$$E\left\{\Phi_{s_{\varrho_i} s_{\varrho_i}}(f)\right\} = T(f) = \int_{-\infty}^{\infty} \text{rec}\,(f/\varrho_i)\, p_4(\varrho_i)\, \frac{1}{\varrho_i^2}\, d\varrho_i$$

$$T\ (f) = \begin{cases} \dfrac{1}{a^2-b^2} & \text{if} \quad |f| < \dfrac{a-b}{2} \\ \dfrac{1}{2b}\left(\dfrac{1}{2f} - \dfrac{1}{a+b}\right) & \text{if} \quad \dfrac{a-b}{2} < |f| < \dfrac{a+b}{2} \\ 0 & \text{if} \quad \dfrac{a+b}{2} < |f| < \frac{1}{2} \end{cases} \qquad \text{(II.12)}$$

Determination of the crosspower spectra of the input traces

$$E\left\{\Phi_{s_{\varrho_i} s_{\varrho_j}}(f)\right\} \quad T_c(f) = \left[\int_{-\infty}^{\infty} \frac{1}{\varrho} \text{rec}(f/\varrho)\ p_4(\varrho) d\varrho\right]^2$$

$$T_c(f) = \begin{cases} \left(\dfrac{1}{2b}\right)^2 \ln^2\left(\dfrac{a+b}{a-b}\right) & \text{if} \quad |f| < \dfrac{a-b}{2} \\ \left(\dfrac{1}{2b}\right)^2 \ln^2\left(\dfrac{a+b}{2f}\right) & \text{if } \dfrac{a-b}{2} < |f| < \dfrac{a+b}{2} \\ 0 & \text{if } \dfrac{a+b}{2} < |f| < \frac{1}{2} \end{cases} \qquad \text{(II.13)}$$

Determination of the crosspower spectra between input and desired output

$$E\left\{\Phi_{s_a s_{\varrho_j}}(f)\right\} = To(f) = \frac{1}{a}\,\text{rec}(f/a) \int_{-\infty}^{\infty} \text{rec}(f/\varrho)\ p_4(\varrho)\ d\varrho$$

$$To(f) = \begin{cases} \dfrac{1}{a} & \text{if} \quad |f| < \dfrac{a-b}{2} \\ \dfrac{a+b-2f}{2ab} & \text{if} \quad \dfrac{a-b}{2} < |f| < \dfrac{a}{2} \\ 0 & \text{if} \quad \dfrac{a}{2} < |f| < \frac{1}{2} \end{cases} \qquad \text{(II.14)}$$

The functions which especially favour band width deviations from trace to trace therefore are

$$E\left\{\Phi_{ii}(f)\right\} = T(f) \qquad \text{(II.15)}$$

$$E\left\{\Phi_{ij}(f)\right\} = T_c(f)\ \mathrm{sinc}^2(t_c f)\ \mathrm{sinc}(\tau_{ij} f)\ e^{2\pi i t_{ij} f} \qquad \text{(II.16)}$$

$$E\left\{\Phi_{j}(f)\right\} = To(f)\ \mathrm{sinc}(t_c f)\ \ \mathrm{sinc}(\Delta t_j f)\ e^{2\pi i \tau_j f} \qquad \text{(II.17)}$$

All power and crosspower spectra of signals and correlated noise have to be multiplied by certain tapering functions if varying band width from trace to trace is permitted.

APPENDIX III

STACKING FILTER TRANSFER FUNCTION

In case of an even number 2 N of traces, the stacking filter components may be labelled as

$$\left(\underline{A}_{-\left(\frac{2N-1}{2}\right)}(f), \ldots \underline{A}_{-\frac{3}{2}}(f), \underline{A}_{-\frac{1}{2}}(f), A_{\frac{1}{2}}(f), \ldots A_{\left(\frac{2N-1}{2}\right)}(f) \right)$$

then the corresponding functions of section 6.2 become

$$f_{\alpha}(t^*) = \sum_{j=-\left(\frac{2N-1}{2}\right)}^{\left(\frac{2N-1}{2}\right)} a_j(t^*) * \mathrm{sinc}(t^* - \alpha_j) \qquad (6.2.1\ A)$$

$$F_{\alpha}(f) = \sum_{j=-\left(\frac{2N-1}{2}\right)}^{\left(\frac{2N-1}{2}\right)} A_j(f) e^{-2\pi i f \alpha_j} \qquad (6.2.5\ A)$$

$$F(f,\tau) = \sum_{j=-\left(\frac{2N-1}{2}\right)}^{\left(\frac{2N-1}{2}\right)} A_j(f) e^{-2\pi i f j \tau} \qquad (6.2.6\ A)$$

$$F(f,k) = \sum_{\tilde{l}=-n}^{m} \sum_{j=-\left(\frac{2N-1}{2}\right)}^{\left(\frac{2N-1}{2}\right)} a_j(\tilde{l}) e^{-2\pi i (f\tilde{l} - kj)} \qquad (6.2.8\ A)$$

APPENDIX IV

DESIGN OF A GENERAL THREE-DIMENSIONAL MULTICHANNEL VELOCITY FILTER

The two-dimensional recording array of figure 5.1.3.1 is used for the following considerations. Each detector location is sufficiently described by the two variables i,j ($i = 1,..,N_x$; $j = 1,..,N_y$). The $N_x \times N_y$ recorded traces may be assumed to have the form

$$x_{ij}(t) = s(t - \alpha_{ij}) + r(t - \tilde{\alpha}_{ij}) + n_{ij}(t), (i=1,..,N_x; j=1,..,N_y) \quad (IV.1)$$

Signals and noise are supposed to be uncorrelated and $\alpha_{ij}, \tilde{\alpha}_{ij}$ are the various delays. The aim is to filter all arriving plane waves in a specified wedge, not only polarized waves. The filtered output should then optimally approximate the signal s(t). All planes falling into the wedge of figure 5.1.3.1 can be expressed as: $z = -\alpha_1 x - \alpha_2 y$

where α_1 and α_2 may be the following random variables

$$\alpha_1 = \tau_x + \Delta\tau_x/2 + \eta$$

$$\alpha_2 = \tau_y + \Delta\tau_y/2 + \xi$$

with the probability density functions

$$p_1(\eta) = \frac{1}{\Delta\tau_x} \operatorname{rec}\left(\frac{\eta}{\Delta\tau_x}\right) \quad (IV.2)$$

$$p_2(\xi) = \frac{1}{\Delta\tau_y} \operatorname{rec}\left(\frac{\xi}{\Delta\tau_y}\right) \quad (IV.3)$$

The relative arrivals of plane wave signals at the points (i,j) become

$$\alpha_{ij} = (\tau_x + \Delta\tau_x/2 + \eta)i + (\tau_y + \Delta\tau_y/2 + \xi)j$$

Crosscorrelating a signal on trace (i,j) with another one on trace $(\hat{i},\hat{j})$ leads to crosscorrelation functions

$$\varphi_{s_{ij}, s_{\hat{i}\hat{j}}}(\tau) = \varphi_{ss}(\tau + \alpha_{\hat{i}\hat{j}} - \alpha_{ij})$$

By making use of the abbreviations

$$\tau_{ij,\hat{i}\hat{j}} = (\tau_x+\Delta\tau_x/2)(\hat{i}-i) + (\tau_y+\Delta\tau_y/2)(\hat{j}-j)$$

$$\hat{\eta} = \eta(\hat{i}-i)$$

$$\hat{\xi} = \xi(\hat{j}-j)$$

one may express the crosspower spectrum between two signals as

$$\Phi_{s_{ij}s_{\hat{i}\hat{j}}}(f) = \tilde{\Phi}_{ss}(f)e^{2\pi i\tau_{ij,\hat{i}\hat{j}}f} \quad e^{2\pi i\hat{\eta}f} \quad e^{2\pi i\hat{\xi}f} \tag{IV.4}$$

The expectation values for these expressions become with (IV.2) and (IV.3).

$$E\left\{\Phi_{s_{ij}s_{\hat{i}\hat{j}}}(f)\right\} = \tilde{\Phi}_{ss}(f)e^{2\pi i\tau_{ij,\hat{i}\hat{j}}f} \int_{-\infty}^{+\infty}\hat{p}_1(\hat{\eta})e^{2\pi i\hat{\eta}f}d\hat{\eta} \int_{-\infty}^{+\infty}\hat{p}_2(\hat{\xi})e^{2\pi i\hat{\xi}f}d\hat{\xi} \tag{IV.5}$$

$$E\left\{\Phi_{s_{ij}s_{\hat{i}\hat{j}}}(f)\right\} = \tilde{\Phi}_{ss}(f)e^{2\pi i\tau_{ij,\hat{i}\hat{j}}f}\,\mathrm{sinc}(\Delta\tau_x(\hat{i}-i)f)\,\mathrm{sinc}(\Delta\tau_y(\hat{j}-j)f) \tag{IV.6}$$

where

$$\hat{p}_1(\hat{\eta}) = \frac{1}{|\hat{i}-i|}\,p_1\left(\frac{\hat{\eta}}{|\hat{i}-i|}\right)$$

$$p_2(\hat{\xi}) = \frac{1}{|\hat{j}-j|}\,p_2\left(\frac{\hat{\xi}}{|\hat{j}-j|}\right)$$

In a similar way one gets for the crosspower spectra between the desired output signal s(t) and the various input signals

$$E\left\{\Phi_{ss_{ij}}(f)\right\} = \tilde{\Phi}_{ss}(f)e^{2\pi i\tau_{ij}f}\,\mathrm{sinc}\,(\Delta\tau_x if)\,\mathrm{sinc}\,(\Delta\tau_y jf) \tag{IV.7}$$

with $\tau_{ij} = (\tau_x+\Delta\tau_x/2)\,i + (\tau_y+\Delta\tau_y/2)j$

If again all signals are chosen to be broad band, the corresponding expressions for (4.2.1), (4.2.2) and (4.2.3) become

$$E\left\{\Phi_{s_{ij}s_{\hat{i}\hat{j}}}(f)\right\} = \mathrm{rec}(f) \tag{IV.8}$$

$$E\left\{\Phi_{s_{ij}s_{\hat{i}\hat{j}}}(f)\right\} = \mathrm{rec}(f)e^{2\pi i\tau_{ij,\hat{i}\hat{j}}}\mathrm{sinc}(\Delta\tau_x(\hat{i}-i)f)\mathrm{sinc}(\Delta\tau_y(\hat{j}-j)f) \quad (1V.9)$$

$$E\left\{\Phi_{ss_{ij}}(f)\right\} = \mathrm{rec}(f)e^{2\pi i\tau_{ij}} \quad \mathrm{sinc}(\Delta\tau_x if)\ \mathrm{sinc}(\Delta\tau_y jf) \quad (1V.10)$$

These components are sufficient to specify normal equations where various pass and reject regions are allowed in the design (see section 4.2)

Instead of referring to each input trace with the indices (i,j) it is possible to label the traces with one index from 1 to N_xN_y by counting traces in x-direction in one row after the other. This is done below. For reasons of simplicity the computed power and crosspower spectra (1V.8) to (1V.10) are renumbered in the corresponding way.

If $R_{ij}(f)$ $(i=1,..,N_xN_y;\ j=1,..,N_xN_y)$ and $G_j(f)$, $(j=1,.,N_xN_y)$ are the general terms for the power and crosspower spectra of the renumbered components one may write the normal equations as

$$\sum_{i=1}^{N_xN_y} A_i(f)\ R_{ij}(f) = G_j(f), \quad (j = 1,..,N_xN_y)$$

$A_i(f)$,$(i=1,.,N_xN_y)$ are the filter components of the general multichannel velocity filter. These solutions may be obtained in the same way as the solutions of (4.2.4).